

Shaharin Anwar Sulaiman *Editor*

# Energy Efficiency in Mobility Systems

 Springer

# Energy Efficiency in Mobility Systems

Shaharin Anwar Sulaiman  
Editor

# Energy Efficiency in Mobility Systems

 Springer

*Editor*

Shaharin Anwar Sulaiman  
Department of Mechanical Engineering  
Universiti Teknologi PETRONAS  
Seri Iskandar, Perak, Malaysia

ISBN 978-981-15-0101-2                      ISBN 978-981-15-0102-9 (eBook)  
<https://doi.org/10.1007/978-981-15-0102-9>

© Springer Nature Singapore Pte Ltd. 2020

This work is subject to copyright. All rights are reserved by the Publisher, whether the whole or part of the material is concerned, specifically the rights of translation, reprinting, reuse of illustrations, recitation, broadcasting, reproduction on microfilms or in any other physical way, and transmission or information storage and retrieval, electronic adaptation, computer software, or by similar or dissimilar methodology now known or hereafter developed.

The use of general descriptive names, registered names, trademarks, service marks, etc. in this publication does not imply, even in the absence of a specific statement, that such names are exempt from the relevant protective laws and regulations and therefore free for general use.

The publisher, the authors and the editors are safe to assume that the advice and information in this book are believed to be true and accurate at the date of publication. Neither the publisher nor the authors or the editors give a warranty, expressed or implied, with respect to the material contained herein or for any errors or omissions that may have been made. The publisher remains neutral with regard to jurisdictional claims in published maps and institutional affiliations.

This Springer imprint is published by the registered company Springer Nature Singapore Pte Ltd. The registered company address is: 152 Beach Road, #21-01/04 Gateway East, Singapore 189721, Singapore

# Preface

Mobility systems are highly complex nowadays due to high number of population in the world and high population density in cities. To give an idea, the city of Manila, at the time when this book is written, is the most populous city with 43,079 people per square kilometer! Humans need to move around for various reasons on daily basis, and thus sophisticated transportation system is vital especially in highly populated areas. Not only human transportation must be properly planned, the transportations of commodity and various products, and also provision of services, are also the concerns of mobility systems. In relation to high population densities, mobility systems are always related to issues such as traffic jams, fuel economy, emission, health etc. These are global issues and they are primary interests of various United Nations agencies. One way to overcome these problems is to ensure that the mobility systems itself is energy efficient. This book discusses various works from different authors on initiatives that have been taken to attain sustainable mobility systems, in particular on the energy efficiency aspect. It will be a useful reference for various stakeholders in transportation systems. Concurrently, the book provides new thinking on the future of transportation in meeting the challenging future. The editor wishes to express his gratitude to all the contributing authors for their initiatives and dedication in preparing the manuscripts for the book.

Seri Iskandar, Malaysia

Shaharin Anwar Sulaiman

# Contents

<b>1</b>	<b>Introduction to Mobility Systems</b> .....	<b>1</b>
	Shaharin Anwar Sulaiman	
<b>2</b>	<b>Hydrogen Fuel Cell in Vehicle Propulsion: Performance, Efficiency, and Challenge</b> .....	<b>9</b>
	Jundika Candra Kurnia and Agus Pulung Sasmito	
<b>3</b>	<b>Prospect of Composite Tubes Based on Bi-materials for Weight Reduction of Vehicles</b> .....	<b>27</b>
	Tahir Abbas, Hamdan Haji Ya, M. Zaki Abdullah, Suhaimi Hassan and Muhammad Yasar Javaid	
<b>4</b>	<b>Mobility and Health: The Interaction of Activity-Travel Patterns, Overall Well-Being, Transport-Related Social Exclusion on Health Parameters</b> .....	<b>53</b>
	Dimas B. E. Dharmowijoyo and Tri Basuki Joewono	
<b>5</b>	<b>Water in Diesel Emulsion Behavior in High-Pressure Direct Injection System</b> .....	<b>85</b>
	A. Rashid A. Aziz, Mhadi A. Ismael, Morgan Heikal, Firmansyah, Ibrahim B. Dalha and Ezrann Zharif Zainal Abidin	
<b>6</b>	<b>Reactivity Controlled Compression Ignition: An Advanced Combustion Mode for Improved Energy Efficiency</b> .....	<b>101</b>
	Ibrahim B. Dalha, Mior A. Said, Z. A. Abdul Karim, A. Rashid A. Aziz, Firmansyah, Ezrann Zharif Zainal Abidin and Mhadi A. Ismael	
<b>7</b>	<b>Principal, Design and Characteristics of a Free Piston Linear Generator</b> .....	<b>127</b>
	A. Rashid A. Aziz, M. B. Baharom, Ezrann Zharif Zainal Abidin, Firmansyah, Salah E. Mohammed, W. N. Azleen W. Nadhari, Evelyn and M. Noraiman M. Jaffry	

<b>8</b>	<b>Efficient Visualization of Scattered Energy Distribution Data by Using Cubic Timmer Triangular Patches</b> . . . . .	145
	Fatin Amani Mohd Ali, Samsul Ariffin Abdul Karim, Sarat Chandra Dass, Vaclav Skala, Mohammad Khatim Hasan and Ishak Hashim	
<b>9</b>	<b>Biodiesel-Fuelled Direct Injection Compression Ignition Engine</b> . . . . .	181
	Saheed Wasiu	
<b>10</b>	<b>A Study on Handling of Stranded Motorcycles in Malaysia</b> . . . . .	199
	Shaharin Anwar Sulaiman, Choo Sin Keat, Bong Hong Seng, M. Syahir Sazali and M. Ashraf Azhar	

# Contributors

**Tahir Abbas** Department of Mechanical Engineering, Government College University Faisalabad, Faisalabad, Punjab, Pakistan

**Z. A. Abdul Karim** Department of Mechanical Engineering, Universiti Teknologi PETRONAS, Seri Iskandar, Perak, Malaysia

**Ezrann Zharif Zainal Abidin** Centre for Automotive Research and Electric Mobility, Universiti Teknologi PETRONAS, Seri Iskandar, Perak, Malaysia

**Fatin Amani Mohd Ali** Fundamental and Applied Sciences Department, Universiti Teknologi PETRONAS, Seri Iskandar, Perak, Malaysia

**M. Ashraf Azhar** Department of Mechanical Engineering, Universiti Teknologi PETRONAS, Seri Iskandar, Perak, Malaysia

**A. Rashid A. Aziz** Centre for Automotive Research and Electric Mobility, Universiti Teknologi PETRONAS, Seri Iskandar, Perak, Malaysia

**M. B. Baharom** Centre for Automotive Research and Electric Mobility, Universiti Teknologi PETRONAS, Seri Iskandar, Perak, Malaysia

**Ibrahim B. Dalha** Centre for Automotive Research and Electric Mobility, Universiti Teknologi PETRONAS, Seri Iskandar, Perak, Malaysia

**Sarat Chandra Dass** Fundamental and Applied Sciences Department, Universiti Teknologi PETRONAS, Seri Iskandar, Perak, Malaysia

**Dimas B. E. Dharmowijoyo** Department of Civil and Environmental Engineering, Universiti Teknologi PETRONAS, Seri Iskandar, Perak, Malaysia

**Evelyn** Centre for Automotive Research and Electric Mobility, Universiti Teknologi PETRONAS, Seri Iskandar, Perak, Malaysia

**Firmansyah** Centre for Automotive Research and Electric Mobility, Universiti Teknologi PETRONAS, Seri Iskandar, Perak, Malaysia



**Hamdan Haji Ya** Department of Mechanical Engineering, Universiti Teknologi PETRONAS, Seri Iskandar, Perak, Malaysia

**Mohammad Khatim Hasan** Faculty of Information Science and Technology, Centre for Artificial Intelligence Technology, Universiti Kebangsaan Malaysia, Bangi, Selangor, Malaysia

**Ishak Hashim** Faculty of Science and Technology, Centre for Modelling and Data Science, Universiti Kebangsaan Malaysia, Bangi, Selangor, Malaysia

**Suhaimi Hassan** Department of Mechanical Engineering, Universiti Teknologi PETRONAS, Seri Iskandar, Perak, Malaysia

**Morgan Heikal** Centre for Automotive Research and Electric Mobility, Universiti Teknologi PETRONAS, Seri Iskandar, Perak, Malaysia

**Mhadi A. Ismael** Centre for Automotive Research and Electric Mobility, Universiti Teknologi PETRONAS, Seri Iskandar, Perak, Malaysia

**M. Noraiman M. Jaffry** Centre for Automotive Research and Electric Mobility, Universiti Teknologi PETRONAS, Seri Iskandar, Perak, Malaysia

**Muhammad Yasar Javaid** Department of Mechanical Engineering, Government College University Faisalabad, Faisalabad, Punjab, Pakistan

**Tri Basuki Joewono** Department of Civil Engineering, Parahyangan Catholic University, Bandung, Indonesia

**Samsul Ariffin Abdul Karim** Fundamental and Applied Sciences Department, Universiti Teknologi PETRONAS, Seri Iskandar, Perak, Malaysia

**Choo Sin Keat** Department of Mechanical Engineering, Universiti Teknologi PETRONAS, Seri Iskandar, Perak, Malaysia

**Jundika Candra Kurnia** Department of Mechanical Engineering, Universiti Teknologi PETRONAS, Seri Iskandar, Perak, Malaysia

**Salah E. Mohammed** Centre for Automotive Research and Electric Mobility, Universiti Teknologi PETRONAS, Seri Iskandar, Perak, Malaysia

**W. N. Azleen W. Nadhari** Centre for Automotive Research and Electric Mobility, Universiti Teknologi PETRONAS, Seri Iskandar, Perak, Malaysia

**Mior A. Said** Department of Mechanical Engineering, Universiti Teknologi PETRONAS, Seri Iskandar, Perak, Malaysia

**Agus Pulung Sasmito** Department of Mining and Materials Engineering, McGill University, Montreal, Quebec, Canada

**Bong Hong Seng** Department of Mechanical Engineering, Universiti Teknologi PETRONAS, Seri Iskandar, Perak, Malaysia

**Vaclav Skala** Faculty of Applied Sciences, Department of Computer Science and Engineering, University of West Bohemia, Pilsen, Czech Republic

**Shaharin Anwar Sulaiman** Department of Mechanical Engineering, Universiti Teknologi PETRONAS, Seri Iskandar, Perak, Malaysia

**M. Syahir Sazali** Department of Mechanical Engineering, Universiti Teknologi PETRONAS, Seri Iskandar, Perak, Malaysia

**Saheed Wasiu** Malaysia France Institute, University of Kuala Lumpur, Bandar Baru Bangi, Selangor, Malaysia

**M. Zaki Abdullah** Department of Mechanical Engineering, Universiti Teknologi PETRONAS, Seri Iskandar, Perak, Malaysia

# Chapter 1

## Introduction to Mobility Systems



**Shaharin Anwar Sulaiman**

Mobility systems explore the movement of people, things, and ideas. This book is intended to delve into the first two. In many cases, they are referred to as the transportation systems. They are complicated issues nowadays primarily due to the drastic increase in human population and the related consequences. The differences in geographical locations, culture, socioeconomic backgrounds, politics, and many other factors make mobility systems far more complex.

### 1.1 Overview of Mobility Systems

The scope of mobility systems in this book covers, but not limited to, individual mobility (could be as simple as walking), private transports such as cars and bicycles, mass transportation of people and goods, and the related infrastructures. In complex social systems of today, the needs to getting around are significant. Adults commute daily to workplaces, markets, and for various social reasons. Youngsters need to get to schools on a daily basis. Furthermore, people also travel to hospitals, government offices, religious and community places, and for leisure. Beyond personal needs, there are also transportation requirements such as transportation of commodities, delivery of household goods, mail delivery, and a long list of delivery of services.

---

S. A. Sulaiman (✉)  
Department of Mechanical Engineering, Universiti Teknologi  
PETRONAS, 32610 Seri Iskandar, Perak, Malaysia  
e-mail: [shaharin@utp.edu.my](mailto:shaharin@utp.edu.my)

© Springer Nature Singapore Pte Ltd. 2020  
S. A. Sulaiman (ed.), *Energy Efficiency in Mobility Systems*,  
[https://doi.org/10.1007/978-981-15-0102-9\\_1](https://doi.org/10.1007/978-981-15-0102-9_1)

## 1.2 Associated Issues

When the modern transportation systems were introduced during the Industrial Revolution in the eighteenth century, it brought in sudden goodness to the society. The prominent ones were the waterways, railroads, and roads, which involved various forms of vehicles intended primarily for relatively faster and more efficient transport of raw materials and finished products. As a result, the use of animal and human for transportation was reduced tremendously. Not only has this made travel faster, but also the transportation systems have been safer since the period of the Industrial Revolution.

The Industrial Revolution had also resulted in a huge improvement in human health, leading to a tremendous increase in the human population. Consequently, the need for transportation systems also has, since then, increased. The number of motor vehicles nowadays is very high. There were more than 1.3 billion of them reported in 2016 [1]. The sustainability of the present-day transportation systems is a great debate, as it involves issues such as environment, energy, and the society.

In dealing with mobility systems, the associated social aspects and environmental impacts are equally important, particularly in present days when the world's population has already exceeded 7.7 billion [2]. Easily, this implies highly complex mobility situations, which consequently require well-managed and sustainable mobility systems. One of the recent trends nowadays is to have a working-living environment whereby people can minimize traveling since all their needs are designed to be within the same place [3]. While the luxury of this concept may be nice, they are mostly applicable for new developments, and hence other established populated areas or townships [4] will have to deal with the present-day issues related to mobility system.

From the point of view of the governments, it would be ideal for them if their citizens have access to different places for various purposes ranging from work to leisure. There are many factors that must be considered in satisfying the needs of the citizens. They include, for example, status of income, distance, geographical conditions, emissions, etc. For cities, it is usual to have a range of choice of public transportations. On the other hand, rural areas, depending on the government, are sometimes left out, leaving the community to have to figure out their modes of transportation. This would be worse, particularly for the low-income citizens. In Malaysia, there are still areas where public transportation is not accessible to people in certain rural areas.

For developed countries, short-distance transportation for rural areas relies on the heavy taxes imposed on the income of the citizens. Figure 1.1 shows a single-coach train observed in Austria, which was intended to cater for short-distance travel for people in rural areas. The decision for single-coach might have been made in view of the low volume passengers for that area. At the same time, the train operator may probably have to bear some hefty cost due to the low number of passengers. In addition, there is also a need for the operator to coordinate the train traffic in order to accommodate for this small local train network which is sharing the tracks of a bigger train rail network.



**Fig. 1.1** A single-coach train in Europe serving rural area for short-distance travel

While the railway systems are just an example, the mobility systems involve also personal vehicles such as cars, motorcycles, bicycles and many others. These are basically individual machines that can be purchased in the free market in most countries. Since anyone can buy or rent them, their numbers can be uncontrollable, leading to problems such as traffic jams, poor mobility, and high emissions. Those are daily problems that people in the cities are facing. Occasionally, such as during big festivals, like in Malaysia, mass traffic jams at inter-city highways have always been anticipated [5]. This is because during such festivals, people in the cities, especially Kuala Lumpur, would concurrently return to hometown for the celebrations. In this circumstance, it would be common that traffic is almost at a standstill sometimes for more than 10 km on the highway. The neighboring country, Indonesia, had even worse experience when coming to festival seasons. In 2016, it was reported that 12 people died of dehydration and exhaustion while sitting in heavy traffic, which filled up three lanes for several days on the island of Java [6].

In controlling the ownership of individual vehicles, the government of Singapore has a quota system, through the Certificates of Entitlement [7], for which citizens must bid for in order to legally own a vehicle. Such a system, along with various other charges, is imposed because the country is small and has an extremely high population density. Consequently, number of vehicles in the country can be controlled and can be matched with the desired traffic.

Equally important are the pedestrian systems. They are vital in promoting the habit of walking within a community area. There so many benefits of good pedestrian systems. They can be helpful in easing road traffic. More importantly, they could reduce emission and conserve fuel that is resulted from the use of motored vehicles. At the same time, they can be instrumental in promoting a healthy lifestyle. An exemplary pedestrian system in Malaysia is the Canopy Walk at Bandar Sunway [8].

While pedestrian systems are usually intended for relatively short-distance travel, bicycles have greater capability in term of distance and speed. Like pedestrians, bicycles do not consume fuel. The power source and engine for bicycle is the human body. As a matter of fact, cycling is more efficient than any other methods of travel, including walking. In some cities, there are more bicycles than any other vehicles. The trend is due to various promoting factors, usually due to the influence of the government. It is common nowadays to see bicycle paths in many countries; they are mainly intended for recreational use such as the one shown in Fig. 1.2.

When the number of bicycles is high, the associated arising issue would be in managing the traffic in ensuring safety and smoothness of the journey. On safety, it is not just about the cyclists, but also for others such as pedestrians and other road users. The initiatives taken in some developed countries in promoting the use of bicycles are applaudable. Belgium, Germany, Denmark, the Netherlands, and the United Kingdom have, for example, developed freeways dedicated to bicycles, which connect cities [9]. Here, the freeways are intended for long-distance traffic, just for bicycles. The bicycle freeway network in Belgium spans for over 1500 km.



**Fig. 1.2** Typical recreational bicycle paths in Malaysia

In Denmark, it is reported that its investment in a total network of 45 routes of cycle superhighways has resulted in a socioeconomic surplus of €765 million, partly due to improved health, fewer days of sick leave and less time wasted in traffic jams [10].

### 1.3 The Importance of Energy Efficient Systems

At present days, the ambition of countries in providing reliable, affordable and clean energy, while growing their economies, has been expressed in the Paris Agreement [11]. This agreement has a goal of limiting global increase in temperature to below 2 °C. The temperature change, which is very well known as global warming, is a long-term rise in the average temperature of the Earth's climate system, due to various effects. A main contributor to the climate change is the build-up of greenhouse gases, which are trapped in the atmosphere. The highest share of greenhouse gases is water vapor. The second main contributor to greenhouse gases is carbon dioxide emissions, which is more related to human activities. Primarily derived from the combustion of fossil fuels, carbon dioxide emissions have risen dramatically since the start of the Industrial Revolution. Most of the world's greenhouse gas emissions come from top world economies, primarily China, the United States, and the European Union; the per capita greenhouse gas emissions are highest in the United States and Russia [12].

The transportation sector contributes 27% of global carbon dioxide emissions [13]. In addition, diesel vehicles emit short-lived black carbon, which is also known as soot, a consequence of incomplete combustion of hydrocarbons. While soot is also a contributor to global warming, it is also a major component of particulate matter, the air pollutant most closely associated with increased air-pollution related mortality and morbidity.

In reducing emission from transportation, one of the biggest potential is through the avoidance of the use of carbon fuel through electrification of vehicles. Even if the electric power plants are still using fossil fuel, this could be advantageous in the sense that the emission is concentrated at limited places and therefore can be treated more effectively. This is still better than having widespread vehicles releasing emissions in cities or at any places they travel through. Further improvements can be achieved when the sources of fuel for power generation are shifted to renewable energy. Presently, as shown in Table 1.1, several countries have already pledged to phase out conventional internal combustion engine vehicles, in favor of electric vehicle. Although there have been critics on the achievability of such plan, most of the countries are serious and highly committed in their plans. It is clear that internal combustion engine vehicles will be phased slowly out in many countries.

In relation to mobility systems, energy efficiency would be regarded as a high priority. Energy-efficient mobility systems envision transportation future that is safe, affordable, efficient, and accessible. In achieving this, research and development (R&D) will be required in various aspects, namely on the vehicle, traveler, infrastructure, and technology solutions that would lead to increase in mobility

**Table 1.1** Countries that are banning conventional vehicles with internal combustion engines

Country	Source	Year	Notes
United Kingdom	[14]	2020	Starts with Oxford. London in 2030
Costa Rica	[15]	2021	
Italy	[16]	2024	Diesel vehicles in Rome. Milan 2030
Greece	[17]	2025	Diesel cars and vans in Athens
Mexico	[17]	2025	All ICE vehicles in Mexico City
Spain	[17]	2025	Diesel vehicles in Madrid. Barcelona in 2030
Norway	[17]	2025	Diesel cars and vans in Athens
Canada	[18]	2025	10% ZEVs in British Columbia
France	[19]	2025	Diesel vehicles in Paris. France 2040
New Zealand	[14]	2030	Starts with Auckland
India	[20]	2030	
Denmark	[21]	2030	
Ireland	[22]	2030	
Israel	[23]	2030	
The Netherlands	[24]	2030	
Belgium	[25]	2030	Diesel vehicles in Brussels
South Africa	[14]	2030	All ICE vehicles in Cape Town
Germany	[14]	2030	All ICE vehicles in Heidelberg
Ecuador	[14]	2030	All ICE vehicles in Quito
USA	[14]	2030	All ICE in Los Angeles & Seattle
China	[26]	2030	Hainan only. Deadline for whole China to be announced [20]

energy productivity for individuals and businesses. In relation to this, at present, futurists are in favor of electric (battery) vehicles, hybrid vehicles, and fuel cell vehicles. Also, not to forget, the flying cars are presently at their inception. It may be a matter of time before they overcome their barriers. Companies like Uber are looking forward to utilizing them in the near future [27].

Strong supports from the stakeholders are vital in research and development that studies the significance of disruptive forces such as automated, connected, electric and shared vehicles on energy consumption in transportation. At a glance, reduction in energy consumption could be attained through straightforward approaches such as ride-sharing, smooth driving (instead of sudden acceleration), small-sizing of vehicles, and shortening of travel distance. In addition, joint efforts with researchers and different stakeholders are very important in order to understand better how to make use of disrupted technologies in achieving energy-efficient mobility systems.



## 1.4 Summary

Today's mobility systems are very complex as it serves communities of various backgrounds and needs. The trends of mobility systems keep changing over time due to increased challenges related to the increase in human population and growth in technologies and economies. At the same time, the world is facing problems mainly in terms of energy and environment. Global warming is well acknowledged by the society but the appropriate mitigation actions are still lacking. In a bigger picture, the sustainability of systems in the society needs constant improvement. Hence, from the point of view of mobility systems, continuous research and development is required in order to ensure that they are able to cope with the challenges of the future.

## References

1. S.C. Davis, S.E. Williams, R.G. Boundy, *Transportation Energy Data Book*, vol. 36, 2nd edn. (Oak Ridge National Laboratory, Oak Ridge, 2018)
2. United Nations, *World Population Prospects: The 2017 Revision, Key Findings and Advanced Tables* (Department of Economic and Social Affairs, Working Paper No. ESA/P/WP/248, 2017)
3. A.K. Kar, M.P. Gupta, P.V. Ilavarasan, Y.K. Dwivedi, *Advances in Smart Cities: Smarter People, Governance, and Solutions* (CRC Press, Boca Raton, 2017)
4. Green Building Index, *GBI Assessment Criteria for Township, Version 2.0* (Malaysia, 2017)
5. C.L. Leen, A. Yunus, 'Balikkampung' rush: Heavy traffic on all major highways in Malaysia (Jun 23, 2017), <https://www.asiaone.com/malaysia/balik-kampung-rush-heavy-traffic-all-major-highways-malaysia>. Accessed 24 Apr 2019
6. BBC News, Indonesia traffic jam: 12 die in Java gridlock during Ramadan, 8 July 2016, <https://www.bbc.com/news/world-asia-36748008>
7. Singapore Legal Advice, Buying a car in Singapore: a comprehensive guide (2018), <https://singaporelegaladvice.com/law-articles/buying-a-car-in-singapore-a-comprehensive-guide/>. Accessed 24 Apr 2019
8. The Star, Canopy Walk at Bandar Sunway. *Community News*, 8 September 2012
9. Wikipedia, Bike freeway, [https://en.wikipedia.org/wiki/Bike\\_freeway](https://en.wikipedia.org/wiki/Bike_freeway). Accessed 8 May 2019
10. Supercykelstier, About cycle superhighways, <https://supercykelstier.dk/about/>. Accessed 9 May 2019
11. United Nations, Paris agreement (2015), <https://unfccc.int/process-and-meetings/the-paris-agreement/the-paris-agreement>
12. C2ES, Global emissions, <https://www.c2es.org/content/international-emissions/>. Accessed 10 May 2019
13. WHO, Health and sustainable development, World Health Organization, <https://www.who.int/sustainable-development/transport/health-risks/climate-impacts/en/>. Accessed 10 May 2019
14. I. Burch, J. Gilchrist, Survey of global activity to phase out internal combustion engine vehicles, Technical Report (The Center for Climate Protection, Santa Rosa, California, USA, 2018)
15. Brian Spaen, Costa Rica plans to eliminate fossil fuels by 2021. *Greenmatters* (2018), <https://www.greenmatters.com/>. Accessed 9 May 2019

16. J. Dow, Rome latest city to announce car ban, will ban diesel cars from historical center starting 2024. *Electrek*, 28 February 2018, <https://electrek.co/2018/02/28/rome-bans-diesel-cars-2024/>
17. M.J. Coren, Nine countries say they'll ban internal combustion engines. So far, it's just words. *Quartz*, 7 August 2018, <https://qz.com>
18. L. Kretzel, B.C. plans to ban new gas, diesel car sales by 2040. *Citynews*, 20 November 2018, <https://www.citynews1130.com>
19. F. Harvey, Four of world's biggest cities to ban diesel cars from their centres. *The Guardian*, 2 December 2016, [www.theguardian.com](http://www.theguardian.com)
20. Energy World, *China to Set Deadline to Phase Out Conventional Vehicles* (Energy Institute, October 2017), p. 4
21. E.G. Nielson, Denmark embraces electric car revolution with petrol and diesel ban plan. *Reuters*, 2 October 2018
22. E. Burke-Kennedy, Ireland 2040: €22bn to turn State into low-carbon economy. *The Irish Times*, 16 February 2018
23. S. Solomon, Israel aims to eliminate use of coal, gasoline and diesel by 2030. *The Times of Israel*, 27 February 2018
24. B. Schmidt, Amsterdam bans all petrol and diesel cars and motorbikes from 2030. *The Driven*, <https://thedriven.io>, 6 May 2019
25. GJS, Brussel gaatdieselwagensverbannenvanaf 2030, regeringwilookmaatregelentegenbenzinewagens. *Het Nieuwsblad (in Dutch)*, 31 May 2018, <https://www.nieuwsblad.be>
26. W. Priyanto, 2030, Pulau IniLarangPenjualan Mobil Berbahan Bakar Fossil, Tempo.Co (in Indonesian), 11 March 2019 <https://otomotif.tempo.co>
27. C. Reilly, How Uber is getting flying cars off the ground. *CNET*, 25 September 2018

# Chapter 2

## Hydrogen Fuel Cell in Vehicle Propulsion: Performance, Efficiency, and Challenge



Jundika Candra Kurnia and Agus Pulung Sasmito

This chapter provides comprehensive review on the current development of polymer electrolyte membrane fuel cell (PEMFC) in automotive application to assist further development of hydrogen fuel cell and expedite its wide adoption on a commercial scale. Special attention is devoted to the performance and efficiency of PEMFC especially on vehicular application and key issues hindering further development of PEMFC to achieve its commercialization stage. Subsequently, various mitigation strategies proposed to address the aforementioned issues are outlined and discussed. Lastly, further research and development needs of the field are highlighted and discussed.

### 2.1 Introduction

Over the last decades, there has been a growing concern over the severe impact of fossil fuel burning to the environment. Several countries in Europe have announced their decisions to ban fossil-fueled internal combustion engines, especially diesel engines, from their roads in the near future. To replace these internal combustion engine vehicles, communities worldwide have been leaning towards electric vehicle, hybrid vehicle and fuel cell vehicle. At the moments, most of the efforts have been devoted on the development of hybrid vehicle which combines internal combustion engine with an electric motor, as it is deemed as the bridge between the

---

J. C. Kurnia (✉)

Department of Mechanical Engineering, Universiti Teknologi  
PETRONAS, 32610 Seri Iskandar, Perak, Malaysia  
e-mail: [jundika.kurnia@utp.edu.my](mailto:jundika.kurnia@utp.edu.my)

A. P. Sasmito

Department of Mining and Materials Engineering, McGill  
University, 3450 University Street, Montreal, Quebec H3A0E8, Canada

conventional fossil-fueled vehicles with the future electric vehicles. Despite its promising potential, electronic vehicles have several limitations that need to be addressed prior to their wide adoption, i.e., limited battery capacity, relatively long charging time, short battery lifecycle, large size of battery pack, high cost of battery pack and limited availability of charging stations. These limitations, although they will most likely be addressed with advanced technology and material development in the future, have driven the interest in the development of fuel cell vehicles. Fuel cell vehicle offers some advantages as compared to the electric vehicle, such as high energy density of the hydrogen fuel, relatively faster refueling and longer range at lower weight [1–3]. All these advantages can be achieved by fuel cell vehicle while producing only water and heat as their emission. In addition, several countries, especially in Europe, have issued policies which stimulate the development of hydrogen refueling network [4].

Driven by these factors, several fuel cell vehicles and vehicle concepts have been introduced, showcased and produced by some leading automakers. Some of these vehicles are Honda Clarity, Toyota Mirai, Lexus LF-LC, Mercedes-Benz GLC F-CELL, BMW Hydrogen 7, Hyundai Tucson FCEV and Audi h-tron Quattro [5]. Recently, Toyota increased the production of its hydrogen fuel cell vehicle amid growing investment in Japan for fuel cell vehicle. In South Korea, Hyundai announced a similar plan to produce a large amount of fuel cell vehicles over the next decades [6]. As compared to electric vehicle which is widely available globally, only relatively small numbers of fuel cell vehicles are moving on the road, mainly due to the high cost of fuel cell production. Nevertheless, this cost will most likely reduce as vehicle production increases. Several other issues hindering wide adoption of fuel cell vehicles are the fuel cell performance, fuel utilization, and component degradation. As such, numerous studies and development efforts have been conducted and reported. Most of these studies focused on improving the performance and efficiency of the fuel cell. Meanwhile, some studies investigate the feasibility, life cycle analysis and techno-economic aspect of fuel cell vehicle. This chapter will start with a brief introduction on the basic concept of fuel cell, various types of fuel cell and fuel delivery of fuel cell, followed by a discussion on the performance and efficiency of fuel cell and finally prediction on the future studies and development are highlighted and discussed.

## **2.2 Fuel Cell: Basics, Type, Fuel Delivery and Vehicular Application**

Unlike battery which is an energy-storing device, fuel cell is an energy conversion device which converts chemical energy into electricity. As such, it can continuously produce electricity through electrochemical reaction as long as fuel and reactant are supplied. A fuel cell typically consists of electrodes (anode and cathode) and electrolyte which are sandwiched together. Currently, seven types of fuel cells are

available, i.e., polymer electrolyte membrane or proton exchange membrane fuel cells (PEMFCs or PEFCs), direct methanol fuel cell (DMFC), solid oxide fuel cells (SOFCs), alkaline fuel cells (AFCs), phosphoric acid fuel cells (PAFCs), molten carbonate fuel cells (MCFCs) and microbial fuel cell [7]. Table 2.1 summarizes typical operating temperature, application, advantages and disadvantages of these fuel cells [8–10].

**Table 2.1** Various types of fuel cells

Fuel cell	Operating temperature and efficiency	Applications, advantages and disadvantages
Proton exchange membrane fuel cells (PEMFCs or PEFCs)	60–100 °C 40–50%	–Vehicle and portable power source –Low operating temperature, high power density, quick start-up and response to load changes, easy scale-up and high efficiency –Intolerant to CO in impure H <sub>2</sub> and expensive
Direct methanol fuel cell (DMFC)	50–120 °C 20–40%	–Vehicle and small portable power source –No reforming, high power density, and low operating temperature –Low efficiency, methanol crossover, and poisonous byproduct
Solid oxide fuel cells (SOFCs)	800–1000 °C 50–60%	–Central and stand-alone power plant and combined heat and power plant –High efficiency and direct fossil fuel –High temperature, thermal stress failure, coking, and sulfur poisoning
Alkaline fuel cells (AFCs),	50–90 °C 50–70%	–Space application –High efficiency –Intolerant to CO <sub>2</sub> in impure H <sub>2</sub> and air, corrosion, and expensive
Phosphoric acid fuel cells (PAFCs)	175–220 °C 40–45%	–Stand-alone power plant and combined heat and power plant –Tolerant to impure H <sub>2</sub> , commercial –Low power density, corrosion, and sulfur poisoning
Molten carbonate fuel cells (MCFCs)	600–650 °C 50–60%	–Central and stand-alone power plant and combined heat and power plant –High efficiency, near-commercial –Electrolyte instability, corrosion, and sulfur poisoning
Microbial fuel cells (MFCs)	15–45 °C 4–81%	–Reactors for wastewater treatment, charging and discharging supercapacitor, low power application. –A promising moderate environmental impact, neutral pH operation, uses biomass –More complex than traditional fuel cells, low energy produced, scientific curiosity, rather than that of a useful technology

As can be inferred from Table 2.1, applicability and suitability of these fuel cells for a specific application, including vehicular application, requires careful consideration on several critical parameters such as operating parameter, power requirement, fuel availability, and cost. Among these fuel cells, PEMFC is considered as one of the most promising candidates for vehicular application owing to its unique feature, i.e., low operating temperature, high power density, quick start-up and response to load changes, easy scale-up and high efficiency [11].

In a PEMFC, fuel (hydrogen) and oxygen (air) are delivered through a series of channels (typically embedded on an electrically conductive plate) to the active area where the electrochemical reaction occurs between fuel and oxygen-producing electricity, water and heat. To meet the power requirement for certain applications, several fuel cells are stacked to produce the required voltage and power, as illustrated in Fig. 2.1. For this stacked fuel cell, fuel delivery, water management, and thermal management would be crucial. For PEMFC stack, four fuel delivery configurations are commonly adopted, namely, flow through anode, flow through

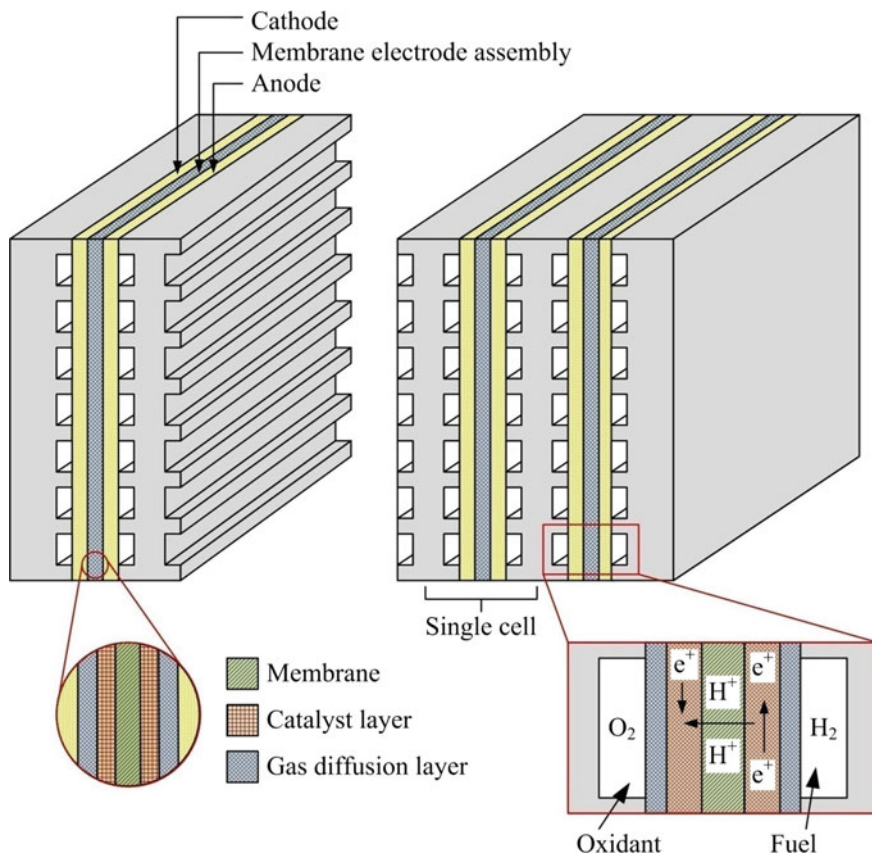


**Fig. 2.1** Schematics of PEMFC stack

anode with recirculation, dead-end anode, and dead-end anode with recirculation [12–15].

The simplest configuration of fuel delivery in PEMFCs is flow-through configuration, in which the fuel (hydrogen) is supplied to the fuel cell continuously. Only part of this fuel is consumed within the cell, some of it is dispersed through the outlet together with the reaction byproduct. This high-pressure excess fuel contributes to the removal of reaction by-products (nitrogen and water) inside the cell, maintaining the performance of the cell. The discharge of excess fuel directly to the atmosphere leads to fuel wastage and environmental pollution. This issue becomes critical in some applications where space for hydrogen storage is limited and confined space where un-reacted hydrogen possesses the potential danger of explosion. To overcome this issue some proposals have been considered and evaluated. The most commonly adopted methods are by recycling the excess fuel from the anode outlet and by supplying the exact amount of fuel required for the electrochemical reaction and seal off the anode outlet, known as dead-end configuration. The former requires liquid and gas separation to remove the water and humidifier to humidify the recycled fuel. This adds complexity to the already complex system. Meanwhile, the former is simpler by sealing off the anode outlet and forcing the fuel to be consumed by the reaction inside the fuel cell. However, this method trigger accumulation of byproduct (liquid water and nitrogen) in the anode side, minimizing fuel access to the active electrochemical reaction area, creating fuel starvation which can lead to cell performance and structure degradation.

To overcome this issue, purging is needed to flash out the accumulated byproduct and recover the cell performance. However, this has to be done carefully as frequent purging will defeat the purpose of dead-end configuration to minimize fuel wastage. Other method combines both dead-end and recirculation configurations. The reason behind this configuration is because the liquid gas separator only separates liquid water from the gas but it does not remove the nitrogen gas component in it. Similar to water accumulation, high concentration of nitrogen will restrict hydrogen access to the fuel cell active area, leading to fuel starvation and degradation of fuel performance and structural integrity. As such, purging is needed to release the accumulated nitrogen. The simplified illustration of these fuel delivery configurations is shown in Fig. 2.2. For fuel cell application in fuel cell vehicle, dead-end is considered as the most promising and suitable fuel delivery owing to its high fuel utilization and simple configuration. It does not need recirculation to achieve high fuel utilization which is critical as vehicle does not offer large compartment to store hydrogen fuel and to accommodate complex recirculation system.

A typical fuel cell vehicle schematic is shown in Fig. 2.3. As can be seen, hydrogen fuel is stored in a special high-pressure storage tank. Before it is supplied to the fuel cell stack, it will pass through pressure controller which control and maintain suitable inlet pressure for the fuel cell stack. A humidifier may be needed to control the humidity of the hydrogen fuel. The overall power cell system work as an electricity producer for supply to the electric motor to drive the vehicle. A cooling system is required to maintain the fuel cell operating at optimum

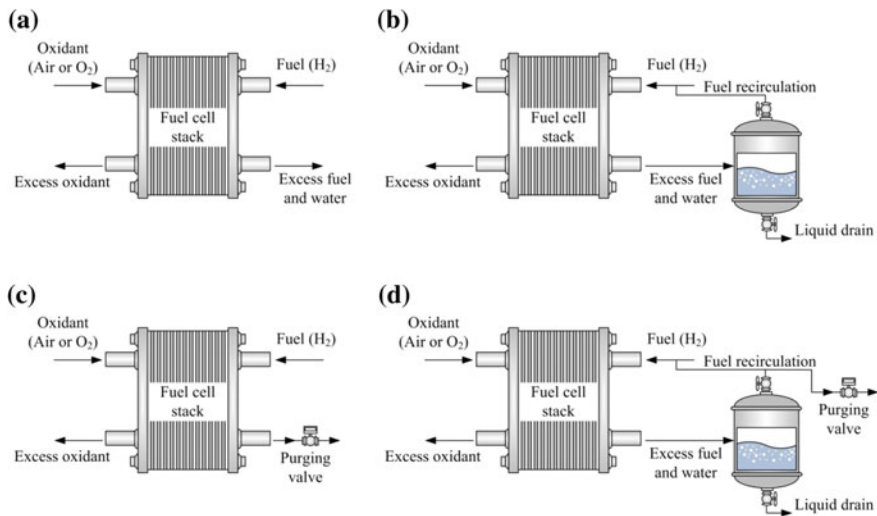


**Fig. 2.2** Fuel delivery configuration in typical fuel cell stacks: **a** flow through anode, **b** flow through anode with recirculation, **c** dead-end anode and **d** dead-end anode with recirculation

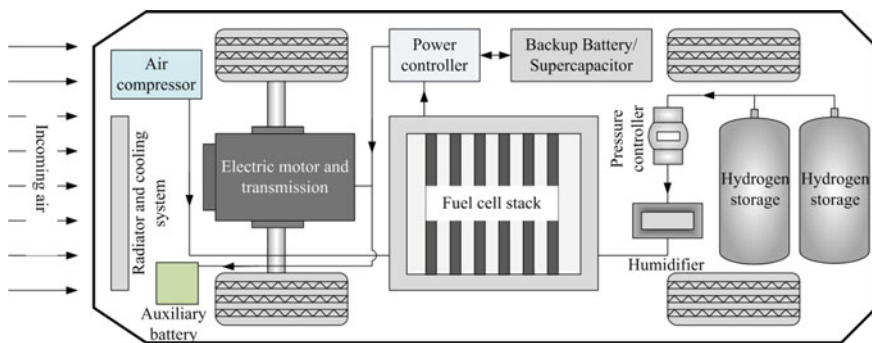


**Fig. 2.3** A typical fuel cell vehicle components

temperature. In addition, a compressor may be needed to compress the incoming air and supply to the fuel cell stack. Note that for some fuel cell vehicles, a more complex system may be adopted, especially when the fuel is not pure hydrogen but hydrogen-rich substances (e.g., methanol, ethanol, and natural gas) for which reformer is needed to convert these fuels into hydrogen gas.

When used in a vehicle propulsion system, fuel cell stack is commonly coupled with battery to provide the power for start-up, back-up should the fuel cell fail and to power auxiliary equipment. Battery is also required to store excess electricity that may be produced from the regenerative braking. In some vehicles, the battery is replaced with super-capacitor to store the excess electricity. As such, fuel cell



vehicle is considered as a hybrid vehicle. Marzougi et al. [16] highlighted that the addition of a supercapacitor and battery in fuel cell-based vehicles allows the possibility of a significant reduction of the hydrogen consumption and an improvement of the vehicle efficiency. Since multiple energy systems are utilized in fuel cell vehicle, energy management system is crucial in determining the overall fuel cell vehicles.

### 2.3 Fuel Cell Performance and Efficiency

Before proceeding further, it is imperative to recall the definition of fuel cell efficiency which is defined as a ratio between the electricity produced and the hydrogen consumed [17]:

$$\eta = \frac{W_{el}}{W_{H_2}} \quad (2.1)$$

where  $W_{el}$  is the electric produced by the fuel cell and  $W_{H_2}$  is the energy of the fuel (hydrogen). Both of them should be expressed in the same unit of in watts or kilowatts. The electric produced by the fuel cell is simply a product of voltage ( $V$ ) and current ( $I$ ), i.e.

$$W_{el} = I \cdot V \quad (2.2)$$

Meanwhile, the energy of the fuel can be estimated from the hydrogen consumption using Faraday's law:

$$W_{H_2} = \Delta H \frac{I}{nF} \quad (2.3)$$

Here,  $\Delta H/nF$  has a dimension of volts. It is commonly referred to as thermoneutral potential and it has a value of 1.482 V for  $\Delta H = 286$  kJ/mol. Therefore, the efficiency of a fuel cell can be expressed as:

$$\eta = \frac{V}{1.482} \quad (2.4)$$

which is directly proportional to the cell potential.

The performance and efficiency of fuel cells is mainly attributed to the fuel availability for the electrochemical reaction, operating temperature, and humidity of the cell. As such, thermal, water and gas management are crucial in determining the performance and efficiency of the fuel cells. Consequently, significant efforts have been devoted to investigating thermal, water and gas management in the fuel cells and their corresponding effect to the fuel cell performance.

Nguyen [18] developed and evaluated a nonconventional gas distribution design with two purposes, i.e., (i) to improve the mass-transport rates of the reactants from the flow channels to the inner catalyst layers of the porous electrodes and (ii) to reduce the electrode water flooding problem in the cathode of proton-exchange-membrane fuel cells. Unlike the conventional design where the inlet and outlet of the flow fields are connected, the new design has its flow fields dead-ended, forcing the reactant to pass through the porous electrode to reach the outlet. The results from Nguyen's study confirmed the ability of the new design to achieve the intended purposes. Jeon et al. [19] evaluated the performance of PEMFC equipped with serpentine flow-fields with a single channel, double channel, cyclic-single channel, and symmetric-single channel patterns. The effect of inlet humidity condition was also evaluated by calculating the distributions of overpotentials, current density distribution, and membrane water content at different cell voltages. The result indicated that the double channel flow-field offered superior performance at high inlet humidity. At low inlet humidity, however, no significant difference on fuel cell performance was observed for the considered flow field designs. Similarly, Rahgoshay et al. [20] evaluated the parallel and serpentine cooling design on maintaining optimum temperature of the PEMFC stacks. It was found that better cooling performance was achieved by adopting serpentine flow field. Sasmito et al. [21] numerically evaluated various gas and coolant channel designs for high-performance liquid-cooled proton exchange membrane fuel cell stacks. The studied designs were parallel, serpentine, oblique-fins, coiled, parallel-serpentine and a novel hybrid parallel-serpentine-oblique-fins designs. The results indicated that the novel hybrid channel design offered superior cell performance, indicated by a lower pumping power and good thermal, water and gas management as compared to conventional channels. Following Sasmito et al. [21], Kerkoub et al. [22] evaluated the effect of channel to rib width ratio with various flow field designs on performance of PEM fuel cell. They reported that decreasing channel width and increasing rib width improved cell performance. In addition, decreasing the channel to rib width ratio led to the increase of the pressure drop and under rib convection. These yielded high reactants speed under the ribs and more homogenous local transport phenomena in the catalysts layer; enhancing the net power density. Afshari et al. [23] proposed the use of metal foam as coolant fluid distributor in the PEMFC. The performance of this metal foam design was compared with parallel and two serpentine designs. It was reported that metal foam design yielded better cooling performance and lower pressure drop. These resulted in better overall fuel cell stack performance and efficiency due to lower parasitic load. Alizadeh et al. [24] evaluated a novel cooling flow field design for PEMFC stack. Looking at the design, it was based on a parallel design with the modified inlet manifold. Different designs were proposed and evaluated. It was concluded that a proper design is critical to prevent hot spot formation and consequently MEA damage.

Looking into the performance and efficiency of fuel cell in vehicle application, Büchi et al. [25] highlighted that efficiency is the main parameter for fuel cell application in automotive field. They compared and evaluated the performance of hydrogen/oxygen PEMFC and hydrogen/air EPMFC. The evaluation considered

overall system from the tank to electric power chain. They reported that when the fuel (hydrogen) and oxidant (oxygen) are produced using conventional path/process using fossil fuel, the fuel to electric current efficiency for both systems (hydrogen/oxygen and hydrogen/air) showed no significant difference. In contrast, when the hydrogen was produced from water by thermolysis or electrolysis, the hydrogen/oxygen system offered better efficiency. Han et al. [26] developed a hybrid FC vehicle simulation model to evaluate the characteristics of FC systems, to optimize the overall FC efficiency and to maximize fuel economy. They indicated that there was a trade-off between power density and overall efficiency: higher power density would reduce efficiency and vice versa. As such, careful balance would be required to achieve optimum condition. In their study, the most critical component determining both power density and efficiency was the compressor: a larger compressor offered higher fuel cell power density but yielded lower fuel cell efficiency. Bang et al. [27] employed a model of fuel cell powered electric vehicle to the performance of the overall vehicle system, fuel economy and the overall efficiency of the system. Both blower and compressor air feeding system were evaluated. Driving cycle FTP-75 was adopted to represent the dynamics of the vehicle. It was reported that combination of vehicle mass and fuel cell efficiency determined the optimum point in power variation. In addition, it was found that compressor air delivery system offered 4.8% higher efficiency than that of the blower air delivery counterpart for FTP-75 driving cycle. It should be noted, however, that for the compressor method, the power loss was mainly contributed by the compressor. Meanwhile, for the blower method, the loss was primarily attributed by the humidifier. Gomez et al. [28] investigated the performance of a dead-end anode PEMFC powered vehicle when subjected to segments of a European driving cycle. They concluded that low purging duration and high purging period were beneficial for fuel cell performance. In addition, they highlighted the importance of coolant flow rate to maintain optimum temperature, and thus optimum performance of the fuel cell stack. Al-Zeyoudi [29] highlighted the importance of air humidity in determining the operation of open cathode PEMFC to power vehicle. Better fuel cell performance was reported during the summer, due to the hot and humid air input. Nevertheless, hot and arid condition was found to deteriorate the performance of the fuel cell, owing to the drying of the membrane which leads to low ionic conductivity. Fly and Thring [30] evaluated and compared evaporative and liquid cooling methods for fuel cell vehicles. They reported that evaporative cooling required smaller radiator frontal area as compared to liquid cooling to maintain the same operating condition in ensuring optimum performance of the fuel cell. This finding indicates the superior performance of the evaporative cooling as compared to the liquid cooling.

Despite extensive studies that were conducted in improving the performance and efficiency of the fuel cell, more studies are needed to further improve the performance of the fuel cell especially on improving the gas distribution and maintaining optimum humidity and temperature for the electrochemical reaction within the cell.

## 2.4 Energy Management in Fuel Cell Vehicles

As stated previously, fuel cell stack will typically be coupled with battery and/or supercapacitor when used in a vehicle propulsion system. As such, relation and interaction between these power/energy systems will be critical in determining the overall vehicle efficiency. Commonly referred to as energy management strategies/systems, this is one of the main focus areas in fuel cell vehicle development. It is therefore not surprising that a significant amount of researchers devoted their efforts to investigate this energy management issue. Feroldi et al. [31] introduced energy management strategies based on the efficiency map for fuel cell hybrid vehicles. Three strategies were evaluated, i.e., (i) operate fuel cell system in an advantageous zone where the efficiency is high, (ii) operate the fuel cell system preferably in its point of maximum efficiency in order to improve the hydrogen economy and (iii) minimize the fuel hydrogen consumption by using optimization. The proposed method offered high system efficiency, mirrored by a high reduction in hydrogen consumption as compared to the base case (fuel cell with no hybridization). On average, 17% reduction in hydrogen consumption was achieved. In their recent study [32], Feroldi and Carignano adopted sizing procedure based on the fulfillment of power requirements, including sustained speed test and stochastic driving cycles, to determine the size of fuel cell and number of supercapacitor required for hybrid vehicles. It was found that a trade-off between the minimum fuel consumption and the minimum installed power was suggested rather than the minimum fuel consumption solution. In addition, it was found that both vehicle mass and reduction on the overall fuel cell efficiency gave rise to hydrogen consumption. Similar approach was taken by Liu and Liu [33] by optimizing power source sizing of fuel cell hybrid vehicles using Pontryagin's minimum principle. However, unlike the previous study, they focused more on battery performance: they optimized battery lifetime while reducing battery energy loss, fuel consumption, and powertrain cost. In their evaluation, they adopted EPA Federal Test Procedure 72 (FTP-72). From the study, they proposed current constraint strategy to lower battery loss and improving the overall system efficiency. Similarly, Xu et al. [34] adopted multi-objective component sizing based on optimal energy management strategy of fuel cell electric vehicles. Their focus was not only on fuel economy but also for system durability. In their study, a two-loop framework based on a dynamic programming algorithm and the Pareto optimal principle was proposed. The system considered was a fuel cell city bus. From their evaluation, they found the optimum battery capacity and fuel cell stacks maximal net output power to ensure both fuel economy and system durability. Carignoni et al. [35] proposed a novel strategy based on the estimation of the energy demand. By implementing the proposed strategy, the fuel economy and the drivability of the vehicle could be achieved.

Li et al. [36] adopted well-to-wheel analysis to compare and evaluate battery-powered and fuel cell powered electric vehicles. They compared several possible scenarios, i.e., with cabin heating and air conditioning off (operation mode A), cabin heating off and air conditioning on (operation mode B) and cabin heating

on and air conditioning off (operation mode C). In addition, they evaluated various fuel pathways including fossil fuel, nuclear energy, and renewable energy resources. When using fossil fuel pathways, the results indicated that battery-powered vehicle consumed less fossil and total energy than fuel cell vehicle for operation modes A and B. The fossil energy usage of fuel cell vehicle was similar to that for battery-powered vehicle when operated with mode C. Similar trend was observed for nuclear and renewable energy pathways where battery-powered vehicle showed superior well-to-wheel energy efficiency for operation modes A and B. A comparable well-to-wheel energy efficiency between battery and fuel cell vehicle was also found for operation mode C when nuclear and renewable energy pathways were adopted.

Unlike most of the previous studies which focused on the overall system or fuel cell efficiency, Williamson et al. [37] investigated the efficiency of the traction motor in a fuel cell vehicle. The main reason for this investigation was that the efficiency of the traction motor determined the overall system efficiency. Similar to other researches, they utilized efficiency map to evaluate the traction motor efficiency. They compared both fuel cell vehicle and hybrid electric vehicle. The advanced vehicle simulator (ADVISOR) software was used owing to its capability to simulate large-sized car over the urban dynamometer-driving schedule and highway fuel economy test drive cycles. The results indicated that hybrid-electric vehicles were more promising than fuel cell vehicles for commercial automotive propulsion applications: hybrid electric vehicles offered 4–8% higher efficiency than fuel cell vehicles. In addition, with the additional cost and fuel (hydrogen) storage issues related to fuel cell vehicles, hybrid electric vehicles gained upper hand as compared to fuel cell vehicles. Using the same software (ADVISOR), Turkmen et al. [38] investigated the performance of a fuel cell ANL50 which was developed by Argonne National Laboratory and had a 50 kW optimal power. They ran it at two different powers (30 and 50 kW) and two different fuels (hydrogen and gasoline). They reported that higher efficiency could be obtained by running the fuel cell with hydrogen rather than using gasoline. Detailed results from their study are shown in Table 6.2. As can be seen, no change in efficiency is observed when the fuel cell is operated at different power. Nevertheless, it could be concluded that vehicle performance is significantly affected by both fuel cell power and fuel cell type.

Etthir et al. [39] proposed and evaluated the design of an adaptive energy management strategy based on Pontryagin's minimum principle for fuel cell vehicles to obtain the best efficiency and power operating points. To evaluate the performance of the proposed adaptive energy management strategy, it will be compared with the hysteresis energy management strategy. The developed adaptive energy management strategy was found to offer superior performance (up to 8.6% more energy) than the hysteresis energy management strategy due to lower hydrogen consumption. Ahmadi and Bathae [40] introduced two energy management strategies to control the energy in the fuel cell hybrid vehicle (FCHV), i.e., fuzzy logic control and operating mode control. To optimize these strategies, genetic algorithm was adopted by off-line simulation through a combined driving

cycle. These control strategies were compared with other approaches like energy management strategy of advanced vehicle simulator software and non-optimized control strategies. The results revealed the superiority of the developed strategies in term of equivalent energy consumption, energy efficiency, and state-of-charge variation as compared to energy management strategies of advanced vehicle simulator software and non-optimized control strategies. Implementation of energy management strategy using dSPACE 1104 controller board was proposed by Marzougoui et al. [16]. When subjected to new European driving cycle, the evaluated fuel cell vehicle adopting the proposed EMS indicated good performance.

As can be inferred from these studies, energy management system is crucial in managing various power system incorporated to the fuel cell vehicle. Addition of battery and supercapacitor can significantly improve the overall efficiency of the vehicle. Introduction of new technology such as regenerative braking also contributes to performance and efficiency improvement. Incorporation of PV to augment fuel cell and battery in fuel cell vehicle was also been reported to enhance the overall efficiency. Again for this multiple power resources, energy management system will play a major role.

## 2.5 Challenges in Automotive Applications

As discussed in the previous section, fuel cell technologies are continuously developing: their performances are steadily improved and more prototypes are introduced. Several countries in Europe and North America have started wide adoption of fuel cell vehicles and developed the supporting infrastructure. Japan, South Korea, and China are progressing towards the same direction. Nevertheless, there are still several challenges hindering the wide adoption of fuel cell for vehicle propulsion. Some of these challenges are the relatively high cost and low reliability of fuel cells, limited space available in the vehicle to support the complex fuel cell system, hydrogen storage inside vehicle, refueling station infrastructure and hydrogen production.

The cost and reliability of fuel cells are the major issues hindering the commercialization of the fuel cell hybrid electric vehicle [41]. In 2017, Whinston et al. [42] reported an expert assessment on the fuel cell cost, durability and power density median to be \$75/kW, 4000 h, and 2.5 kW/L, respectively. Nevertheless, the ranges are widely varied between \$40 and \$500/kW for the fuel cell cost, 1200–12,000 h for the fuel cell durability and the power density range of 0.5–4 kW/L. While the current median cost of \$75/kW is close to the U.S. Department of energy target for fuel cell price (\$40/kW) on 2020, most respondents expect that the target price will not be achieved until 2050. Meanwhile, they expected that the target on a power density of 3 kW/L would be achieved only by 2035. Heavy use of expensive platinum catalyst has been considered as the main factor hindering the application of fuel cell for transportation [43]. Despite the effort taken by the fuel cell vehicle manufacturer to reduce the requirement of platinum catalyst to a mere 30 g, it is still

significantly higher than the amount of precious metal used in internal combustion engine counterparts which is around is 2–8 g. To be a viable option to replace internal combustion engine vehicles, the overall cost of fuel cell vehicle has to be US\$ 30/kW while the cost of fuel cell stack should be US\$ 15/kW [44].

Another factor that becomes the main obstacle in the commercial application of fuel cell in automotive industry is the fuel cell durability [45]. As revealed previously, the fuel cell durability is ranging between 1200 and 12,000 h while the expected are 5000 h operation under drive cycle conditions or 40,000 h for stationary conditions with less than 10% performance decay [44]. This issue is worsening if the limited space within the vehicle is considered, which lead to restriction of the amount of components and fuel that can be accommodated within the vehicle. Usually, dead-end anode is preferable for fuel cell vehicle application due to its high fuel utilization, which means minimum fuel wastage and minimum fuel storage. However, dead-end anode operation significantly reduces the cell durability if not treated properly. A careful purging mechanism is needed to recover fuel cell performance, reduce cell degradation, and lengthening its life time. However, incorporating purging mechanism which impose requirement for additional component may possess big challenge to the already limited space within the vehicle.

On top of fuel cell cost and durability, hydrogen storage is another issue that needs to be addressed to ensure successful adoption of fuel cell vehicle. The importance of this issue was raised by several studies. One of these studies was conducted by Burkert [46]. Unlike most studies that blame the high cost of catalyst is the main reason behind the slow adoption of fuel cell in commercial market, he highlighted that the cost of platinum in fuel cell stacks was not the main issue hindering the wide-adoption of fuel cell. Instead, he cited that hydrogen storage tank was the major cost component in fuel cell vehicle. Currently, there is no easy or immediate solution for hydrogen storage in the vehicle. Hydrogen is typically stored using three possible storage methods, i.e., compressed gas, cryogenic liquid, and metal hydride. Among these methods, the former is widely adopted for fuel cell vehicle, owing to its technical simplicity, high reliability, acceptable efficiency, and affordability [47]. Despite its advantages, the process of compressing the hydrogen is volumetrically and gravimetrically inefficient [48]. The second method, cryogenic liquid, is often used as concentrated form of hydrogen storage. Due to its liquid form, it can store more hydrogen fuel than the compressed hydrogen gas tank. Although the technology appears to be very promising as it overcomes the problem of first method, in term of gravimetric and volumetric efficiency, it possesses problems dealing with the uptake and release of hydrogen, high hydrogen liquefaction rate that causes large energy loss, hydrogen boil-off and tank cost [49]. Recently, metal hydride storage has also been evaluated for hydrogen storage in vehicle. The issue is that the metal hydrides ages with cycle, reducing the capacity of the hydrogen tank [50].

If all problems related with the fuel cell vehicle are assumed to be well addressed, the next challenges that need to be overcome are related to the hydrogen production and refueling station. Hydrogen production is widely considered as an

energy-intensive process (through electrolysis, thermolysis or steam reforming). While steam reforming is one of the most efficient paths to produce hydrogen, it may undermine the overall advantages of fuel cell vehicle as the green vehicle. As such, some studies have suggested to produce hydrogen using solar, wind, or nuclear energy. In addition, there are several paths have been proposed to produce hydrogen including, plasma arc decomposition, biomass gasification, dark fermentation, photocatalysis, biophotolysis, artificial photosynthesis, photoelectrolysis and other methods [51]. Most of these technologies, however, are still under research and development stage. Therefore, more studies are required to bring these technologies to their commercialization stage.

One of the core advantages of fuel cell vehicle as compared to the battery electric vehicle is the ability to be continuously operated as long as the fuel is supplied to the fuel cell just like internal combustion engine. Therefore, similar to internal combustion engine, fuel cell vehicle need to be refueled when it is running out of hydrogen fuel. Unlike refueling internal combustion engine vehicle where the fuel is liquid in the environment condition, its gaseous nature at the environment condition poses challenge for the fuel cell vehicle refueling process. As compared to the traditional fossil fuel refueling station, the availability of hydrogen refueling is significantly smaller, posing difficulties for the fuel cell vehicle owner to refuel their vehicle. At the moment hydrogen refueling stations only available in certain parts of Europe, North America, Japan, and South Korea.

## 2.6 Future Directions

All this while, most of the studies on fuel cell vehicle have been focusing on improving the performance, efficiency, and durability of the fuel cell stack when implemented as the power source in the vehicle. This trend is expected to continue until wide commercialization of fuel cell vehicle occurs. In fact, continuous research and development on the fuel cell performance, efficiency and durability will still be needed to further improve it post-commercialization of the fuel cell vehicle.

On another note, one factor hindering with the adoption of fuel cell in vehicle power train is heavy use of expensive platinum catalyst. Therefore, more studies will be conducted to develop fuel cell with require small amount or no platinum coating. Some of the initial studies are the development of fuel cell with n Ultralow-Pt-Content Core-Shell Catalyst [52] and a low-cost, high-performance zinc-hydrogen peroxide fuel cell [53].

On vehicle system level, development of energy management system will remain to be the main focus in fuel cell vehicle research and development. An effective and efficient energy management system will ensure the optimum operation of the vehicle and maintaining the maximum overall efficiency. To further increase the overall system efficiency of fuel cell vehicle, a hybrid system combining several power sources will be proposed and evaluated. Some studies on this initiative have been conducted and reported. Ezzat et al. [54], for example,



proposed a new integrated fuel cell-photovoltaic-battery system and compared its performance with the base fuel cell-battery system. Their results indicated that the overall energy and exergy efficiencies slightly increase from 39.5% to 39.9% and from 56.3% to 56.6%, respectively at a current density of 1150 mA/cm<sup>2</sup> with the introduction of PV arrays. In addition, a hydrogen fuel saving of 561 g could be achieved for 3 h continuous operation at peak power of 98.3 kW. Lv et al. [55] evaluated the efficiency improvement when regenerative brake is adopted to the fuel cell vehicle. The tested vehicle was subjected to the new European driving cycle. They proposed two parameters in their evaluation, i.e., the contribution ratio to energy efficiency improvement and the contribution ratio to driving range extension. From the testing using the driving cycle, the contribution ratio to energy efficiency improvement and the contribution ratio to driving range extension of up to 11.2% and 12.6%, respectively were recorded by adopting regenerative braking. Fathabadi [56] proposed a novel fuel cell/supercapacitor hybrid power source for fuel cell hybrid electric vehicle. The system consisted of a 90 kW proton exchange membrane fuel cell stack used as the main power source combined with a 600 F supercapacitor bank auxiliary energy storage device. It was claimed a whopping efficiency of 96.2% can be achieved as compared to the state-of-the-art power sources of fuel cell electric vehicles. In addition, excellent acceleration and high maximum speed can be achieved by the proposed system. More studies on the incorporation of other power sources to fuel cell vehicle are expected in the future.

On hydrogen production, research and development will be directed towards the production of hydrogen using renewable energy resources. More studies on life cycle analysis are expected as they provide a guideline on the most sustainable pathways in producing and delivering fuel for fuel cell vehicle. Development of hydrogen storage for both fuel cell vehicle and hydrogen refueling station will be focused on the material storage and storage processes.

## 2.7 Summary

For decades, hydrogen fuel cell or polymer exchange membrane fuel cells have been predicted to replace internal combustion engine in the future vehicles. Their low operating temperature, high power density, quick start-up and response to load changes and high efficiency make them a promising candidate for propulsion systems of environmentally friendly vehicles. Despite its great potential, polymer exchange membrane fuel cell has not been widely adopted and it has not reached its mature commercialization stage yet. The fuel cell performance, fuel utilization, component degradation, and cost are some main issues that need to be addressed. In addition, development of energy management system is crucial to manage interaction between various power sources (fuel cell, batter, supercapacitor) available in the fuel cell vehicle. Lastly, production of hydrogen from renewable resources will remain the main focus for future development together with efficient hydrogen storage and distribution system.

## References

1. K. Kojima, K. Fukazawa, Current status and future outlook of fuel cell vehicle development in Toyota. Meet. Abstr. **MA2015-02**(37), 1310 (2015)
2. T. Yoshida, K. Kojima, Toyota MIRAI fuel cell vehicle and progress toward a future hydrogen society. *Electrochem. Soc. Interface* **24**(2), 45–49 (2015)
3. T. Suzuki, Fuel cell stack technology of Toyota. Meet. Abstr. **MA2016-02**(38), 2560 (2016)
4. S. Nistor, S. Dave, Z. Fan, M. Sooriyabandara, Technical and economic analysis of hydrogen refuelling. *Appl. Energy* **167**, 211–220 (2016)
5. J.C. Kurnia, A.P. Sasmito, T. Shamim, Performance evaluation of a PEM fuel cell stack with variable inlet flows under simulated driving cycle conditions. *Appl. Energy* **206**, 751–764 (2017)
6. S. Philips, Japan is betting big on the future of hydrogen cars. *NPR.org*. Available: <https://www.npr.org/2019/03/18/700877189/japan-is-betting-big-on-the-future-of-hydrogen-cars>. Accessed 21 Mar 2019
7. N. Sulaiman, M.A. Hannan, A. Mohamed, E.H. Majlan, W.R. Wan Daud, A review on energy management system for fuel cell hybrid electric vehicle: Issues and challenges. *Renew. Sustain. Energy Rev.* **52**, 802–814 (2015)
8. C. Santoro, C. Arbizzani, B. Erable, I. Ieropoulos, Microbial fuel cells: From fundamentals to applications. A review. *J. Power Sources* **356**, 225–244 (2017)
9. K. Sopian, W.R. Wan Daud, “Challenges and future developments in proton exchange membrane fuel cells. *Renew. Energy* **31**(5), 719–727 (2006)
10. A.P. Sasmito, *Modeling of Transport Phenomena in Polymer Electrolyte Fuel Cell Stacks: Thermal, Water, and Gas Management*. Thesis, National University of Singapore, 2010
11. Y. Wang, K.S. Chen, J. Mishler, S.C. Cho, X.C. Adroher, A review of polymer electrolyte membrane fuel cells: technology, applications, and needs on fundamental research. *Appl. Energy* **88**(4), 981–1007 (2011)
12. P. Koski, L.C. Pérez, J. Ihonon, Comparing anode gas recirculation with hydrogen purge and bleed in a novel PEMFC laboratory test cell configuration. *Fuel Cells* **15**(3), 494–504 (2015)
13. I.-S. Han, J. Jeong, H.K. Shin, PEM fuel-cell stack design for improved fuel utilization. *Int. J. Hydrogen Energy* **38**(27), 11996–12006 (2013)
14. J.-J. Hwang, Effect of hydrogen delivery schemes on fuel cell efficiency. *J. Power Sources* **239**, 54–63 (2013)
15. H.-Y. Lee, H.-C. Su, Y.-S. Chen, A gas management strategy for anode recirculation in a proton exchange membrane fuel cell. *Int. J. Hydrogen Energy* **43**(7), 3803–3808 (2018)
16. H. Marzougui, M. Amari, A. Kadri, F. Bacha, J. Ghouili, Energy management of fuel cell/battery/ultracapacitor in electrical hybrid vehicle. *Int. J. Hydrogen Energy* **42**(13), 8857–8869 (2017)
17. F. Barbir, *PEM Fuel Cells: Theory and Practice* (Academic Press, Cambridge, 2012)
18. T.V. Nguyen, A gas distributor design for proton-exchange-membrane fuel cells. *J. Electrochem. Soc.* **143**(5), L103–L105 (1996)
19. D.H. Jeon, S. Greenway, S. Shimpalee, J.W. Van Zee, The effect of serpentine flow-field designs on PEM fuel cell performance. *Int. J. Hydrogen Energy* **33**(3), 1052–1066 (2008)
20. S.M. Rahgoshay, A.A. Ranjbar, A. Ramiar, E. Alizadeh, Thermal investigation of a PEM fuel cell with cooling flow field. *Energy* **134**, 61–73 (2017)
21. A.P. Sasmito, J.C. Kurnia, A.S. Mujumdar, Numerical evaluation of various gas and coolant channel designs for high performance liquid-cooled proton exchange membrane fuel cell stacks. *Energy* **44**(1), 278–291 (2012)
22. Y. Kerkoub, A. Benzaoui, F. Haddad, Y.K. Ziari, Channel to rib width ratio influence with various flow field designs on performance of PEM fuel cell. *Energy Convers. Manag.* **174**, 260–275 (2018)

23. E. Afshari, M. Ziaei-Rad, Z. Shariati, A study on using metal foam as coolant fluid distributor in the polymer electrolyte membrane fuel cell. *Int. J. Hydrogen Energy* **41**(3), 1902–1912 (2016)
24. E. Alizadeh, S.M. Rahgoshay, M. Rahimi-Esbo, M. Khorshidian, S.H.M. Saadat, A novel cooling flow field design for polymer electrolyte membrane fuel cell stack. *Int. J. Hydrogen Energy* **41**(20), 8525–8532 (2016)
25. F.N. Büchi et al., On the efficiency of an advanced automotive fuel cell system. *Fuel Cells* **7**(2), 159–164 (2007)
26. J. Han, M. Kokkolaras, P.Y. Papalambros, Optimal design of hybrid fuel cell vehicles. *J. Fuel Cell Sci. Technol.* **5**(4), 041014–041014 (2008)
27. J. Bang, H.-S. Kim, D.-H. Lee, K. Min, Study on operating characteristics of fuel cell powered electric vehicle with different air feeding systems. *J. Mech. Sci. Technol.* **22**(8), 1602–1611 (2008)
28. A. Gomez, A.P. Sasmito, T. Shamim, Investigation of the purging effect on a dead-end anode PEM fuel cell-powered vehicle during segments of a European driving cycle. *Energy Convers. Manage.* **106**, 951–957 (2015)
29. H. Al-Zeyoudi, A.P. Sasmito, T. Shamim, Performance evaluation of an open-cathode PEM fuel cell stack under ambient conditions: case study of United Arab Emirates. *Energy Convers. Manag.* **105**, 798–809 (2015)
30. A. Fly, R.H. Thring, A comparison of evaporative and liquid cooling methods for fuel cell vehicles. *Int. J. Hydrogen Energy* **41**(32), 14217–14229 (2016)
31. D. Feroldi, M. Serra, J. Riera, Energy Management Strategies based on efficiency map for Fuel Cell Hybrid Vehicles. *J. Power Sources* **190**(2), 387–401 (2009)
32. D. Feroldi, M. Carignano, Sizing for fuel cell/supercapacitor hybrid vehicles based on stochastic driving cycles. *Appl. Energy* **183**, 645–658 (2016)
33. C. Liu, L. Liu, Optimal power source sizing of fuel cell hybrid vehicles based on Pontryagin's minimum principle. *Int. J. Hydrogen Energy* **40**(26), 8454–8464 (2015)
34. L. Xu, C.D. Mueller, J. Li, M. Ouyang, Z. Hu, Multi-objective component sizing based on optimal energy management strategy of fuel cell electric vehicles. *Appl. Energy* **157**, 664–674 (2015)
35. M.G. Carignano, R. Costa-Castelló, V. Roda, N.M. Nigro, S. Junco, D. Feroldi, Energy management strategy for fuel cell-supercapacitor hybrid vehicles based on prediction of energy demand. *J. Power Sources* **360**, 419–433 (2017)
36. M. Li, X. Zhang, G. Li, A comparative assessment of battery and fuel cell electric vehicles using a well-to-wheel analysis. *Energy* **94**, 693–704 (2016)
37. S. Williamson, M. Lukic, A. Emadi, Comprehensive drive train efficiency analysis of hybrid electric and fuel cell vehicles based on motor-controller efficiency modeling. *IEEE Trans. Power Electron.* **21**(3), 730–740 (2006)
38. A.C. Turkmen, S. Solmaz, C. Celik, Analysis of fuel cell vehicles with advisor software. *Renew. Sustain. Energy Rev.* **70**, 1066–1071 (2017)
39. K. Ettahir, M. Higueta Cano, L. Boulon, K. Agbossou, Design of an adaptive EMS for fuel cell vehicles. *Int. J. Hydrog. Energy* **42**(2), 1481–1489 (2017)
40. S. Ahmadi, S.M.T. Bathaee, Multi-objective genetic optimization of the fuel cell hybrid vehicle supervisory system: fuzzy logic and operating mode control strategies. *Int. J. Hydrogen Energy* **40**(36), 12512–12521 (2015)
41. T. Fletcher, R. Thring, M. Watkinson, An energy management strategy to concurrently optimise fuel consumption & PEM fuel cell lifetime in a hybrid vehicle. *Int. J. Hydrogen Energy* **41**(46), 21503–21515 (2016)
42. M.M. Whiston, I.L. Azevedo, S. Litster, K.S. Whitefoot, C. Samaras, J.F. Whitacre, Expert assessments of the cost and expected future performance of proton exchange membrane fuel cells for vehicles. *PNAS* **116**(11), 4899–4904 (2019)
43. V. Yarlagadda et al., Boosting fuel cell performance with accessible carbon mesopores. *ACS Energy Lett.* **3**(3), 618–621 (2018)

44. A. de Frank Bruijn, G.J.M. Janssen, PEM fuel cell materials: Costs, performance, and durability, in *Fuel Cells and Hydrogen Production: A Volume in the Encyclopedia of Sustainability Science and Technology*, 2nd Edition, ed. T.E. Lipman, A.Z. Weber (Springer, New York, 2019), pp. 195–234
45. J. Li et al., Fuel cell system degradation analysis of a Chinese plug-in hybrid fuel cell city bus. *Int. J. Hydrogen Energy* **41**(34), 15295–15310 (2016)
46. A. Burkert, Fuel cells—From euphoria to disillusionment. *ATZ Worldw* **121**(4), 8–13 (2019)
47. M. Li et al., Review on the research of hydrogen storage system fast refueling in fuel cell vehicle. *Int. J. Hydrogen Energy* (2019)
48. S. Niaz, T. Manzoor, A.H. Pandith, Hydrogen storage: materials, methods and perspectives. *Renew. Sustain. Energy Rev.* **50**, 457–469 (2015)
49. M. Hirscher, *Handbook of Hydrogen Storage: New Materials for Future Energy Storage* (Wiley, Hoboken, 2010)
50. D. Zhu, D. Chabane, Y. Ait-Amirat, A. N'Diaye, A. Djerdir, Estimation of the state of charge of a hydride hydrogen tank for vehicle applications, in *2017 IEEE Vehicle Power and Propulsion Conference (VPPC)* (2017), pp. 1–6
51. I. Dincer, C. Acar, Review and evaluation of hydrogen production methods for better sustainability. *Int. J. Hydrogen Energy* **40**(34), 11094–11111 (2015)
52. A. Kongkanand, N.P. Subramanian, Y. Yu, Z. Liu, H. Igarashi, D.A. Muller, Achieving high-power PEM fuel cell performance with an ultralow-Pt-content core-shell catalyst. *ACS Catal.* **6**(3), 1578–1583 (2016)
53. L. An, T.S. Zhao, X.L. Zhou, X.H. Yan, C.Y. Jung, A low-cost, high-performance zinc–hydrogen peroxide fuel cell. *J. Power Sources* **275**, 831–834 (2015)
54. M.F. Ezzat, I. Dincer, Development, analysis and assessment of a fuel cell and solar photovoltaic system powered vehicle. *Energy Convers. Manag.* **129**, 284–292 (2016)
55. C. Lv, J. Zhang, Y. Li, Y. Yuan, Mechanism analysis and evaluation methodology of regenerative braking contribution to energy efficiency improvement of electrified vehicles. *Energy Convers. Manag.* **92**, 469–482 (2015)
56. H. Fathabadi, Fuel cell hybrid electric vehicle (FCHEV): Novel fuel cell/SC hybrid power generation system. *Energy Convers. Manag.* **156**, 192–201 (2018)

# Chapter 3

## Prospect of Composite Tubes Based on Bi-materials for Weight Reduction of Vehicles



**Tahir Abbas, Hamdan Haji Ya, M. Zaki Abdullah, Suhaimi Hassan and Muhammad Yasar Javaid**

This chapter provides a study related to energy absorption and failure modes of thin-walled tubes under axial compression. The study was to focus on partial wrapping of light-weight thin-walled aluminium tube with glass/epoxy, which is very significant to enhance the safety of automobiles. Partially wrapped aluminium tube samples have been prepared according to the L9 Taguchi design orthogonal array, by applying various fiber orientations, composite layers and partially wrapped area via filament winding process. The study revealed that the optimum combination of fiber orientation, composite layers, and the partially wrapped area was  $\pm 55^\circ$ , 6, and 30% respectively. This combination was achieved via the analysis of variance (ANOVA), and the main plot effect analysis. Moreover, this combination also has 81.92, and 62.08% higher values of specific energy absorption (SEA), and 47.67 and 1.54% more values of crush force efficiency (CFE) as compared to the simple aluminium tube and its predecessor the steel tube, respectively. The results show the two-lobe diamond failure mode of this combination ( $\pm 55^\circ$ , 6, and 30%). The findings demonstrate the ability of the approach as a reliable and light-weight solution for energy absorbers with a high value of SEA and CFE.

---

T. Abbas · M. Y. Javaid

Department of Mechanical Engineering, Government College University Faisalabad, Kotwali Rd, Gurunanakpura, Faisalabad, Punjab 38000, Pakistan

H. Haji Ya (✉) · M. Zaki Abdullah · S. Hassan

Department of Mechanical Engineering, Universiti Teknologi PETRONAS, 32610 Seri Iskandar, Perak, Malaysia  
e-mail: [Hamdan.ya@utp.edu.my](mailto:Hamdan.ya@utp.edu.my)

© Springer Nature Singapore Pte Ltd. 2020

S. A. Sulaiman (ed.), *Energy Efficiency in Mobility Systems*,

[https://doi.org/10.1007/978-981-15-0102-9\\_3](https://doi.org/10.1007/978-981-15-0102-9_3)

### 3.1 Introduction

Thin-walled tubes are generally utilized in automobiles and the aerospace industry as energy absorbers. Thin-walled tubes absorb more energy when they are subjected to axial compression [1]. They have been applied in numerous crashworthy structures, such as the front chassis of cars and aircraft units [2, 3]. Any structure that absorbs impact energy and dissipates it in some other forms like plastic or friction is defined as a crashworthy structure [4]. Under axial crushing thin-walled metallic tubes collapse in plastic and stable failure mode, and this property makes them attractive in crashworthy applications [5, 6].

Onwards, weight reduction is also important and it is possible to achieve 25% reduction in overall weight of the vehicle by replacing a steel structure with aluminium [7]. Although a detailed study on axial compression of thin-walled metal tubes is available, they are less efficient in energy absorption as compared to thin-walled composite tubes tested under axial loading as mentioned in [8]. Moreover, the metallic parts used in designing car body parts are being replaced by composite materials owing to their high value of stiffness to weight ratio. However, their composite brittle nature makes them less suitable for applications that need energy absorption [9]. That is why research on hybrid tubes is going on now. Aluminium is also light-weight, but its cost is higher as compared to steel [10]. Additionally, as mentioned in [11] glass fibers have low cost as compared to other materials. Hybrid tubes are developed by a combination of metal and composite materials, hence providing more energy absorption and strength as compared to conventional tubes.

### 3.2 Method of Study

The experimental work was divided into different phases which consisted of the selection of the material, partial wrapping of the aluminium tube samples, using the filament winding technique. Aluminium tube samples were partially wrapped according to the L9 array of the Taguchi method. These partially wrapped aluminium tube samples were tested using a universal testing machine (UTM). To see the effect of the fiber angle, composite layers, and partially wrapped area on the specific energy absorption (SEA) and crush force efficiency (CFE), the analysis of variance (ANOVA) was carried out via the Taguchi method on experimental results obtained from the partially wrapped aluminium tube samples under quasi-static testing. The main plot effect analysis was also carried out to find out the best combination of the fiber angle, composite layers, and partially wrapped area for higher SEA and CFE values. The overall research methodology is shown in Fig. 3.1.

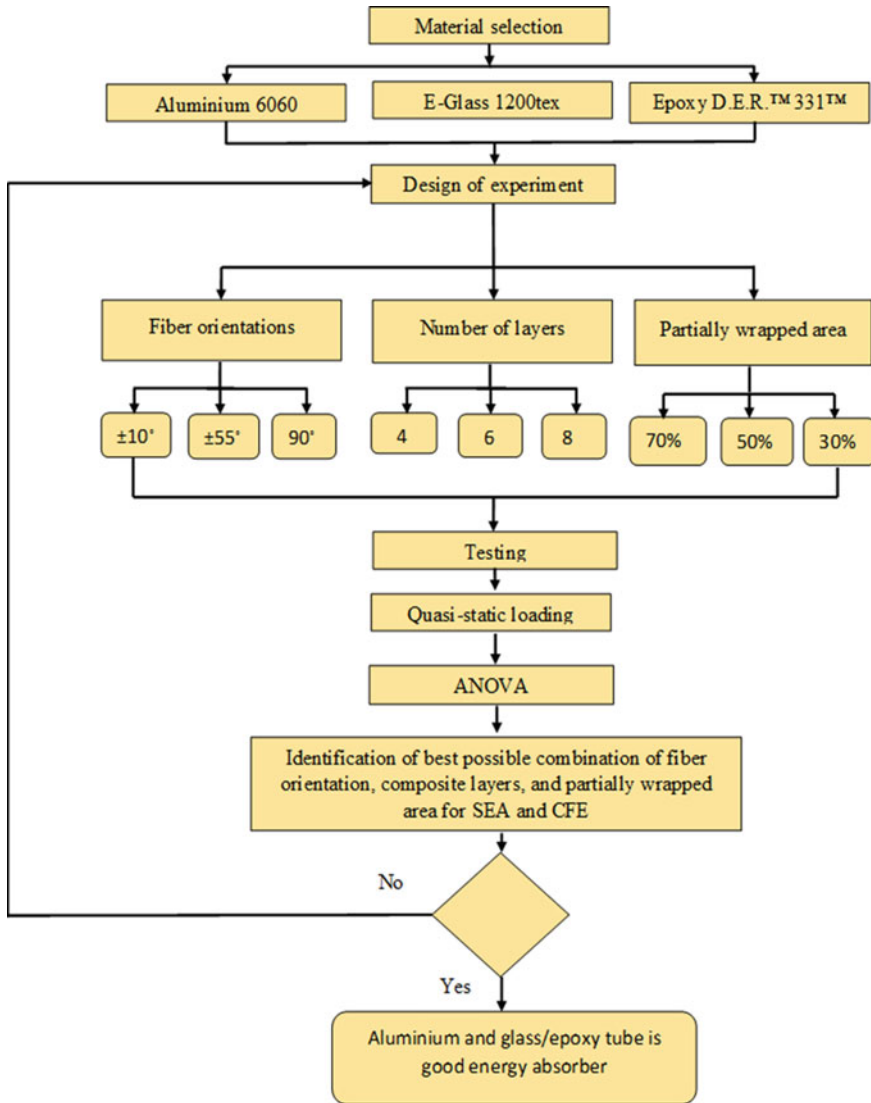


Fig. 3.1 Overall research methodology

### 3.3 Materials

The reason for and specifications of the materials used in this research work are explained thoroughly in the following sections.

### **3.3.1 Aluminium**

The commercially available grade ‘AA6063’ aluminium alloy was used in this work. This aluminium alloy was purchased from (Emirates Global Aluminium) EGA supplier from Dubai. Aluminium was the most suitable choice because of its medium density as compared with other metals [10].

### **3.3.2 Reinforcement**

The commercially available grade of the E-glass reinforcement with the name of ‘Direct Roving External Pullout E-glass 1200tex’ was used in this study. This grade of E-glass was purchased from China National Building Material (Group) Corp. The reason behind the selection of the ‘E’ glass fiber is its low cost as discussed in [11, 12]. Furthermore, it has good behaviour in energy absorption as discussed in [13].

Additionally, as demonstrated in [13], at a small winding angle the carbon-epoxy tube showed a maximum energy absorption, but as the winding angle increased its energy absorption decreased. On the other hand, the E-glass-epoxy tubes contradicted this behaviour, their energy absorption increased up to the 60° winding angle and remained constant after that. So, it is also necessary to explore the effect of winding angle on the partially wrapped tubes.

### **3.3.3 Matrix**

The commercially available grade of liquid epoxy resin D.E.R<sup>TM</sup> 331 was used in this research work. This epoxy grade was purchased from DOW supplier from North America. This grade of epoxy resin is designed for automotive coatings and filament winding. The hardener EPAMINE PC 39 was used for curing of the epoxy resin. EPAMINE PC 39 is an aliphatic amine with a long pot life.

## **3.4 Filament Winding Machine**

For the partial wrapping of the aluminium tubes with the glass/epoxy filament winding machine was used at SIRIM as shown in Fig. 3.2.



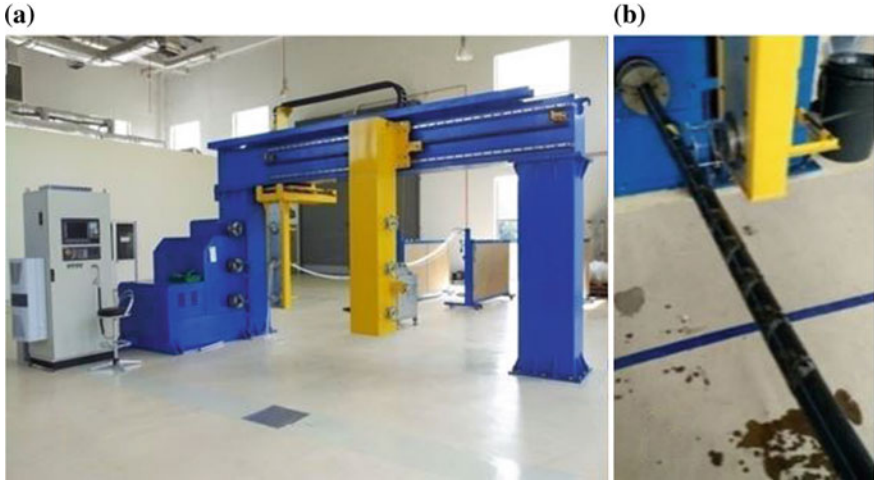


Fig. 3.2 a Filament winding machine. b Partial wrapping of specimen

### 3.5 Universal Testing Machine (UTM)

Quasi-static testing of the partially wrapped hybrid aluminium-glass/epoxy samples was conducted using the, GT-7001-LS20, universal testing machine (UTM) at Universiti Teknologi Petronas as shown in Fig. 3.3.

Fig. 3.3 Universal testing machine



### 3.6 Partial Wrapping of the Aluminium Tube Specimens

Aluminium alloy ‘AA6063’ tubes of a one-meter length were used for partial wrapping with glass/epoxy. These aluminium tubes were fixed to the filament winding machine. After that direct roving glass fibers were mixed with epoxy resin D.E.R<sup>TM</sup> 331 to partially wrap the aluminium tubes with different fiber orientations ( $\pm 10^\circ$ ,  $\pm 55^\circ$ , and  $90^\circ$ ), composite layers (4, 6, and 8), and partially wrapped areas (70, 50, and 30%). The EPAMINE PC 39 hardener was used as a curing agent for the epoxy resin. The weight ratio of the resin to the catalyzer was chosen (100:33) as per manufacturer’s recommendations. The surface of aluminium tubes was cleaned with acetone to remove any contamination. After the filament winding, the partially wrapped hybrid aluminium-glass/epoxy specimens were cured for three hours at  $60^\circ\text{C}$  according to the manufacturer’s recommendation. After the curing process, for the appropriate collapse mode, the chosen length of the partially wrapped hybrid aluminium tube was 200 mm to avoid Euler buckling [14].

Figures 3.4, 3.5, 3.6 and 3.7 show the dimensions and designations of prepared samples, S1 to S9, respectively. Additionally, the details of the partially wrapped samples are listed in Table 3.1. According to the L9 orthogonal array, there are nine combinations of fiber orientations, composite layers and partially wrapped areas, so a total of 45 samples were tested using the universal testing machine.

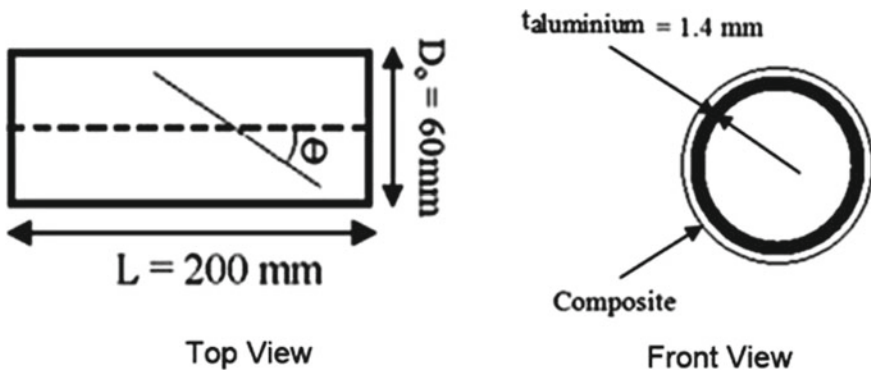
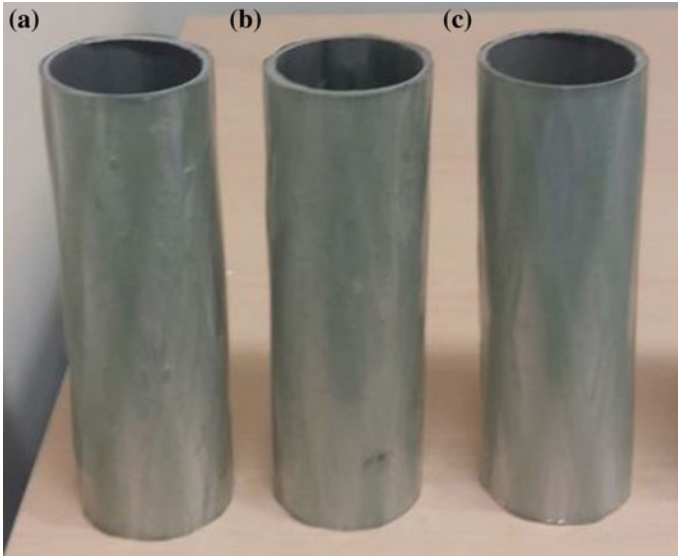
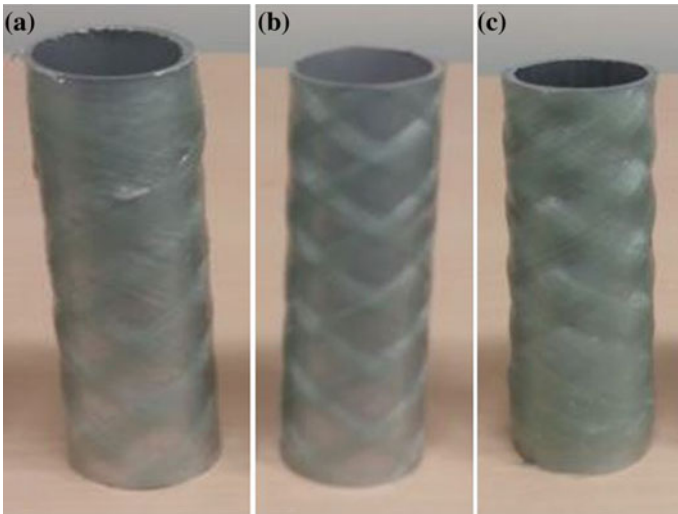


Fig. 3.4 Dimensions of the aluminium tubes



**Fig. 3.5** Partially wrapped aluminium tubes. **a** Sample 1 (S1), **b** Sample 2 (S2), and **c** Sample 3 (S3)



**Fig. 3.6** Partially wrapped aluminium tubes. **a** Sample 4 (S4), **b** Sample 5 (S5), and **c** Sample 6 (S6)

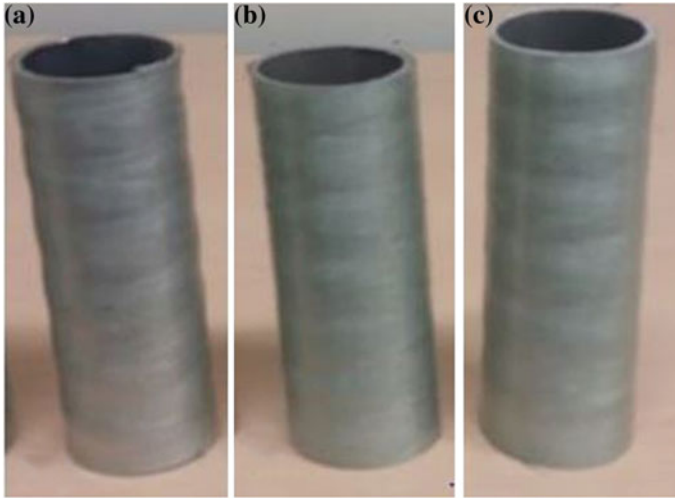


**Fig. 3.7** Partially wrapped aluminium tubes. **a** Sample 7 (S7), **b** Sample 8 (S8), and **c** Sample 9 (S9)

**Table 3.1** Details of the partially wrapped aluminium tube samples

Partially wrapped aluminium tubes	Designations	Fiber orientation	Composite layers	Partially wrapped area (%)	Mass (kg)
Unwrap	Unwrap				0.19
Sample 1	S1	$\pm 10^\circ$	4	70	0.26
Sample 2	S2	$\pm 10^\circ$	6	50	0.25
Sample 3	S3	$\pm 10^\circ$	8	30	0.27
Sample 4	S4	$\pm 55^\circ$	4	50	0.20
Sample 5	S5	$\pm 55^\circ$	6	30	0.20
Sample 6	S6	$\pm 55^\circ$	8	70	0.32
Sample 7	S7	$90^\circ$	4	30	0.23
Sample 8	S8	$90^\circ$	6	70	0.22
Sample 9	S9	$90^\circ$	8	50	0.25

### 3.7 Specific Energy Absorption and Crush Force Efficiency

The specific energy absorption and crush force efficiency were calculated by [15–17]:

$$E_{abs} = \int_0^{\delta_{max}} P \delta d \delta \quad (3.1)$$

Here,  $P$  denotes the crushing load, and  $\delta$  and  $\delta_{\max}$  are the final and initial distances of the crushing structure. The SI unit for the total energy absorbed ( $E_a$ ) is kJ.

$$P_m = \frac{1}{\delta} \int_0^{\delta} P \delta d \delta \quad (3.2)$$

$$\text{SEA} = \frac{E_{\text{abs}}}{m} \quad (3.3)$$

$E_{\text{abs}}$  and  $m$  represent total energy absorbed and original mass of specimen, respectively

$$\text{CFE} = \frac{P_{\text{mean}}}{P_{\text{max}}} \quad (3.4)$$

$P_{\text{mean}}$  and  $P_{\text{max}}$  are average and maximum loads respectively.

### 3.8 Selection of Parameters

It was noticed that the fiber orientation, composite layers, and partially wrapped area can affect the specific energy absorption and crush force efficiency of a partially wrapped hybrid tube. Furthermore, the reason behind selection of the ( $\pm 10^\circ$ ) fiber orientation was that in the axial direction, fibers have more ability to carry out axial loads, and in the ( $\pm 55^\circ$ ) fiber orientation, the hoop strength of the fibers is more as compared to axial the strength [18]. In addition to this, fibers oriented at  $90^\circ$  have the maximum hoop strength [19]. Moreover, the reason behind the selection of the composite layers (4, 6, and 8) is that, as the number of composite layers increases, the energy absorption also increases; but, it is not a linear relationship because a high number of composite layers can also become the reason for a catastrophic failure, thus reducing the energy absorption [5, 20].

As discussed earlier, for the light-weight design of hybrid tubes, partially wrapped areas of (70, 50, and 30%) were chosen to see the effect of this parameter on the SEA and CFE values in combination with the fiber orientation and composite layers. So, in this experimental work, a total of three parameters were studied. Three levels of each parameter were selected because any non-linear behaviour amongst the parameters can only be studied if parameters are set on more than two levels [21]. So, these parameters were set on three levels. All the ranges of the parameters were determined according to their strength and their effect on the specific energy absorption and crush force efficiency. Table 3.2 shows the levels of selected parameters.

According to the full factorial design, a total of 33 experiments were required. Furthermore, the filament winding process and the quasi-static testing of partially

**Table 3.2** Levels of the selected parameters

Column	Parameter	Level 1	Level 2	Level 3
A	Fiber orientation	$\pm 10^\circ$	$\pm 55^\circ$	$90^\circ$
B	Composite layers	4	6	8
C	Partially wrapped area	70%	50%	30%

wrapped tubes also involved cost and time for the 33 experiments. So, to carry out this study within the time and budget limits, the Taguchi Orthogonal array (OA) has been used. For the three factors at the three levels, standard Taguchi orthogonal array has been used to put up all the factors with their levels. Further discussion on the selection of the OA is provided in the following section.

### 3.9 Selection of the Orthogonal Array (OA)

The selection of the orthogonal array was based on total DOF of fiber orientation, composite layers, and partially wrapped area. These three parameters had three levels so each of them had two DOF. Hence, the total DOF needed is six. According to Taguchi's method, the total degree of freedom needed to carry out experiments must be equal to or less than the total degree of freedom of the selected orthogonal array. So, an orthogonal array (L9) with 8 DOF in which all parameters with their levels can be accommodated was selected.

As discussed before, it is time-consuming to conduct experiments with the full factorial design. Therefore, with the help of the orthogonal array (OA), the total number of experiments was reduced to nine. In the L9 orthogonal array, the fiber orientation was assigned as A, the composite layer was assigned as B, and partially wrapped area was assigned as C as shown in Table 3.3. For a detailed understanding of the Taguchi method, it can be found in design of experiments using the Taguchi approach [22].

**Table 3.3** Design of the experiment using the L9 Orthogonal Array

Trial No.	A	B	C
1	1	1	1
2	1	2	2
3	1	3	3
4	2	1	2
5	2	2	3
6	2	3	1
7	3	1	3
8	3	2	1
9	3	3	2

### 3.10 Results and Discussions

The experimental results for the partially wrapped aluminium tubes were prepared according to Sect. 3.6, and the experiments were conducted on these specimens subjected to quasi-static loading. The collapse mode and the energy absorption capability during the quasi-static loading were explored. The ANOVA and the main effects' analysis were used to determine the best combination of the fiber orientation, composite layers, and partially wrapped area.

### 3.11 Quasi-static Testing of Aluminium Tubes

Quasi-static tests of partially wrapped aluminium tube samples, and unwrapped aluminium tube samples were conducted using the universal testing machine. The speed of the machine was fixed at 5 mm/min. The collapse modes and energy absorption characteristics of the partially wrapped and plain aluminium tube samples were analyzed.

### 3.12 Collapse Modes and Load-Displacement Curves

There a was total of nine configurations of partially wrapped aluminium tube samples as discussed in the Taguchi L9 array. These configurations were made with combination of different fiber orientations, composite layers, and partially wrapped areas. These nine configurations were designated as Sample 1 (S1), Sample 2 (S2), Sample 3 (S3), Sample 4 (S4), Sample 5 (S5), Sample 6 (S6), Sample 7 (S7), Sample 8 (S8), and Sample 9 (S9).

Load displacement curves for all the samples are presented in Figs. 3.8, 3.9, and 3.10, respectively. Moreover, specific energy absorption and crush force efficiency are calculated and listed in Table 3.4.

In Table 3.5, Figs. 3.11 and 3.12 the crashworthiness parameters of specimens are illustrated. It is observed that the S5 partially wrapped aluminium tube had the best combination of fiber orientation, composite layers, and partially wrapped area. This is because it had SEA and CFE values of 25.56 kJ/kg and 60.77%, respectively, which were higher as compared with the other combinations of fiber orientation, composite layers, and partially wrapped area.

Table 3.6 shows the comparison of the partially wrapped aluminium tube with the partially wrapped steel tube by [23]. It is concluded that, the partially wrapped aluminium tube (S5) with the fiber orientation ( $\pm 55^\circ$ ), composite layers (6), and partially wrapped area (30%) had 81.92 and 62.08% higher SEA values as

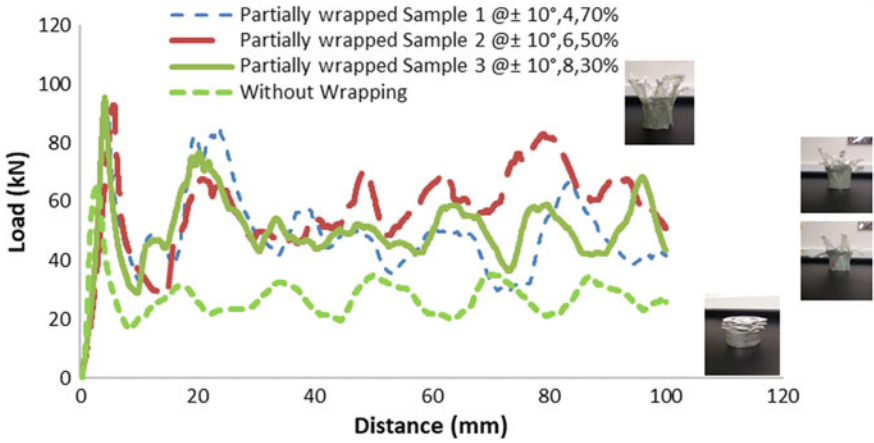


Fig. 3.8 Load-displacement curves of the partially wrapped aluminium tube Samples 1, 2 and 3 and of an unwrapped aluminium tube

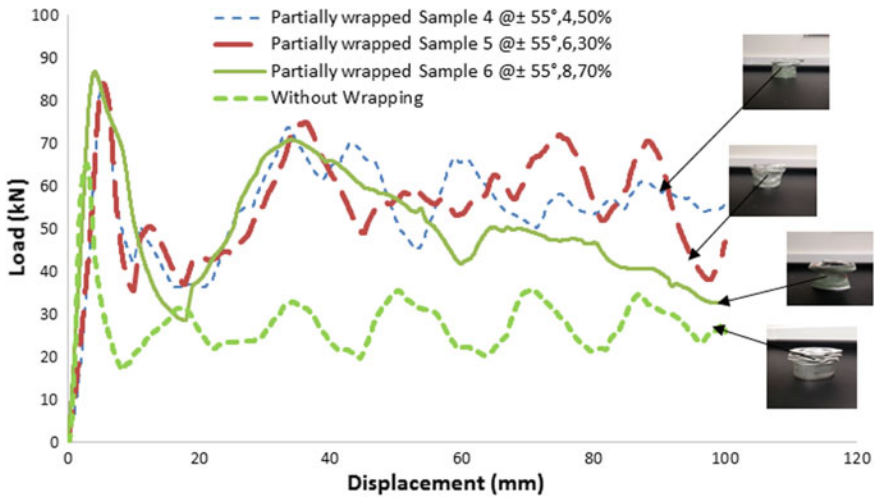
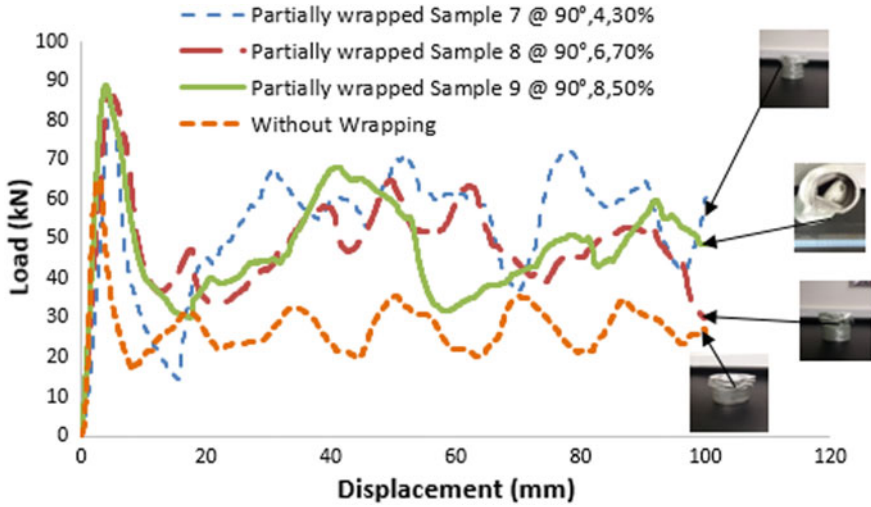


Fig. 3.9 Load-displacement curves of the partially wrapped aluminium tube Samples 4, 5, and 6 and of an unwrapped aluminium tube







compared with the unwrapped aluminium and partially wrapped steel tubes. Similarly, it had 47.67 and 1.54% higher CFE values as compared with the unwrapped aluminium and partially wrapped steel tubes.








**Fig. 3.10** Load-displacement curves of the partially wrapped aluminium tube samples 7, 8 and 9 and of an unwrapped aluminium tube

**Table 3.4** Failure modes of the partially wrapped aluminium tube samples

Sr. no	Samples	Failure mode	No. of folds	Cut view
1	S1	3-lobe diamond	6	
2	S2	3-lobe diamond	7	
3	S3	Mixed mode	5	
4	S4	3-lobe diamond	9	
5	S5	2-lobe diamond	11	
6	S6	Euler buckling	5	

(continued)

**Table 3.4** (continued)

Sr. no	Samples	Failure mode	No. of folds	Cut view
7	S7	3-lobe diamond	7	
8	S8	diamond	8	
9	S9	Euler buckling	4	

### 3.13 Results of the L<sub>9</sub> Orthogonal Array (OA) Experiments

In this research, the Taguchi method based systematic approach to the design of the experiments was used to determine the best combination of fiber orientation, composite layers, and partially wrapped area that had more influence on the specific energy absorption (SEA), and crush force efficiency (CFE) of the partially wrapped aluminium tubes. Considering the applications of the partially wrapped tubes in automobiles, a final product with high specific energy absorption and crush force efficiency is desirable. All test runs of the partially wrapped aluminium tubes have been conducted using the universal testing machine, and results have been presented in Table 3.7.

### 3.14 S/N Ratio and Data Normalization

For better performance of the energy absorber, higher values of specific energy absorption and crush force efficiency are desired, so the-higher-the-better S/N ratio formula has been applied. These calculated values were added up to a combined value (C) after normalizing, Table 3.8. The purpose of addition of these values was to study the effect of fiber orientation, composite layers, and partially wrapped area on the SEA and CFE, simultaneously.

**Table 3.5** Crashworthiness parameters

Parameters of crashworthiness	Al tube	S1	S2	S3	S4	S5	S6	S7	S8	S9
TEA (kJ)	2.67	4.71	4.76	4.67	4.75	5.12	4.85	4.64	4.62	4.56
SEA (kJ/kg)	14.05	18.11	19.04	17.3	23.72	25.56	15.15	20.17	20.91	18.24
$P_{max}$ (kN)	65.09	91.91	93.76	95.61	83.96	84.11	86.88	84.81	86.15	88.69
$P_{mean}$ (kN)	26.79	47.11	47.66	46.71	47.45	51.12	48.54	46.45	46.19	45.60
CFE (%)	41.15	51.25	50.83	48.85	56.51	60.77	55.87	54.76	53.62	51.41

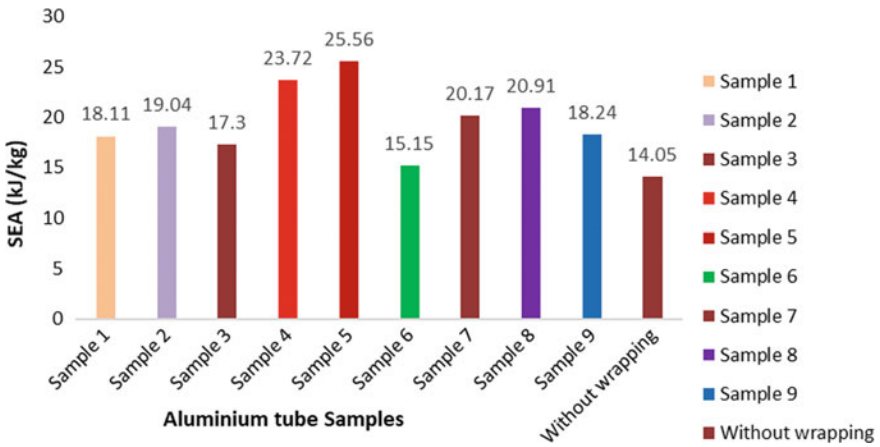


**Fig. 3.11** Specific energy absorption comparison of the partially wrapped and an unwrapped aluminium tube samples

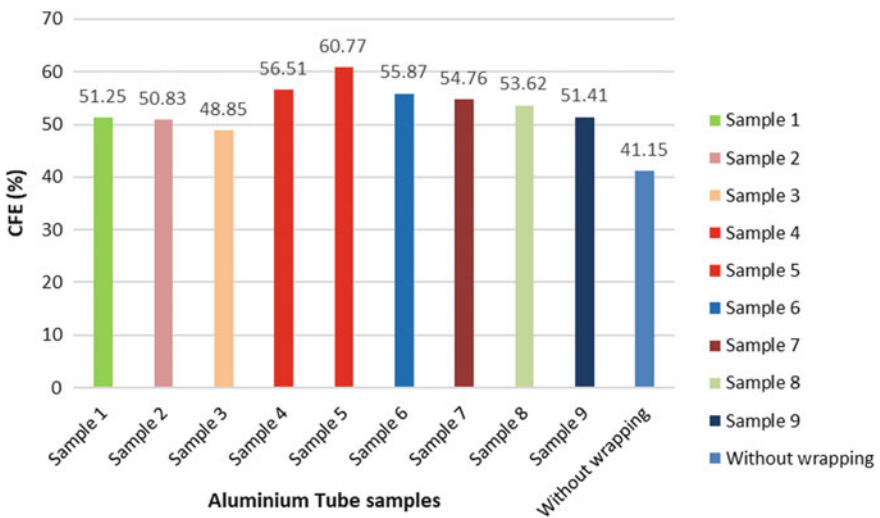





**Fig. 3.12** Crush force efficiency comparison of the partially wrapped and unwrapped aluminium tube samples

### 3.15 Analysis of Variance (ANOVA)

To determine the effect of fiber orientation, composite layers, and partially wrapped area on the specific energy absorption and crush force efficiency, the ANOVA was performed. The relative contribution of each parameter was also computed using

**Table 3.6** Comparison of the partially wrapped aluminium tube with the partially wrapped steel tube

Tubes	SEA (kJ/kg)	CFE (%)	Collapse Modes	
Partially wrapped aluminium tube (S5)	25.56	60.77	2-lobe diamond mode	
Without wrapping	14.05	41.15	3-lobe diamond mode	
Partially wrapped steel tube [23]	15.77	59.85	Asymmetric	

**Table 3.7** Experimental results of the partially wrapped aluminium tubes

Trial No.	Factors			Response	
	A	B	C (%)	SEA (kJ/kg)	CFE (%)
1	±10°	4	70	18.11	51.25
2	±10°	6	50	19.04	50.83
3	±10°	8	30	17.3	48.85
4	±55°	4	50	23.72	56.51
5	±55°	6	30	25.56	60.77
6	±55°	8	70	15.15	55.87
7	90°	4	30	20.17	54.76
8	90°	6	70	20.91	53.62
9	90°	8	50	18.24	51.41

**Table 3.8** S/N ratios and data normalization of experimental results

Trial No.	S/N ratio (dB)		Normalized		
	X	Y	X	Y	C
1	25.16	34.19	0.34	0.22	0.56
2	25.59	34.12	0.44	0.18	0.62
3	24.76	33.78	0.25	0.00	0.25
4	27.50	35.04	0.86	0.66	1.52
5	28.15	35.67	1.00	0.72	1.72
6	23.61	34.94	0.00	0.61	0.61
7	26.09	34.77	0.55	0.52	1.07
8	26.41	34.59	0.62	0.43	1.05
9	25.22	34.22	0.35	0.24	0.59

the ANOVA. Table 3.9 shows the quantities of the ANOVA; which are, the degree of freedom (DOF), the sum of squares (SS), variance, F-ratio and percentage contribution of each parameter. According to Roy [22], a parameter is considered

**Table 3.9** Analysis of variance table for experimental results

Column	Parameter	DOF	Sum of squares	Variance	F-ratio	Percentage
A	Fiber orientation	2	0.98	0.49	49	50.53
B	Composite layers	2	0.74	0.38	37	37.89
C	Partially wrapped area	2	0.11	0.06	6.0	4.74
All others/error		2	0.07	0.01		2.63
Total		8	1.90			100

insignificant if its influence is less than 10% of the highest parameter. From the ANOVA in Table 3.9, it has been concluded that fiber orientation and composite layers were significant using a 90% confidence level. Although partially wrapped area did not contribute too much.

### 3.16 Analysis of Main Effects

Before carrying out the main plot effect analysis, the interaction plots of the parameters were plotted, and it was noticed that the interaction plot lines were crossing each other, so it means that interaction between the parameters existed and they can affect the SEA and CFE values at an individual level as well. This is shown in Figs. 3.13, 3.14, 3.15, 3.16, 3.17 and 3.18. From Fig. 3.13, it has been concluded that interaction of the fiber orientation ( $\pm 55^\circ$ ) and the composite layers (6) would give higher energy absorption. Similarly, from Fig. 3.14, it is observed that the interaction of fiber orientation ( $\pm 55^\circ$ ) and the partially wrapped area (30%) would give higher value of the SEA. Figure 3.15 depicts that the interaction of the composite layers (6) and the partially wrapped area (30%) would give a high value of the SEA.

From Fig. 3.16, it has been concluded that the interaction of the fiber orientation ( $\pm 55^\circ$ ) and the composite layers (6) would give a higher value of CFE. Similarly, from Fig. 3.17, it is observed that the interaction of fiber orientation ( $\pm 55^\circ$ ) and the partially wrapped area (30%) would provide a high value of the CFE. Figure 3.18 depicts that the interaction of the composite layers (6) and partially wrapped area (30%) would offer high value of CFE.

In addition to this, to see the effect of an independent variable on a dependent variable, the main effect analysis has been carried out. Each parameter at various levels was summed up to figure out the average performance. For example, parameter A (Fiber orientation) at level 1 was denoted by  $\bar{A}_1$  to represent its average performance. In the orthogonal array L9, all the results in which parameter A was

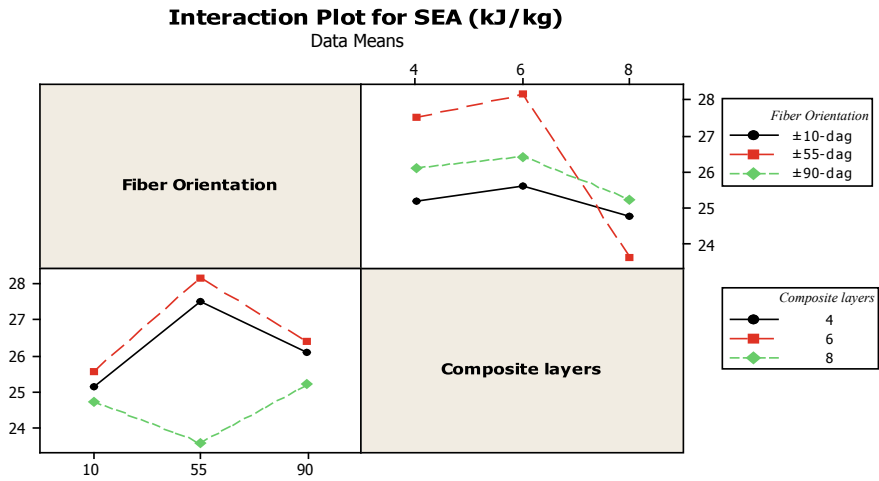


Fig. 3.13 Interaction plot of the fiber orientation and the composite layers for the SEA (kJ/kg)

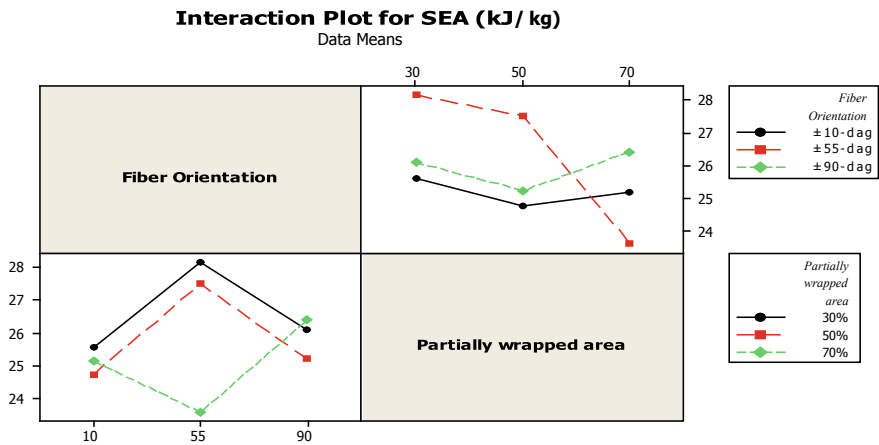


Fig. 3.14 Interaction plot of the fiber orientation and the partially wrapped area for the SEA (kJ/kg)

present were added and then divided by the number of trials. In a similar way, the average performance of  $\bar{A}_2$  and  $\bar{A}_3$  was calculated as given below:

$$\begin{aligned} \bar{A}_1 &= (T_1 + T_2 + T_3)/3 \\ &= (0.56 + 0.62 + 0.25)/3 = 0.47 \end{aligned}$$

$$\begin{aligned} \bar{A}_2 &= (T_1 + T_2 + T_3)/3 \\ &= (1.52 + 1.72 + 0.61)/3 = 1.28 \end{aligned}$$

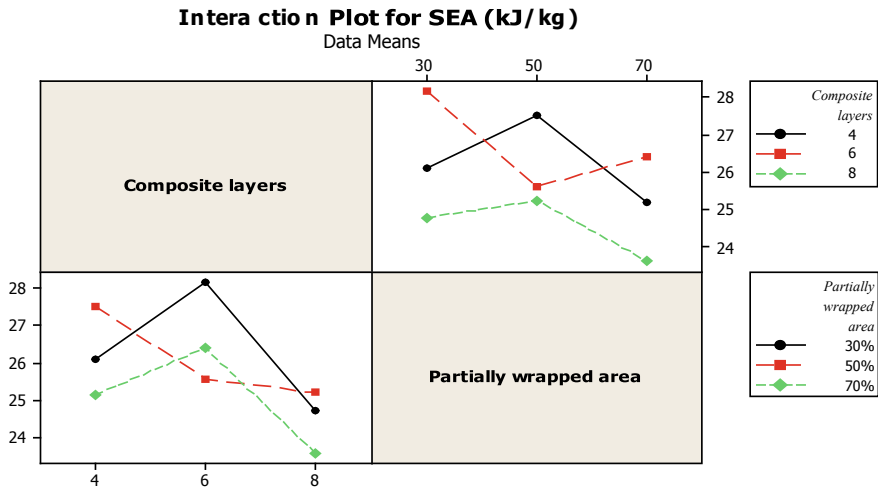


Fig. 3.15 Interaction plot of the composite and the partially wrapped area for the SEA (kJ/kg)

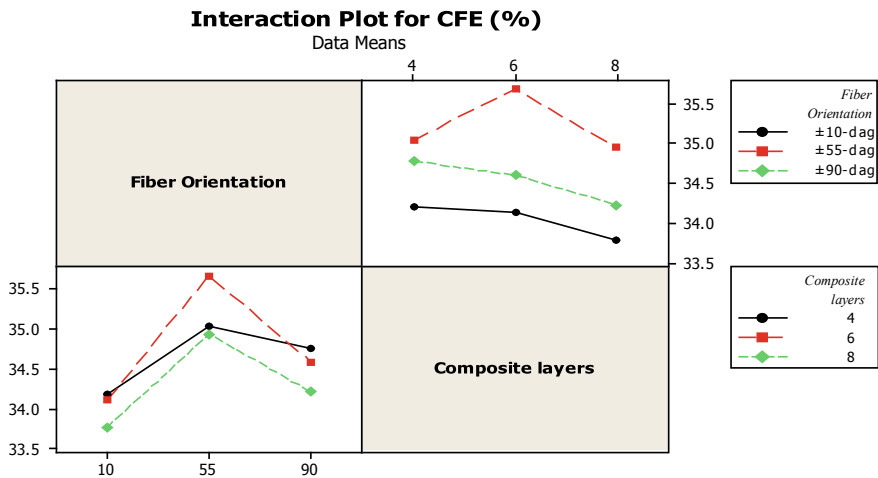


Fig. 3.16 Interaction plot of the fiber orientation and the composite layers for the CFE (%)

$$\bar{A}_3 = (T_1 + T_2 + T_3)/3$$

$$= (1.27 + 1.21 + 0.68)/3 = 0.91$$

The main effects' analysis on the results of the specific energy absorption and crush force efficiency was performed in two stages. In the first stage, the main effects' analysis was performed on the SEA and CFE values, separately. Any change in the fiber orientation, composite layers, and partially wrapped area could



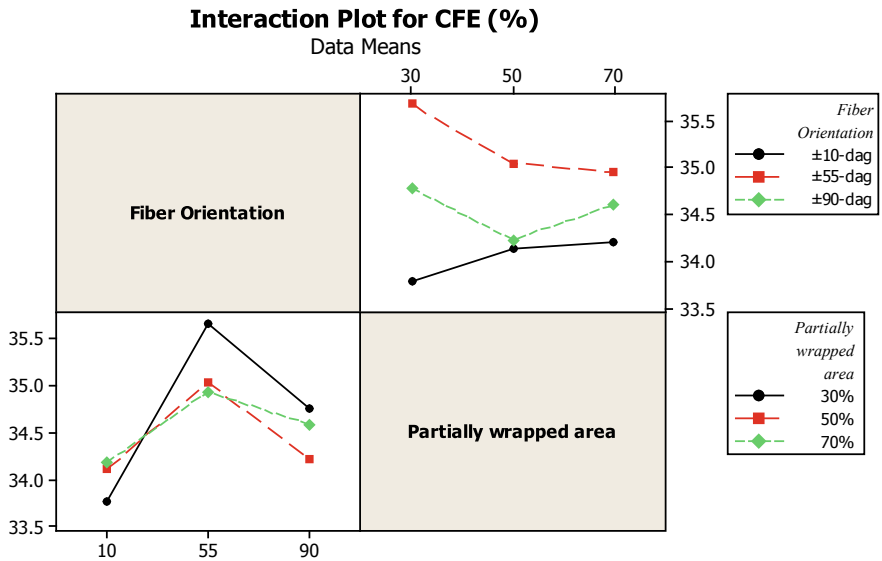


Fig. 3.17 Interaction plot of the fiber orientation and the partially wrapped area for CFE (%)

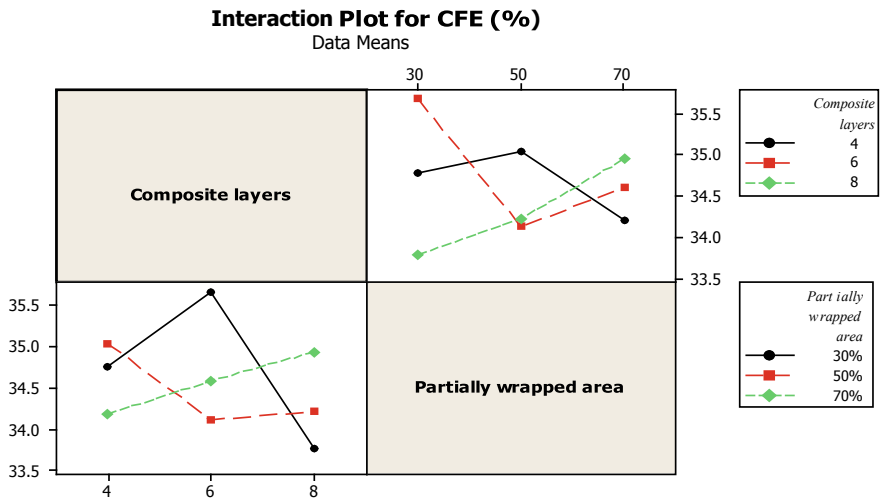


Fig. 3.18 Interaction plot of the composite layers and the partially wrapped area for the CFE (%)

**Table 3.10** Main effects' analysis of the specific energy absorption

Column	Parameter	Level 1	Level 2	Level 3
A	Fiber orientation	25.17	26.42	25.91
B	Composite layers	26.25	26.72	24.53
C	Partially wrapped area	25.06	26.11	26.33

**Table 3.11** Main effects' analysis of the crush force efficiency

Column	Parameter	Level 1	Level 2	Level 3
A	Fiber orientation	34.03	35.67	34.53
B	Composite layers	34.67	34.62	34.32
C	Partially wrapped area	34.57	34.46	34.56

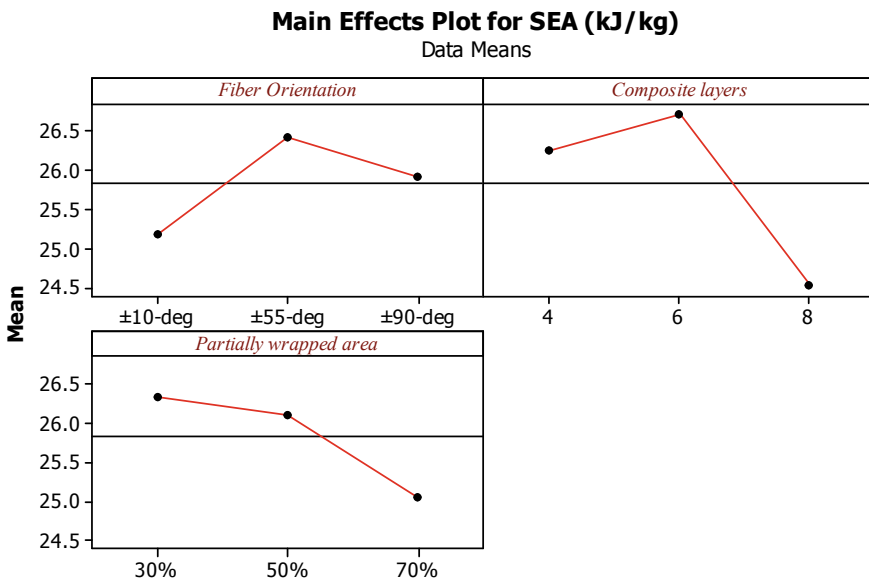


**Fig. 3.19** Main effects' plot for the specific energy absorption

change the SEA and CFE values. Therefore, the individually computed main effects' analysis on the SEA and CFE is shown in Tables 3.10 and 3.11. For a better interpretation of the results of the main effects, the analysis is shown in Figs. 3.19 and 3.20.

From Figs. 3.19 and 3.20, it is clear that the specific energy absorption and crush force efficiency both had a different optimal combination of parameters. So, it is important that all parameters have only one optimal combination to enhance the specific energy absorption and crush force efficiency. As discussed earlier, the

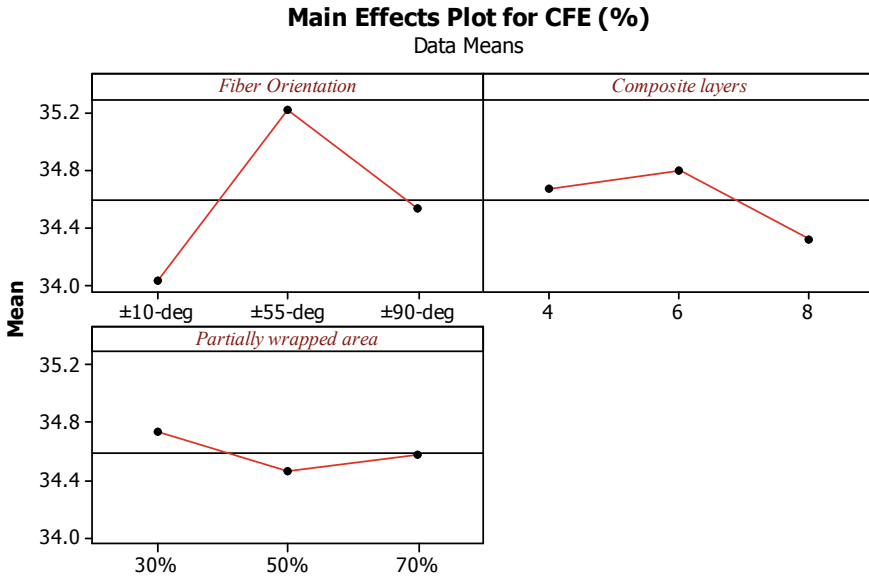


Fig. 3.20 Main effects’ plot for the Crush force efficiency

Table 3.12 Main effects’ analysis of the combined SEA and CFE

Column	Parameter	Level 1	Level 2	Level 3
A	Fiber orientation	0.48	1.29	0.90
B	Composite layers	1.05	1.13	0.48
C	Partially wrapped area	0.74	0.91	1.01

specific energy absorption and crush force efficiency S/N ratio values were summed up to get one value after being normalized. Therefore, for the combined value of the SEA and CFE the main effects’ analysis was computed and is shown in Table 3.12. From Fig. 3.21, it is noticed that the specific energy absorption and crush force efficiency were both greatly influenced by changing the fiber orientation, composite layers, and partially wrapped area. The optimal combination of the fiber orientation, composite layers, and partially wrapped area that resulted with statistically high values of the SEA and CFE was  $A_2/B_2/C_3$ . From the main effects’ plot, as shown in Fig. 3.21, these parameters have the optimal values of  $\pm 55^\circ$  fiber orientation, 6 composite layers, and a 30% partially wrapped area.

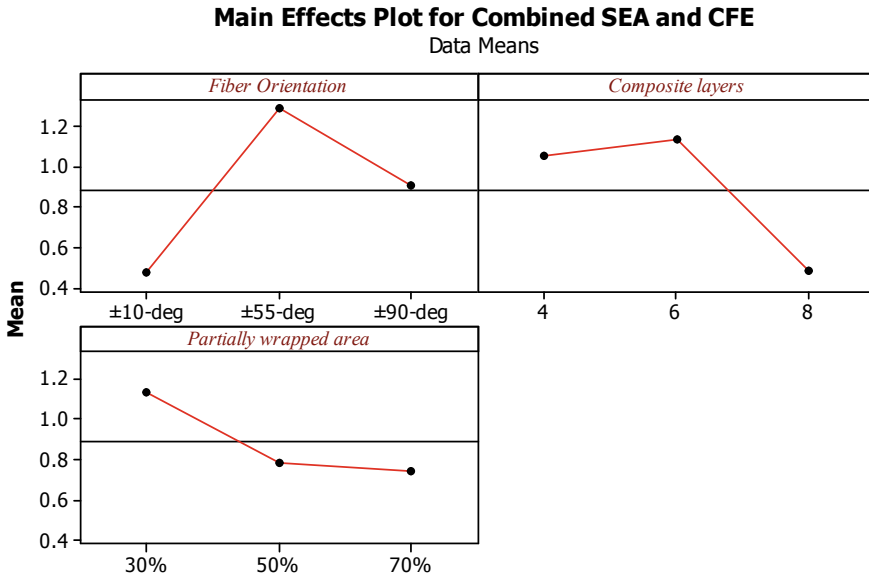


Fig. 3.21 Main effects’ plot of the combined SEA and CFE

### 3.17 Summary

This chapter described the experimental investigation of the collapse modes and specific energy absorption, and the crush force efficiency of the partially wrapped aluminium tubes subjected to quasi-static loading. Various combinations of fiber orientations, composite layers, and partially wrapped areas were used to develop the partially wrapped aluminium tube samples according to the Taguchi design. The analysis of variance has been conducted to find out the best combination of fiber orientation, composite layers and partially wrapped area for a specific energy absorption and crush force efficiency. The combination ( $\pm 55^\circ$ , 6, and 30%) has 81.92, and 62.08% higher values of specific energy absorption (SEA), and 47.67 and 1.54% more values of crush force efficiency (CFE) as compared to the simple aluminium tube and its predecessor the steel tube, respectively. The experiments that were conducted on different partially wrapped aluminium tubes revealed that partially wrapped aluminium tubes are better in energy absorption and crush force efficiency as compared to unwrapped aluminium tubes.

## References

1. A. Alghamdi, Collapsible impact energy absorbers: an overview. *Thin-Walled Struct.* **39**, 189–213 (2001)
2. N.D. Flesher, *Crash Energy Absorption of Braided Composite Tubes* (Stanford University, Stanford, 2006)
3. G.L. Farley, R.M. Jones, *Energy-Absorption Capability of Composite Tubes and Beams* (DTIC Document, 1989)
4. A. Chathbai, *Parametric Study of Energy Absorption Characteristics of a Rectangular Aluminum Tube Wrapped With E-Glass/Epoxy* (Wichita State University, 2007)
5. M. Bambach, M. Elchalakani, X.L. Zhao, Composite steel–CFRP SHS tubes under axial impact. *Compos. Struct.* **87**, 282–292 (2009)
6. M. Bambach, Fibre composite strengthening of thin-walled steel vehicle crush tubes for frontal collision energy absorption. *Thin-Walled Struct.* **66**, 15–22 (2013)
7. M. Langseth, O. Hopperstad, Static and dynamic axial crushing of square thin-walled aluminium extrusions. *Int. J. Impact Eng.* **18**, 949–968 (1996)
8. C. Bisagni, Experimental investigation of the collapse modes and energy absorption characteristics of composite tubes. *Int. J. Crashworthiness* **14**, 365–378 (2009)
9. R.M. Lima, Z. Ismarrubie, E. Zainudin, S. Tang, Effect of length on crashworthiness parameters and failure modes of steel and hybrid tube made by steel and GFRP under low velocity impact. *Int. J. Crashworthiness* **17**, 319–325 (2012)
10. C. Leyens, M. Peters, *Titanium and Titanium Alloys: Fundamentals and Applications* (Wiley, Hoboken, 2006)
11. P. Balaguru, A. Nanni, J. Giancaspro, *FRP Composites for Reinforced and Prestressed Concrete Structures: A Guide to Fundamentals and Design for Repair and Retrofit* (Taylor & Francis, Abingdon, 2008)
12. A. Mamalis, M. Robinson, D. Manolakos, G. Demosthenous, M. Ioannidis, J. Carruthers, Crashworthy capability of composite material structures. *Compos. Struct.* **37**, 109–134 (1997)
13. G.L. Farley, *Relationship Between Mechanical-Property and Energy-Absorption Trends for Composite Tubes*, vol. 3284 (National Aeronautics and Space Administration, Office of Management, Scientific and Technical Information Program, 1992)
14. K. Andrews, G. England, E. Ghani, Classification of the axial collapse of cylindrical tubes under quasi-static loading. *Int. J. Mech. Sci.* **25**, 687–696 (1983)
15. S.C.K. Yuen, G.N. Nurick, The energy-absorbing characteristics of tubular structures with geometric and material modifications: an overview. *Appl. Mech. Rev.* **61**, 020802 (2008)
16. Z. Ahmad, Impact and energy absorption of empty and foam-filled conical tubes, Ph.D. Thesis, Queensland University of Technology, 2009
17. N. Jones, *Structural Impact* (Cambridge University Press, Cambridge, 1989)
18. D. Hull, T. Clyne, *An Introduction to Composite Materials* (Cambridge University Press, Cambridge, 1996)
19. R. Keal, *Post Failure Energy Absorbing Mechanisms of Filament Wound Composite Tubes* (University of Liverpool, Liverpool, 1983)
20. R. Kalhor, S.W. Case, The effect of FRP thickness on energy absorption of metal-FRP square tubes subjected to axial compressive loading. *Compos. Struct.* **130**, 44–50 (2015)
21. A. Lakshminarayanan, V. Balasubramanian, Process parameters optimization for friction stir welding of RDE-40 aluminium alloy using Taguchi technique. *Trans. Nonferrous Metals Soc. China* **18**, 548–554 (2008)
22. R.K. Roy, *Design of Experiments Using the Taguchi Approach: 16 Steps to Product and Process Improvement* (Wiley, Hoboken, 2001)
23. M. Abbasi, S. Reddy, A. Ghafari-Nazari, M. Fard, Multiobjective crashworthiness optimization of multi-cornered thin-walled sheet metal members. *Thin-Walled Struct.* **89**, 31–41 (2015)

# Chapter 4

## Mobility and Health: The Interaction of Activity-Travel Patterns, Overall Well-Being, Transport-Related Social Exclusion on Health Parameters



Dimas B. E. Dharmowijoyo and Tri Basuki Joewono

This chapter provides a descriptive analysis of research development in mobility and health. The relationship between daily activity-travel participations and health parameters is not straightforward. It seems that overall well-being and transport-related social exclusion can mediate the relationship between daily activity-travel patterns and health conditions. More advanced model such as a hierarchical SEM can be used for further analysis.

### 4.1 Introduction

Individuals' activity-travel behaviour is complex. Treating individuals' activity-travel behaviour as an independent entity which varies in only socio-demographic and built environment manners is underestimating the complex mechanism behind decision-making process of individuals. Conventional method, which based on cross-sectional observation, was found to fail in explaining and forecasting individuals' travel needs and demands [1, 2]. More than 9 out of 10 rail projects were overestimated and approximately 50% of all road projects showed a difference between actual and forecasted demand of more than  $\pm 20\%$  [2]. The conventional approach assumes that the individual engages in similar travel and activities every day and, therefore, such approach encompasses only inter-personal variability [3]. Conventional method, or normally called trip-based analysis, may fail in addressing

---

D. B. E. Dharmowijoyo (✉)

Department of Civil and Environmental Engineering, Universiti  
Teknologi PETRONAS, 32610 Seri Iskandar, Perak, Malaysia  
e-mail: [dimas.bayu@utp.edu.my](mailto:dimas.bayu@utp.edu.my)

T. B. Joewono

Department of Civil Engineering, Parahyangan Catholic University,  
Jalan Ciumbuleuit 94, 40117 Bandung, Indonesia

the interdependencies among trips and activities, temporal constraints on activity scheduling, and activities among individuals within a household or within their social networks [4]. This form of analysis disregards the mechanisms especially with respect to individuals' time-space constraints [5–7].

Decision-making process in shaping individuals' activity-travel participations is influenced by their personal, household and social characteristics and their socio-environmental or built environment conditions. The time and space prism concept reveals that an individual retains multiple characteristics in multiple dimensions such as personal, household, social and spatial dimensions. The interaction of individuals' characteristics in multiple dimensions will create a specific needs and constraints of individuals to form their daily activity-travel participations. Husband, wife and a child will have a different role within a household and will attach with a different set of activities and travel set as well by their personal characteristics such as gender and age. Moreover, the engagement of an individual with their society such as part of a particular company and/or part of a certain school and neighbourhoods will also influence the formation of a set of activities and travels in interaction with the individuals' other characteristics.

Hägerstrand [5] argued that understanding the different formation of activities and travels on a given day is subject of three types of constraints: capability, coupling, and authority constraints which describe individuals' constraints on personal level, household and social level, and socio-environmental conditions. These constraints will complement each other, thus will interact with each other in conjunction with someone's needs to form one's daily space-time prism. The conditions and variability of other resources, such as availability and service level of the infrastructure and public transport network, the selection of possible activity locations within reachable distances, access to various travel modes, and amount of money to spend, would provide individuals with opportunities to engage in more/less activities with more/less dispersed locations within possible time constraints. This complex mechanism means that everyone is unique and failing to capture these interactions biases the analyses and the predictions. Understanding the concept might reveal a different perspective on mobility. There is a case, individuals from larger household, who needs to commute farther to reach their working place and requires visiting more than one out-of-home activity locations in order to drop/to pick other household members, and/or to meet other people, and/or to do other activities in different locations, tend to be difficult to be free from motorised mode. However, massive dependency of motorised mode is not also good in considering its impact to congestion and physical health conditions.

People have fluctuation of needs and desires on different day that might be also influenced by the changing of environmental conditions and the constraints on personal, household and social, and socio-environmental levels. Given the condition may make the time-space prisms and paths also differ from day to day [5, 8–12]. The exclusion of day-to-day variation can diminish complexity manner of our models and can miss the complete picture of individuals' needs and desires in term of travel. It will misinterpret how people manage their undertaken activities and travels within the complex interactions of changing needs, constraints and

opportunities offered in time and space dimensions on daily basis. Moreover, the variability analysis also predicts how the individual plans and optimises different activity-travel pattern within changing situations of needs and built environmental situations [9, 11–14].

Another aspect that can shape the variability of daily activity-travel behaviour is the variability of daily other household members' activity-travel patterns [14–17]. When a household member is undertaking more trips or spending more travel time budget approaching his/her maximum travel time budget, another household member will perform in-home activities longer [16, 17]. Joint activities among household members tend to influence reducing of workers and students' out-f-home maintenance activities [14, 16]. Previous studies tried to include the correlation of other household members' and individuals' activity-travel behaviour using one or two independent variables. Such a method will consider the influence of social contacts on any dependent variable. However, this method does not influence estimation parameter of the model. With first method, any suggested policy as a result of estimated parameter will not consider the presence of other people in individuals' activity participation. Another alternative is using multilevel modelling. In this method, the estimation parameter of each model will take in the inclusion of other people in each activity in a certain period. Multilevel modelling will reveal the complexity of individuals' decision-making process.

Additionally, any health or emotional problems may also influence individuals' activity-travel participation. Health indicators will uncover another dimension of individuals' capability factors which, in some extents, cannot be only explained by conventional time and space variables such as socio-demographic, socio-economic, and time-use and activity participation. When utilising individuals' health indicators, previous studies exhibit any relation among having better health in term of physical, mental and social with individuals' activity-travel behaviour. Previous studies exhibit a correlation of having better social cohesion or social capital on individuals' activity-travel behaviour [18–20]. Moreover, walking and cycling behaviour and taking more percentage of public transport is also influenced by having better physical health [19, 20].

At the same time, how individuals spend their time engaging in different activities and trips may influence their physical, mental and social health. Showing how individuals' health condition influences the individuals' activity and travel participation may be more straightforward compared with the other way around. [19, 21, 22]. There have not yet been any studies which have detangled the direct correlations between individuals' health conditions and their time-use and activity participation [19, 21, 22]. Relation between individuals' activity-travel behaviour and health is complex. Some aspects in health such as physical health tend to have direct relation to individuals' activity-travel behaviour such as through participation into public transport or non-motorised transportation more often [20, 23–28]. However, Wee and Ettema [29] emphasised that more detail variables in explaining how often individuals spend on moderate and vigorous physical activities will reveal indirect correlation of activity-travel behaviour on physical health factor. On relation between activity-travel behaviour, and social and mental health, social



exclusion and social capital [18, 30–34], and/or subjective well-being [29] were assumed to mediate relation between individuals' activity-travel behaviour on their mental and social health performances. Furthermore, some studies also showed a relation between having more organised activity-travel patterns with having better mental and social health [22, 35].

WHO [36] and Suzukamo et al. [37] defined social and mental health as the presence of social and mental illness. The social and mental illness could be happened due to individuals' problems on their physical condition, general health and emotional which affect their social and mental health. Well-being focus on wider spectrum of mental illness [29] which may not always be related to the presence of social and mental illness. Social and mental health factors may limit individuals' participation in certain activities which may influence individuals' well-being level. On the other hand, how the way individuals experience during a day will show whether someone is on social and mental health problems or not. Therefore, individuals' daily or overall well-being may bridge the relation between individuals' activity-travel behaviour and health conditions.

Activities and travels are materialised actions of human in their efforts of satisfying their needs and desires shaped by their constraints in a complex manner within time-space limitation. Understanding on how individuals shape their activity-travel behaviour due to their personal and social characteristic within multidimensional and multi-hierarchical time and space perspective and its correlation with health factors may be able to suggest a certain policy that can ensure improvement of individuals' health, particularly social and mental health. Moreover, when someone undertakes a set of activities and travels that correspond with a positive health condition in multiple definitions, it can be also as a result of a long-term process. Performing a particular set of activity-travel participation can be a result of a long contemplation that creates a particular attitude and believes [38–40] implemented in daily activities and travels. Therefore, healthy daily life is a lifestyle implemented into daily activities and travels. As materialised actions of a human, finding out how to reach a particular healthy level in multiple dimensions should be also required in order to spread the healthy lifestyle to society.

In term of mental health, social exclusion might bridge the relationship with activity and travel participation. Planning and setting built environment conditions are only facilitating individuals to do suggested activities for improving their well-being or health into a particular level. However, intervening individuals' decision to participate in a particular activity may suggest a particular attitude or motive which can create internal motivations of individuals in performing set of activities for improving their subjective well-being and health conditions.

The present study tackles the research gap mentioned above. The interaction among individuals' and other household members' time-use and activity participation, physical geographical conditions, perception on particular built environment conditions and socio-economic/socio-demographic will be applied to influence individuals' daily and global well-being and health performances in a complex manner. The subjective well-being is assumed to mediate the relation between daily activity-travel behaviour and health conditions in multiple definitions, whereas

transport-related social exclusion will mediate the relationship between daily activity-travel participations and mental health conditions.

## 4.2 The 2013 Bandung Metropolitan Area Dataset

### 4.2.1 *The Bandung Metropolitan Area*

The Bandung Metropolitan Area (BMA) is located 200 km or three hours' drive southeast of Jakarta. It is 768 m above sea level in the basin of the central mountainous plateau region of West Java. BMA covers the City of Bandung as the capital city of West Java Province with its fringe: Municipality of Bandung in the south part of area, Municipality of West Bandung in the west and north part, City of Cimahi in the west part of area and some districts within Municipality of Sumedang in the east part of area. The area encompasses around 7.89 million people and 3382.89 km<sup>2</sup> [41].

BMA suffers unplanned mixed with the strong city centre and very low road capacity level and low performance of public transport systems [41]. There were efforts to adopt compact development approach with creating multiple centres in 2003 Masterplan which divided Bandung into six secondary urban centres and one primary urban centre on the east side of the city [42, 43]. However, most of the movements are still attracted to the city centre. These factors may make BMA area particularly city centre suffers from severe road congestion which makes BMA's travellers take motorcycles to reduce their travel costs and time. Unplanned mixed land use makes BMA travellers have more choices within- a closer range in which to conduct their activities along with their travel routes. These conditions influence the size, spread, orientation, and variability of daily activity spaces [44]. BMA has informal transit system with marginal railway operation in serving West-East corridor and indigenous public transport systems called *angkot* and *ojeg*. *Angkot* (operated as mini-bus as in developed country case) and *ojeg* (motorcycle taxi) have no specific stops or can stop everywhere. *Angkot* tends to have fixed networks without a proper frequency in which operate near the city centre or in a populated area in the west and south part of the City of Bandung. *Ojeg* totally has no fixed network as taxis in the developed country case and serves the other areas not served by *angkots* [43, 45, 46].

### 4.2.2 *The 2013 BMA Dataset*

The BMA dataset was collected in 2013 [20, 47]. It contains a number information of individuals' time-use and activity participation in conjunction with another multidimensional information such as household, physical activity and lifestyle,

social and family engagements, mental and social health conditions, individual's subjective characteristics, and subjective well-being data. The time-use and activity participation were collected for 21 consecutive days and for 732 individuals and 191 households. The dataset provides opportunities to investigate complexity and variability of individuals' activity-travel behaviour.

The household data section included information on household composition and individuals' subjective measurement of accessibility and subjective neighbourhood questions. As in the developing country case, unpredictable traffic conditions, frequently highly congested and unpattern mixed land use may cause the objective measurement of accessibility cannot capture the reality of accessibility measurement of individuals' home resident. Therefore, a subjective measurement of accessibility was used to capture how far individuals' home resident from basic public amenities. Moreover, household data section was also incorporated by subjective neighbourhood questions. The subjective neighbourhood questions contain four questions with five Likert scale possible answers. The answers are range from strongly agree to strongly disagree.

Moreover, in the household data section, it also contains the information of how many days on average within a week, individuals undertake social and family interactions. The answer could be no day into 7 days. Another question related to social and family interactions is how long respondents spend the time in average to perform social and family interactions during a day? The answers to this question will be in seven Likert scales from very short time until very long time in a day.

The dataset collected activity diary rather than a travel diary. The dataset captured twenty-three types of in-home and out-of-home activity categorizations. The activity classification is categorised into mandatory and discretionary activities which each of category will be divided into in-home and out-of-home activities considering whether the activities are undertaken at home or out-of-home. Activities are categorised as mandatory when a particular activity is defined to be difficult to be re-scheduled [48] with higher temporal and spatial fixity such as working, going to school and pick up/drop activities [49]. Whereas, activities with higher temporal and spatial flexibility which can be easily re-scheduled is classified as discretionary activities such as grocery shopping and leisure activities [48, 49]. In term of discretionary activities, discretionary activities for satisfying household and personal physiological and biological needs [50] were defined as maintenance activities such as housekeeping and nursing activities, grocery shopping, health treatment activities and other service activities (such as going to the bank, post office) [14]. For this study, out-of-home maintenance activities were separated into grocery shopping and another out-of-home maintenance. Moreover, leisure activities were discretionary activities undertaken within an individual's available time either in-home or out-of-home for satisfying cultural and physiological needs such as socialising, entertainment activities, sport and recreational activities [50]. For this study, out-of-home leisure activities were divided into out-of-home socialising and recreation, and sports activities.

This dataset also includes multitasking activities. Multitasking activities were defined as concurrent activities which contained primary and secondary activities

[51, 52] for satisfying different needs and desires at the same time. In this case, multitasking activities were defined as combining mandatory activities (such as work/school, eating, sleeping), maintenance activities (such as nursing, grocery shopping), and active leisure activities such as doing sport or reading a book with passive leisure activities, such as entertainment and socialising [52]. In this case, socialising was defined as meeting with other people such as with other household members, or nonhousehold members.

The questionnaire contained a section with health-related quality of life (QoL) questions and its potential influencing factors. Health-related QoL was developed based on SF-36 (Short-Form 36), one of the most widely used generic measures for health-related surveys. This set of questions has been adopted by more than 11 countries [19]. It contains eight subscales that consider physical, social and mental health, which are measured in categories such as physical functioning (PF), limitations on role functioning according to physical health (RP), bodily pain (BP), general health (GH), mental health (MH), limitations on role functioning due to emotional problems (RE), social functioning (SF) and vitality (VT). As suggested by [37], PF, RP and BP will be defined as physical health, RP, SF and RE as social health, and BP, GH, VT, SF, MH as mental health. Profile of the sample is shown in Table 4.1. More detail information regarding the dataset can be found in Dharmowijoyo et al. [20] and Dharmowijoyo [47].

In this study, for capturing the individual's daily subjective well-being, each individual was asked: *'How would you describe your experience today in considering all aspects such as the activities, travels and built environment situations?'*. The response contains seven Likert scale range from 'very bad' to 'very good'. It is part of domain-specific well-being that assesses the well-being condition on a particular day, considering all dimensions, including activities, travels and other aspects [39, 53].

In term of overall well-being, the structure of well-being in general consists of three components: the presence of positive feelings, the absence of negative feelings and overall satisfaction with life [54, 55]. The first and second components are referred to as affective component, whereas the last is defined as a judgmental or cognitive component.

In measuring life satisfaction or happiness, it was possible in BMA 2013 dataset to include affective and cognitive components of life satisfaction. In survey time, respondents were asked with two questions related to affective and cognitive components of life satisfaction. The question related with the affective component is *'How do you feel your life in general?'*. Respondents answered the affective component question into two dimensions called valence and activation [39, 53, 55–57].

For valence dimension, the respondents were asked to rate in 7 Likert scale ranges from sad to happy, whereas for activation dimension, respondents rated in 7 Likert scale ranges from passive or quietness to active or arousal. Two categories were added to cover a combination of emotions of different position between valence and activation dimensions with a range from depressed/dull to excited/joyful, and distress to content/calm.

**Table 4.1** Profile of the samples used in the study

Variables	Percentage or mean
<i>Socio-demographic characteristics at individual level</i>	
Male	52.10%
Worker and non-worker	43.64 and 31.05% <sup>a</sup>
Isa dependent child ( $\leq 14$ years old)	12.73%
Young-adult (aged 15–22 years old)	18.60% <sup>a</sup>
Aged 23–45 and 45–55 years old	44.76 and 14.27% <sup>a, c</sup>
Part of low income (<IDR 3 million/month) and medium income households (IDR 3–6 million/month)	75.20 and 15.80% <sup>a</sup>
<i>Household characteristics</i>	
Number of household members	4.52
Number of dependent children per household	0.83
Number of motorised vehicles per household	1.77
Reside within the inner city boundary of BMA and within Greater BMA	44.90 and 37.90% <sup>a</sup>
<i>Trips engagements and travel time spent on weekdays (weekends)<sup>b</sup></i>	
Number of trips	2.64 (2.29)
Number of trip chains	1.26 (1.08)
Percentage of using motorised mode	39.19% (36.77%)
Percentage of using public transport	14.88% (9.55%)
Percentage of using non-motorised mode	34.49% (32.08%)
Total travel time spent from Monday to Friday (minutes)	74.87(69.35)
<i>Time spent for different activities on weekdays (weekends)<sup>b</sup></i>	
Time spent for in-home mandatory activities (minutes)	693.17 (738.18)
Time spent for in-home leisure and maintenance activities (minutes)	308.23 (363.09)
Time spent for working/school activities (minutes)	298.85 (161.99)
Time spent for out-of-home grocery shopping (minutes)	13.11 (21.62)
Time spent for out-of-home social-recreational (minutes)	51.72 (61.52)
Time spent for out-of-home other maintenance and sport (minutes)	5.04 (24.75)
<i>Percentage of time engaging with multitasking activities within certain activity on weekdays (weekends)<sup>b</sup></i>	
Percentage of time engaging with multitasking activities within travel activities	6.89% (5.22%)
Percentage of time engaging with multitasking activities within out-of-home mandatory activities	7.11% (3.64%)
Percentage of time engaging with multitasking activities within out-of-home discretionary activities	17.84% (11.85%)
<i>Built environment variables<sup>c</sup></i>	

(continued)

**Table 4.1** (continued)

Variables	Percentage or mean
Km-length of road and railway per square-km within the respondents' residential location	38.57 and 4.83
Density of industrial and trade centre or wholesale centre area per square-km within the respondents' residential location	0.024 and 0.005
Density of government office and settlement area <sup>d</sup> per square-km within the respondents' residential location	0.012 and 0.484
<i>Perceived accessibility variables</i>	
Perceived number of public transport lanes passing respondent's resident	2.57
Perceived travel time to CBD and shopping centre area (minutes)	31.27 and 15.85
Perceived travel time to grocery store and park (minutes)	8.34 and 18.29
Perceived travel time to the nearest place to stop public transport (minutes)	14.50
<i>Subjective neighbourhood questions</i>	
Agree to perceive that you have good neighbours and reside in a friendly and peace neighbourhood?	3.87
Agree to perceive to have adequate access to good basic social right facilities in your neighbourhood in term of health, education, social-community, and shopping facilities?	3.50
Agree to perceive to stay in a neighbourhood with good infrastructure, parking space and sanitation?	3.41
Agree perceive that your neighbourhood has good traffic condition?	3.26
<i>Involvement of social and political, and family participation</i>	
How many days on average within a week, individuals spend time for social and political activities with their community/society? (days)	3.26
How long in average individuals spend social and political participation during a day?	3.53
The average variability in individuals' activity-travel patterns on particular days compared to other days	51.23
<i>Social Inclusion Index</i>	0.00

<sup>a</sup>The remaining is students (25.31%), part of high-income households (8.90%) and reside within CBD of BMA (17.20%)

<sup>b</sup>The values in brackets show the percentage/mean values on weekends, otherwise is on weekdays

<sup>c</sup>The density is calculated based on the built area in only horizontal plane in km<sup>2</sup> divided by total area in km<sup>2</sup>. The measurement is excluded the area on vertical plane

<sup>d</sup>Following the definition of density of certain built area, living in a denser settlement area does not always mean to live in a populated area. More populous area can mean an area which contains low-density settlement area in horizontal plane (but denser in vertical plane)

<sup>e</sup>Both groups represent groups with different time and space constraints which may have a different working quality level and time allocation [60] and different activity-travel patterns in Indonesia context [44]

On the other hand, the cognitive component was measured using Satisfaction with Life Scale (SLWS) [58, 59]. In SWLS, participants were asked some questions: 'The condition of my life is excellent', 'In most ways, my life is excellent', 'I am satisfied with my life', 'So far I have gotten the important things I want in life',

and ‘*If I could live over, I would change almost nothing*’. Participants rated those questions in 7 Likert scale ranging from ‘*Does not agree at all*’ to ‘*Agree completely*’. Affective and cognitive components shape global life satisfaction or happiness index of individuals. Figure 4.1 illustrates the factor loadings that shape the score of overall subjective well-being.

In this study, social exclusion/inclusion is assumed to be influenced by transport-related dimension [61, 62]. Limitation in term of social and transport disadvantages is assumed to be the main resources why someone tends to have limited social participation and lack access to various basic public amenities in geographical manners. Observed variables of transport and social disadvantages will use the definition by Lucas [62]. Figure 4.2 shows the observed variables of transport and social disadvantages in this study. In this research, the distance to various basic public amenities is represented by the perception of having longer travel time to various basic public amenities (such as school, bank, post office, hospital, government offices, park, grocery store and shopping centre). Having low social participation can be represented by time-use variables such as how many days in a week and how many hours per day someone will spend social and political activities, and travel parameters such as number of trips, trip chains and total travel time. Activity-travel behaviour research has revealed that higher number of trips/trip chains and total travel time correspond with bigger size of activity space

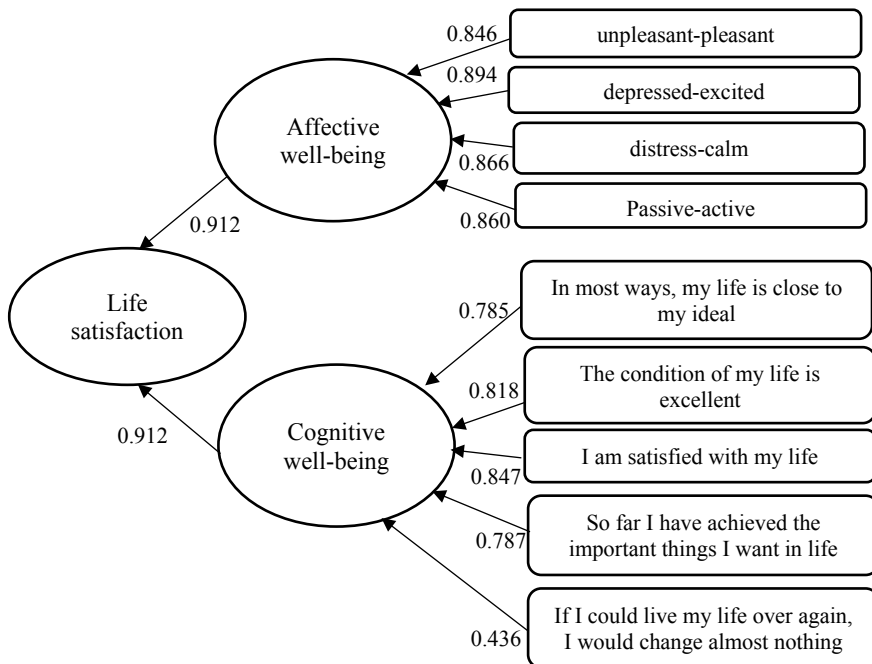


Fig. 4.1 Measurement model of life satisfaction

[13, 16, 44, 63, 64] and more maintenance and leisure activities [44, 65–70]. From the definition, the ones who have the highest risk of social and transport disadvantages are the ones who have the lowest opportunities and access to various basic public amenities, and to social networks. However, there is a possibility the ones part of social disadvantage group, may not have transport disadvantage problems and may have high access to various public amenities and to social networks.

According to Lucas [62], social and transport disadvantages interact with the distance/travel time to various basic public amenities and number of connected

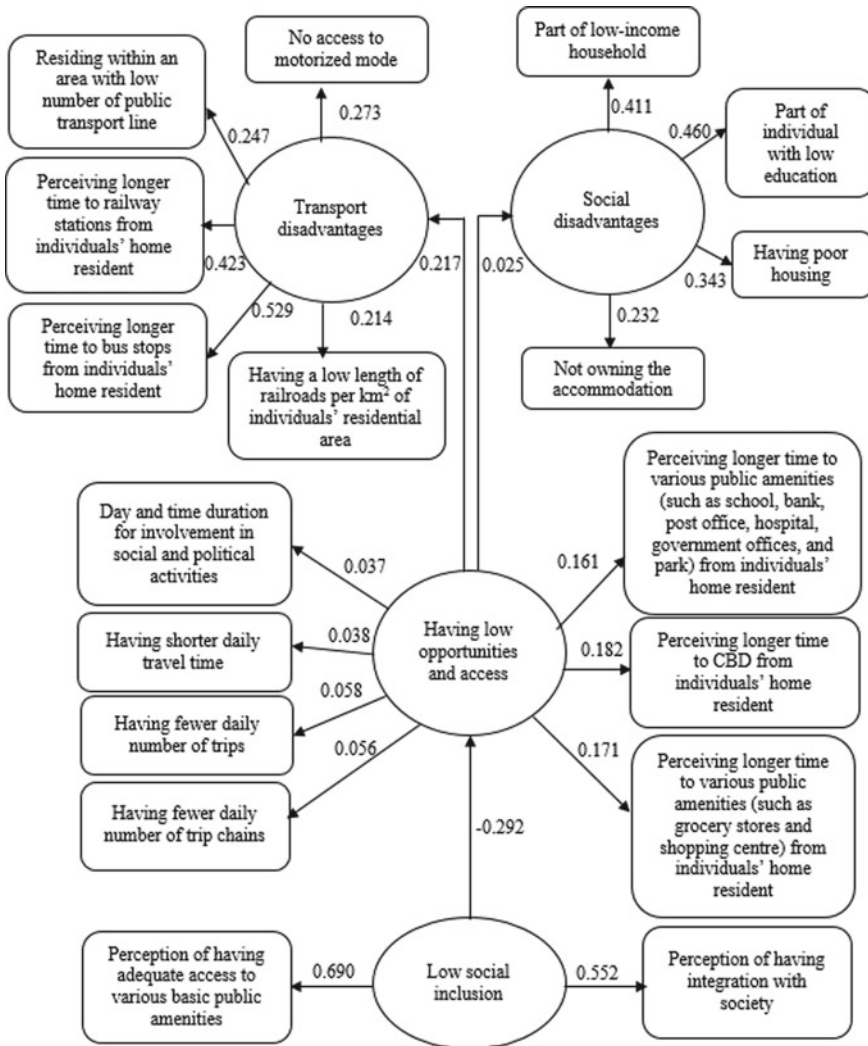


Fig. 4.2 Factor loadings of the observed variables used to estimate the Social Inclusion Index



social networks and social capital component on social exclusion/inclusion. Moreover, modified from Lucas [62], having low opportunities and access to various factors (such as to various public amenities in geographical manners and to social networks/social capital) is assumed to interact with perception of having adequate access not in geographical access and of having integration with society. In the BMA dataset, the individuals' perceptions of whether they have adequate access (in terms of opportunity) to basic social rights facilities and good infrastructure, sanitation and parking spaces may represent whether individuals attain adequate or inadequate access to basic social rights as defined in various reports [61, 62, 71, 72]. For integration with society, there is a question that can represent the lack of normative integration, which is: *'Do you perceive that you have good neighbours and reside in a friendly and peaceful neighbourhood?'* The question contains answers based on a 5-point Likert scale ranging from totally disagree to totally agree.

All variables are used to create a 'social inclusion index' obtained from factor scores of all questions related to transport-related social exclusion/social inclusion, using a basic principle component analysis with a single-factor solution. The factor scores are standardised variables with a mean of zero and a variance of one across the sample which essentially carries the same information in a more compact form [73, 74]. Factor score is the common method of uncovering latent variables (such as social exclusion or inclusion) which have multidimensional interpretations [75]. The factor scores also produce factor loadings of multidimensional information that influence the latent factor scores. The factor loadings show the interrelationships among variances of multidimensional information that shape social inclusion. Figure 4.2 shows the factor loadings that shape factor scores of the social inclusion index. Lower negative scores indicate a higher risk of being socially excluded.

### **4.3 Activity-Travel Participation, Daily Experience, Overall Subjective Well-Being on Health Conditions**

From this section, authors try to show the effect of multiple spatiotemporal variables on daily experience, overall subjective well-being, and health parameters. As discussed above the health parameters contain three definitions: physical, social and mental health. As expected multiple spatiotemporal variables such as time-use and activity participations, travel parameters, and built environment conditions have an effect on individuals' daily experience, overall well-being, and physical, social and mental health. It is shown that the fluctuation of daily experience might be occurred due to participation of different type of activities and travels on the given days.

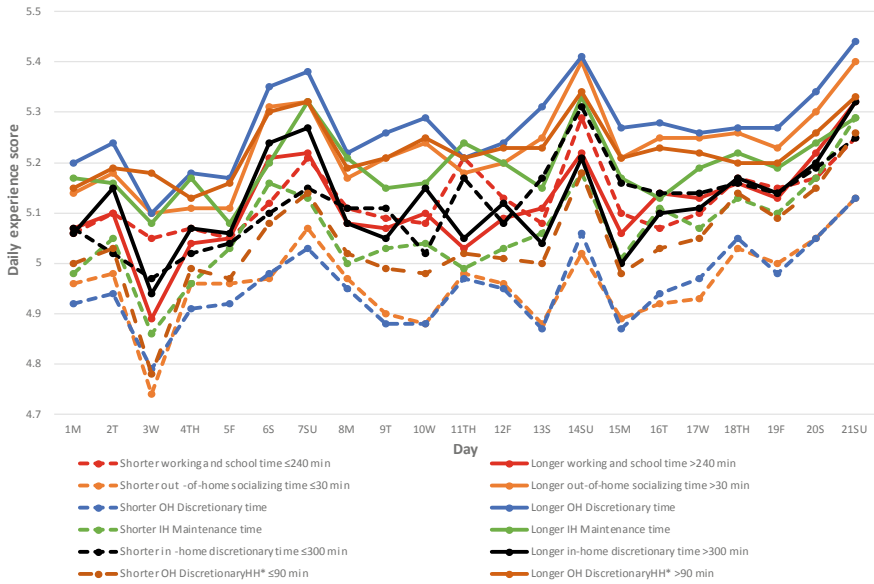
Undertaking fewer time for obligation activities such as working and studying and more time for leisure activities particularly out-of-home might be the reason why daily experience shows the highest level on weekend days. It is shown in Fig. 4.3 that travellers who undertake out-of-home discretionary and in-home

maintenance activities may correspond with better daily experience. The level of daily experience tends to be lower when someone undertakes longer working and studying time. Performing shorter working and studying may be observed to have better daily experience on weekdays. Someone who engages more trips, travel longer and resides in areas with denser population may correspond to have better daily experience than the ones who have fewer trips, shorter travel time and residing in less dense areas. Figure 4.3 also exhibits the influence of other household members' discretionary activity time-use on people's daily experience. It is shown that people who have longer time of other household members' out-of-home discretionary activities may correspond to have better daily experience. It may indicate joint discretionary activities particularly on weekdays as argued as well in previous results in developed countries [4, 76, 77] and developing country case [16, 17].

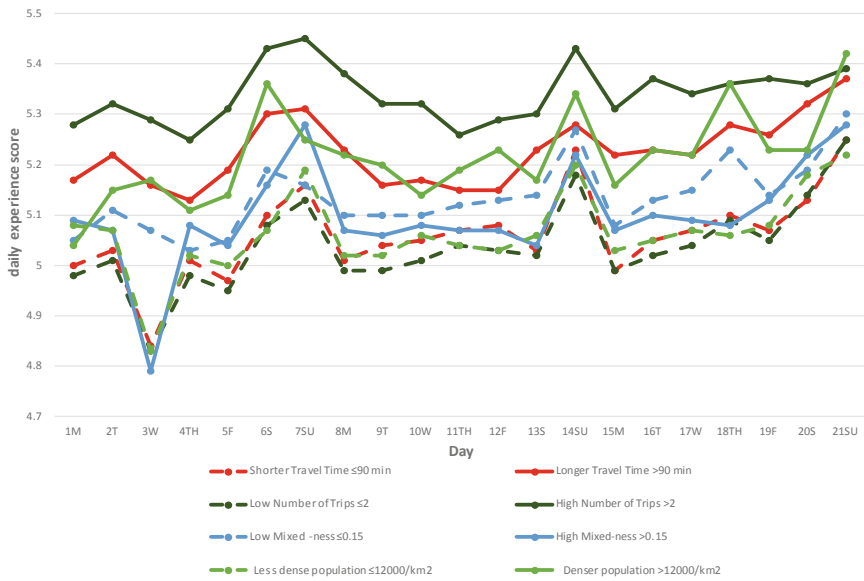
Figures 4.4, 4.5, 4.6 and 4.7 show how people tend to have different time-use and activity participation when they have different level of overall subjective well-being and health conditions. It might support argument that overall subjective well-being and health conditions are results of long-term process [39, 40]. People may do a particular set of activities with a specific configuration, may meet a specific person and/or visit particular locations as a result of a long-term process represented by long-term variables such as overall well-being, and health condition variables. Undertaking longer working and studying, out-of-home discretionary and travel time may correspond with better overall well-being as shown in Fig. 4.4. Similar result may be exhibited when someone performs shorter time to in-home discretionary activities. In term of health conditions, better physical and social health conditions may be found to correspond with longer working and studying and travel time, and shorter in-home discretionary time as shown in Figs. 4.5 and 4.6. There is no pattern of out-of-home discretionary time for physical and social health. In Fig. 4.6, having better social health may not correspond with having longer out-of-home discretionary time but having frequent out-of-home social visits within longer travel time [77–79]. However, in Fig. 4.7 better mental health conditions may correspond with a shorter time to working and studying and in-home discretionary activities, and longer travel and out-of-home discretionary time. It means that opportunities to engage with social contacts in out-of-home activities might be more related to correspond with better mental health than social health as revealed in this study.

Figures 4.4, 4.5, 4.6 and 4.7 also show the effect of other household members' activity and travel time use to overall well-being and health performance. Having a longer time of other household members' out-of-home discretionary activities may correspond with better mental health but may worsen physical and social health conditions. Moreover, having a longer time for other household members' work and school time may correspond with better overall well-being, but with worse mental health.

Different configuration in undertaking daily trips may correspond in different overall well-being conditions as shown in Table 4.2. Moreover, engaging in more trip chains (>1) may correspond with better physical and social health, whereas performing more trips within one chain may correspond opposite conditions.



(a) Time-use and activity patterns



(b) Travel patterns and built environment conditions

**Fig. 4.3** Daily self-reported well-being of individuals for various activities, travel parameters and geographical situations

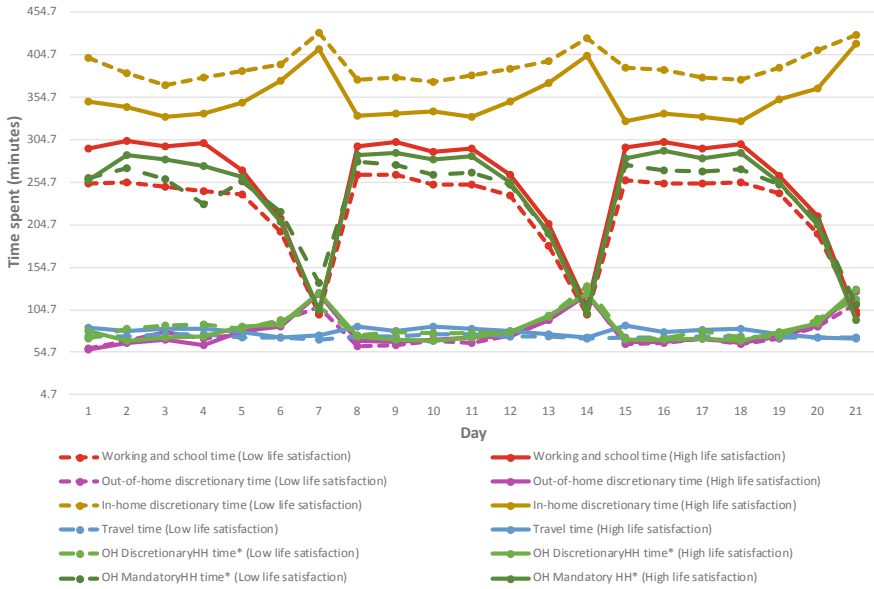


**Fig. 4.4** Daily time-use for different activities and travel of people based on their overall well-being

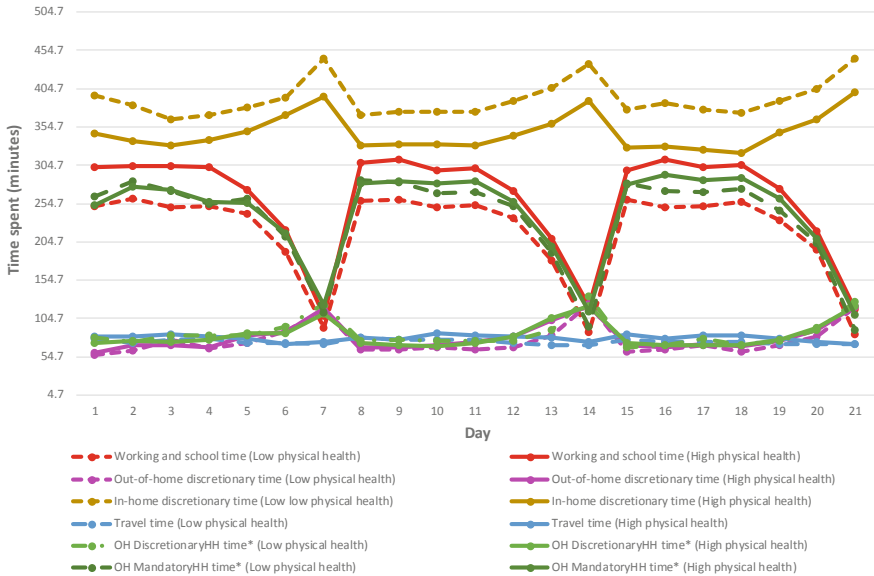


**Fig. 4.5** Daily time-use for different activities and travel of people based on their physical health

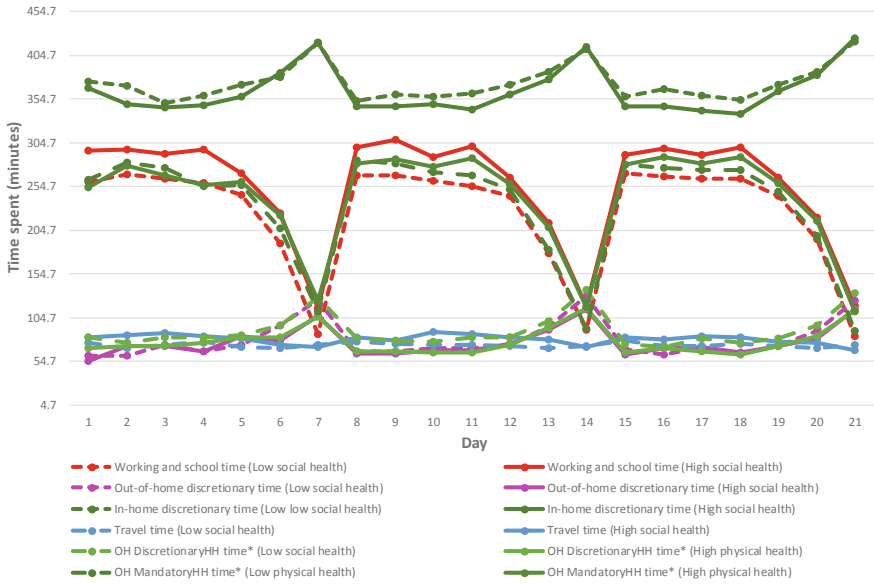


Fig. 4.6 Daily time-use for different activities and travel of people based on their social health

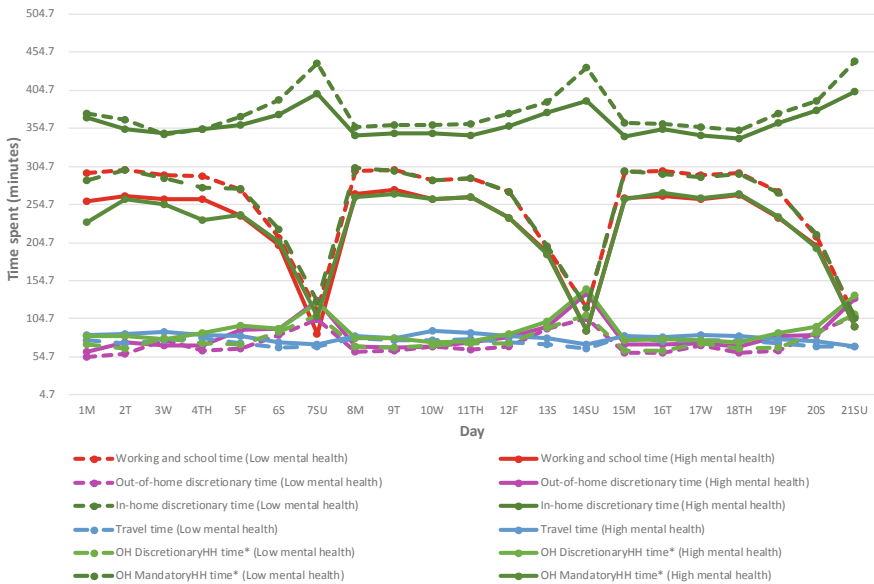


Fig. 4.7 Daily time-use for different activities and travel of people based on mental health

**Table 4.2** Daily time-use for different activities, travel parameters and geographical conditions of people based on their life satisfaction, physical health, social health, and mental health

Variables	Overall subjective well-being	Physical health	Social health	Mental health
High number of trips >2	-0.06	-0.23	-0.16	-0.12
Low number of trips $\leq 2$	0.02	-0.04	-0.11	0
High number of trip chains >1	0.05	-0.07	-0.07	-0.03
Low number of trip chains $\leq 1$	-0.04	-0.1	-0.17	-0.03
High land use diversity >0.10	-0.02	-0.19	-0.27	-0.13
Low land use diversity $\leq 0.10$	0.01	-0.01	-0.01	0.04
High population density >12,000	0.06	0.03	0.15	0.2
Low population density $\leq 12,000$	-0.04	-0.16	-0.27	-0.16
High public transport lines >2	-0.04	-0.07	-0.1	0.12
Low public transport lines $\leq 2$	0.05	-0.12	-0.15	-0.22
High daily experience >5	0.13	0.01	-0.05	0.04
Low daily experience $\leq 5$	-0.13	-0.19	-0.19	-0.11
High overall well-being >0		-0.02	-0.09	0.04
Low overall well-being $\leq 0$		-0.19	-0.17	-0.14

Undertaking more trip chains may correspond with performing a discretionary trip more often than might correspond with better physical and social health. Focus to social health, undertaking more trip chains might correspond with performing more socialising trips which may correspond with more meaningful stops trip [77, 79–81]. Particular geographical conditions might correspond with better overall well-being, but worse health indicators. For example, high land-use diversity might correspond with better health condition, but worse overall well-being. However, people who reside within denser population tend to have better health conditions and overall subjective well-being. More populated area tends to be closer with grocery store, park, shopping centre and other basic amenities whereas more diverse land use tend to be farther from public amenities. Moreover, more populated areas might also have better integration system with settlers which may correspond with positive value of mental health. The impact of daily experience on overall subjective well-being and health indicators may be linear. Having positive daily experience might correspond with positive overall well-being, and physical

and mental health conditions. The linearity of the relationship between daily experience and health conditions might be also found in the relationship between overall well-being and health indicators.

Table 4.3 displays how someone from a particular socio-demographic group may correspond with having a particular activity and travel pattern, and life satisfaction and health level. From Fig. 4.5, someone from household with 3–5 members tends to have more balanced life with balance time to do obligation (such as work and maintenance activities) and leisure activities and having longer travel time as well than the ones from other household groups. Having more balance time to do obligation and leisure activities may make someone from middle household to correspond with having better health condition than other household groups, and better life satisfaction than household with one and more than 5 members as found in research in developed country [22], and developing country [20, 35]. A couple may correspond with the best overall well-being level than other household groups, but a couple is likely to have worse physical health condition than persons from a household with more than 2 members and to have worse social and mental health than persons from household with 3–5 members. Undertaking more time spent for out-of-home socialising, in-home leisure and travel, and less time for work and maintenance activities may help people with no child to have better overall well-being and health condition than someone with a dependent child/children. Whereas, younger and employed individuals may correspond to engage with more out-of-home activity and travel time which make them have better overall well-being and health condition than senior citizen and non-worker, respectively.

#### 4.4 Activity-Travel Participation and Social Exclusion on Mental Health

Figure 4.8 exhibits the relationship between individuals' and other household members' daily work and out-of-home discretionary activity time use by different social inclusion indices of individuals. In these graphs, 'high social inclusion' refers to someone with above zero ( $>0$ ) social inclusion index, whilst low social inclusion index means someone who has a social inclusion index the same as or below zero ( $\leq 0$ ). Crucially to this paper, the ones who have better social inclusion tends to have different activity and travel participation on daily basis from the ones who have worse social inclusion. It also shows that the different arrangement of activity and travel participation on weekdays and weekends may decide the level of social inclusion of people. Moreover, the difference in socio-demographic variables may also correspond with having a low or high social inclusion index.

In Fig. 4.8, it seems that those who have better social inclusion index may correspond to undertake longer time for social and recreational activities all the time, but only for Sunday. However, the ones who have better social inclusion index tend to correspond with longer time for other household members'

**Table 4.3** Individuals' daily work and discretionary activity time-use, life satisfaction and health indicator by different socio-demographic groups

Variables	Single	Couple	Medium number Household <sup>a</sup>	High number Household <sup>a</sup>	No child	Low number of children <sup>b</sup>	High number of children <sup>b</sup>	Female	Male
Out-of-home mandatory	515.10	256.08	240.17	228.86	232.16	242.85	263.8	165.85	307.33
Out-of-home other maintenance	0	2.49	4.31	5.26	3.20	6.04	1.18	6.17	2.68
Out-of-home maintenance	17.14	132.02	145.03	147.025	120.66	179.00	173.93	235.68	59.37
Out-of-home socialising	62.86	46.47	54.08	55.95	58.80	52.00	36.81	41.68	65.04
Percentage of use motorised mode	3.81	37.38	49.59	37.29	47.00	46.23	42.86	31.6	62.74
Number of trips	2.05	2.63	2.54	2.38	3.00	2.50	2.28	2.15	2.84
Number of trip chains	1.00	1.16	1.14	1.11	1.00	1.13	0.63	1.02	1.25
Total travel time	35.71	70.69	78.66	73.67	80	75.56	61.88	55.7	95.88
In-home leisure	152.14	276.77	241	242.11	263.08	230.00	217.93	247.25	242.06
In-home maintenance	17.14	113.95	124.25	129.26	101.85	139.00	174.55	206.27	48.61
In-home discretionary activities	169.28	390.72	365.25	371.37	364.93	369.00	392.48	453.52	290.67
Overall subjective well-being	-0.37	0.08	-0.02	0.01	0.04	0	-0.12	-0.04	0.04
Physical health	-0.64	-0.36	0.05	-0.35	-0.08	0	-0.10	-0.16	-0.02
Social health	-0.43	-0.20	0.03	-0.50	-0.02	0	-0.25	-0.14	-0.10
Mental health	-0.37	-0.12	0.07	-0.26	-0.01	0	-0.33	-0.09	0.02

(continued)



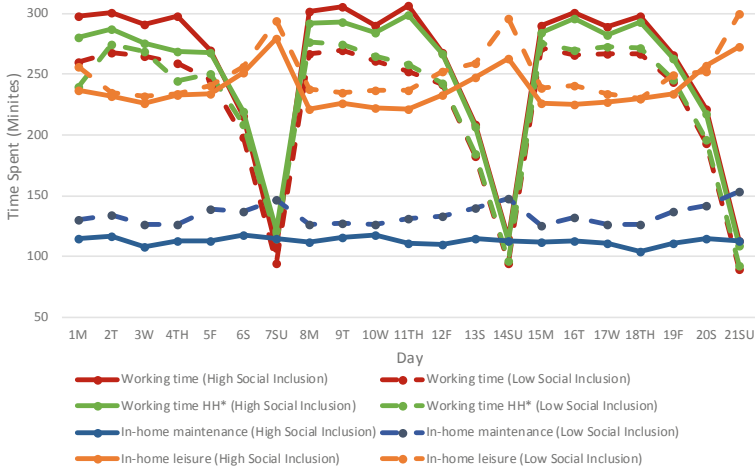
**Table 4.3** (continued)

Variables	Young persons <sup>c</sup>	Working age persons <sup>c</sup>	Senior Citizens <sup>c</sup>	Low and Middle Income	High Income	Workers and students	Non workers	CBD and suburban residents	Greater BMA residents
Out-of-home mandatory	254.42	255.05	125.02	241.01	223.34	320.72	107.99	239.12	241.21
Out-of-home other maintenance	0.82	3.60	13.45	4.66	1.26	2.19	7.85	4.72	2.12
Out-of-home maintenance	81.89	152.41	144.67	77.41	89.79	84.86	239.6	142.97	150.48
Out-of-home socialising	75.03	49.96	50.39	52.82	63.9	60.32	43.33	52.78	60.24
Percentage of use motorised mode	56.09	49.345	21.42	45.27	55.43	60.67	26.99	45.55	61.60
Number of trips	2.36	2.56	2.34	2.48	2.72	2.71	2.18	2.49	2.61
Number of trip chains	1.05	1.15	1.1	1.12	1.21	1.21	1.04	1.14	1.14
Total travel time	88.44	77.36	56.81	75.23	90.23	93.89	48.63	73.96	92.82
In-home leisure	228.45	232.44	338.77	243.23	257.74	215.56	291.39	255.15	179.11
In-home maintenance	72.52	135.39	122.69	125.94	107.86	71.11	210.27	122.51	135.35
In-home discretionary activities	300.97	367.83	461.46	369.17	365.60	286.67	501.66	377.66	314.46
Overall subjective well-being	-0.01	0.07	-0.42	0	0	0.1	-0.17	-0.03	0.16
Physical health	0.17	-0.03	-0.80	-0.09	-0.09	0.07	-0.35	-0.10	-0.03
Social health	0.03	-0.1	-0.47	-0.11	-0.27	-0.08	-0.19	-0.10	-0.24
Mental health	0.04	-0.03	-0.16	-0.03	0	0.02	-0.12	-0.05	0.08

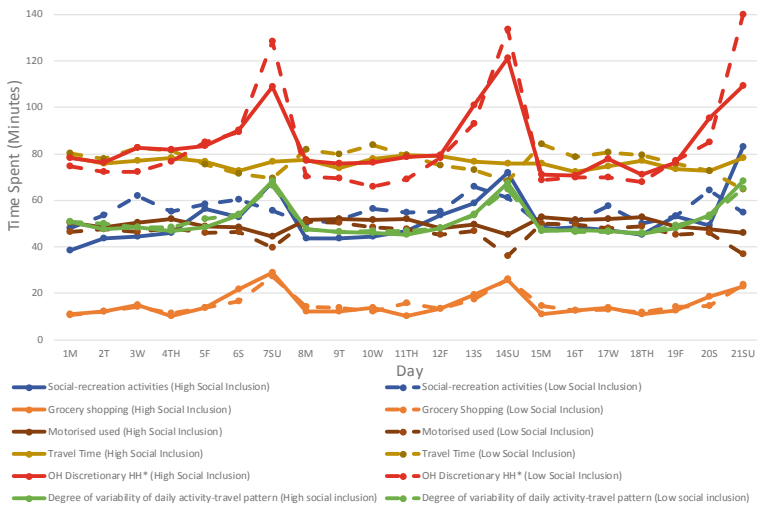
<sup>a</sup>Medium number household means households with 3-5 members in the household, whereas high number household means households with above 5 members in the household

<sup>b</sup>Low number of children means households with 1-3 dependent child/children in the household, whereas high number of children means households with above dependent children in the household

<sup>c</sup>Younger travellers are someone at age below 22 years, working-age persons are someone at age between 23 and 55 years, and senior citizens are someone at age above 55 years old



(a) Individuals' daily working and in-home discretionary time use by social inclusion index



(b) Individuals' daily and out-of-home discretionary time use and travel parameters by social inclusion index

**Fig. 4.8** Individuals' daily activity-travel pattern by social inclusion and mental health index (\*Working HH and OH discretionary HH means other household members' daily work and out-of-home discretionary activity time spent)



(c) Individuals’ daily working, in-home and out-of-home discretionary time use by mental health index

Fig. 4.8 (continued)

out-of-home discretionary activities on weekdays. Having longer other household members’ out-of-home discretionary time may indicate joint out-of-home discretionary activities on weekday time as shown as well in previous results in developed [14, 76, 82] and developing countries [16, 17]. It may mean that having better social inclusion may correspond with having longer time engagement with other household members on weekdays, then focus to do social and recreation activities on Sunday. Moreover, the ones who have more working time may also correspond with having better social inclusion condition than the ones who work shorter time. The ones who work longer time may indicate someone who has full employment and has better payment. Moreover, the ones who work longer may have higher level of interaction with others particularly in the working place (e.g. [80, 83]) and having higher social capital [84] compared to the ones who work less. The results in Fig. 4.2 also shows that someone may have a similar degree of variability of daily activity-travel pattern, but the configuration of undertaken activity and travel participation during might be more important in defining social inclusion level of someone.

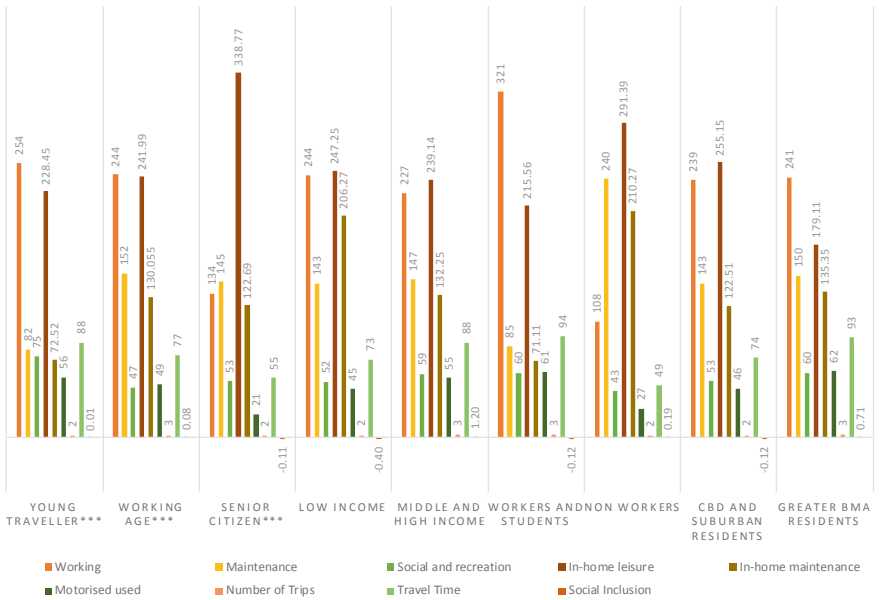
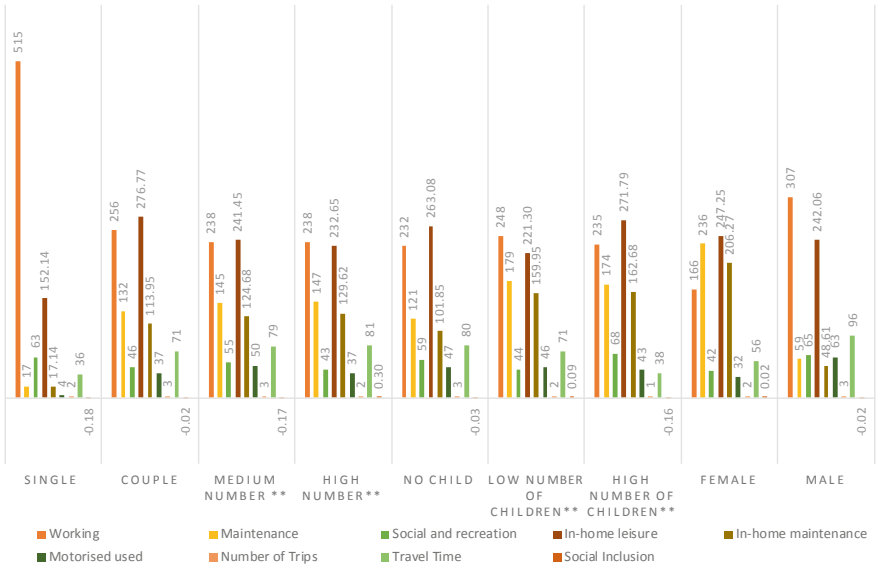
Figure 4.9 demonstrates how personal and household characteristics may correspond with having different time investments for different activity-travel behaviour on average. Socio-demographics may represent people’s various basic roles within personal, social and spatial dimensions, which may correspond with different

social inclusion indices. In Fig. 4.9, someone who has better social inclusion condition such as the ones who have high number of household members and a low number of dependent child, young-adult travellers, and workers and students tends to have balance time for working, out-of-home and in-home discretionary activities, and to correspond with longer time of other household members' out-of-home discretionary time. Someone who has 1–3 dependent child/children may only correspond with shorter time for out-of-home discretionary activities and other household members' out-of-home discretionary activities than someone with no child, but within their out-of-home discretionary time, those with a low number of dependent children may spend more hours with other household members. In addition, although senior citizens may spread their out-of-home time across various activities, they appear to have the longest time allocation for in-home discretionary activities. It seems that although they have no time pressure, they may have less social contact. Having less social contact may make senior citizens spend most of their time at home within flexible time-space constraints. This may be the reason why senior citizens correspond to having the lowest social inclusion compared to their younger counterparts [62, 72].

This section tries to explore how time-use and spatial variables may explain why someone is defined as socially included or not. Ensuring to have more social contact and have joint activities with other household members is hypothesised to correspond with positive result of social inclusion condition as indicated in previous studies in developed country context [14, 82]. It also shows that a good redistribution of performed out-of-home social and recreation activities and other household members' out-of-home discretionary time between weekdays and weekends, may correspond with positive social inclusion result. Daily activity-travel behaviour may provide a more complete picture in terms of capturing people's activity-travel participation in meaning of considering trade-off mechanism between weekdays and weekends overlooked when capturing only one-day or not including weekday-weekend observation of activity and travel participation [11–14, 20]. Moreover, personal, household, social and spatial characteristics of someone may correspond with specific activity-travel pattern as shown in Fig. 4.3. Managing daily activity-travel time-use to organise out-of-home activities particularly for having more social contacts within working, and social and recreation time, and joint activity time with other household members' might correspond with a positive result on social inclusion. However, this section only provides bivariate analysis without considering the interaction among time and space variables.

## 4.5 Summary

This study tries to show how day-to-day activity-travel participations and travel parameters may correspond with daily subjective well-being, overall well-being, and different health parameters such as physical, social and mental health in descriptive analysis. Moreover, it is also expected that different daily time-use and



◀**Fig. 4.9** Individuals' daily work and out-of-home discretionary time use, social inclusion and mental health by different socio-demographic groups. \*Working HH and OH discretionary HH means other household members' daily work and out-of-home discretionary activity time spent [\*\*'Medium number' refers to households with 3–5 members within the household, whereas 'high number' means households with more than 5 (>5) members within the household. Moreover, 'low number of children' refers to household with 1–3 dependent children, whereas 'high number of children' means households with more than 3 (>3) dependent children. \*\*\*Young and working-age travellers' mean travellers with ages between 15–22 years old and 23–55 years old, whereas 'senior citizen' means travellers with ages above 55 years old (>55 years old)]

activity-travel participations may also correspond with social inclusion and mental health. From the analysis, it is shown that, with bivariate analysis, day-to-day activity and travel patterns tend to have a correlation with daily experience and overall well-being, and different health parameters. Different daily activity and travel patterns tend to correspond with different social inclusion and mental health conditions. However, previous studies showed that with more advanced models the correlation between time-use and activity-travel participations and health parameters are not straight forward [19, 20, 22]. Few variables such as overall well-being and social inclusion may mediate the relationship between daily time-use and activity participations, and health parameters.

Some studies argued that overall well-being might mediate the relationship between time-use and activity-travel participations. People tend to try to maintain their specific life domain such as family, social and leisure domains on a particular level by undertaking specific activities on a daily level in which correspond with better overall well-being [85, 86]. The efforts of maintaining the specific life domains on particular level might also represent how people try to satisfy their needs and desires on higher level such as love needs as argued by Maslow [85]. Moreover, the positive well-being has been described as an important component of mental health [87–91] or the absence of depression [92]. Moreover, people with positive subjective well-being report better physical health and fewer unpleasant physical symptoms [93–95]. Positive well-being was also found to shape more often social activities [90, 96, 97]. It means that there is a possibility that someone with better overall subjective well-being has better social health as well. Therefore, in travel behaviour research overall subjective well-being has been argued to mediate the relationship between time-use and activity-travel participation on daily level with various health conditions [29].

In addition, previous studies have uncovered the complex relationship between activity-travel pattern and mental health [19, 21, 22, 29]. However, some studies have revealed the link between social exclusion with mental health mostly in developed countries [68, 98–100]. Previous studies used limited definition of social exclusion as determinants of mental health such as social support and meaningful time-use [98], loneliness [100] and neighbourhood condition in social meaning [101]. Stanley et al. [31] revealed the correlation between reducing the risk of social exclusion with well-being. Well-being might refer to a broader aspect of mental health which not only includes the existence of mental illness which is different

from mental health [29]. Transport-related social exclusion is assumed to involve multidimensional factors of social participation such as the degree of integration with society, connection with various social networks in term of time spent for socialising and political activities, number of performed trips/discretionary trips and total travel time spent, and whether someone has adequate access to various access to basic public amenities in geographical and non-geographical manners. Transport-related social exclusion will extend the meaning of ‘loneliness’ and taking solitary informal activities [100], social support [98], and residing in a better neighbourhood [101]. Moreover, transport-related social exclusion is assumed to carry time-space information such as life stage, household size, the degree of dependent children, undertaken activities and travels, type of travel mode, built environment condition in geographical and social meaning, and the degree of variability daily activity-travel pattern on multiple days. Therefore, transport-related social exclusion is hypothesised to be a proxy of activity-travel pattern in linking with mental health.

This study encourages to investigate the relationship between time-use and activity-travel participation and multiple health parameters mediated by overall well-being and transport-related social inclusion index. More advanced models such as Structural Equation Modelling (SEM) can be used to explore the relationships. Moreover, to include the nested observations of individuals’ activity and travel patterns, modification of SEM with using a hierarchical Structural Equation Modelling (SEM) can be utilised as well [102, 103]. A hierarchical SEM combines structural equation modelling and multilevel modelling. Multilevel modelling is a model that can include nested observations of individuals’ activity and travel patterns such as daily observations and other household members’ activity-travel pattern variations. Those variations have been shown by research to contribute to a better picture of individuals’ daily activity-travel pattern. Due to different needs and constraints on a different day, people do different activity and travel participation on a different day. Moreover, the difference in daily activity-travel patterns is also influenced by variations of other household members’ activity-travel patterns.

## References

1. M. Fox, Transport planning and the human activity approach. *J. Transp. Geogr.* **3**(2), 105–116 (1995)
2. B. Flyvberg, M.K.S. Holm, S.L. Buhl, How in(accurate) are demand forecasts in public work projects? The case of transportation. *J. Am. Plan. Assoc.* **71**(2), 131–146 (2005)
3. M. Senbil, R. Kitamura, The optimal duration for a travel survey: empirical observations. *IATSS Res.* **33**(2), 54–61 (2009)
4. M.G. McNally, in *The Four Step Model in Handbook of Transport Modelling*, ed. by D.A. Hensher, K.J. Button, pp. 35–52 (2000)
5. T. Hägerstrand, What about people in regional sciences? *Reg. Sci. Assoc.* **247**(21) (1970)
6. H.J.A. Miller, Measurement theory for time geography. *J. Geogr. Anal.* **37**, 17–45 (2005)
7. T. Neutens, T. Schwanen, F. Witlox, The prism of everyday life: towards a new research agenda for time geography. *Transp. Rev.* **31**(1), 25–47 (2011)

8. R. Schlich, K.W. Axhausen, Habitual travel behaviour: evidence from a six-week travel diary. *Transportation* **30**, 13–36 (2003)
9. M. Chikaraishi, A. Fujiwara, J. Zhang, K.W. Axhausen, D. Zumkeller, Changes in variations of travel time expenditure: some methodological considerations and empirical results from German mobility panel. *Transp. Res. Rec.* **2230**, 121–131 (2011)
10. C. Raux, T.Y. Ma, E. Cornelis, Variability versus stability in daily travel and activity behaviour: the case of a one week travel diary (2011). Available on line at [https://halshs.archives-ouvertes.fr/file/index/docid/612610/filename/Raux\\_et\\_al\\_Variability\\_vs\\_stability.pdf](https://halshs.archives-ouvertes.fr/file/index/docid/612610/filename/Raux_et_al_Variability_vs_stability.pdf)
11. A. Moiseeva, H.J.P. Timmermans, J. Choi, C.H. Joh, Sequence alignment analysis of activity-travel pattern's variability using eight weeks' diary data. *Transp. Res. Record* **2412**, 49–56 (2014)
12. Y.O. Susilo, K.W. Axhausen, Stability in individual daily activity-travel-location patterns: a study using the Herfindahl-Hirschman Index. *Transportation* **41**, 995–1011 (2014)
13. Y.O. Susilo, R. Kitamura, An analysis of the day-to-day variability in an individual's action space: exploration of 6-week Mobidrive travel diary data. *Transp. Res. Rec.* **1902**, 124–133 (2005)
14. H. Kang, D.M. Scott, Exploring day-to-day variability in time use for household members. *Transp. Res. Part A* **44**, 609–619 (2010)
15. L.P. Kostyniuk, R. Kitamura, Life cycle and household time-space paths: empirical investigation. *Transp. Res. Rec.* **879**, 28–37 (1982)
16. D.B.E. Dharmowijoyo, Y.O. Susilo, A. Karlström, Relationships among discretionary activity duration, travel time spent and activity space indices in the Jakarta Metropolitan Area, Indonesia. *J. Transp. Geogr.* **54**, 148–160 (2016)
17. C. Liu, Y.O. Susilo, D.B.E. Dharmowijoyo, Investigating intra-household interactions between individuals' time and space constraints. *J. Transp. Geogr.* **73**, 108–119 (2018)
18. R.D. Putnam, *Bowling Alone: The Collapse and Revival of American Community* (Simon and Schuster, New York, 2001)
19. J. Zhang, Urban forms and health promotion: an evaluation based on health-related QOL indicators. 13th World Conference on Transport Research (WCTR), 2013
20. D.B.E. Dharmowijoyo, Y.O. Susilo, A. Karlström, Collecting a multidimensional three-weeks household time-use and activity diary in the Bandung Metropolitan Area. *Transp. Res. Part A* **80**, 231–246 (2015)
21. E. Hunt, E. McKay, I. Perry, Measuring and mapping adolescent time use and wellbeing—an occupational perspective. International Association of Time Use Research 33rd Annual Conference, 1–3 August: Abstracts (IATUR, Oxford, 2011). Available at: <http://iatur2011.timeuse.org/files/iatur2011/FINAL%20abstracts%20for%20programme.pdf>. Accessed 21 Sept 12
22. E. Hunt, E. McKay, D.L. Dahly, A.P. Fitzgerald, I.J. Perry, A person-centred analysis of the time use, daily activities, and health related quality of life of Irish school-going late adolescent. *Qual. Life Res.* **24**, 1303–1315 (2015)
23. J.N. Morris, A.E. Hardman, Walking to health. *Sports Med.* **23**(5), 306–332 (1997)
24. P. Oja, I. Vuori, O. Paronen, Daily walking and cycling to work: their utility as health-enhancing physical activity. *Patient Educ. Couns.* **33**, S87–S94 (1998)
25. F.B. Hu, M.J. Stampfer, G.A. Colditz, A. Ascherio, K.M. Rexrode, W.C. Willett, J.E. Manson, Physical activity and risk of stroke in women. *J. Am. Med. Assoc.* **283**(22), 2961–2967 (2000)
26. A. Wagner, C. Simon, P. Ducimetière, M. Montaye, V. Bongard, J. Yarnell, D. Arveiler, Leisure-time physical activity and regular walking or cycling to work are associated with adiposity and 5 y weight gain in middle-aged men: the PRIME study. *Int. J. Obes.* **25**(7), 940–948 (2001)
27. J.E. Manson, P. Greenland, A.Z. LaCroix, M.L. Stefanick, C.P. Mouton, A. Oberman, D.S. Siscovick, Walking compared with vigorous exercise for the prevention of cardiovascular events in women. *N. Engl. J. Med.* **347**(10), 716–725 (2002)



28. S. Handy, in *Health and travel in Handbook of Sustainable Travel Gärling*, ed. by T. Ettema, D. Friman (Springer, Dordrecht/Heidelberg/New York/London, 2014)
29. B. van Wee, D. Ettema, Travel behaviour and health: a conceptual model and research agenda. *J. Transp. Health* **3**(3), 240–248 (2016)
30. M. Marmot, The social environment and health. *Clin. Med.* **5**(3), 244–248 (2005)
31. J.K. Stanley, D.A. Hensher, J.R. Stanley, D. Vella-Bodrick, Mobility, social exclusion and subjective well-being: exploring the links. *Transp. Res. Part A* **45**(8), 789–801 (2011)
32. M. Pantell, D. Rehkopf, D. Jutte, S.L. Syme, J. Balmes, N. Adler, Social isolation: a predictor of mortality comparable to traditional clinical risk factors. *J. Publ. Health* **103**(11), 2056–2062 (2013)
33. S.M. Mohnen, B. Völker, H. Flap, S.V. Subramanian, P.P. Groenewegen, The influence of social capital on individual health: is it the neighbourhood or the network? *Soc. Indic. Res.* **1–20** (2014)
34. M. Choi, M. Mesa-Frias, E. Nüesch, J. Hargreaves, D. Prieto-Merino, A. Bowling, J. P. Casas, Social capital, mortality, cardiovascular events and cancer: a systematic review of prospective studies. *Int. J. Epidemiol.* **43**(6), 1895–1920 (2014)
35. D.B.E. Dharmowijoyo, Y.O., Susilo, A. Karlström, A., Analysing the complexity of day-to-day individual activity-travel patterns using a multidimensional sequence alignment model. *J. Transp. Geogr.* **64**, 1–12 (2017)
36. World Health Organization, *Reducing Risks: Promoting Healthy Life: World Health Report 2002* (World Health Organization, Geneva)
37. Y. Suzukamo, S. Fukuhara, J. Green, M. Kosinski, B. Gandek, J.E. Ware, Validation testing of three-component model of Short Form-36 scores. *J. Clin. Epidemiol.* **64**, 301–308 (2011)
38. D. Kahneman, A.B. Krueger, D.A. Schkade, N. Schwarz, A. Stone, A survey method for characterizing day life experience: the day reconstruction method. *Science* **306**(5702), 1776–1780 (2004)
39. T. Schwanen, D. Wang, Well-being, context and everyday activities in space and time. *Ann. Assoc. Am. Geogr.* **104**(4), 833–851 (2014)
40. A. Pred, Structuration and place: on the becoming of sense of place and structure of feeling. *J. Theor. Soc. Behav.* **12**(1), 45–68 (1983)
41. Y.O. Susilo, T.B. Joewono, W. Santosa, W., An exploration of public transport users' attitudes and preferences towards various policies in Indonesia. *J. East. Asia Soc. Transp. Stud.* **8**, 1202–1216 (2010)
42. S.D. Arifwidodo, Exploring the effect of compact development policy to urban quality of life in Bandung. *City Cult. Soc.* **3**, 303–311 (2012)
43. A.K.M. Tarigan, S. Sagala, D.A.A. Samsura, D.F. Fisabilillah, H.A. Simarmata, M. Nababan, Bandung City, *Indonesia Cities* **50**, 100–110 (2016)
44. D.B.E. Dharmowijoyo, Y.O. Susilo, A. Karlström, Day-to-day inter- and intra-personal variability of individuals' activity spaces in a developing country. *Environ. Plan. B* **41**, 1063–1076 (2014)
45. T.B. Joewono, H. Kubota, User perception of private paratransit operation in Indonesia. *J. Publ. Transp.* **10**(4), 99–118 (2007)
46. T.B. Joewono, H. Kubota, User satisfaction with paratransit in competition with motorization in Indonesia: anticipation of future implications. *Transportation* **34**(3), 337–354 (2007)
47. D.B.E. Dharmowijoyo, The complexity and variability of individuals' activity-travel patterns in Indonesia. Doctoral Thesis at KTH Royal Institute of Technology
48. I.G. Cullen, V. Godson, Urban networks: the structure of activity patterns. *Progr. Plan.* **4**, 1–96 (1975)
49. T. Schwanen, M.P. Kwan, F. Ren, How fixed is fixed? Gendered rigidity of space-time constraints and geographies of everyday activities. *Geoforum* **39**, 2109–2121 (2008)
50. G. Akar, K.J. Clifton, S.T. Doherty, Discretionary activity location choice: in-home or out-of-home. *Transportation* **38**, 101–122 (2011)

51. S. Kenyon, G. Lyons, Introducing multitasking to the study of travel and ICT. *Transp. Res. Part A* **41**, 161–175 (2007)
52. G. Circella, P.I. Mokhtarian, L.K. Poff, A conceptual typology of multitasking behaviour and polichronicity preferences. *Intl. J. Time Use Res.* **9**(1), 59–107 (2012)
53. D. Ettema, T. Gärling, L.E. Olsson, M. Friman, M. Out-of-home activities, daily travel and subjective well-being. *Urban Geogr.* **32**(6), 871–883 (2010)
54. E. Diener, *The Science of Well-Being: The Collected Works of Ed Diener*, vol. 1. (Kluwer, Dordrecht, 2009)
55. J. De Vos, T. Schwanen, V. Van Acker, F. Witlox, Travel and subjective well-being: A focus on findings, methods and future research needs. *Transp. Rev.* **33**(4), 421–442 (2013)
56. J.A. Russell, A circumplex model of affect. *J. Pers. Soc. Psychol.* **39**(6), 1161–1187 (1980)
57. J.A. Russell, Core affect and the psychological construction of emotion. *Psychol. Rev.* **110** (1), 145–172 (2003)
58. E. Diener, E.A. Emmons, R.J. Larsen, S. Griffen, The satisfaction with life scale. *J. Pers. Assess.* **49**, 71–75 (1985)
59. M. Friman, T. Gärling, D. Ettema, L.E. Olsson, How does travel affect emotional well-being and life satisfaction? *Transp. Res. Part A* **106**, 170–180 (2017)
60. V. Skirbekk, Age and individual productivity. Working papers of the Max Planck Institute for demographic research
61. S. Kenyon, G. Lyons, J. Rafferty, Transport and social exclusion: investigating the possibility of promoting inclusion through virtual mobility. *J. Transp. Geogr.* **10**, 207–219 (2002)
62. K. Lucas, Transport and social exclusion: where are we now? *Transp. Policy* **20**, 105–113 (2012)
63. S. Schönfelder, K.W. Axhausen, Activity spaces: measures of social exclusion? *Transp. Policy* **10**(4), 273–286 (2003)
64. Md Kamruzzaman, J. Hine, Analysis of rural activity space and transport disadvantage using a multi-method approach. *J. Transp. Geogr.* **19**, 105–120 (2012)
65. A. Páez, R.G. Mercado, S. Farber, C. Morency, M. Roorda, *Mobility and Social Exclusion in Canadian Communities: An Empirical Investigation of Opportunity Access and Deprivation from the Perspective of Vulnerable Groups* (Policy Research Directorate Strategic Policy and Research, Toronto, Canada, 2009)
66. A. Páez, R.G. Mercado, S. Farber, C. Morency, M. Roorda, Relative Accessibility Deprivation Indicators for Urban Settings: Definition and Application to Food Deserts in Montreal. *Urb. Stud.* **47**(7), 1415–1438 (2010)
67. Department for Transport, National Travel Survey, Available from <https://www.gov.uk/government/collections/national-travel-survey-statistics> (2014)
68. R.L. Macket, R. Thoreau, Transport, social exclusion and health. *J. Transp. Health* **2**, 610–617 (2015)
69. D.O. Hernandez, H. Titheridge, Mobilities of the periphery: informality, access, and social exclusion in the urban fringe in Columbia. *J. Transp. Geogr.* **55**, 152–164 (2016)
70. S. Özkazanç, F.N.Ö. Sönmez, Spatial analysis of social exclusion from a transportation perspective: a case study of Ankara metropolitan area. *Cities* **67**, 74–84 (2017)
71. A. Church, M. Frost, K. Sullivan, Transport and social exclusion in London. *Transp. Policy* **7**, 195–205 (2000)
72. J.C. Vrooman, S.J.M. Hoff, The disadvantaged among the Dutch: a survey approach to the multidimensional measurement of social exclusion. *Soc. Indic. Res.* **113**, 1261–1287 (2013)
73. J. Hair, R. Anderson, R. Tatham, W. Black, *Multivariate Data Analysis*, 5th edn. (Prentice Hall, Englewood Cliffs, 1998)
74. J. Anable, ‘Complacent car addicts’ or ‘aspiring environmentalists’ identifying travel behaviour segments using attitude theory. *Transp. Policy* **12**, 65–78 (2005)

75. G. DiStefano, M. Peteraf, G. Verona, Dynamic capabilities deconstructed: a bibliographic investigation into the origins, development, and future directions of the research domain. *Ind. Corp. Change* **19**, 1187–1204 (2011)
76. H. Kang, D.M. Scott, D.T. Doherty, An investigation of planning priority of joint activities in the household activity scheduling process. *Transp. Res. Rec.* **2134**, 82–88 (2009)
77. P.L. Mokhtarian, Travel as a desired end, not just a means. *Transp. Res. Part A* **39**, 93–96 (2005)
78. R. Kitamura, Y.O. Susilo, Does a grande latte really stir up gridlock? Stops in commute journeys and incremental travel. *Transp. Res. Record* **198–206**, 2006 (1985)
79. J. Jain, G. Lyons, The gift of travel time. *J. Transp. Geogr.* **16**(2), 81–89 (2008)
80. D.B.E. Dharmowijoyo, Y.O. Susilo, A.K.M. Tarigan, T. Joewono, Multitasking activities and daily subjective well-being. Submitted to *Transportation Research Part A*, 2019
81. M. Rizki, T. Joewono, D.B.E. Dharmowijoyo, P.F. Belgiawan, Multiple multitasking activities during travel and travel usefulness in Bandung Metropolitan Area. Submitted to *Transportation* (2019)
82. Y.O. Susilo, A. Avineri, The impacts of household structure to the day-to-day variability of individual and household stochastic travel time budget. *J. Adv. Transp.* **48**, 454–470 (2017)
83. C.D. Ryff, Happiness is everything, or is it? Explorations of the meaning of psychological well-being. *J. Pers. Soc. Psychol.* **52**(6), 1069–1081 (1989)
84. J.F. Helliwell, R.D. Putnam, The social context of well-being. *Philos. Trans. R. Soc. Lond. Ser. B Biol. Sci.* **359**(1449), 1435–1446 (2004)
85. A.H. Maslow, *Motivation and Personality* (Harper & Row, New York, 1970)
86. S. Oishi, E.F. Diener, E.M. Suh, R.E. Lucas, Value as a moderator in subjective well-being. *J. Pers.* **67**(1), 158–184 (1999)
87. M. Jahoda, *Current Concepts of Positive Mental Health* (Basic Book, New York, 1958)
88. E. Diener, M.E.P. Seligman, Very happy people. *Psychol. Sci.* **13**, 81–84 (2002)
89. S. Cohen, W.J. Doyle, T.B. Turner, C.M. Alper, D.P. Skoner, Emotional style and susceptibility to the common cold. *Psychosom. Med.* **65**, 652–657 (2003)
90. S. Lyubomirsky, L. King, E. Deiner, The benefits of frequent positive affect: does happiness lead to success? *Psychol. Bull.* **131**, 803–855 (2005)
91. E. Diener, M.Y. Chan, Happy people live longer. *Health Well-Being* **3**(1), 1–43 (2011)
92. E.C. Chang, A.S. Farrehi, Optimism/pessimism and information-processing styles: can their influences be distinguished in predicting psychological adjustment. *Pers. Individ. Differ.* **31**, 555–562 (2011)
93. M. Pinqart, S. Sorensen, Influence of socioeconomic status, social network, and competence on subjective well-being in later life: a meta-analysis. *Psychol. Aging* **15**, 187–224 (2000)
94. D.K. Mroczek, A. Spiro, Change in life satisfaction during adulthood: findings from the veterans' affairs normative aging study. *J. Pers. Soc. Psychol.* **88**, 189–202 (2005)
95. M. Standage, F.B. Gillison, N. Ntoumanis, D.C. Treasure, Predicting students' physical activity and health-related well-being: a prospective cross-domain investigation of motivation across school physical education and exercise settings. *J. Sport Exerc. Psychol.* **34**(1), 37–60 (2012)
96. S. Mishra, Leisure activities and life satisfaction in old age: a case study of retired government employees living in urban areas. *Act. Adapt. Aging* **16**, 7–26 (1992)
97. R.E. Lucas, Pleasant affect and sociability: Towards a comprehensive model of extraverted feelings and behaviors. *Dissertation Abstracts International*, vol. 61, no. 10-B, p. 5610. (UMI No. AA19990068)
98. J.N. Scanlan, A.C. Bundy, L.R. Matthews, Investigating the relationship between meaningful time use and health in 18 to 25-year-old unemployed people in New South Wales, Australia. *J. Commun. Appl. Soc. Psychol.* **20**, 232–247 (2010)

99. S. Boniface, R. Scantlebury, S.J. Watkins, J.S. Mindell, Health implications of transport: evidence of effects of transport on social interactions. *J. Transp. Health* **2**, 441–446 (2015)
100. I. Shergold, Taking part in activities, an exploration of the role of discretionary travel in older people's well-being. *J. Transp. Health* **12**, 195–205 (2019)
101. M. Tajalli, A. Hajbabaie, On the relationships between commuting mode and public health. *J. Transp. Health* **4**, 267–277 (2017)
102. D.B.E. Dharmowijoyo, Y.O. Susilo, A. Karlström, The day-to-day variability in travellers' activity-travel patterns in the Jakarta Metropolitan Area. *Transportation* **43**(4), 601–621 (2016)
103. D.B.E. Dharmowijoyo, Y.O. Susilo, A. Karlström, On complexity and variability of individuals' discretionary activities. *Transportation* **45**(1), 177–204 (2018)

# Chapter 5

## Water in Diesel Emulsion Behavior in High-Pressure Direct Injection System



A. Rashid A. Aziz, Mhadi A. Ismael, Morgan Heikal, Firmansyah, Ibrahim B. Dalha and Ezrann Zharif Zainal Abidin

This chapter describes the approaches used in micro-explosion studies, fundamentals of the micro-explosion processes, and the main factors influencing the micro-explosion behavior. Moreover, this chapter briefly discussed the effect of injection equipment on the dispersed water droplets size and the results related to their micro-explosion behavior.

### 5.1 Introduction

Water-in-diesel emulsions potentially favor the occurrence of micro-explosions when exposed to elevated temperatures, thereby improving the mixing of fuels with the ambient gas. Different methods have been proposed to classify the use of water in the engine cylinder, including through injection into the intake manifold [1], an injection of water into the cylinder [2, 3], and emulsification of water and diesel prior to injection into the chamber [4]. Different methods have been implemented to introduce water into the engine cylinder, as illustrated in Fig. 5.1.

However, there is a growing body of literature that recognizes the presence of water as emulsified diesel fuel reduces harmful emissions, while simultaneously improving the combustion process. The emulsion is formed from immiscible liquids, the oil (continuous phase) and water droplets (disperse phase) being tied together with the aid of chemical additives—so-called surfactants [5]. The emulsions can be classified into two types: water-in-oil emulsion (W/O) and oil-in-water emulsion (O/W). Figure 5.2 illustrates the two-phase emulsions. The stability mechanisms of those emulsions are quite different. In the case of O/W emulsions,

---

A. R. A. Aziz · M. A. Ismael (✉) · M. Heikal · Firmansyah · I. B. Dalha · E. Z. Z. Abidin  
Centre for Automotive Research and Electric Mobility, Universiti Teknologi PETRONAS,  
32610 Seri Iskandar, Perak, Malaysia  
e-mail: [mhadi\\_g03348@utp.edu.my](mailto:mhadi_g03348@utp.edu.my)

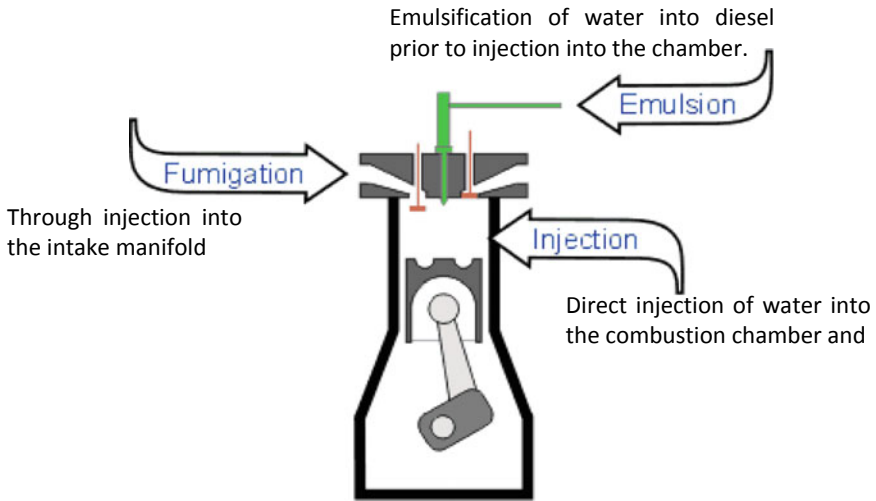
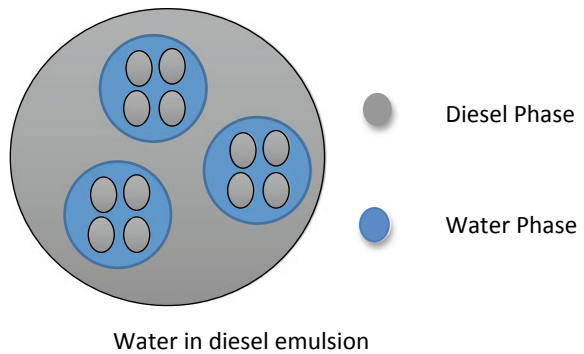


**Fig. 5.1** Water addition methods

**Fig. 5.2** Concept of oil-in-water-in-oil and water-in-oil-in-water emulsions



both steric and electrostatic repulsions are used, however, only steric forces are expected to stabilize the emulsion in the case of W/O, because of the low electrical conductivity of the continuous phase [6]. Furthermore, the emulsion can be characterized into two types based on the emulsification phases, namely two- and three-phase emulsions. In case of two-phase emulsion (O/W), a small quantity of oil is dispersed in a large volume of water, whereas in W/O emulsion, the oil and water are reversed. The O/W emulsion is generally used in pharmaceutical, food, cosmetics and such other areas whereas W/O is considered as an alternative to diesel [7, 8].

With water-in-diesel emulsion, the vaporization of water during the spray causes a reduction of NO<sub>x</sub> emission [9], while secondary atomization improves the combustion process due to better air-fuel mixing [10]. For the secondary atomization of emulsions, both micro-explosion and puffing are the key factors that

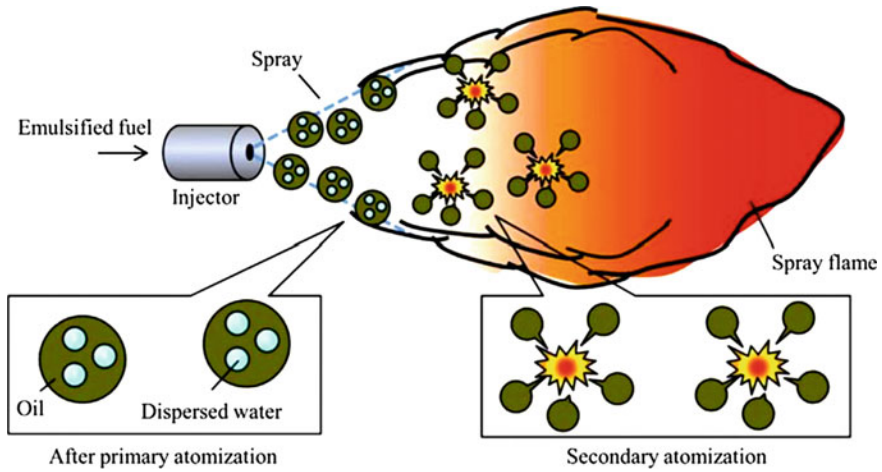


**Fig. 5.3** Schematic of the occurrence of micro-explosion process

influence the fuel mixing process. Micro-explosion is when droplets burst into smaller droplets due to explosive boiling of the dispersed water inside a continuous oil phase (immiscibility and different volatility of the two liquid components) which causes the disruption of the parent drops and, hence, secondary atomization. Puffing is when water droplets (or vapor) erupt from the surface of the parent droplet without its complete breakup. Figure 5.3 shows a schematic diagram of how the micro-explosion process enhances the secondary atomization.

A considerable amount of literature has been published on micro-explosion and puffing using single droplet experiments [11]. These studies have confirmed that large isolated droplets of emulsified fuel lead to puffing and/or micro-explosion, with their occurrences depending on several factors. The coalescence and phase separation of emulsions are among the most important factors. Other factors include the type and amount of surfactant, water content in the emulsion and the size of the dispersed water droplets. A higher surfactant content was found to delay the micro-explosion occurrences [12], while in contrast, the increase of water content in the emulsion was found to decrease the emulsion stability and enhance the intensity of micro-explosion [13]. The optimum water concentration in the emulsion was found to be 10% [14]. The intensity of micro-explosion was found to be higher with dispersed water droplet sizes larger than 10  $\mu\text{m}$  [15]. However, with a reduction in the dispersed water droplets size to 2  $\mu\text{m}$ , the temperature required for micro-explosion increased [26]. The dispersed droplet size was functioning optimally at 4.7  $\mu\text{m}$  [16]. The increase in the breakup rate caused by mechanical stirrers results in smaller droplet sizes [15], whilst in larger droplet sizes, the coalescence rate of dispersed phase increased.

To control the secondary atomization of water-in-diesel emulsion it is essential to control the sizes and numbers of the dispersed phase. It should be noted that the emerging emulsions from the injector nozzle are significantly different compared

with the unused fuel in the tank [17]. Therefore, in order to control the micro-explosion of emulsified fuels, it is essential to control the water content, number, and size distributions of the dispersed phase after the injection system.

The objective of this work is to address the effect of injection pressure on the distribution of water dispersed phase and micro-explosion behavior. This article begins by describing the emulsion preparation and then characterizes the emulsion characteristics after it is pumped through a common rail system. It then goes on to examine the spray of the pumped emulsions (10% water concentration at injection pressures of 500, 1000, and 1500 bar) into a high-temperature gas environment and the puffing and/or micro-explosion of the droplets were visualized.

## 5.2 Experimental Method

The experiments started with water-in-diesel emulsion preparation. The emulsions were characterized at different injection pressures, which is described in Sect. 5.2.3. The collected samples from the spray were tested under Leidenfrost conditions and the droplets' micro-explosion behavior was visualized using high-speed video recordings (Sect. 5.2.4) and freely falling droplets (Sect. 5.2.5).

### 5.2.1 *Emulsion Preparation and Stability*

A Span 80 (a lipophilic surfactant) with a hydrophilic–lipophilic balance (HLB) of 4.3 was used as the emulsifying agent to prepare 10% (v/v) water-in-diesel emulsion. A gravitational method [18–20] was used to characterize the stability of the emulsion. For this purpose, a mechanical stirrer running at 1000 rpm for 10 min was used to blend the emulsion, which was then stored in cylindrical tubs. Then, the de-emulsifications of the blends were recorded at different times and the separation of the layer. For the first 4 h, the emulsion was stable; it then exhibited some de-emulsification after this time. However, a complete separation was observed after three days.

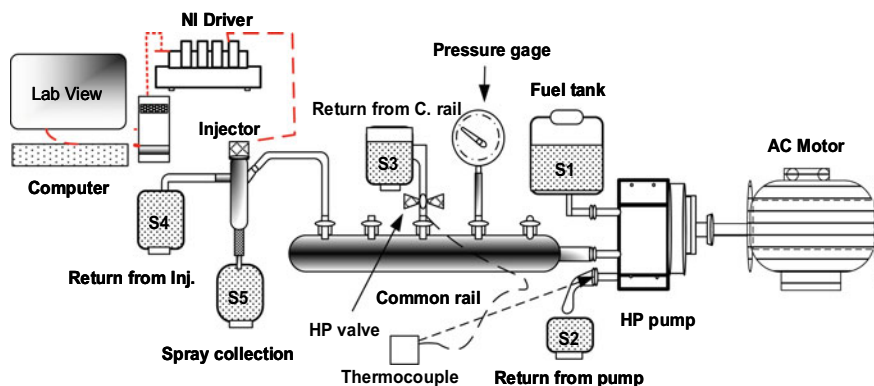
### 5.2.2 *Physical Properties*

The viscosity and density of the neat diesel and emulsions were measured using a Lovis 2000 M viscometer (Anton Paar, Graz, Austria) and an Anton Paar density meter (DMA 4500 M). The pendant drop method (OCA 15EC, Data Physics, Graz, Austria) and isoperibol calorimeter (AC-350, Leco, Graz, Austria) were used to measure the surface tension and calorific value. The properties of all fuels tested are shown in Table 5.1.



**Table 5.1** Properties of neat diesel and water-in-diesel emulsions

Water content (%v/v)	0 (Neat diesel)	5	10	15
Density at 25 °C (kg/m <sup>3</sup> )	825	841	850	858
Viscosity at 40 °C (mm <sup>2</sup> /s)	3.21	5.06	8.33	9.35
Calorific value (MJ/kg)	43.20	42.09	39.25	36.30
Surface tension (N m)	27.1	32.1	31.3	26.6

**Fig. 5.4** Schematic of the experimental setup

### 5.2.3 Fuel Injection System

A high-pressure injector (solenoid valve servo-actuated injector, Denso (Tokyo, Japan), with a 6-hole nozzle and orifice diameter of 0.2 mm) was used to spray the emulsions. The experimental setup used in the present study is the same as that of the authors' previous work [21]. This injection system provided flexibility in controlling the injection timing, injection duration, and the rail pressure. Different injection pressures were used while the injection duration was kept constant at 3 ms for all the experiments. The schematic of the experimental setup is shown in Fig. 5.4.

### 5.2.4 Hot Plate Technique

The experimental set-up used in this study was the same as the previous study by Khan et al. [22] and is shown in Fig. 5.5. A high-speed camera (8001-Phantom Miro M310, Wayne, New Jersey 07470 USA, USA) coupled with high long-distance Microscope-K2 (Boulder, Colorado, USA), a Type-K thermocouple and data logger were synchronized to evaluate the micro-explosion event and

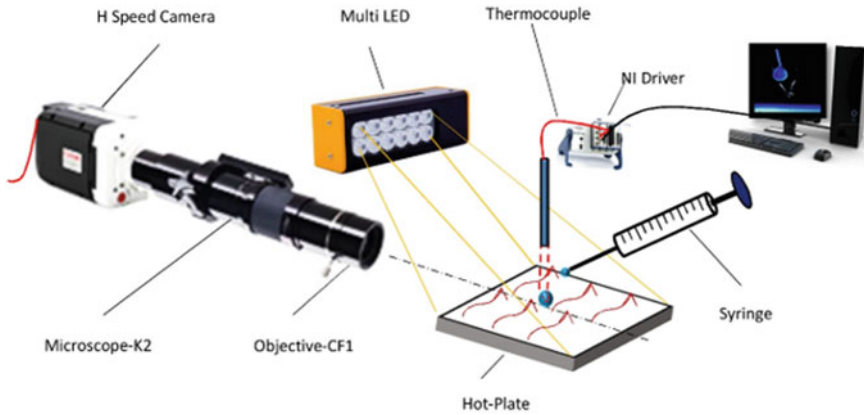


**Fig. 5.5** Experimental setup for the visualization technique

record the profile of droplet temperature during the event. The camera triggering was set when the thermocouple temperature reached 150 °C for all emulsion samples. A controlled hot plate was maintained at 500 °C before dropping the droplet using a syringe with an internal needle diameter of 0.3 mm. The droplet was suspended above the hot plate onto the endpoint of the thermocouple wire (0.03 mm diameter with a bead of 0.08 mm) and the gap between the end of thermocouple and the hot plate was kept at 2 mm using a feeler gauge. To ascertain the thermocouple reading, we immersed two thermocouples into hot water at 10 different temperatures.

To avoid transfer of heat to the needle tip, which may affect the droplet before it is dispensed, the droplet was suspended manually after the thermocouple recorded the required temperature, and the needle promptly retracted. A direct visualization system was used to record the event. A Multi LED (LT-V8-15 -Tokyo, Japan) was used as the source of illumination in the same direction as the camera. The image acquisition rate was set at 500 fps with a resolution of 1280 × 800 pixels and exposure 300 μs throughout all the experiment. The image sequences of the emulsion droplet, as well as the temperature history, were recorded.

### **5.2.5 Free Falling Droplet Experimental Setup**

A shadowgraph imaging system was developed to acquire detailed records of the spray droplets as shown in Fig. 5.6. It consisted of a high-speed video camera (Phantom Miro M310) coupled with a long-distance microscope (Type K2), zoom lens (CF1 objective) and a Multi LED (LT-V8-15) for illumination was positioned opposite to each other. The experiments were performed with a resolution of 256 × 800 pixels (0.0185 mm/pixel), frame rates of 12,000 frames per second

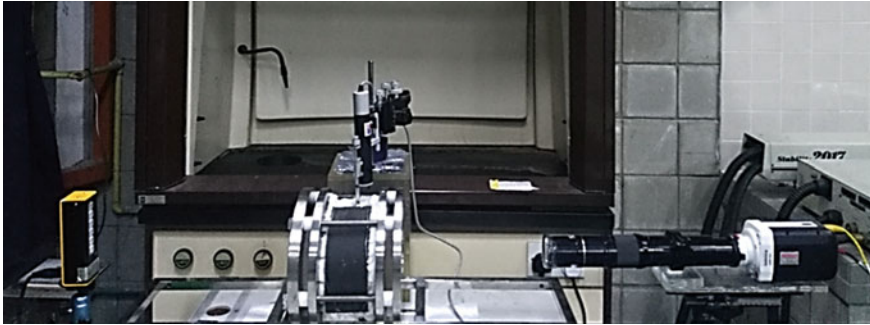


**Fig. 5.6** Experimental setup for shadow imaging visualization system

(fps) and exposure time  $2 \mu\text{s}$ . The minimum spray droplets measured were  $20 \mu\text{m}$ , and smaller sizes were not included due to experimental uncertainty. Droplets were not ignited during these experiments. To determine a sufficient number of droplets, each sample was repeated several times while keeping the same experimental condition.

### 5.3 Impact of Injector Nozzle on the Dispersed Droplet Size

Figure 5.7 shows the physical appearance of the samples for 10% water content. The initial appearance of these emulsions was turbid, as expected for a macro-emulsion, the appearance of all the emulsion samples became more translucent after injection. This suggests that either a considerable proportion of the water separated (or evaporated) out of the emulsion, or the emulsion shifted to a nano-emulsion with dispersed diameters smaller than  $100 \text{ nm}$  [23]. In both cases, a fundamental change in the emulsion's properties was required to alter the visual appearance of the samples, which would ultimately impact the mixing and combustion of the blends.

Figure 5.8 shows the effect of injector nozzle shear on a water-in-diesel emulsion made with 15%W in the fuel tank (1 bar) and different injection pressure as seen under an optical microscope at  $50\times$  magnification. The injector nozzle shifted the emulsion distributions' modes to a smaller diameter and the dispersed water droplet size decreased steadily with the increase in injection pressure. This is caused by the elevated shear and temperatures exerted by the injector's nozzle onto the emulsion.

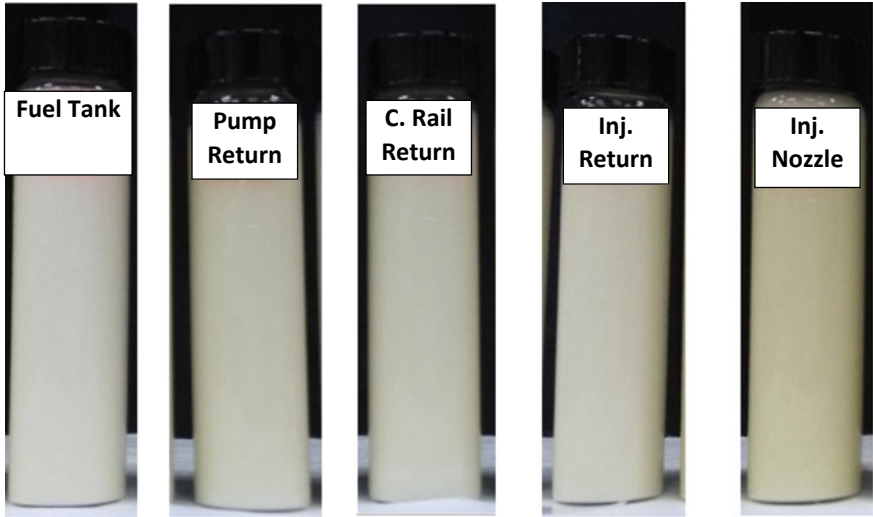


Fig. 5.7 Physical appearance of the samples for 10% water concentration

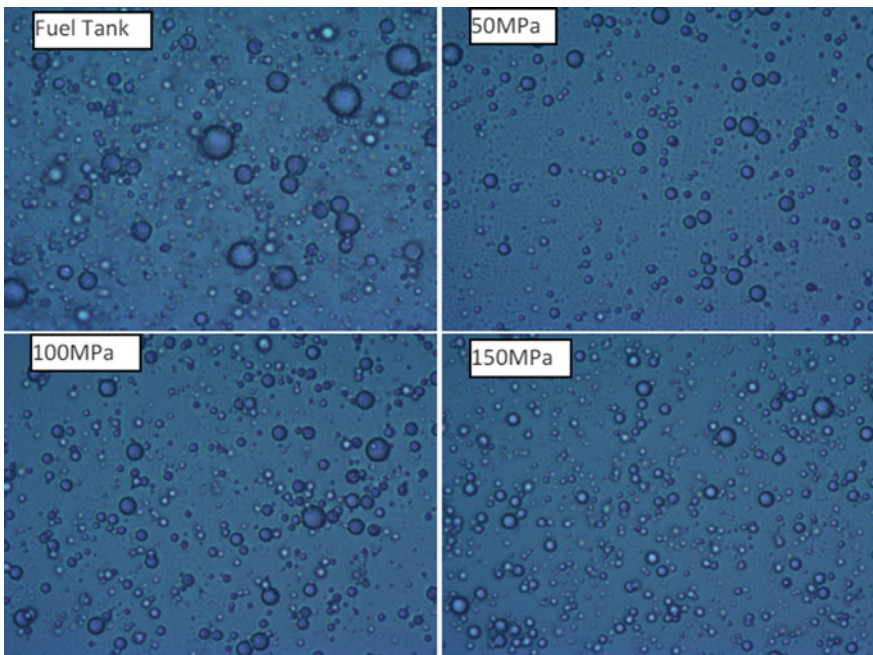


Fig. 5.8 Images of water-in-diesel emulsion samples for 15%v/v water content, examined under an optical microscope at 50× magnification for the emulsion in the fuel tank, and after injection at 50, 100 and 150 MPa

### ***5.3.1 Water Droplet Size Distribution in a Single Droplet Emulsion***

The dispersed water droplets distribution in the emulsion before the injection system at fuel tank (A) and after the injector nozzle were measured at different injection pressures: 50 MPa (B), 100 MPa (C) and 150 MPa (D) and presented in Fig. 5.9. It can be seen that the size and number of the dispersed water droplets were significantly affected by the injector nozzle, with the distributions of droplets size and number increasing with the increase in injection pressure. Indeed, in the injector nozzle, the emulsion was subjected to an intense turbulent and shear flow fields, which led to the breakup of the dispersed phase into smaller droplets.

The mean droplet diameter for samples A, B, C, and D were 5.58, 2.57, 1.2, and 0.7  $\mu\text{m}$ , respectively. The dispersed droplet size in the fuel tank is several times (7.9 times) larger than the droplets found after the injection equipment. These observations support the hypothesis that the emulsion in the fuel tank does not represent the actual fuel spray. Therefore, this reduction in size distribution could significantly reduce the propensity for the emulsion to explode while mixing inside the combustion chamber.

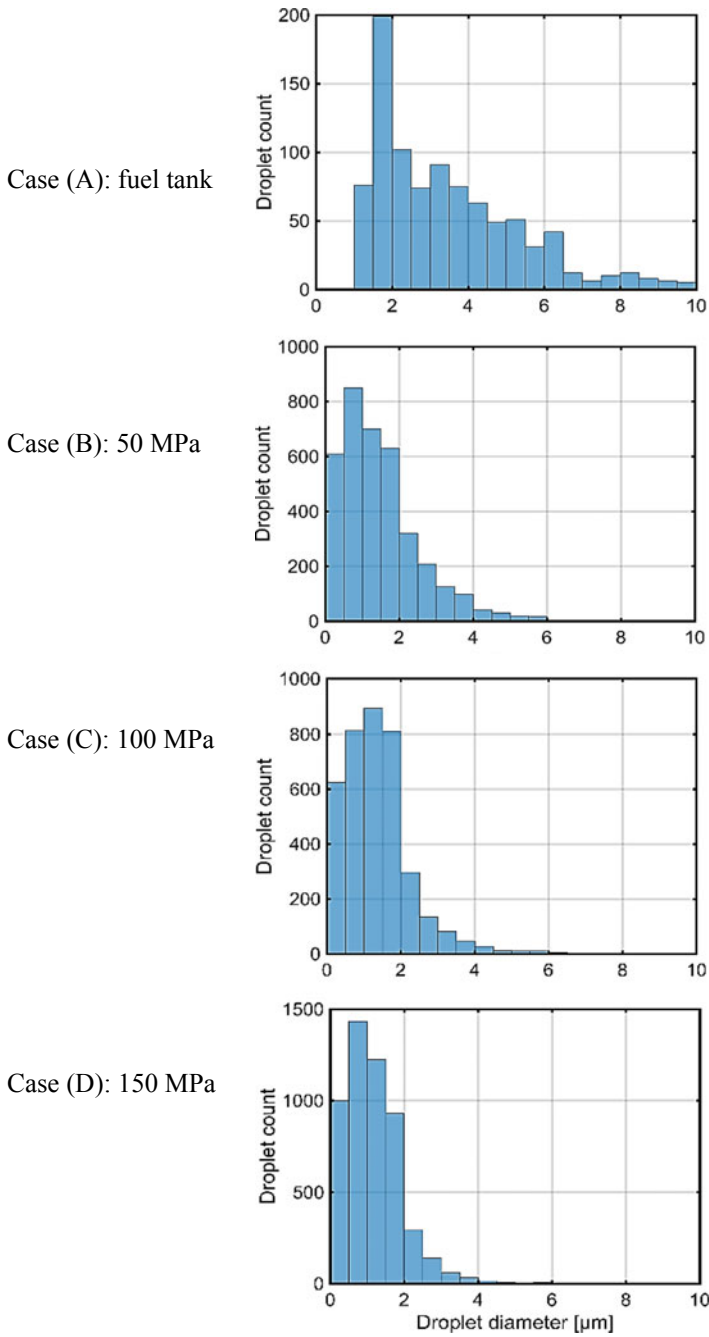
### ***5.3.2 Impact of Injector Nozzle on Micro-Explosion Behavior***

Figure 5.10 shows image sequences of a droplet for the evolution of micro-explosion phenomena of emulsion made with 15% water concentration by volume. Samples from the fuel tank (A) and after the injection pressure at 150 MPa were tested at the Leidenfrost conditions to determine the effect of injection pressure on the micro-explosion phenomena.

The results showed that the micro-explosion behavior was significantly affected by the injector shearing, hence. With the increase of injection pressure, micro-explosion time was delayed (from 1.4 s in the fuel tank to 2.5 after the injector at 150 MPa) due to reduction in dispersed water droplet size and water content in the emulsion.

### ***5.3.3 Droplet Puffing/Micro-Explosion for Free Falling Droplets***

To further investigate the effect of fuel injection system on the droplet micro-explosion behavior, the emulsion samples were collected after injection at 50, 100, and 150 MPa. These samples were then injected into the combustion chamber using the micro-syringe (0.3 mm  $\emptyset$ ), into an environment with a gas



**Fig. 5.9** Droplet counts distribution for the emulsions used in the experiments of 10%W (fuel tank A) and at different injection pressures for Cases (B), (C) and (D)

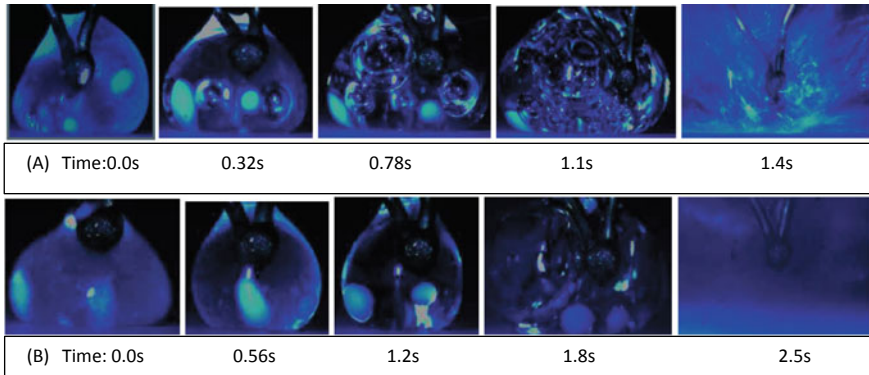


**Fig. 5.10** Sequences of images showing micro-explosion behavior of an emulsion made with 15% water content taken from (a) the tank and (b) after the injection at 150 MPa

temperature of 723 K. The images in Fig. 5.11a show the spray droplets behavior at 1.25 ms and 2.4 ms after injection while Fig. 5.11b focuses on magnified droplets at different times. The images reveal that, even for very fine droplets, water vapor erupts from the droplets resulting in secondary atomization. As shown in Fig. 5.11a, most of the spray droplets were non-spherical near the injector nozzle and do not breakup due to the high surface tension [24]. As can be seen in Fig. 5.11b Case (I), the droplets became spherical during water evaporation, and puffing occurred at 3.5 ms prior to evaporation.

Figure 5.11b Case (II), shows puffing occurred twice for the same droplet which is thought to be due to the high-water concentration. Also, the distribution of water inside the droplets was not always the same. A complete micro-explosion can be seen clearly in Case (III) with a droplet diameter of 100  $\mu\text{m}$  at 6.12 ms. However almost all smaller droplets burst instantaneously, and very fine secondary droplets were produced and evaporated. Qualitatively, a similar behavior was observed in Case (IV) with increasing waiting time of 7.34 ms. Interestingly, in Case (V) the ejected droplet was observed to undergo further micro-explosion. These results confirm that residence time is a significant factor for micro-explosion outcomes. Longer waiting times increase the probability of micro-explosion.

### 5.3.4 Temporal Variation of Spray Droplets Size

In this section, the dynamics of micro-explosion and puffing were tracked for a falling emulsified fuel droplet and an attempt was made to understand the mechanism and the stages involved in the secondary atomization. Both spray droplet size and velocity were measured as shown in Figs. 5.12 and 5.13. In all cases, although the droplet's evaporation progressed, their size gradually increased as the spray moved downstream (Fig. 5.12). It can, therefore, be assumed that the rate of droplet

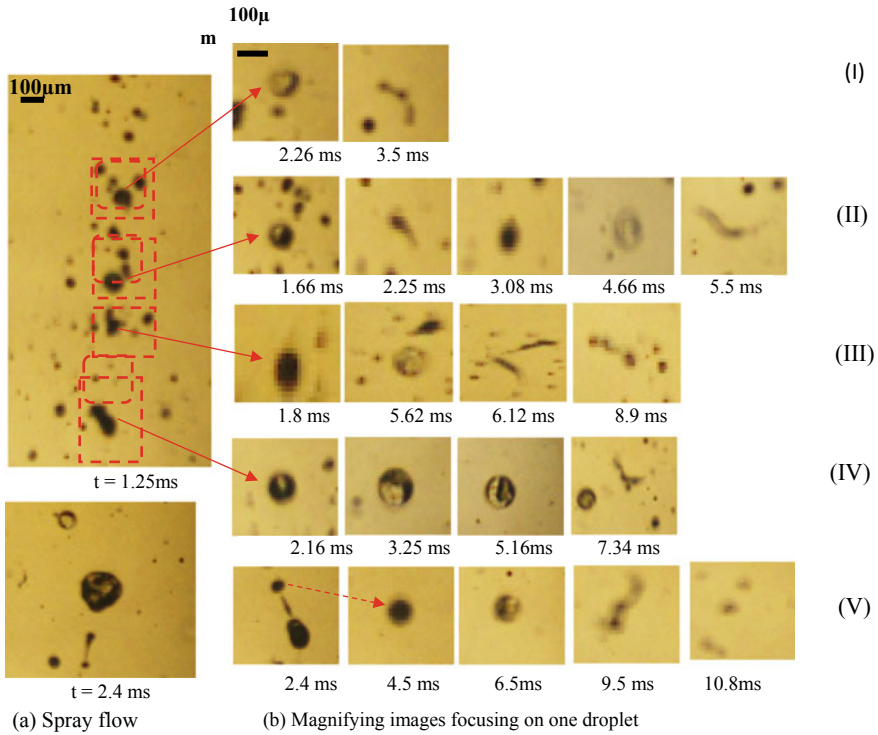


**Fig. 5.11** Sequences of spray flow droplets of 10% water concentration at 723 K showing droplet puffing and micro-explosion

thermal expansion due to water evaporation was greater than the droplet shrinkage caused by the evaporation from droplet. It should be noted that at low initial droplet velocities (2–3 m/s) and with laminar motion of the counter flow of high-temperature gases (slower than 2 m/s), the probability of coalescence of droplets as they moved parallel to each other was minimized [25].

In the first stage ( $t = 0\text{--}2\text{ ms}$ ), the droplets were non-spherical as they left the micro-syringe. The size of the droplets tended to decrease abruptly and followed an oscillatory path. In the second stage ( $t = 2\text{--}5\text{ ms}$ ), as the droplet stabilized and converged towards sphericity, their size continued to increase due to water evaporating inside the droplet until it reached the puffing limit, the point where the droplet ebullition occurred. The droplets oscillation decreased as they became more spherical and moved in a straight path. In the third stage ( $t = 5\text{--}10\text{ ms}$ ), droplets 1, 3 and 4 underwent puffing, reduced in size giving birth to satellite droplets. However, droplet 2 continued to increase in size over time with lower velocity compared to other droplets (Fig. 5.13) until it reached the puffing limit at a much later stage ( $t = 10\text{--}16\text{ ms}$ ). As the size of the parent emulsion droplet increased, the droplet velocity and the puffing time also increased as shown by Case 3 and Case 4.



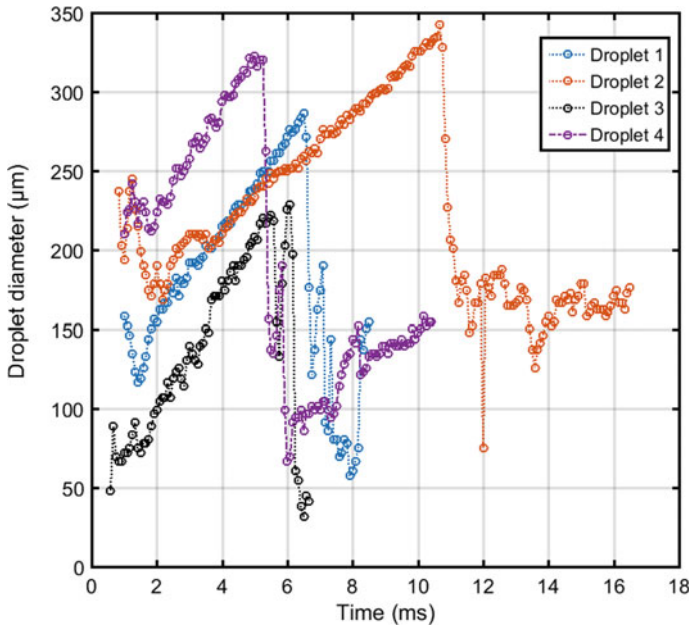


**Fig. 5.12** Effect of different droplet size on time to puffing of 10% water content sprayed at 100 MPa injection pressure

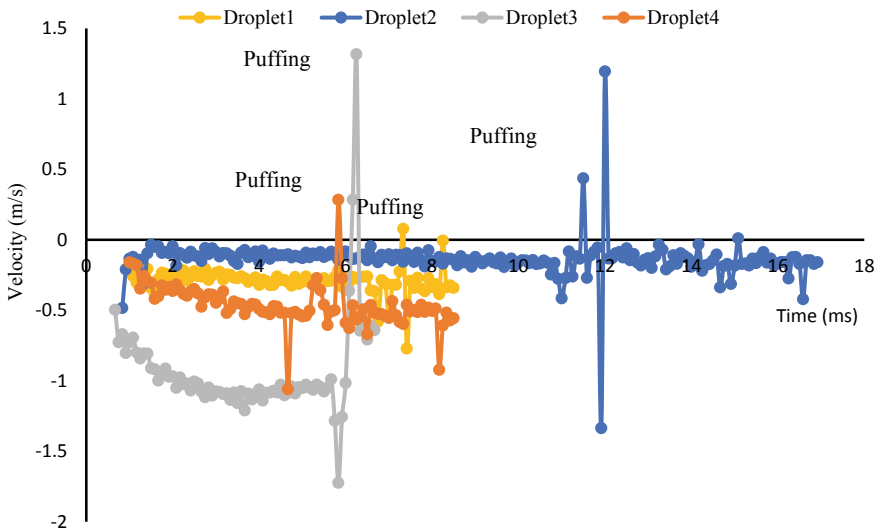


**Fig. 5.13** Plots of different droplet size (1, 2, 3 and 4) speed versus time of 10% water content sprayed at 100 MPa injection pressure

However, the physics differed in Case 1 and Case 4 which can be attributed to the dispersed size of the water content within the parent emulsion droplet and the location of the vapor nuclei [26, 27]. Again, in Cases 1 and 2, a similar behavior was observed, however, their time to puffing were different although their initial droplet sizes and their velocities were almost the same. It is also observed that in some cases the droplets tended to grow in size again after puffing indicating the partial utilization of water dispersed within the parent droplet. This could be because of partial coalescence of dispersed water droplets [17], and as a result complete micro-explosion was not observed. In this case, the satellite droplets may have the potential to undergo further puffing.

## 5.4 Summary

The evolution of micro-explosion and puffing phenomenon for a single emulsion droplet under Leidenfrost and free-falling droplets were visualized with a microscopy high-resolution images. The dispersed droplet sizes reduce significantly after being injected through the nozzle's orifices. Micro-explosion was found to be affected by the injection equipment, with the micro-explosion time delayed with the increase of injection pressure. This led to the suggestion that the injected emulsion induced a lower coalescence rate and, hence, delayed the micro-explosion occurrence. The spray falling droplets were found to be affected by both the initial size of the dispersed water droplets and parent spray droplet. The probability of micro-explosion in freely falling droplets was very rarely compared to that of single droplet in Leidenfrost technique due to shorter waiting time.

## References

1. X. Tauzia, A. Maiboom, S.R. Shah, Experimental study of inlet manifold water injection on combustion and emissions of an automotive direct injection diesel engine. *Energy* **35**(9), 3628–3639 (2010)
2. E. Arabaci, Y. İçingür, H. Solmaz, A. Uyumaz, E. Yilmaz, Experimental investigation of the effects of direct water injection parameters on engine performance in a six-stroke engine. *Energy Convers. Manag.* **98**, 89–97 (2015)
3. F. Bedford, C. Rutland, P. Dittrich, F. Wirbeleit, Effects of direct water injection on di diesel engine combustion. *SAE Pap.* **1**, 2938 (2000)
4. X. Ma, F. Zhang, K. Han, Z. Zhu, Y. Liu, Effects of intake manifold water injection on combustion and emissions of diesel engine. *Energy Procedia* **61**, 777–781 (2014)
5. G. Lv, F. Wang, W. Cai, H. Li, X. Zhang, Influences of addition of hydrophilic surfactants on the W/O emulsions stabilized by lipophilic surfactants. *Colloids Surf. Physicochem. Eng. Asp.* **457**(1), 441–448 (2014)
6. E. Blomberg, E. Poptoshev, P. Claesson, Surface forces and emulsion stability, in *Encyclopedic Handbook of Emulsion Technology* (2001), pp 305–326

7. R. Najjar, S. Heidari, Modified diesel prepared by stabilization of water as nanodroplets in diesel/colla oil blend: study of phase behavior and affecting parameters. *Fuel* **214**(May 2017), 497–504 (2018)
8. B.K. Debnath, U.K. Saha, N. Sahoo, An experimental way of assessing the application potential of emulsified palm biodiesel toward alternative to diesel. *J. Eng. Gas Turbines Power* **136**(February 2014), 1–12 (2016)
9. Z. Wang et al., Effects of water content on evaporation and combustion characteristics of water emulsified diesel spray. *Appl. Energy* **226**(1037), 397–407 (2018)
10. Z. Wang et al., Experimental investigation on spray, evaporation and combustion characteristics of ethanol-diesel, water-emulsified diesel and neat diesel fuels. *Fuel* **231** (April), 438–448 (2018)
11. M.A. Ismael, M.R. Heikal, A.R.A. Aziz1, C. Crua, An overview of experimental techniques of the investigation of water-diesel emulsion characteristics droplets micro-explosion. *ARPN J. Eng. Appl. Sci.* **11**(20), 11975–11981 (2016)
12. B. Kichtavov, A. Korshunov, A. Kiverin, A. Saveliev, The role of explosive boiling in the process of foamed emulsion combustion. *Int. J. Heat Mass Transf.* **119**, 199–207 (2018)
13. M.Y. Khan, Z.A.A. Karim, A.R.A. Aziz, R. Morgan, C. Crua, Puffing and microexplosion behavior of water in pure diesel emulsion droplets during Leidenfrost effect. *Combust. Sci. Technol.* **189**(7), 1186–1197 (2017)
14. V. Califano, R. Calabria, P. Massoli, Experimental evaluation of the effect of emulsion stability on micro-explosion phenomena for water-in-oil emulsions. *Fuel* **117**, 87–94 (2014)
15. Y. Kimoto, K., Owashi, Y., & Omae, The vaporizing behavior of the fuel droplet of water-in-oil emulsion on the hot surface. *Bull. JSME*, **258**(29), 4247–4255, 1986
16. E. Mura, C. Josset, K. Loubar, G. Huchet, J. Bellettre, Effect of dispersed water droplet size in microexplosion phenomenon for water in oil emulsion. *At. Sprays* **20**(9), 791–799 (2010)
17. M.A. Ismael, M.R. Heikal, A.R.A. Aziz, F. Syah, E.Z. Zainal, C. Crua, The effect of fuel injection equipment on the dispersed phase of water-in-diesel emulsions. *Appl. Energy* **222**, 762–771, 2018
18. S.S. Reham, H.H. Masjuki, M.A. Kalam, I. Shancita, I.M. Rizwanul Fattah, A.M. Ruhul, Study on stability, fuel properties, engine combustion, performance and emission characteristics of biofuel emulsion. *Renew. Sustain. Energy Rev.* **52**, 1566–1579 (2015)
19. B.K. Debnath, U.K. Saha, N. Sahoo, An experimental way of assessing the application potential of emulsified palm biodiesel toward alternative to diesel. *J. Eng. Gas Turbines Power* **136**(2), 021401 (2013)
20. C.Y. Lin, S.A. Lin, Effects of emulsification variables on fuel properties of two- and three-phase biodiesel emulsions. *Fuel* **86**(1–2), 210–217 (2007)
21. M.A. Ismael, M.R. Heikal, M.B. Baharom, Spray characteristics of a diesel-cng dual fuel jet using the schlieren imaging technique. *Int. J. Mater. Mech. Manuf.* **3**(3), 145–151 (2015)
22. M.Y. Khan, Z.A. Abdul Karim, A.R.A. Aziz, I.M. Tan, Experimental investigation of microexplosion occurrence in water in diesel emulsion droplets during the Leidenfrost effect. *Energy & Fuels* **28**(1), 7079–7084 (2014)
23. D.J. McClements, Nanoemulsions versus microemulsions: terminology, differences, and similarities. *Soft Matter* **8**(6), 1719–1729 (2012)
24. M. Agrawal, A.R. Premlata, M.K. Tripathi, B. Karri, K.C. Sahu, Nonspherical liquid droplet falling in air. *Phys. Rev. E* **95**(3), 033111 (2017)
25. R.S. Volkov, G.V. Kuznetsov, P.A. Strizhak, Influence of droplet concentration on evaporation in a high-temperature gas. *Int. J. Heat Mass Transf.* **96**, 20–28 (2016)
26. J. Shinjo, J. Xia, L.C. Ganippa, A. Megaritis, Physics of puffing and microexplosion of emulsion fuel droplets. *Phys. Fluids* **26**(10), 103302 (2014)
27. J.C. Lasheas, L.T. Yap, F.L. Dryer, Effect of the ambient pressure on the explosive burning of emulsified and multicomponent fuel droplets. *Symp. Combust.* **20**(1), 1761–1772 (1985)

# Chapter 6

## Reactivity Controlled Compression Ignition: An Advanced Combustion Mode for Improved Energy Efficiency



**Ibrahim B. Dalha, Mior A. Said, Z. A. Abdul Karim, A. Rashid  
A. Aziz, Firmansyah, Ezrann Zharif Zainal Abidin  
and Mhadi A. Ismael**

This chapter reviews reactivity controlled compression ignition (RCCI), which is an advanced combustion mode. RCCI is capable of improving thermal efficiency and reducing nitrogen oxides (NO<sub>x</sub>) and soot emission. However, it has high specific fuel consumption, unburned hydrocarbon (UHC) and carbon monoxide (CO) emissions, and thus requiring appropriate strategies. The effects of some strategies were found to influence advanced combustion phase and reduced UHC and CO emissions to a certain extent while maintaining RCCI reputability or otherwise. The use of bio-based low reactivity fuels (LRF) in RCCI combustion serves as a substitute for gasoline in reactivity stratification. Depending on the LRF used, utilization of biodiesel enables controlled combustion phase, extended load and significantly reduce soot and CO emissions, but it increases NO<sub>x</sub> and UHC emissions through NO<sub>x</sub> is compromised with biodiesel blends. The use of biodiesel can serve a greater advantage over conventional diesel when appropriate LRF and strategy are used especially for medium to higher blends or pure biodiesel.

---

I. B. Dalha (✉) · A. R. A. Aziz · Firmansyah · E. Z. Z. Abidin · M. A. Ismael  
Centre for Automotive Research and Electric Mobility, Universiti Teknologi PETRONAS,  
32610 Seri Iskandar, Perak, Malaysia  
e-mail: [irobabangida13@gmail.com](mailto:irobabangida13@gmail.com)

M. A. Said · Z. A. Abdul Karim  
Department of Mechanical Engineering, Universiti Teknologi PETRONAS,  
32610 Seri Iskandar, Perak, Malaysia

© Springer Nature Singapore Pte Ltd. 2020  
S. A. Sulaiman (ed.), *Energy Efficiency in Mobility Systems*,  
[https://doi.org/10.1007/978-981-15-0102-9\\_6](https://doi.org/10.1007/978-981-15-0102-9_6)

## 6.1 Introduction

Internal combustion (IC) engines have served as the primary power source in transportation systems and other engineering machineries since decades ago, though they remain as the major source of UHC, CO, NO<sub>x</sub>, soot, and greenhouse gases [1]. Numerous researches were carried out on different aspects of IC engine suggesting strategies for reducing fuel consumption, emissions and increasing engine efficiency. Recently, the attention of researchers has been focusing on low-temperature combustion (LTC) technologies for achieving lower emissions and higher efficiency as compared to other methods. LTC is a desired concept in advanced diesel combustion technologies which has the potentiality of meeting the most stringent environmental legislations alongside improved efficiencies. LTC has different combustion techniques that include homogenous charge compression ignition (HCCI), premixed charge compression ignition (PCCI) and RCCI combustion. These techniques have similar fundamental principles but differ in their modes of operation. To overcome certain difficulties of LTC such as high-pressure rise rate, combustion phase control, and extended operation limit, RCCI can be adopted.

## 6.2 LTC Mode

Low-Temperature Combustion (LTC) is a generic term referred to advanced combustion concepts with the ultimate goal of lowering combustion temperatures while achieving high efficiency and minimum exhaust emissions. It is an emerging idea of modern combustion science which works on the same fundamental principle as 4-stroke engine and uses basic elements of compression ignition (CI) and spark ignition (SI) engines [2]. During the intake stroke, fuel–air mixture is introduced into the cylinder and compression followed. As a result of the compression, in-cylinder temperature and pressure increases and subsequently the mixture auto-ignite. Fuel oxidation and subsequent chemical energy release succeed auto-ignition. This quick heat release resulted in pressure rise in a significantly shorter time span compared to conventional engines. During LTC, the peak temperature can be as low as 2000 K which can result in drastic reduction in NO<sub>x</sub> formation due to the low activation energy of N–O bond formation reactions. To achieve LTC, the use of high injection pressure and resized nozzle diameters are required to reduce the equivalence ratio and decrease the in-cylinder temperature [3]. In addition, utilization of long ignition delay period allows adequate time for mixing prior to the start of combustion; thus, rich regions in the combustion chamber are reduced and soot formation is mitigated [4]. LTC can yield higher specific heat ratios because the engine is operating on lean fuel–air mixture resulting in more work done.

## 6.3 Fundamentals of RCCI Combustion

Fundamentally, RCCI is an advanced dual-fuel combustion technology that employs the use of two fuels of different reactivity to achieve in-cylinder fuel blending and adopt some strategies such as multiple injection and rate of exhaust gas recirculation for controlled reactivity in the cylinder resulting in improved or optimized combustion duration and magnitude, thereby developing high thermal efficiency and reduced NO<sub>x</sub> and particulate matter (PM) emissions. However, this section covers the basic elements and fundamental principles of RCCI operation.

### 6.3.1 Principles of RCCI Combustion

The main objective of RCCI is to achieve the desired combustion duration and magnitude. From onset, the LRF such as gasoline or biogas is injected into the intake manifold through a port fuel injector and premixed with air, then charged into the cylinder through the intake manifold during the intake stroke. Subsequently, the fuel with higher reactivity such diesel, biodiesel or a blend of fuels is injected into the charged mixture in the cylinder through a direct injector with a single or multiple injection strategies during the compression stroke. The fuels can be injected at a given interval of time governing the reactivity stratification for the desired combustion phase. The early injected high reactivity fuel (HRF) gets to the squish region while the late injection served as a source of ignition, eventually reactivity stratification is formed. By strategically modulating the fuels ratio and injection timings, the reactivity gradient formed in the cylinder enabled a controlled combustion phase and mitigated the pressure rise rate along with the peak heat release rate. The schematic diagram of RCCI engine concept is shown in Fig. 6.1. During its combustion process, the combustion starts from the areas occupied by HRF and proceeds to the areas of LRF. This process enables better expansion during combustion of the premixed mixture which resulted in high thermal efficiency, low-pressure rise rates and low exhaust emissions.

Kokjohn et al. [5] in their comparison of RCCI with the conventional diesel engine, found that for the conventional engine the NO<sub>x</sub> emission was tripled, while soot emission was six times higher by magnitude, along with a 16.4% increase in gross indicated efficiency as compared to RCCI. Similarly, Benajes et al. [6] parametrically studied a heavy-duty CI engine for RCCI combustion mode. In comparison with the conventional diesel combustion, they reported a little decrease in NO<sub>x</sub> emission and a significant reduction in soot emission for RCCI combustion. This signifies that RCCI combustion is capable of reducing NO<sub>x</sub> and soot emissions drastically compared to conventional diesel combustion. The combustion mode is much beneficial to increase thermal efficiency though it has high specific fuel consumption (SFC), UHC and CO emissions [7]. Different techniques were used to reduce fuel consumption, UHC and CO emissions while maintaining RCCI reputability.

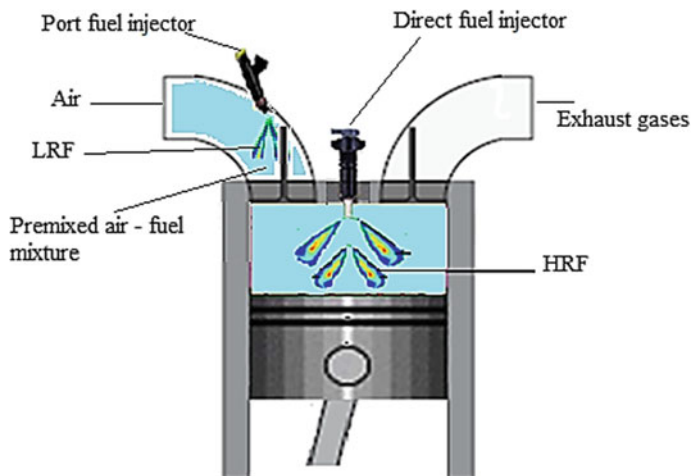


**Fig. 6.1** The schematic diagram of RCCI engine fundamentals

### **6.3.2 Fuel Reactivity Stratification in RCCI**

When the reactivity is determined purely by the amount of fuels being used, it is termed global reactivity while when it relates to spray penetration and entrainment of fuel directly injected with the mixture it is termed reactivity stratification [4]. However, fuel stratification occurs when two fuels of different reactivity are injected into the cylinder by port and direct injection strategy thereby creating layers known as stratification. Fuel reactivity stratification influences combustion characteristic to a greater extent, though stratification created by the injection of HRF is affected by the in-cylinder mixing of the fuels and many other factors such as engine load, equivalence ration, fuel blends, temperature and so on. Mikulski and Bekdemir [8] studied the potential of RCCI with direct-injected natural gas (NG). It was observed that gaseous fuel stratification improves combustion efficiency with reduced methane and CO emission meanwhile a decrease in NO<sub>x</sub> and a slight increase in UHC were recorded. The NG stratification shows an increase in combustion efficiency by 11% at low loads and the potentiality of increase in combustion efficiency decreased with the increase in engine loads.

### **6.3.3 Mixing and Auto-Ignition Processes of RCCI**

Auto-ignition is an outcome of physical and chemical processes in combustion and its characteristic depends mainly on the composition, molecular size, and structure of the test fuel. Auto-ignition in RCCI combustion mode combines the techniques of conventional diesel and HCCI engines. This involves port injection of a

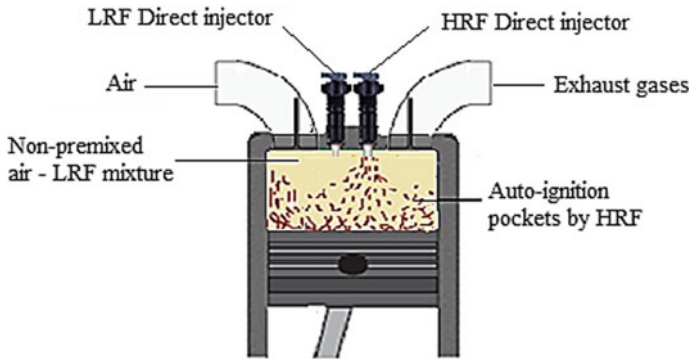


**Fig. 6.2** Formation of auto-ignition pockets and staged ignition in dual direct injection mode

homogenous charge mixture of fuel with low cetane number which is similar to that of HCCI and direct injection of high cetane number fuel to create charge stratification like that of conventional diesel engine. The low cetane number fuel can also be injected directly as in the case of dual direct injection. The HRF injected at high pressure towards the centerline reaches the piston bowl rim area and makes the mixture more reactive due to more concentration of HRF resulting in auto-ignition. The mixture reactivity is a peak around the bowl rim area and more of the auto-ignition pockets are formed in those areas as depicted in Fig. 6.2. Very early direct injection timing resulted in more mixing of the mixture in the cylinder, thereby making the mixture almost homogenous. The homogeneity of the mixture reduces its reactivity stratification and affects the auto-ignition process in RCCI leading to similar auto-ignition which causes abrupt combustion and excessive peak pressure rise rate. Benajes et al. [6] carried out a detailed analysis of air–fuel mixing process using one-dimensional spray model and reported that auto-ignition of diesel injected initiated the combustion. The rise in temperature and pressure in the combustion chamber facilitated the flame propagation of the lean mixture across the zone. Reduction in the fuel ratio caused more ignition delay, which consequently extended the mixing time, and thus lowering the first combustion stage while enhancing the second one. However, with the advanced injection timing, the aforementioned effects were more pronounced.

### 6.3.4 Rate of Heat Release in RCCI

Heat release rate occurs due to the formation of rich zones as a consequence of more fuel concentration in the squish area. It defines the rate at which chemical energy is converted into thermal energy during combustion. The HRF reacts at low temperature, releasing sufficient energy to ignite the LRF. During the process of heat release in RCCI combustion, low- and high-temperature heat releases occur.



A low-temperature reaction takes place at a temperature lower than that of auto-ignition, hence creating a two-stage ignition. The peak low-temperature heat release at the first stage is governed by HRF with negative temperature coefficient while the second-highest temperature heat release depends on the premixed fuel. This staged ignition process enables an increase in combustion duration with reduced peak heat release rate. However, heat release rate affects directly the rate of pressure rise and subsequently the power produced. It is a function of many factors such as advanced injection timing, lower heat transfer, increased specific heat ratio, and increased thermal efficiency.

## 6.4 RCCI Operational Variables

RCCI combustion is influenced directly or indirectly by numerous factors. The effects of some factors under certain circumstances are controllable while those of other factors are beyond control. In this section, attention is given to some controllable variables that significantly affect RCCI combustion as considered by many researchers in their experimental variables. These include but not limited to injection timing, injection pulses, fuel spray angle, fuel ratio, equivalence ratio, intake air temperature, and premixed ratio.

### 6.4.1 *Pilot Fuel Injection Timing*

Injection strategy is applied in the process of injecting HRF which is one of the significant techniques that enabled enhanced performance of RCCI engine. In the event of injection timing, as a particular crank angle degree at which the HRF is injected into the cylinder, there are many variables that can be manipulated to improve the technique for effective performance. For instance; single or double (retarded and advanced) injection timing can be adopted to ascertain its influence on certain parameters such as heat release rate, and varying the injection pulses of HRF into single, double or triple pulses. In addition, injection timing has an influence in advancing combustion phase and reducing UHC and CO emission to certain extent while maintaining NO<sub>x</sub> emission at a comparable level. However, as reported by some researchers it might influence an increase in peak pressure rise rate. Nazemi and Shahbakhti [9] found that the optimum performance was obtained when the start of injection timing was at 53°BTDC, 580 bar injection pressure and a premixed ratio of 0.76. Also, the UHC and CO emissions were reduced by 23% and 39% respectively, while gross indicated efficiency and combustion were improved. The smallest local reactivity gradient manifested at the most advanced start of injection timing, which resulted in combustion instability. Zhang et al. [10] reported that increasing direct injection quantity resulted to advanced peak pressure rise rate and heat release rate while direct injection timing has a great influence on

combustion phase. However, a controlled combustion phase was achieved with an improved indicated thermal efficiency and extended operation range.

### **6.4.2 Pilot Fuel Injection Pulses**

HRF distribution can be influenced by the number of pulses in the injection strategy thus shaping the in-cylinder reactivity distribution. Numerous researchers investigated the effects of the number of pulses on CI engine performance. Double injection should be used for RCCI operation from low to mid load while single injection should be used for high to full load operation, mainly to avoid excessive in-cylinder pressure gradients [3]. Tong et al. [11] found that when palm oil dimethyl ester was used as HRF with single injection strategy, the load was extended to 1.76 MPa IMEP which was significantly higher compared to that of conventional gasoline–diesel operation using an optimized double injection strategy which was about 1.39 MPa IMEP. Also, a stable and controllable RCCI operation was achieved with increased indicated thermal efficiency, reduced soot, and comparable NO<sub>x</sub> emission.

### **6.4.3 Pilot Fuel Injection Pressure**

Injection pressure is one of the injection strategic parameters used while injecting HRF to enable enhanced performance and fuel economy of the RCCI engine [4]. Poorghasemi et al. [12] demonstrated that by decreasing the injection pressure from 450 to 300 bar, the gross indicated efficiency increases by 5% and combustion phase was retarded by 4 crank angle degrees. Simultaneous reduction in UHC and CO emissions along with NO<sub>x</sub> was achieved by reducing injection pressure with first advanced start of injection timing. Zhang et al. [10] reported that low injection pressure affects fuel atomization while high injection pressure resulted to misappropriation. However, it was observed that direct injection pressure had little effect on combustion phase, though controlled combustion was achieved with an improved indicated thermal efficiency and extended operation range.

### **6.4.4 Pilot Fuel Spray Angle**

Fuel spray angle is an important fuel injection parameter for RCCI engine operation. All types of spray generate a particular droplet distribution depending on the geometry of the atomizer, supply conditions, and fluid injected. The geometrical parameters such as spray angle provides some information regarding the injected fuel phases, hence spray parameters interact with the combustion processes. The

spray angle depends on the injection pressure and fuel viscosity hence it varies with the fuel types. Furthermore, the spray angle plays a role in the occurrence of combustion because the mixing depends on the angle formed by the sprayed fuel and oxidizing air [13]. Nazemi and Shahbakhti [9] used 3D computational fluid dynamics combustion model to study the effects of spray angle, SOI timing, injection pressure and premixed ratio on the performance and emission characteristics of RCCI engine. It was found that when the spray angle was decreased from  $74^\circ$ , which was the base condition, to  $55^\circ$ , UHC and CO were decreased by 27% with the increase in gross indicated efficiency and improved combustion. The location of first stage heat release was found to be independent of spray angle variation while the spray angle has the major effect on combustion phase.

#### **6.4.5 Fuels Energy Fraction**

An energy fraction of the premixed and pilot injected fuel is important in dual-fuel engine. Energy fraction, which is the ratio of either premixed or pilot injected fuel to the total energy input, affects the in-cylinder reactivity which is a measure of the fuel cetane number. Modulating the fuel ratio or energy fraction changes the in-cylinder reactivity and eventually affect in-cylinder pressure and temperature, heat release rate, ignition delay time and the combustion characteristics in general [14]. Kakaee et al. [15] studied the effects of diesel fuel mass fraction in the early start of injection on combustion and emission characteristics of RCCI engine. The results show that combustion takes place early with the increasing diesel mass fraction at early start of injection, though there was a slight increase in peak pressure rise rate. It was evidenced from some findings that energy fraction did not only affect combustion characteristics but also engine-out emissions. To a certain extent, it helps in controlling UHC and CO emissions that are still some drawbacks in RCCI combustion.

#### **6.4.6 Premixed Air to Fuel Ratio**

Premixed ratio referred to the amount of LRF mixed with the air before entering the cylinder, unlike the term energy fraction which is the ratio of either pilot or premixed fuel to the total energy input. Premixed ratio does not only influence combustion characteristics but also has great influence on engine-out emissions as reported in the literature; Nazemi and Shahbakhti [9] and Wang et al. [16] reported that besides improvement in combustion phase, premixed ratio could facilitate an increase in RCCI engine efficiency and suppress the tendency of having ringing intensity during operation as a consequence of reduced peak pressure rise rate. In addition, premixed ratio plays a role in reducing NO<sub>x</sub> and soot emissions. However, increase in premixed ratio can be disadvantageous by promoting UHC and CO

emissions. Employing certain techniques to improve the premixed mixture can help to reduce UHC and CO emissions.

## 6.5 RCCI Combustion Control Strategies

Combustion phase control is an important phenomenon in RCCI, in fact, is the factor that predicts the effectiveness and reliability of any combustion mode in compression ignition engine.

### 6.5.1 *Split Injection (SPI) Strategy*

This strategy involves splitting the injection into fraction at the targeted timing which is the strategy employed to effect control of combustion phase. The 1st and 2nd start of injection timings have significant effects on RCCI engine combustion and emission characteristics. Splitting the injection into pulses can enable reduced burning duration which implies improved combustion duration and likely its magnitude along with reduced NO<sub>x</sub> and soot emissions. According to Molina et al. [3] and Tong et al. [11] single injection suppressed peak pressure rise rate which facilitated load extension to higher limit. It was evident that the fraction of the delayed injection resulted in reduced NO<sub>x</sub> emission. However, Li et al. [18] found that double injection strategy resulted in longer ignition delay. As summarized in Table 6.1, the SPI strategy can potentially enable improved thermal efficiency and moderately advanced combustion phase with acceptable peak pressure rise rate. In addition, upon selecting other appropriate variables along with SPI strategy, UHC, CO, and PM emissions can be reduced with acceptable NO<sub>x</sub>.

### 6.5.2 *Exhaust Gas Recirculation (EGR) Strategy*

To achieve optimum RCCI operation conditions, EGR is highly required especially under high loads condition to enable reduction in peak pressure rise rate. When internal EGR is used, mixture homogeneity of the charge is greatly affected by EGR rate. Also, when EGR is not completely mixed with the charge in the cylinder, mixture stratification occurs thus affecting ignition timing and combustion duration [4]. Therefore, EGR is one of the effective parameters for combustion control. Wang et al. [31] found that very low NO<sub>x</sub> and PM emissions along with high thermal efficiency were achieved on gasoline–diesel RCCI at moderate to high loads. For an extended RCCI operation to higher loads, an increased EGR rate and fuel ratio alongside advanced diesel injection timing could be employed to minimize the in-cylinder global reactivity of the charge thereby mitigating premature

**Table 6.1** Projected attributes of strategies on combustion and emission parameters in RCCI

Mode	Strategies	Effects on emission					Effects on combustion			References
		NOx	PM	UHC	CO	CA50	TE	PPRR		
RCCI	Split injection (SPI)	↔	↓	↓	↓	↔	↑	↔	[17-27]	
RCCI	Exhaust gas recirculation (EGR)	↓	↔	↑	↑	↓	↔	↑	[19, 28-34]	
RCCI	Dual direct injection (DDI)	↓	↓	↔	↓	↑	↑	↓	[8, 33, 35-38]	
RCCI	Dual-mode operation (DMO)	↓	↔	↑	↑	↑	↔	↓	[28, 39, 40]	
RCCI	Variable valve timing (VVT)	↓	↓	↑	↑	↑	↑	↓	[41]	
RCCI	Fuel additives (FA)	↓	-	↑	↓	-	↑	-		
RCCI	Variable compression ratio (VCR)	-	-	-	-	-	-	-		
RCCI	Close loop control (CLC)	-	-	-	-	-	-	-		

*Note* (↑) stands for advance in CA50 or high values for TE and PPRR while (↓) stands for retard in CA50 or low values for TE and PPRR while (↔) represent the relatively constant for TE, PPRR, NOx, PM, UHC and CO emissions as averaged based on the listed inferences

combustion, peak pressure rise rate, and high peak in-cylinder pressure. However, control of combustion phase might be difficult when very high EGR rate is used. According to Pedrozo et al. [32] the mean gas temperatures in the cylinder increased due to higher utilization of EGR rates and global equivalence ratios which resulted in higher exhaust gas temperature with lower UHC and CO emissions. The use of internal EGR reduces NO<sub>x</sub> formation because of lower oxygen concentration and higher heat capacity while indicated thermal efficiency was improved and remained constant with the increase in throttling. As shown in Table 6.1, EGR rate has no significant benefit to combustion parameters, UHC and CO emissions but certainly advantageous to suppressing NO<sub>x</sub> and soot emissions.

### 6.5.3 Dual Direct Injection (DDI) Strategy

Dual direct injection involves the use of two separate injectors to inject the LRF and HRF at different injection timing and pressure to create in-cylinder reactivity gradient thereby forming fuel stratification. An in situ mixing of air with LRF in the cylinder could possibly avoid trapping premixed air–fuel mixture in the crevice region, hence UHC and CO emissions during RCCI combustion, which is due to premixed air–fuel mixture trapped in the crevice region, could relatively be reduced [4, 42]. Lim and Reitz [33] used dual direct injection in RCCI combustion and concluded that engine load was extended to 21 bar IMEP at a speed of 1800 rpm with the EGR rate of 46%. High thermal efficiency of 48.7% was achieved with very low NO<sub>x</sub>, soot and CO emissions. Utilization of the piston geometry and important regions by the two injectors resulted to achieving such load extension. Utilizing huge quantity of fuel during first injection timing enables effective control of combustion by maximizing evaporative cooling in the squish region. Luong et al. [43] employed dual direct fuel strategy in RCCI combustion. The authors concluded that there was lower peak heat release rate with longer combustion duration at high pressure while the ignition delay changed with increase in injection timing due to the evaporative cooling effects of the dual direct-injected fuels. The strategy enabled precise control of combustion phase and peak heart release rate through modulation of the directly injected LRF, which was more effective when the injection occurred during the high-temperature combustion regime. In summary, Table 6.1 reveals that DDI strategy can potentially enable improved combustion phase, thermal efficiency and minimized peak pressure rise rate. Besides, upon selecting other appropriate variables along with DDI strategy, all emissions can be reduced.

### 6.5.4 Dual-Mode Operation (DMO) Strategy

The quest to improve LTC operation suggests this strategy, in which the engine starts an operation on particular combustion mode and subsequently switched to

another mode with the view to controlling combustion phase. The system combined conventional compression or spark ignition and LTC mode to achieve clean and efficient operation. Garcia et al. [39] reported an increase in UHC and CO emissions with RCCI/Conventional diesel combustion than dual-mode dual-fuel concept. The DMO yielded ultra-low NO<sub>x</sub> emission reduction without the use of after-treatment systems as similarly reported by Benajes et al. [40]. According to them, the reduction in NO<sub>x</sub> and soot emissions were more pronounced along with higher thermal efficiency when E85 was used as LRF compared to gasoline in DMO. Based on the summary of the few researches, as shown in Table 6.1, dual-mode operation can potentially advance combustion phase, minimize peak pressure rise rate and improve thermal efficiency. Similarly, Table 6.1 further reveals that the mode is beneficial to reducing NO<sub>x</sub> and soot emissions with likelihood of increasing CO and UHC emissions. When other strategies such as EGR and DDI are used together with DMO, the aforementioned benefits can be maximized along with reduction in CO and UHC emissions.

### ***6.5.5 Variable Valve Timing (VVT) Strategy***

VVT enables achievement of variable opening and closing of intake and exhaust valves timing during operation. With early and late intake valve closing timing, the compression ratio can be flexible and adjusted; hence the thermodynamic state of the in-cylinder charge can effectively be controlled, which is beneficial for the control of LTC phase. However, VVT is an effective way of controlling NO<sub>x</sub> and soot emissions while reducing maximum in-cylinder pressure and peak pressure rise rate, hence it could suppress the ringing intensity [41]. Xu et al. [41] optimized numerically the RCCI combustion with VVT at various loads conditions. The result showed that combining RCCI with VVT strategy enabled achievement of Euro VI limit for NO<sub>x</sub> with significantly reduced soot emission at low and medium load conditions while fuel consumption was found comparable at all load conditions. Table 6.1 shows that VVT has similar benefits and potentialities with DMO; hence with the combination of EGR and DDI, it can be more advantageous.

### ***6.5.6 Other Potential Strategies***

To utilize a single fuel in RCCI combustion instead of using two fuels with different reactivity, the use of fuel additives (FA) comes in. The strategy of using cetane number improvers on a single LRF to improve its reactivity and inject directly into the cylinder in place of HRF thereby creating reactivity gradient is known as single fuel strategy in RCCI [4]. Besides, FA can be used to improve the reactivity of some blended fuels.

Compression ratio is a parameter used to indicate the extent of compression and the process of compression increases the temperature and pressure of the charge in the cylinder causing rapid fuel evaporation, mixing and subsequent combustion. The strategy of varying compression ratio was employed by some researchers to improve combustion performance and emission characteristics of CI engine. Therefore, variable compression ratio (VCR) has great potentiality in improving performance parameters along with the decrease in CO, HC, and soot emissions in dual-fuel combustion modes though most of the researchers unanimously reported its challenge of increase in NO<sub>x</sub> emissions due to increase in in-cylinder temperature at higher compression ratios. However, these signify that the benefits of VCR in reducing CO and HC emissions can be extended to RCCI combustion.

To track and be able to optimize combustion phasing, RCCI requires feedback and control systems. Mixture reactivity and direct injection timing in RCCI needs to be controlled precisely during steady-state and transient operation conditions. Precise control of combustion has been a greatest challenge in RCCI and yet very little is done for such accomplishment.

## 6.6 Liquid LRF in RCCI for Improved Performance

Low reactivity fuels (LRF) are fuels characterized with a high octane number that are usually port-injected during RCCI combustion. Those commonly used in RCCI include gasoline, NG, methanol, and ethanol [4]. Recently butanol and dimethyl furan were also considered as LRFs in RCCI engine. In addition to NG, biogas and syngas are promising gaseous LRF utilized in RCCI combustion. However, these fuels can also be directly injected during RCCI combustion by modification of the engine to enable DDI. To limit the scope of the chapter, this section covers the use of bio-based LRF in RCCI as summarized in Table 6.2.

### 6.6.1 *Dimethyl Furan as LRF in RCCI Combustion*

Dimethyl furan (DMF) is also a second-generation biofuel with high octane number and energy density thus it can serve as a substitute to gasoline in IC engine. However, DMF can be produced directly from biomass materials with much less energy consumption compared to ethanol [29]. DMF superior properties called the attention of researchers to investigate its workability in IC engine. Zheng et al. [29] investigated experimentally the combustion and emission of RCCI engine fueled with biodiesel–DMF. The authors reported that its combustion resulted in high NO<sub>x</sub> emission due to lower latent heat value. Figure 6.3 indicates that both alcohols and DMF exhibited similar emission trends in reactivity with biodiesel. Both reduce CO and PM with an increase in UHC and NO<sub>x</sub> relative to change in some parameters such as EGR.



**Table 6.2** Summarized effects of LRF on combustion and emission attributes of RCCI engine

Mode	Reactivity fuels		Effects on combustion				Effects on emission				References	
	HRF	LRF	CA50	TE	PPRR	NOx	PM	UHC	CO			
RCCI	Biodiesel	Gasoline	↔			↑	↓			[22]		
			↔	↑	↑	↑	↓	↓	↓	[11]		
					↔	↔	↔	↑	↓		[18]	
							↓	↓	↓	↓	↓	[44]
					↔	↑	↔	↑	↓	↓	↓	[24]
RCCI	Biodiesel	Methane	↑		↑	↓	↓	↓	↓	[23]		
			↔		↔	↑	↓	↓	↓	[45]		
			↑		↑	↓	↓	↓	↓	↓	[46]	
			↑		↑	↓	↓	↓	↓	↓		
					↑	↑	↓	↓	↓	↓	↓	[47]
RCCI	Biodiesel	Ethanol	↑		↑	↔	↓	↑	↑	[29]		
					↔	↓	↑	↑	↑	[48]		
						↔	↓	↓	↓	↓	[19]	
RCCI	Biodiesel	Butanol	↑		↑	↓	↓	↑	↑			
			↑		↔	↓	↑	↑	↑	[28]		
					↑	↓	↓	↓	↑	↑	[29]	
RCCI	Biodiesel	DMF	↑		↑	↑	↓	↑	↑			
			↑		↑	↑	↑	↑	↑	↓	[29]	

Note (↑) stands for advance in CA50 or high values for TE and PPRR and (↓) stands for retard in CA50 or low values for TE and PPRR while (↔) represent the relatively constant for TE and PPRR but shows comparison to conventional methods for NOx, PM, UHC and CO emissions

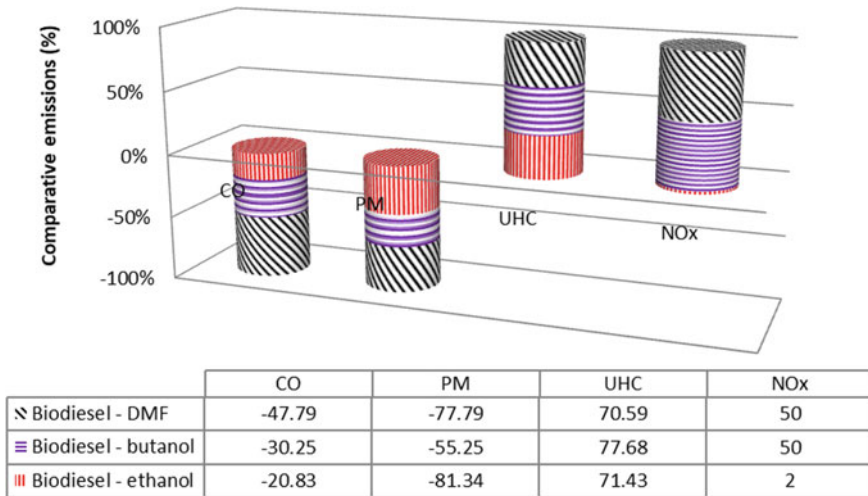


**Fig. 6.3** Emissions of biodiesel with alcohols and DMF in RCCI compared to conventional biodiesel

### 6.6.2 Use of Alcohols as LRF in RCCI Combustion

Alcohols are oxygenated in nature and can be produced from renewable substances such as agricultural products. This class of fuel is beneficial for cleaner combustion and reduced sole dependence on fossil energy. Methanol, ethanol, and butanol as alcoholic fuels are the most prominent alternatives due to their physico-chemical properties [49]. Methanol can be produced from natural gas, coal, biomass, or recovered through flashing vaporization in continuous production of biodiesel. Though methanol is produced at low cost but has some drawbacks such as lower calorific value, toxicity and poor solubility in diesel [50]. It is an environmentally and economically attractive fuel and can be used in a diesel engine as blended, fumigated or directly injected fuel. The attention of most researchers focused on blending methanol with diesel though requires an additive due to poor solubility. The use of biodiesel with a high fraction of methanol as reactivity fuels in RCCI coupled with the use of EGR and other appropriate strategies, the load can be extended with low emissions. Comparatively, it was observed from the studies of Li et al. [17, 26] that when diesel was used instead of biodiesel, the methanol mass fraction and intake temperature along with advanced SOI positively affected the combustion phase and engine-out emissions, except for NOx, due to high temperature.

Ethanol is a renewable fuel produced from biomass-based materials through alcoholic fermentation of food materials such as; sugar beet, sugar cane, corn, or wheat and non-food materials such as straw, feedstock, and waste wood. Due to low reactivity and good volatility, ethanol is a good substitute for gasoline. It is

commonly used for gasoline engine though blending bio-ethanol in diesel is recently receiving researchers' attention. Although ethanol has poor miscibility in diesel, it can be dissolved in biodiesel at any given proportion [29]. The ethanol reactivity is more beneficial to suppressing in-cylinder temperature thereby reducing NO<sub>x</sub> emission and PPRR with the likelihood of extending load to a higher limit as summarized in Table 6.2. However, the findings of Zheng et al. [29] showed that use of ethanol as LRF mitigated the persistent effect of biodiesel that resulted to high NO<sub>x</sub> emission. This effect similarly manifested in their findings, Pedrozo et al. [32], Benajes et al. [40] and Liu et al. [34] when diesel was used as HRF. The use of anhydrous ethanol and diesel enabled reduced UHC and CO emissions, but when hydrous ethanol was used the UHC and CO emissions increases while NO<sub>x</sub> emissions reduce in both cases.

Butanol is a first-generation renewable fuel produced from biomass-based materials through alcoholic fermentation of sugar beet, sugar cane, corn, or wheat [51]. The quest to avoid the use of food materials, lignocellulosic biomass such as woods, grasses, and agricultural wastes are converted to butanol [29, 51]. It is among the widely recognized alcohol fuels and attracted the attention of researchers, over methanol and ethanol, due to higher calorific value, miscibility in diesel, lower vapor pressure and non-corrosiveness. Its higher energy density, lower volatility, and hydrophilicity make it less corrosive and more suitable for transportation system [29]. Table 6.2 portrays that butanol and biodiesel reactivity is also beneficial to suppressing in-cylinder temperature thereby reducing NO<sub>x</sub> emission and peak pressure rise rate with the likelihood of extending load to higher limit compared to conventional method though UHC and CO emissions may not breakeven due to crevices and higher latent heat vaporization of bio-based alcohols causing lower regional temperature. Figure 6.3 indicates that both ethanol and butanol exhibited similar emission trends in reactivity with biodiesel.

## **6.7 Gaseous LRF in RCCI for Improved Performance**

As discussed in Sect. 6.6, gaseous fuels are also used as LRF in RCCI combustion ranging from fossil to bio-based. However, this section covers the benefits of using methane, biogas and syngas as gaseous fuel in reactivity stratification.

### **6.7.1 Methane as LRF in RCCI**

Methane as renewable energy is produced through bioconversion of the most abundant lignocellulosic biomass, animal manure, and food waste. Besides, methane is the major constituent in NG and potent greenhouse gases that can also be trapped from NG industries and other sources such as wastewater anaerobic treatment among others. It remained one of the sources that emitted greenhouse

gases with adverse environmental effects and can be utilized to reduce such effects [52]. Utilization of methane gas as fuel in IC engine can contribute to substantial environmental and economic benefits. The use of methane in CI engine gave higher thermodynamic conversion efficiencies while its high octane number minimizes the tendency of having an engine knocking at higher compression ratio [53]. The use of methane as LRF along with biodiesel is advantageous in getting stable combustion with improved thermal efficiency and reduced CO and UHC emissions as shown in Table 6.2. However, NO<sub>x</sub> emission increases when these fuels are used and addition of hydrogen gas still favored the said increase though the emission decreases compared to conventional NG–Diesel RCCI. Generally, the use of methane is highly beneficial to improve combustion parameters except for peak pressure rise rate.

### 6.7.2 Biogas as LRF in RCCI

Biogas is produced from anaerobic digestion of organic compounds like food wastes, animal wastes, and cellulosic biomass. It constitutes methane (CH<sub>4</sub>), carbon dioxide (CO<sub>2</sub>) and small percentage of nitrogen (N<sub>2</sub>). There are certain quantities of undesirable contaminants such as hydrogen sulfide (H<sub>2</sub>S), ammonia (NH<sub>4</sub>) and silicon oxides (SiO<sub>2</sub>) depending upon the biogas sources and could be detrimental to any thermal conversion device. It is an important renewable energy source with numerous applications and can replace fossil natural gas in internal combustion engine and deter its environmental impacts [54]. Hence, it is highly desirable to remodel RCCI combustion mode for effective and hitch-free performance using biomass-based gaseous fuels such as biogas.

Wang et al. [21] studied experimentally, simulated biogas–diesel RCCI performance. The result indicated controlled combustion phase due to prime injection timing while excessive pilot injection retarded the combustion. However, higher indicated thermal efficiency and CO emission were observed with controlled NO<sub>x</sub> and soot emissions. When certain strategies were used the persistent high CO emission relatively reduced as depicted in Fig. 6.4. It is shown in Fig. 6.4 that with the use of non-premixed port injection strategy, the CO emission was reduced significantly at medium to high load condition which could be attributed to high oxygen concentration at high load resulting to more complete combustion. When B5 diesel was used, the CO emission was reduced significantly at all load conditions signifying the benefit of using oxygenated fuel in RCCI. Qian et al. [20] reported the performance of two types of four-component syngas simulated as biogas operated on RCCI mode. Analytically, when the strategy of varying HRF injection parameters was used along with biogas as LRF, it offered a great advantage in combustion control, increased thermal efficiency and suppressed soot and NO<sub>x</sub> emissions due to low in-cylinder temperature and heat losses though the soot emission was affected by the increase in biogas premixed ratio.

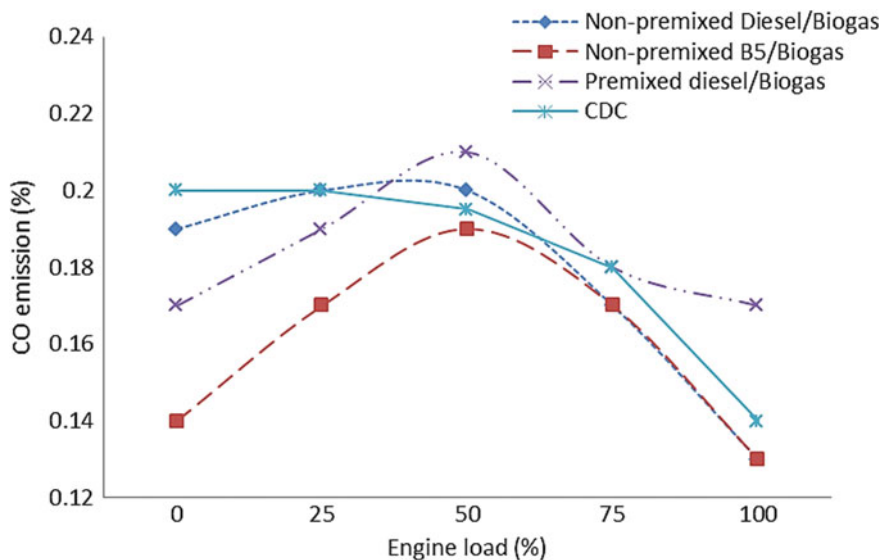


**Fig. 6.4** CO emission during non-premixed port injection of biogas and direct injection of different HRF

The significance of using biogas in suppression NO<sub>x</sub> is depicted in Fig. 6.5. It can be observed from Fig. 6.5 that biogas–diesel RCCI is more advantageous in reducing NO<sub>x</sub> than biogas–B5 RCCI due to little increase in in-cylinder temperature because of biodiesel concentration. Besides, the investigation on the effects of non-premixed port injection strategy in RCCI shows great potentiality in reducing UHC emission though remained relatively high compared to conventional diesel combustion as shown in Fig. 6.6.

### 6.7.3 Syngas as LRF in RCCI

Syngas is a biomass-based gaseous fuel obtained through the process of gasification or by reforming of flue gases through reaction with methane in the presence of catalysts. It is a CO<sub>2</sub> rich gaseous fuel composed of combustible and non-combustible gases such as; CO, H<sub>2</sub>, CH<sub>4</sub>, N<sub>2</sub>, and CO<sub>2</sub>. Syngas, as a desirable substitute to gaseous fossil fuels, has the potentiality to reduce engine-out emissions [27]. The presence of hydrogen in syngas improves its laminar burning velocity and extends its flammability limit. Hence, the lean combustion of the syngas–air mixture can be achieved, which can improve fuel efficiency and reduce NO<sub>x</sub> and PM emissions [27]. The use of syngas gives way to consistent combustion at low load as a consequence of a higher octane number and longer ignition delay of NG compared to other fuels [55]. However, the application of syngas in CI engine is

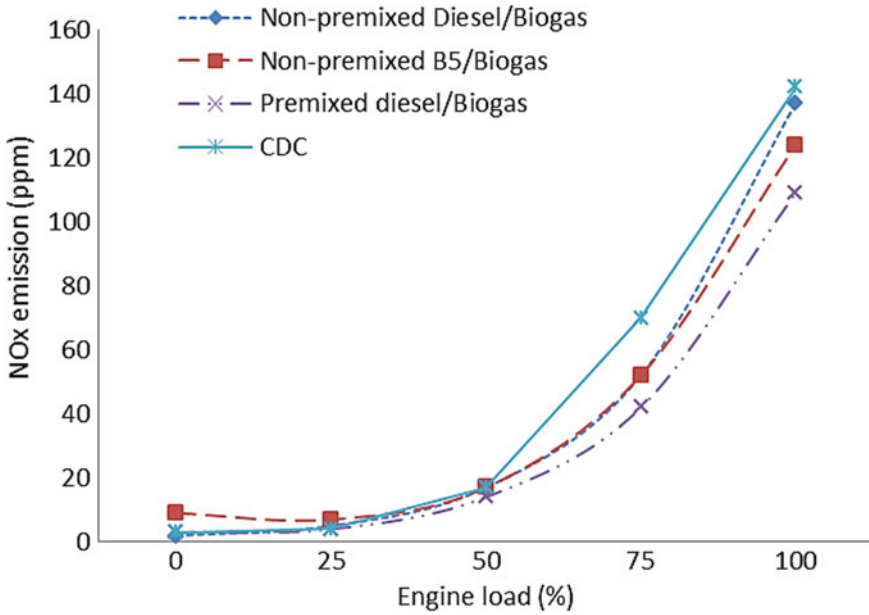


**Fig. 6.5** NOx emissions during non-premixed port injection of biogas and direct injection of different HRF

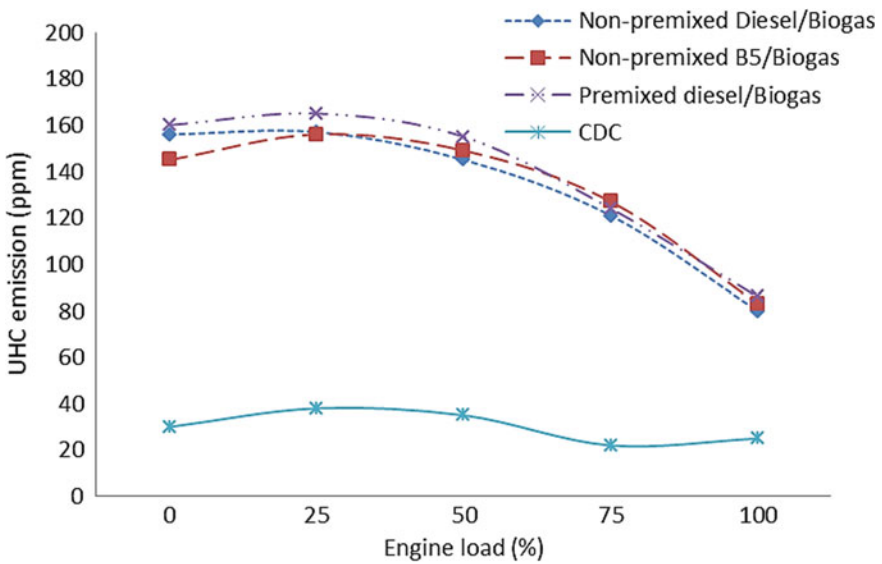


**Fig. 6.6** UHC emissions during non-premixed port injection of biogas and direct injection of different HRF

making way in advanced RCCI combustion. Rahnama et al. [55] reported that adding a proportion of hydrogen and syngas as additives improve combustion processes with reduced UHC and CO emissions of the RCCI engine at low load but peak pressure rise rate and high ringing intensity limited the engine operation at high load. However, use of hydrogen as dilution behaves otherwise. In another study, Rahnama et al. [56] used 3% by volume syngas in air, which enabled achievement of advanced combustion phase because of short ignition delay and combustion duration. More so, syngas addition improved combustion efficiency and suppresses CO emission. Xu et al. [27] computationally optimized syngas composition in syngas–diesel RCCI engine. The results indicated that higher fraction of H<sub>2</sub> in syngas was most desirable and yielded RCCI operation with high efficiency, moderate combustion and low emissions at full load. The use of early pilot fuel injection and high premixed ratio considerably reduced NO<sub>x</sub> emission with the corresponding efficient combustion.

## 6.8 Use of High Reactivity Fuel for Improved RCCI Performance

On the other hand, HRFs are fuels with high cetane number directly injected into the engine during RCCI combustion. The commonly used HRF are diesel and biodiesel [4]. Biodiesels are renewable mono alkyl esters derived from fatty acid esters of biological materials such as waste plants and animal fats. Biodiesel can be produced from various feedstock sources, from 1st, 2nd, and 3rd generation edible and non-edible oils, and can be utilized as direct-injected HRF. However, the most widely used sources for RCCI are Polyoxymethylene dimethyl ethers, palm oil waste, waste fish oil, waste cooking oil, safflower oil, and pangomia pinnata oil. Biodiesel can replace fossil diesel in IC engine and reduces harmful emissions while retaining the life-cycle emission of CO [57]. It has numerous advantages such as renewability, biodegradability, lubricity, high flash point, miscibility with fossil diesel and its ability to substitute fossil diesel in CI engines. Besides, it has some disadvantages like NO<sub>x</sub> emission, high cloud and pours points, lower energy content, lower oxidative ability, and poor performance at low temperature compared to conventional diesel.

The use of biodiesel in RCCI indicated controllable combustion with improved thermal efficiency that could be attributed to moderate combustion phase and minimized rate of heat transfer through the cylinder wall. It might likely cause rise in maximum in-cylinder pressure though in most cases within acceptable limit and became inauspicious when the load is extended to a higher limit. Specifically, the use of pure biodiesel indicated advanced combustion phase and improved thermal efficiency with acceptable peak pressure rise rate while use of blended biodiesel indicated retarded combustion phase and moderate thermal efficiency with higher peak pressure rise rate. For instance, an investigation of non-premixed port injection

of biogas–B5 diesel RCCI shows that more stable combustion, higher indicated thermal efficiency and lower SFC could be achieved as compared to conventional diesel RCCI. The combustion phase was advanced from low to medium load and retarded at high load while the break SFC decreased with the increase in load.

The highest indicated thermal efficiency of 37.45% was obtained at half load as shown in Figs. 6.7 and 6.8. However, the use of biodiesel irrespective of fraction drastically reduces soot with moderately acceptable NOx and CO emissions as a consequence of in-cylinder temperature which was lower than that of soot and NOx formation temperature. Besides, the use of biodiesel raises the UHC emission meanwhile both UHC and CO emissions could be attributed to the lower in-cylinder temperature caused by the amount of biodiesel or the amount of LRF entering the crevices.

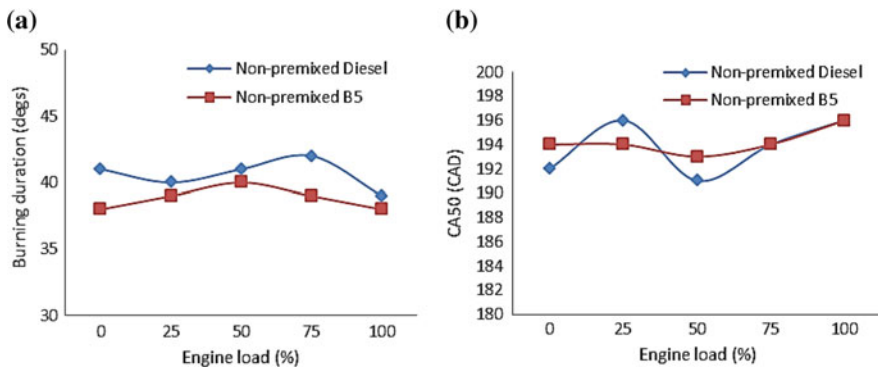


**Fig. 6.7** Variation of **a** burning duration and **b** combustion phase of RCCI with non-premixed port injected biogas

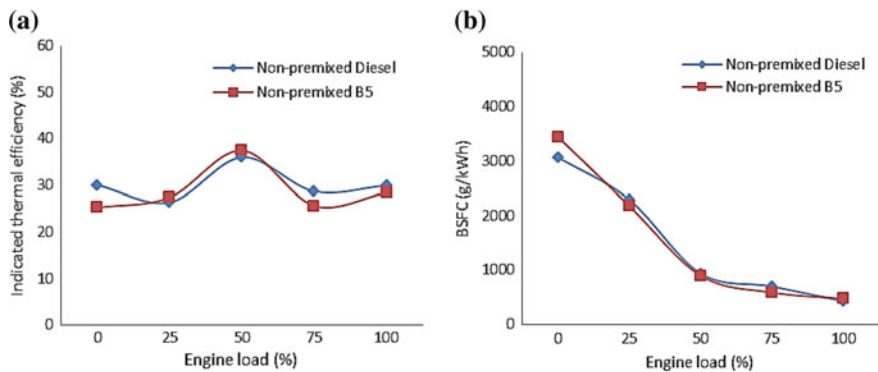


**Fig. 6.8** Variation of **a** indicated thermal efficiency and **b** specific fuel consumption of RCCI with non-premixed port-injected biogas



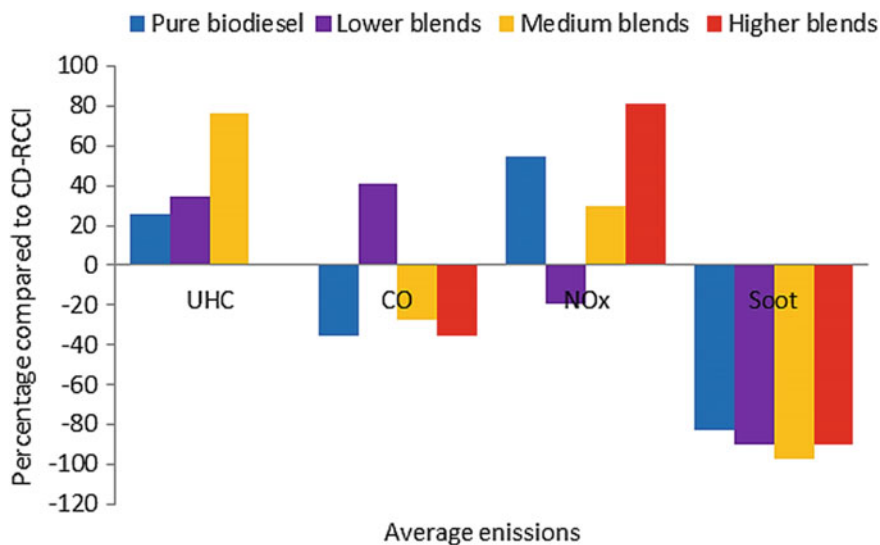


**Fig. 6.9** Comparative averaged emissions of pure and various blending ranges

However, Fig. 6.9 which is constructed based on average emissions indicates that use of pure biodiesel could increase NOx and UHC emission with reduced CO and soot emissions. In contrast, use of lower biodiesel blends indicated a rise in UHC and CO emissions with the corresponding decrease in NOx and soot emissions. This relatively simulates the trend of conventional diesel RCCI hence could be attributed to the fact that the effects of the oxygenated fuel do not actually manifest at lower blending ratios. As the biodiesel blends increase to medium level, NOx emission increases with further increase in UHC emission while CO emission decrease and kept the reputability of RCCI for significant reduction in soot emission. Similar trends manifested with higher biodiesel blends though the higher biodiesel blends further suppress the CO and soot emission which is clearly indicating the benefits of using oxygenated fuel in RCCI.

Conclusively, this inferred that use of biodiesel as HRF in RCCI is beneficial to improve combustion with a significant reduction in soot and CO emissions but increase NOx and UHC emissions. The use of biodiesel could serve a greater advantage over conventional diesel when appropriate LRF and strategies are used more especially medium to higher blends or pure biodiesel. The use of lower biodiesel blends requires careful selection of other low reactivity biofuels along with appropriate combination of strategies that can simultaneously reduce all emissions.

## 6.9 Summary

RCCI as an advanced and promising combustion mode is capable improving combustion and thermal efficiency with reduction in nitrogen oxides and soot emission though has high specific fuel consumption, unburned hydrocarbon, and carbon monoxide emission calling for appropriate strategies. Different strategies such as split injection, EGR rate among others were used to improve RCCI performance. Effects of these strategies influence advanced combustion phase and reduced UHC and CO emissions to a certain extent while maintaining RCCI reputation or otherwise. The use of some liquid biofuels as LRF in RCCI combustion has been gaining ground to serve as a substitute to gasoline in reactivity control. Alcohols improve the oxygen content, homogeneity in fuel distribution and in-cylinder temperature during the combustion. The use of these fuels enabled reduced soot and CO emissions along with thermal efficiency but UHC emission increases while NO<sub>x</sub> compromise with biodiesel blends. Depending on the LRF used, high reactivity fuels particularly biodiesel enables controlled combustion phase and extended load in RCCI engine due to minimized peak pressure rise rate with significant reduction in soot and CO emissions but increase NO<sub>x</sub> and UHC emissions. The use of biodiesel can serve a greater advantage over conventional diesel when appropriate LRF and strategy are used especially for medium to higher blends or pure biodiesel. The use of lower biodiesel blends requires careful selection of other low reactivity biofuels along with appropriate combination of strategies that can simultaneously reduce all emissions.

## References

1. Y. Qian, H. Li, D. Han, L. Ji, Z. Huang, X. Lu, Octane rating effects of direct injection fuels on dual fuel HCCI-DI stratified combustion mode with port injection of N-heptane. *Energy* **111**, 1003–16 (2016)
2. A.K. Agarwal, P.S. Akhilendra, K.R. Maurya, Evolution, challenges and path forward for low temperature combustion engines. *Progr. Energy Combust. Sci.* **61**, 1–56 (2017)
3. S. Molina, A. García, J.M. Pastor, E. Belarte, I. Balloul, Operating range extension of RCCI combustion concept from low to full load in a heavy-duty engine. *Appl. Energy* **143**, 211–27 (2015)
4. J. Li, W. Yang, D. Zhou, Review on the management of RCCI engines. *Renew. Sustain. Energy Rev.* **69**, 65–79 (2017)
5. S.L. Kokjohn, R.M. Hanson, D.A. Splitter, R.D. Reitz, Fuel reactivity controlled compression ignition (RCCI): a pathway to controlled high-efficiency clean combustion. *Intl. J. Eng. Res. Spec. Issue Pap.* **12**, 209–26 (2010)
6. J. Benajes, S. Molina, A. García, E. Belarte, M. Vanvolsem, An investigation on RCCI combustion in a heavy duty diesel engine using in-cylinder blending of diesel and gasoline fuels. *Appl. Therm. Eng.* **63**, 66–76 (2014)
7. I.B. Dalha, M.A. Said, Z.A.A. Karim, F. Firmansyah, Strategies and methods of RCCI combustion: a review, in *AIP Conference Proceedings 2035*, vol. 030006, pp. 030006-1–5, 2018

8. M. Mikulski, C. Bekdemir, Understanding the role of low reactivity fuel stratification in a dual fuel RCCI engine—a simulation study. *Appl. Energy* **191**, 689–708 (2017)
9. M. Nazemi, M. Shahbakhti, Modeling and analysis of fuel injection parameters for combustion and performance of an RCCI engine. *Appl. Energy* **165**, 135–150 (2016)
10. C. Zhang, L. Xue, Y. Li, Combustion characteristics and operation range of a RCCI combustion engine fueled with direct injection N-heptane and pipe injection. *Energy* **125**, 439–448 (2017)
11. L. Tong, H. Wang, Z. Zheng, R. Reitz, M. Yao, Experimental study of RCCI combustion and load extension in a compression ignition engine fueled with gasoline and PODE. *Fuel* **181**, 878–886 (2016)
12. P. Kamran, K.S. Rahim, A. Ehsan, K.I. Behrouz, S. Mehdi, J.D. Naber, Effect of diesel injection strategies on natural gas/diesel RCCI combustion characteristics in a light duty diesel engine. *Appl. Energy* **199**, 430–446 (2017)
13. A. Amoresano, C. Allouis, M. Di Santo, P. Iodice, G. Quaremba, V. Niola, Experimental characterization of a pressure swirl spray by analyzing the half cone angle fluctuation. *Exp. Thermal Fluid Sci.* **94**, 122–33 (2018)
14. A. Yousefi, M. Birouk, Investigation of natural gas energy fraction and injection timing on the performance and emissions of a dual-fuel engine with pre-combustion chamber under low engine load. *Appl. Energy* **189**, 492–505 (2017)
15. A. Kakaee, P. Rahnema, A. Paykani, CFD study of reactivity controlled compression ignition (RCCI) combustion in a heavy-duty diesel engine. *Periodica Polytechnica Transp. Eng.* **43**, 177–83 (2015)
16. H. Wang, X. Zhao, L. Tong, M. Yao, The effects of DI fuel properties on the combustion and emissions characteristics of RCCI combustion. *Fuel* **227**, 457–68 (2018)
17. Y. Li, M. Jia, Y. Liu, M. Xi, Numerical study on the combustion and emission characteristics of a methanol/diesel reactivity controlled compression ignition (RCCI) engine. *Appl. Energy* **106**, 184–97 (2013)
18. J. Li, X. Ling, D. Liu, W. Yang, D. Zhou, Numerical study on double injection techniques in a gasoline and biodiesel fueled RCCI (reactivity controlled compression ignition) engine. *Appl. Energy* **211**, 382–92 (2018)
19. J. Benajes, S. Molina, A. García, J. Monsalve-Serrano, Effects of direct injection timing and blending ratio on RCCI combustion with different low reactivity fuels. *Energy Convers. Manag.* **99**, 193–209 (2015)
20. Y. Qian, Y. Zhang, X. Wang, X. Lu, Particulate matter emission characteristics of reactivity controlled compression ignition engine fueled with biogas/diesel dual fuel. *J. Aerosol Sci.* **113**, 166–177 (2017)
21. X. Wang, Y. Qian, Q. Zhou, X. Lu, Modulated diesel fuel injection strategy for efficient-clean utilization of low-grade biogas. *Appl. Therm. Eng.* **107**, 844–52 (2016)
22. J. Li, W.M. Yang, H. An, D. Zhao, Effects of fuel ratio and injection timing on gasoline/biodiesel fueled RCCI engine: a modeling study. *Appl. Energy* **155**, 59–67 (2015)
23. J. Liu, F. Yang, H. Wang, M. Ouyang, Numerical study of hydrogen addition to DME/CH<sub>4</sub> dual fuel RCCI engine. *Int. J. Hydrogen Energy* **37**, 8688–97 (2012)
24. H. Liu, Q. Tang, X. Ran, X. Fang, M. Yao, Optical diagnostics on the reactivity controlled compression ignition (RCCI) with micro direct-injection strategy. *Proc. Combust. Inst.* **000**, 1–9 (2017)
25. D.Z. Zhou, W.M. Yang, H. An, J. Li, Application of CFD-chemical kinetics approach in detecting RCCI engine knocking fueled with biodiesel/methanol. *Appl. Energy* **145**, 255–64 (2015)
26. Y. Li, M. Jia, Y. Chang, Z. Xu, G. Xu, H. Liu, Principle of determining the optimal operating parameters based on fuel properties and initial conditions for RCCI engines. *Fuel* **216**, 284–95 (2018)
27. Z. Xu, M. Jia, Y. Li, Y. Chang, G. Xu, L. Xu, Computational optimization of fuel supply, syngas composition, and intake conditions for a syngas/diesel RCCI engine. *Fuel* **234**, 120–34 (2018)

28. Z. Zheng, M. Xia, H. Liu, R. Shang, G. Ma, M. Yao, Experimental study on combustion and emissions of N-Butanol/biodiesel under both blended fuel mode and dual fuel RCCI mode. *Fuel* **226**, 240–51 (2018)
29. Z. Zheng, M. Xia, H. Liu, X. Wang, M. Yao, Experimental study on combustion and emissions of dual fuel RCCI mode fueled with biodiesel/n-Butanol, biodiesel/2,5-dimethylfuran and biodiesel/ethanol. *Energy* **148**, 824–38 (2018)
30. Y. Li, M. Jia, Y. Chang, Y. Liu, M. Xie, T. Wang, L. Zhou, Parametric study and optimization of a RCCI (reactivity controlled compression ignition) engine fueled with methanol and diesel. *Energy* **65**, 319–32 (2014)
31. Y. Wang, M. Yao, T. Li, W. Zhang, Z. Zheng, A parametric study for enabling reactivity controlled compression ignition (RCCI) operation in diesel engines at various engine loads. *Appl. Energy* **175**, 389–402 (2016)
32. V.B. Pedrozo, I. May, T.D.M. Lanzanova, H. Zhao, Potential of internal EGR and throttled operation for low load extension of ethanol—diesel dual-fuel reactivity controlled compression ignition combustion on a heavy-duty engine. *Fuel* **179**, 391–405 (2016)
33. J.H. Lim, R.D. Reitz, High load (21 Bar IMEP) dual fuel RCCI combustion using dual direct injection. *J. Eng. Gas Turbines Power* **136**, 101–514 (2014)
34. H. Liu, G. Ma, B. Hu, Z. Zheng, M. Yao, Effects of port injection of hydrous ethanol on combustion and emission characteristics in dual-fuel reactivity controlled compression ignition (RCCI) mode. *Energy* **145**, 592–602 (2018)
35. M. Wissink, R.D. Reitz, Direct dual fuel stratification, a path to combine the benefits of RCCI and PPC. *SAE Intl. J. Eng.* **8**, 01–0856 (2015)
36. C. Kavuri, J. Paz, S.L. Kokjohn, A comparison of reactivity controlled compression ignition (RCCI) and gasoline compression ignition (GCI) strategies at high load, low speed conditions. *Energy Convers. Manag.* **127**, 324–41 (2016)
37. Firmansyah, A.A.A. Rasheed, M. Heikal, Z.A.A. Karim, Diesel/CNG mixture autoignition control using fuel composition and injection gap. *Energies* **10**, 1639 (2017)
38. J.H. Lim, R. Reitz, Improving high efficiency reactivity controlled compression ignition combustion with diesel and gasoline direct injection. *Proc. Inst. Mech. Eng. Part D, J. Automob. Eng.* **227**, 17–30 (2013)
39. A. García, J. Monsalve-Serrano, R.V. Rückert, M.E. Santos Martins, Evaluating the emissions and performance of two dual-mode RCCI combustion strategies under the world harmonized vehicle cycle (WHVC). *Energy Convers. Manag.* **149**, 263–74 (2017)
40. J. Benajes, A. García, J. Monsalve-Serrano, S.R. Lago, Fuel consumption and engine-out emissions estimations of a light-duty engine running in dual-mode RCCI/CDC with different fuels and driving cycles. *Energy* **157**, 19–30 (2018)
41. G. Xu, M. Jia, Y. Li, Y. Chang, T. Wang, Potential of reactivity controlled compression ignition (RCCI) combustion coupled with variable valve timing (VVT) strategy for meeting euro 6 emission regulations and high fuel efficiency in a heavy-duty diesel engine. *Energy Convers. Manag.* **171**, 683–98 (2018)
42. A. Paykani, A. Kakaee, P. Rahnama, R.D. Reitz, Progress and recent trends in reactivity-controlled compression ignition engines. *Int. J. Engine Res.* **17**, 481–524 (2016)
43. M.B. Luong, R. Sankaran, G.H. Yu, S.H. Chung, C.S. Yoo, On the effect of injection timing on the ignition of lean PRF/Air/EGR mixtures under direct dual fuel stratification conditions. *Combust. Flame* **183**, 309–21 (2017)
44. J. Li, W.M. Yang, D.Z. Zhou, Modeling study on the effect of piston bowl geometries in a gasoline/biodiesel fueled RCCI engine at high speed. *Energy Convers. Manag.* **112**, 359–68 (2016)
45. A. Ghareghani, R. Hosseini, M. Mirsalim, S.A. Jazayeri, An experimental study on reactivity controlled compression ignition engine fueled with biodiesel/natural gas. *Energy* **89**, 558–67 (2015)
46. S.S. Kalsi, K.A. Subramanian, Experimental investigations of effects of hydrogen blended CNG on performance, combustion and emissions characteristics of a biodiesel fueled reactivity controlled compression ignition engine. *Intl. J. Hydr. Energy* **42**, 4548–60 (2017)

47. D.Z. Zhou, W.M. Yang, H. An, J. Li, C. Shu, A numerical study on RCCI engine fueled by biodiesel/methanol. *Energy Convers. Manag.* **89**, 798–807 (2015)
48. Z.M. Isik, A. Hüseyin, Analysis of ethanol RCCI application with safflower biodiesel blends in a high load diesel power generator. *Fuel* **184**, 248–60 (2016)
49. S. No, Application of bio-butanol in advanced CI engines—a review. *Fuel* **183**, 641–58 (2016)
50. D.K. Jamuwa, D. Sharma, S.L. Soni, Experimental investigation of performance, exhaust emission and combustion parameters of compression ignition engine with varying ethanol energy fractions. *Energy* **127**, 544–57 (2017)
51. E.G. Giakoumis, C.D. Rakopoulos, A.M. Dimaratos, D.C. Rakopoulos, Exhaust emissions with ethanol or N-butanol diesel fuel blends during transient operation: a review. *Renew. Sustain. Energy Rev.* **17**, 170–90 (2013)
52. M. Farzaneh-gord, M.S. Pahlevan-zadeh, Measurement of methane emission into environment during natural gas purging process. *Environ. Pollut.* **242**, 2014–26 (2018)
53. G.D. Blasio, G. Belgiorno, C. Beatrice, Effects on performances, emissions and particle size distributions of a dual fuel (methane-diesel) light-duty engine varying the compression ratio. *Appl. Energy* **204**, 726–40 (2017)
54. N. Duic, M. Vujanovic, G. Krajac, Sustainable development of energy, water and environment systems for future energy technologies and concepts. *Energy Convers. Manag.* **125**, 1–14 (2016)
55. P. Rahnama, A. Paykani, R.D. Reitz, A numerical study of the effects of using hydrogen, reformer gas and nitrogen on combustion, emissions and load limits of a heavy duty natural gas/diesel RCCI engine. *Appl. Energy* **193**, 182–98 (2017)
56. P. Rahnama, A. Paykani, V. Bordbar, R.D. Reitz, A numerical study of the effects of reformer gas composition on the combustion and emission characteristics of a natural gas/diesel rcci engine enriched with reformer gas. *Fuel* **209**, 742–53 (2017)
57. V.K. Shahir, C.P. Jawahar, P.R. Suresh, Comparative study of diesel and biodiesel on ci engine with emphasis to emissions—a review. *Renew. Sustain. Energy Rev.* **45**, 686–97 (2015)

# Chapter 7

## Principal, Design and Characteristics of a Free Piston Linear Generator



**A. Rashid A. Aziz, M. B. Baharom, Ezrann Zharif Zainal Abidin, Firmansyah, Salah E. Mohammed, W. N. Azleen W. Nadhari, Evelyn and M. Noraiman M. Jaffry**

This chapter introduces the working principle, potential applications and current developments of free-piston engines (FPE) used for electricity generation. FPE is essentially a type of internal combustion engine (ICE) with its crankshaft mechanism removed to reduce total weightage and friction losses. However, since engine control conventionally relies heavily on crankshaft, an alternative control system is required for FPE. Therefore, studies are conducted on a free-piston linear generator (FPLG) prototype evaluating the optimum control and operation parameters to obtain best performance.

### 7.1 Introduction

Fossil fuels are considered as unsustainable energy source due to its harmful emission and limited availability. Based on data from BP Statistical Review of World Energy, current known oil reserve is only sufficient for less than 50 years at the current rate of usage [1]. Even before it actually runs out, lack of alternative fuels will drive oil prices up dramatically due to its limited availability. Furthermore, on environmental point of view, completely depleting these reserves will produce 746 billion tons of carbon [2]. This amount is almost thrice as much as the carbon budget (275 billion tons) to maintain global temperature rise below 2 °C set at the UN Paris climate agreement.

As awareness on unsustainability of fossil fuel-powered internal combustion engines (ICE) increases, hybrid and electric vehicles are becoming increasingly popular. These types of vehicle rely partially or fully on electric power to drive the

---

A. R. A. Aziz · M. B. Baharom · E. Z. Z. Abidin · Firmansyah · S. E. Mohammed · W. N. A. W. Nadhari · Evelyn (✉) · M. N. M. Jaffry  
Centre for Automotive Research and Electric Mobility, Universiti Teknologi PETRONAS,  
32610 Seri Iskandar, Perak, Malaysia  
e-mail: [evelyn@utp.edu.my](mailto:evelyn@utp.edu.my)

vehicle motion. These mean that dependency on fossil fuels can be dramatically reduced or even completely eliminated. Since electricity can be generated through renewable energy sources such as solar and wind, this makes it a more sustainable option for the future.

Currently, hybrid vehicles are more feasible than electric vehicles considering the availability of charging stations and affordability of the vehicles itself. Charging stations are yet to be as widely available as conventional petrol or diesel fueling stations, especially in developing countries. Hybrid cars also generally cost less than electric cars, which makes it more accessible to general public instead of only for the wealthy few. After all, the objective is to increase usage volumes enough for it to actually make a noticeable difference.

One of the simplest types of hybrid vehicles is the Series Hybrid Electric Vehicle (SHEV) where wheels are fully driven by electric motors. Additionally, an on-board generator is installed as range extender where ICE is used to convert conventional fossil fuels into additional electricity when required. This additional feature improves the vehicles' versatility to be operated anywhere without the worry of unavailability of charging stations. Until infrastructures supporting fully electric vehicles are more developed worldwide, SHEV is the most suitable transitional system currently available.

Since the ICE in SHEV is used solely for electricity generation instead of wheel rotation, components such as the crank mechanism are no longer necessary. For electricity generation purpose, linear motion could perform just as well if not better than rotational motion. This is the idea behind the invention of free-piston engine (FPE), where crank mechanism is eliminated to enable the piston to move freely in linear motion. More details on working principle of FPE will be laid out in the next section of this chapter.

Currently, one of the best fuel options for FPE is compressed natural gas (CNG) which is considered as the safest, cleanest, and most widely available among fossil fuels. It burns completely and produces less greenhouse emissions. Price of CNG also remains mostly constant even when gasoline or diesel price fluctuates dramatically. Lastly, production capability is predicted to be in abundance through 2040 [3], further ensuring affordability and availability. This period should provide plenty time for global development to accommodate full transition to electric vehicles.

Pescara [4] was the pioneer on the development of free-piston engine concept in 1928 through his patent. Unfortunately, by the mid-20th century, this concept has lost its appeal and studies were then abandoned. Once it starts regaining traction, investigation mainly focuses on its potential application to produce power for high hydraulic loads vehicles such as off-highway heavy machineries and forklift trucks. Recently, interest in free-piston engine is increasing due to its prospective application in hybrid-electric vehicle as it tends to have higher efficiency. Numerous groups of researchers worldwide are currently exploring the option of electricity generator using free-piston engine for application in hybrid-electric vehicle [5].

When used as electricity generation device, free-piston engine is often referred to as free-piston linear generator (FPLG). Electricity is produced through conversion of the linear motion of internal combustion engine. It operates in a similar principle of a

conventional internal combustion engine (ICE) where fuel combustion will generate high-pressure gas which will be the driver for piston movement within the cylinder. The difference lies in the absence of crankshaft mechanism in the configuration of FPLG. This design allows free motion in a linear path for the piston without the crankshaft causing any limitation [6]. Additional advantage is higher efficiency from the reduction in friction loss from crankshaft mechanism which is a common issue occurring in conventional ICE. Areas with more complicated structure such as between piston rings, cylinder wall, and piston skirt, also in crankshaft, cam-shaft bearings, and in the valves will cause the most friction losses [7].

The structure of FPLG consists of two main components which are the free-piston engine and a linear alternator made of permanent magnets and windings. Starting of engine is achieved through operating the linear alternator in motoring mode where alternating current is received to drive the piston. Combustion can be initiated once the required frequency has been reached, which will then continue on to induce reciprocating motion of the piston. Windings of the linear alternator will then generate electric current as a result from the piston linear motion. Different types of linear alternator will result in a different amount of power output as well. Classifications of linear alternators are typically based on its magnet arrangements, types, and phase structure [8].

There are two types of FPLG, four-stroke, and two-stroke, which is the more preferable one between the two. Four-stroke FPLG is less investigated due to the need for a more complex control system for the opening and closing of its valves. This means that it presents greater motion control issues compared to the two-stroke variant. There is a risk of the valves and piston colliding without a proper control system [9]. Another reason for two-stroke being more desirable is from a study by Jia et al. [10] which compared two and four-stroke free-piston engine generator. They found that higher indicated power and electric power is produced by two-stroke engine at the same throttle opening with four-stroke engine. This is caused by the four-stroke engine using up more of the generated power for its motoring processes.

## 7.2 General Operating Characteristics

After studying motion characteristics of double piston FPE, Xiao et al. [11] equalized the system to a forced vibration with adjustable stiffness and damping. Basing their mathematical analysis on Newton's second law, they concluded that a combination of factors such as external excitation, stiffness, moving mass, and damping will affect the amplitude. As even small changes in the aforementioned factors will significantly alter the amplitude, a comprehensive control system is required to prevent collision between piston and cylinder head from too high of an oscillation amplitude. Possible solutions to prevent such incident from occurring include increasing damping coefficient or lowering the amount of excitation force by reducing fuel mass, advancing ignition timing, or increasing the load.

Additional issues often found in FPE is misfiring, caused by the excitation force not corresponding with damping dissipation or even ceasing due to insufficient



input energy to overcome dissipation force. Consequently, oscillation amplitude will decrease gradually and eventually the piston motion will diminish. To avoid this, an adequate amount of external excitation must be provided.

While conventionally starting of ICE is done by cranking it over several revolutions, this method is not a viable option for FPE due to the elimination of crankshaft mechanism. An experiment involving a combination of two stages to start a dual-piston, two-stroke, spark-ignited FPE prototype is done by Jia et al. [12]. The first stage is the motoring phase, where electric machine is run as a motor to provide the required motoring force. In the second stage, delivery and ignition of fuel will be started after the piston has reached sufficient speed and compression ratio for combustion.

The linear electric machine will provide constant motoring force in the same direction as the velocity of the piston during the first stage. Displacement amplitude as well as peak in-cylinder pressure will continuously increase to obtain the optimal parameters for ignition. Fuel will be injected and then ignited once the signal based on piston position initiate the triggering process. The feasibility of such starting method has been proven through the experiments conducted. On the other hand, some issues as misfiring and notable cycle-to-cycle variation seem to occur quite frequently. Therefore, further optimization on certain parameters of injection and ignition is required for the engine to perform optimally.

Absence of crankshaft provides FPLG with additional advantage compared to conventional ICE in the form of unlimited piston position. Acceleration of FPLG piston is customizable to reduce the amount of time spent at top dead center (TDC). Since pressure and temperature tends to be the highest when piston is at this position, shortening the occurrence duration of this condition will result in lower heat transfer loss [6]. This theory is validated by an experiment done by Achten et al. [13] where it was found that when compared with conventional ICE, FPE had significantly faster combustion.

Further verification comes from a similar result presented by Tikkanen et al. [14]. Additionally, Feng et al. [15] through a numerical simulation conducted on diesel-fueled FPLG observed that around TDC, FPLG had higher acceleration than conventional ICE. Moreover, combustion in FPLG tends to result in lower average cylinder temperature, hence less NO<sub>x</sub> emission as well as energy loss from heat release. Combustion optimization can also be done by operation of homogenous charge compression ignition (HCCI) with the addition of adjustable compression ratio of FPLG. This will result in improvement in terms of thermal efficiency and emissions [16].

### 7.3 Research Methodology

Free piston linear generator dynamic and combustion characteristic can be analyzed from two perspectives which are numerical and experimental. From numerical analysis, the estimation of the performance of FPLG could be done prior to prototyping. This could save cost and time to analyze and optimize FPLG.

### 7.3.1 Working Principle

A two-stroke FPLG consists of combustion chamber, bounce chamber, and linear generator as shown in Fig. 7.1. The combustion chamber is where the main energy is released to translate the piston back and forth in a way that the EMF could be generated through the linear generator. Using the dual piston configuration, the piston moves back and forth by assistance of the bounce chamber.

The high acceleration of the piston after combustion allows the piston to travel to BDC as well as create the compression stroke at bounce chamber. The compression at bounce chamber does not contribute much on the power generation compared to combustion. This is because the bounce chamber compression objective is to build up the potential energy so that the piston can bounce back for the second compression stroke.

The bounce chamber shown in Fig. 7.2 consists of two pneumatic ports where each port connects to its own solenoid valve. The two pneumatic valves control the air mass of the bounce to control the piston TDC and BDC. Before starting the piston must be move to TDC, compressed air inject from both pneumatic host to project the motion of piston to TDC. One of the ports then changes to exhaust configuration such that the air inject early escape from the chamber and hence the bounce pressure set to be at atmospheric pressure. Next, the starting operation,

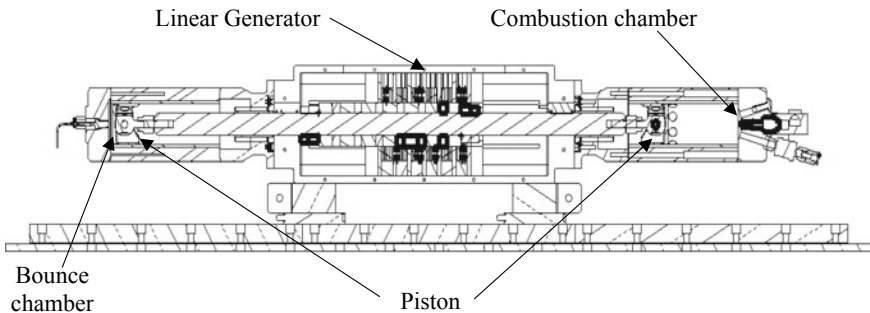


**Fig. 7.1** Cross-section of FPLG

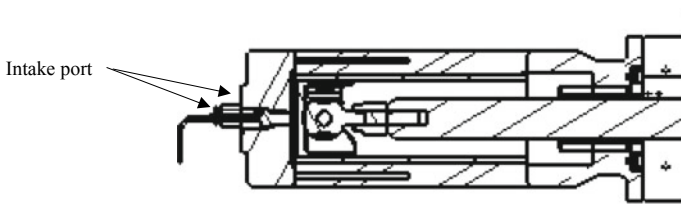


**Fig. 7.2** Bounce chamber cross-section

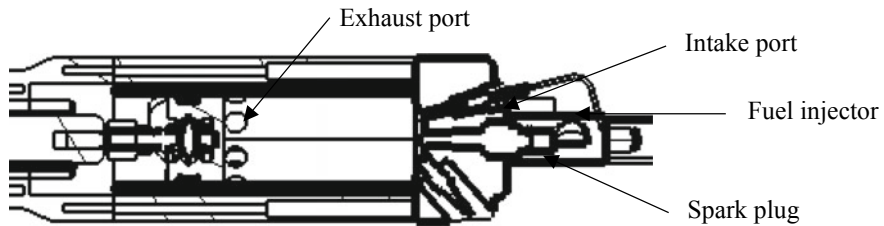
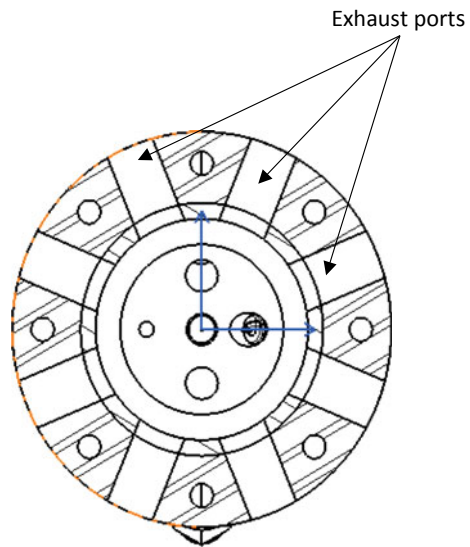


**Fig. 7.3** Combustion chamber cross-section

**Fig. 7.4** Exhaust cross-section on combustion chamber



at which the piston is at TDC, the compressed air supplied to the combustion chamber through pneumatic port as shown in Fig. 7.3 to create induction force and push the piston to BDC. Once it reaches the BDC, the piston will bounce back from the bounce chamber effect in compression stroke.

During the compression stroke stage, the fuel injection and spark ignition timing are set by the piston position. These two parameters are essential in determining the optimize operation condition of FPLG. The pneumatic port on the combustion chamber is controlled using the solenoid valve and the one-way valve to provide backflow during compression and combustion. The passive exhaust port is selected for FPLG exhaust. The exhaust hole in Fig. 7.4 is created through the circumference of combustion chamber wall to allow more residual gas escape to ambient after combustion and increase the trapping efficiency of scavenging system. The overall visual for FPLG motion from starting process is shown in Fig. 7.5.

Moreover, the kinetic energy of the piston translates to electrical energy by the linear alternator, as shown in Fig. 7.6. The linear alternator uses the Halbach-array

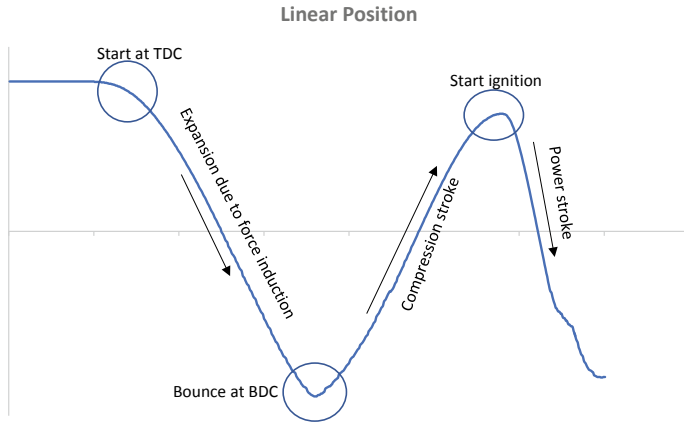


Fig. 7.5 FPLG motion profile

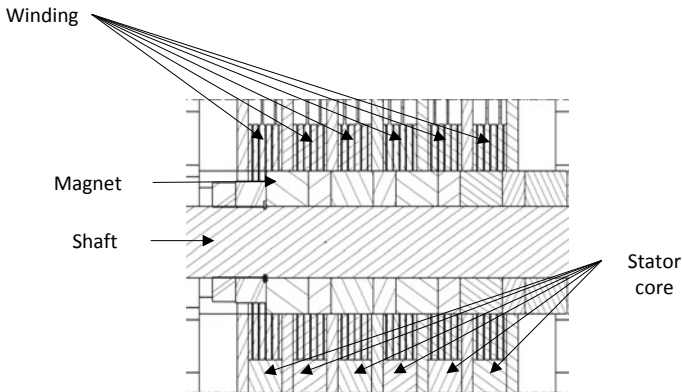


Fig. 7.6 Linear alternator configuration

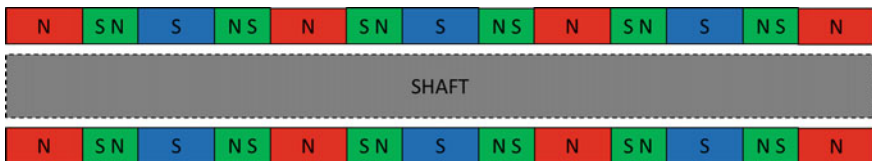


Fig. 7.7 Halbach-array magnet

view on arrangement on the magnet translator, as illustrated in Fig. 7.7, so that the flux density cut by the winding core is high. This is because the Halbach-array allows the flux intensity is higher on one side which in this case the outer region of the translator compared to inner region. In addition, with this arrangement the

amount of flux leakage could be minimized. The distinguished characteristic of the linear alternator in comparison to other linear alternators is that the movement of the piston is not governed by it. Most of the FPLG developed, the concept of linear motor is applied parallel with the linear generator to increase the precision of piston control [12, 17, 18].

### 7.3.2 Governing Equation

First, the dynamic motion is described as follows:

$$F = ma = A \times (P_l - P_r) \quad (7.1)$$

On the other hand, the combustion model is used to calculate the pressure acting on the combustion and bounce chamber of the FPLG. By applying the first law of Thermodynamics for closed system,

$$\frac{dU}{dt} = \frac{dQ}{dt} - \frac{dW}{dt} \quad (7.2)$$

where  $U$ ,  $Q$ , and  $W$  represent internal energy, heat addition and work done on the system while  $t$  is the simulation of time of modeling. Internal energy can be defined as:

$$\frac{dU}{dt} = mC_v \frac{dT}{dt} \quad (7.3)$$

Therefore, Eq. (7.2) becomes:

$$mC_v \frac{dT}{dt} = \frac{dQ}{dt} - P \frac{dV}{dt} \quad (7.4)$$

By using Mayer's relation and ideal gas law to derive Eq. (7.4) and rearranging the equation:

$$C_p = C_v + R \quad (7.5)$$

$$\gamma = \frac{C_p}{C_v} \quad (7.6)$$

$$mR \frac{dT}{dt} = P \frac{dV}{dt} + V \frac{dP}{dt} \quad (7.7)$$

After derivation, the Eq. (7.4) is rearranged as shown by:

$$dP = (\gamma - 1) \frac{dQ}{dt} - \frac{P}{V} \frac{dV}{dt} \quad (7.8)$$

Equation (7.8) is rearranged such that the rate of heat release (ROHR) could be obtained from the pressure and volume of the FPLG:

$$\frac{dQ}{dt} = -\frac{\gamma P}{\gamma - 1} \frac{dV}{dt} - \frac{V}{\gamma - 1} \frac{dP}{dt} \quad (7.9)$$

From the rate of heat release, the mass fraction burn (MFB) is calculated by:

$$\text{MFB} = \frac{\text{Accumulated ROHR}}{\text{Maximum accumulated ROHR}} \quad (7.10)$$

The electrical power output of the FPLG is measured from the load bank that is connected with the FPLG. The equation of electrical power output is:

$$P_E = I^2 R \quad (7.11)$$

where  $P_E$  is electrical power output,  $I$  is the current and  $R$  is the resistor of the FPLG.

### 7.3.3 Test Setup

As for the test setup, the FPLG and auxiliary system configured as shown in Fig. 7.8. Data logging and motion control of FPLG utilized the data acquisition system supplied by National Instruments. An assembly consisted of CNG gas tank, pressure regulators, Micro Motion mass flow meter, and injector is used to supply fuel gas to the system. A two-stage pressure regulator system is used to help maintain a constant downstream fuel line pressure at 18 bar. In-cylinder pressure and piston linear displacement are observed using two separate types of sensors connected to the aforementioned data acquisition system. Readings on linear displacement are provided by a linear displacement magnetic encoder while in-cylinder pressure is measured using a Kistler piezoelectric pressure transducer connected to a Kistler charge amplifier.

The experiments conducted to verify the overall performances of the FPLG are divided into three-stage. The first stage of experiment is to see the dynamic and thermodynamic behavior of the FPLG at starting process. The physical parameters are defined in Table 7.1.

Using the parameter set in Table 7.1, the FPLG combustion performances are observed and recorded. The recorded data is analyzed such that the comprehensive understanding of FPLG prototype for future development.

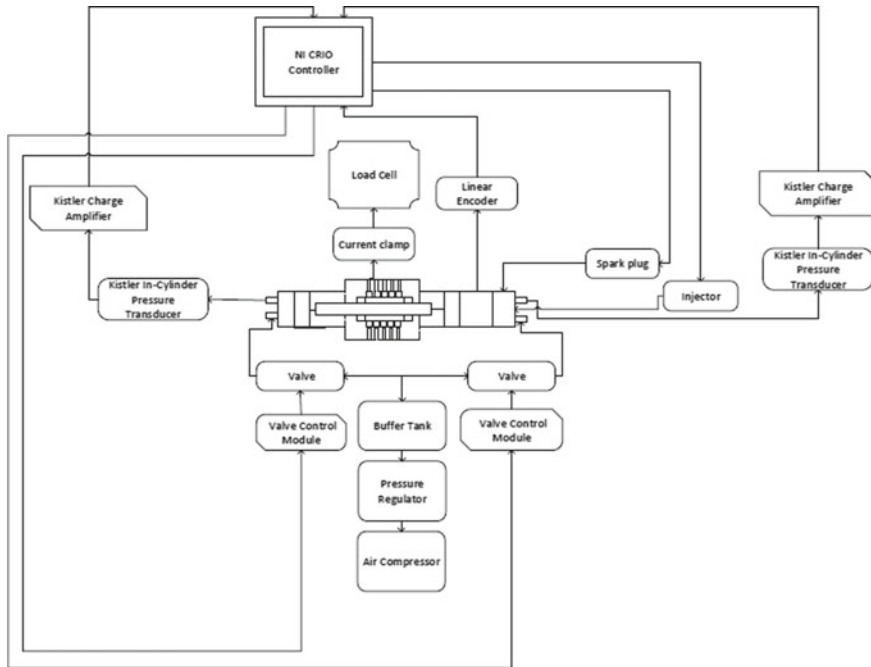


**Fig. 7.8** Schematic of the FPLG system

**Table 7.1** Physical parameter of FPLG

Parameter	Description
Strokes	2
Bore	56 mm
Stroke length	84 mm
Exhaust port open (EPO)	72.5 mm (from TDC)
Fuel type	CNG
Equivalence ratio (ER)	1.4
Injection position (INJ)	42 mm (from TDC)
Ignition position (IGN)	20 mm (from TDC)
Ignition type	Spark ignition
Maximum compression ratio	9.48
Moving mass	7 kg

For the second stages of experiment, the combustion characteristic of the FPLG using CNG fuel ins investigate to find the maximum operating condition. The ER is varied for this purpose. The variation of ER is defined by controlling the duration of injection. From the duration of injection, the mass flow rate of fuel is determined. The heat release and indicated thermal efficiency is then calculated to identify the

**Table 7.2** Equivalence ratio parameter

Test	2.1	2.2	2.3
ER	1.4	1.6	1.8

**Table 7.3** Injection position parameter

Test	3.1	3.2	3.3
INJ (mm)	39	42	45

equivalence ratio at which the FPLG operates at its best. The indicated thermal efficiency equation is given by:

$$\eta_t = \frac{\text{THR}}{Q_{\text{in}}} \quad (7.12)$$

where THR is total heat release and  $Q_{\text{in}}$  is:

$$\begin{aligned} Q_{\text{in}} &= \dot{m}_{\text{fuel}} \times Q_{\text{LHV}} \\ \dot{m}_{\text{fuel}} &= \text{mass flow rate of fuel} \\ Q_{\text{LHV}} &= \text{Low heating value of the fuel} \end{aligned} \quad (7.13)$$

Table 7.2 presents the variation of Equivalence ratio. Other parameters remain as stated in Table 7.1.

After the optimum equivalence ratio has been determined, the combustion investigation continues further by analyzing the combustion control strategy. The control strategy of FPLG differs from conventional engine, therefore injection timing parameter has to be redefined relative to piston displacement. This could be achieved by using the control system to change the fuel injection position. At this stage, the fuel injection position effects on combustion characteristic as well as power generation is examined. Table 7.3 shows the variation of injection position on FPLG performance test while fixed the other parameter as in Table 7.1.

## 7.4 Results and Discussions

Since the linear motion of FPLG is not restricted by crankshaft, cycle-to-cycle variation will occur in piston displacement. Figure 7.9 shows the velocity profile of FPLG with operating parameters described in Table 7.1. Compression stroke represents the phase where the bounce mechanism drives piston motion from BDC to TDC. Afterwards, power stroke occurs after combustion happened and moves the piston from TDC back to BDC. During compression stroke, piston velocity will reach maximum of 2 m/s and start decreasing halfway through the stroke length before coming to a complete halt at TDC. This happens as the result of gradual



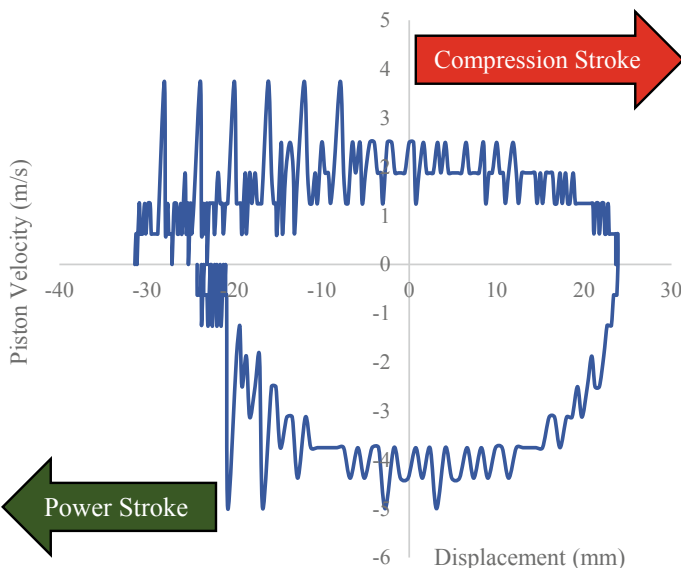


**Fig. 7.9** Variation of velocity with displacement of the FPLG's piston [19]

pressure drop in bounce chamber due to expansion while pressure is rising simultaneously in combustion chamber due to compression.

Subsequently, due to sudden pressure rise in combustion chamber after ignition, piston velocity is increased to a maximum value of 4 m/s while traveling back to BDC. The rise of piston velocity produces high mechanical power which then translates the piston towards BDC and increases the bounce pressure for combustion stroke. At this time, the electrical power output becomes significant. This operation continues is repeated again during continuous cycle. The high mechanical output after combustion can be observed in P–V diagram in Fig. 7.10. The P–V curve has a similar shape as Otto cycle curve which indicates that the combustion process occurs almost at constant volume region.

Experimental works are carried out for various equivalence ratios to evaluate its effect on overall performance. Three different values of equivalence ratios used are 1.4, 1.6, and 1.8. Figure 7.11 shows that there is no significant change in power output produced. However, Fig. 7.12 shows that maximum combustion pressure of 37.24 bar is obtained at ER 1.6. When it is further increased to ER 1.8, pressure is actually reduced to 32 bar which is even lower than what is obtained by ER 1.4. Therefore, it is found that ER 1.6 would provide the best condition for combustion. This result is further supported in Fig. 7.13 where maximum power profile is also obtained at ER 1.6.

Additional studies are also executed to observe the effect of various injection positions at fixed equivalence ratio of 1.0. Three different injection positions are considered, ranging from 39, 42, and 45 mm from TDC. The output parameters

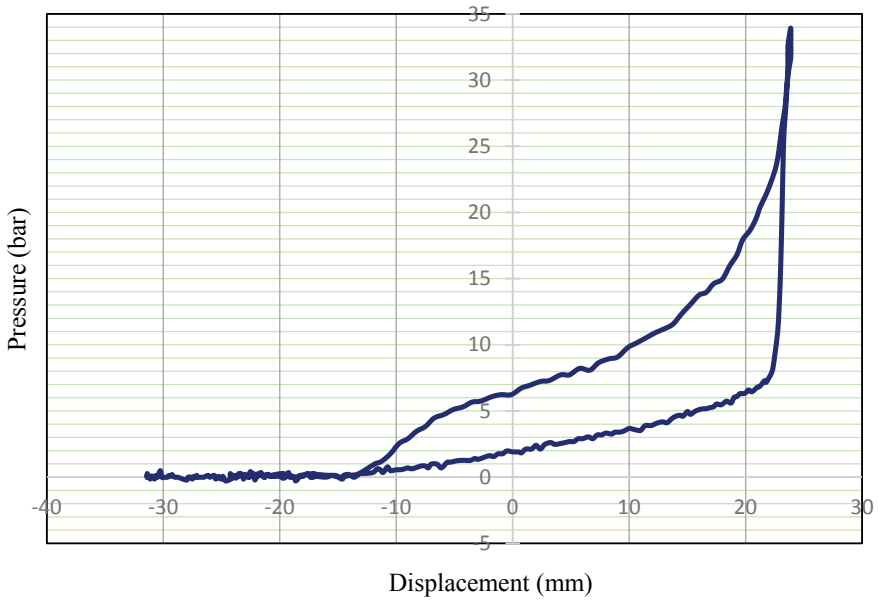


Fig. 7.10 Pressure–Displacement diagram of the FPLG [19]

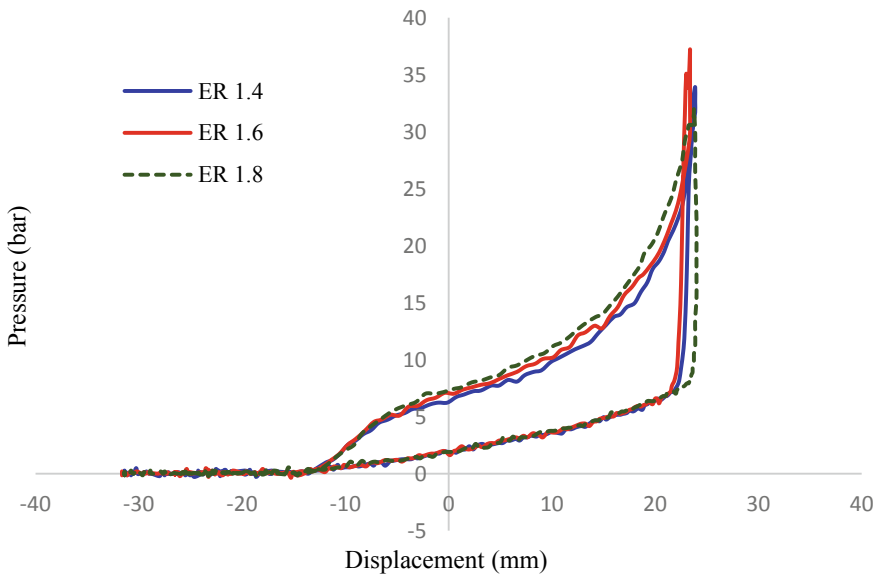


Fig. 7.11 Pressure–Displacement diagram for various equivalence ratios [19]

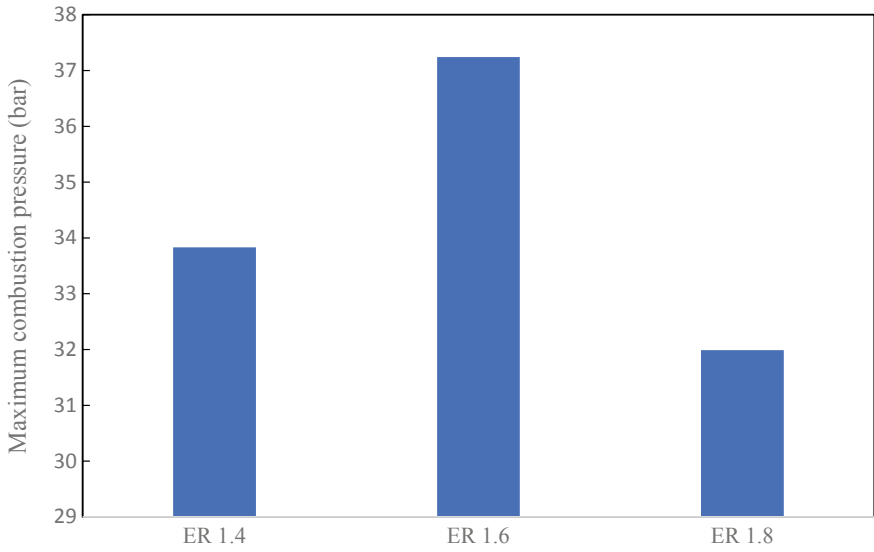


Fig. 7.12 Maximum combustion pressure for various equivalence ratios

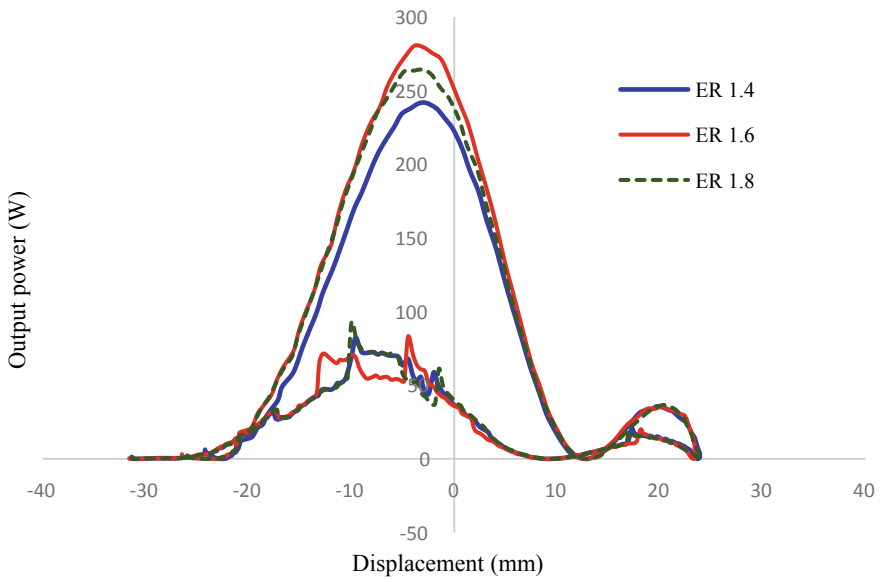
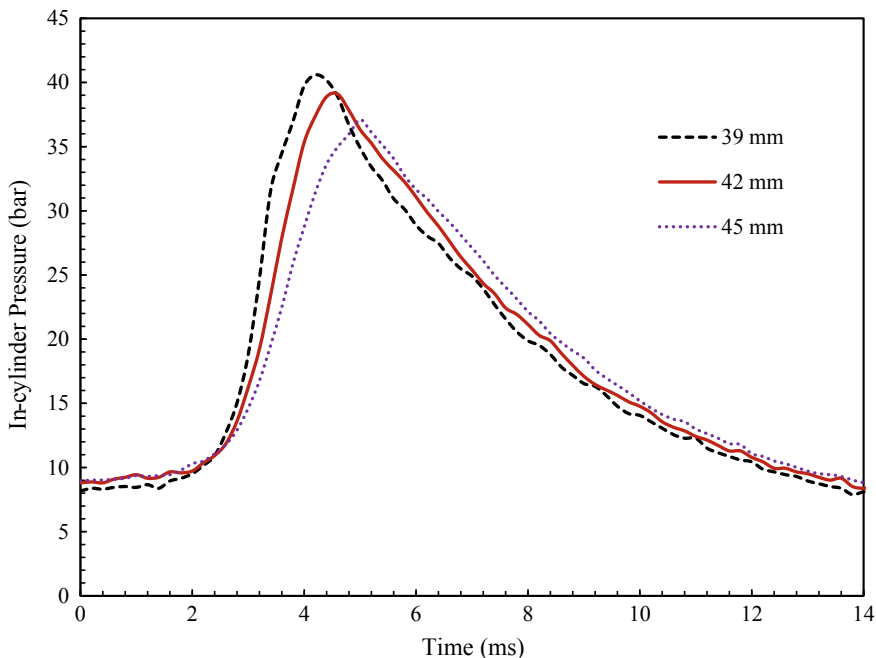


Fig. 7.13 Variation of output power with piston displacement for various equivalence ratio [19]



**Fig. 7.14** Variation of in-cylinder pressure with time for different injection positions [20]

evaluated are in-cylinder pressure, heat release rate, and mass fraction burned. It can be observed from Fig. 7.14 that for the case when injection position is at 39 mm, maximum peak in-cylinder pressure of 40.59 bar took place 4.2 ms after ignition was started. If the injection is moved to the midpoint of the stroke at 42 mm, maximum pressure of 39.1 bar is obtained 4.6 ms after ignition. Lastly for 45 mm, 37.11 bar is observed at 5 ms.

The results of the heat-release rate for different injection position are shown in Fig. 7.15. The lowest value of heat release rate is experienced for the case of injection position of 45 mm, that is about 0.19 kJ/ms, while the fastest value of the heat release is 0.38 kJ/ms occurs for the case of 39 mm. It can be said that both in-cylinder pressure and heat release rate have similar characteristics behavior. For the case of 45 mm injection position, the in-cylinder pressure and the heat release rate is shown to be low, and this is mainly due to the longer ignition delay period as a result of improper fuel mixing.

Figure 7.16 illustrates the effect of mass fraction burned (MFB) for three different injection positions. It is clear that the improvement of combustion rate is more evident at injection position of 39 mm. It can be observed from the figure that the combustion duration decreases with the decrease in injection position from 45 to 39 mm and this could be due to the reduction in ignition delay period.

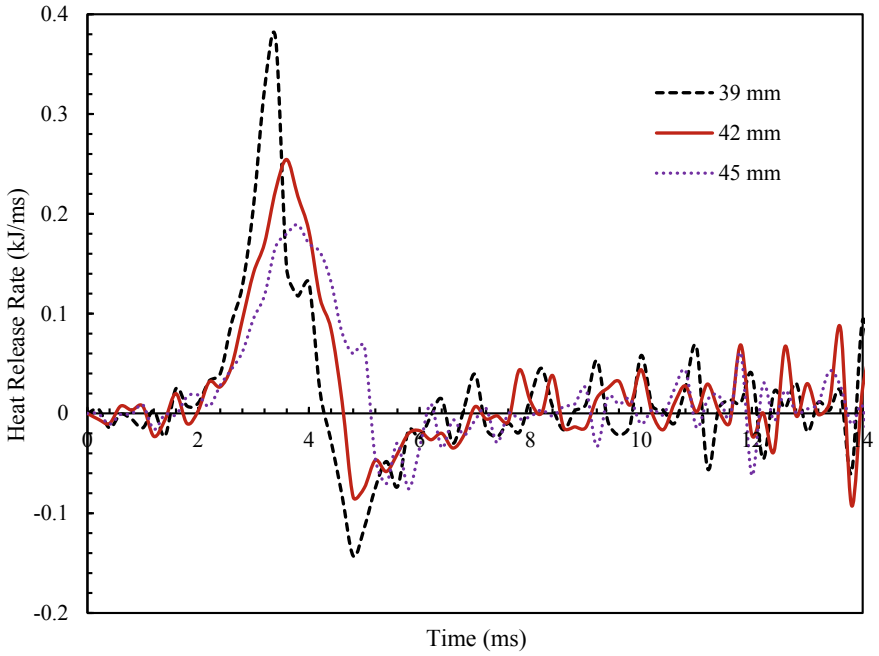


**Fig. 7.15** Temporal variation of heat release rate for different injection positions of the FPLG [20]

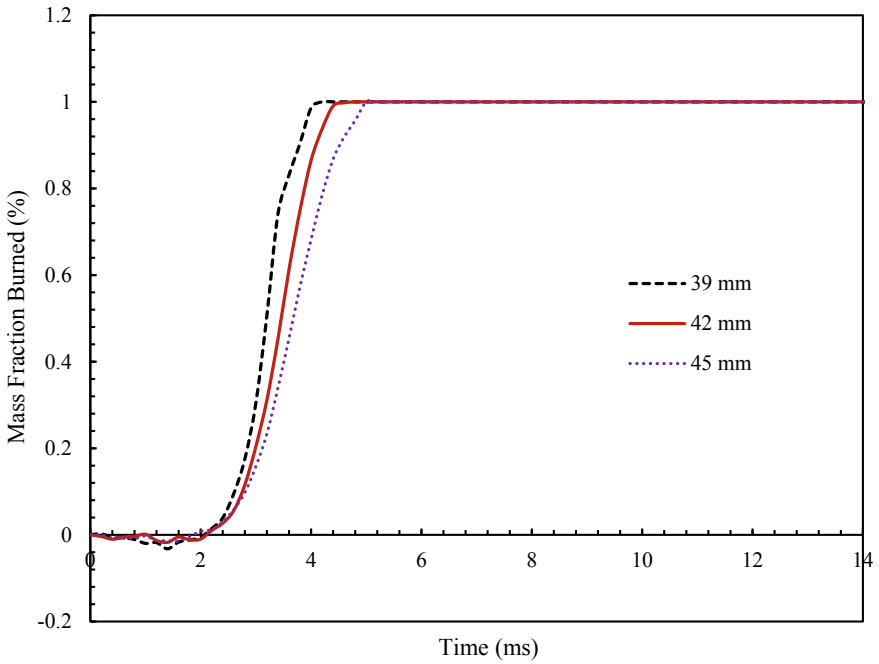


**Fig. 7.16** Temporal variation of mass fraction burned (MFB) for various injection positions [20]

## 7.5 Summary

Free piston linear generator has a great potential as on-board generator to extend the range of hybrid vehicle. It provides better versatility than fully electric vehicle by enabling the use of conventional fossil fuels when required. As a result, efficiency and environmental friendliness of electric vehicles can be maintained without the worry of unavailability of charging stations when it runs out of battery. Furthermore, due to elimination of need for rotational motion, crankshaft mechanism conventionally found in internal combustion engine is no longer required in FPLG. This simpler and lighter configuration has resulted in possibility for even better efficiency. Research groups worldwide have shown major interest in these types and engine and have come out with equally encouraging results. This study has found that by controlling certain parameters such as equivalence ratio and injection position, performance of FPLG can be further improved.

## References

1. BP, Full report—BP Statistical Review of World Energy 2018. Available: <https://www.bp.com/content/dam/bp/business-sites/en/global/corporate/pdfs/energy-economics/statistical-review/bp-stats-review-2018-full-report.pdf>. Accessed 21 Mar 2019
2. IPCC, *Climate Change 2013: The Physical Science Basis. Contribution of Working Group I to the Fifth Assessment Report of the Intergovernmental Panel on Climate Change*, ed. by T. F. Stocker, D. Qin, G.-K. Plattner, M. Tignor, S.K. Allen, J. Boschung, A. Nauels, Y. Xia, V. Bex, P.M. Midgley (Cambridge University Press, Cambridge, United Kingdom and New York, 2013), 1535 pp
3. J. Sherol, Natural gas to lead as fossil fuels dominate global energy mix through 2040, say exporters, [www.naturalgasintel.com](http://www.naturalgasintel.com), 11 Dec 2018. Available: <https://www.naturalgasintel.com/articles/116748-natural-gas-to-lead-as-fossil-fuels-dominate-global-energy-mix-through-2040-say-exporters>. Accessed 21 Mar 2019
4. P.R. Pateras, in *Motor-Compressor Apparatus*, ed. by Google Patents (1928)
5. R. Mikalsen, A. Roskilly, A review of free-piston engine history and applications. *Appl. Therm. Eng.* **27**, 2339–2352 (2007)
6. R. Mikalsen, A. Roskilly, The design and simulation of a two-stroke free-piston compression ignition engine for electrical power generation. *Appl. Therm. Eng.* **28**, 589–600 (2008)
7. R. Wakabayashi, M. Takiguchi, T. Shimada, Y. Mizuno, T. Yamauchi, The effects of crank ratio and crankshaft offset on piston friction losses. SAE Technical Paper 0148-7191, 2003
8. N.B. Hung, O. Lim, A review of free-piston linear engines. *Appl. Energy* **178**, 78–97 (2016)
9. Z. Xu, S. Chang, Prototype testing and analysis of a novel internal combustion linear generator integrated power system. *Appl. Energy* **87**, 1342–1348 (2010)
10. B. Jia, A. Smallbone, Z. Zuo, H. Feng, A.P. Roskilly, Design and simulation of a two-or four-stroke free piston engine generator for range extender applications. *Energy Convers. Manag.* **111**, 289–298 (2016)
11. J. Xiao, Q. Li, Z. Huang, Motion characteristic of a free piston linear engine. *Appl. Energy* **87**, 1288–1294 (2010)
12. B. Jia, G. Tian, H. Feng, Z. Zuo, A. Roskilly, An experimental investigation into the starting process of free-piston engine generator. *Appl. Energy* **157**, 798–804 (2015)

13. P.A. Achten, J.P. van den Oever, J. Potma, G.E. Vael, Horsepower with brains: the design of the chiron free piston engine. SAE Technical Paper 0148-7191, 2000
14. S. Tikkanen, M. Lammila, M. Herranen, M. Vilenius, First cycles of the dual hydraulic free piston engine. SAE Technical Paper 0148-7191, 2000
15. H. Feng, C. Guo, C. Yuan, Y. Guo, Z. Zuo, A.P. Roskilly et al., Research on combustion process of a free piston diesel linear generator. *Appl. Energy* **161**, 395–403 (2016)
16. H.I. Sherazi, Y. Li, Homogeneous charge compression ignition engine: a technical review, in *Automation and Computing (ICAC), 2011 17th International Conference on*, 2011, pp. 315–320
17. E.Z. Zainal Abidin, A.A. Ibrahim, A.R.A. Aziz, S.A. Zulkifli, Effect of motoring voltage on compression ratio of a free-piston linear generator engine. *J. Mech. Eng. Sci.* **8**, 1393–1400 (2015)
18. M.R. Hanipah, A.R. Razali, The numerical assessment of motion strategies for integrated linear motor during starting of a free-piston engine generator. *IOP Conf. Ser.: Mater. Sci. Eng.* **257**, 012054 (2017)
19. W.N.A.W. Nadhari, N.A. Ramlan, S.E. Mohammed, S. Munir, F. Firmansyah, A.A. Aziz, M.R. Heikal, Performance characteristics of free piston linear generator on different equivalence ratio. *AIP Conf. Proc.* **2035**(1), 060003 (2018)
20. S.E. Mohammed, N.A. Ramlan, A.R.A. Aziz, F. Firmansyah, Z. Ezrann Zainal, Investigation of late fuel injection position on the combustion of free piston engine, in *AIP Conference Proceedings*, vol. 2035, no. 1, p. 050002, 2018

# Chapter 8

## Efficient Visualization of Scattered Energy Distribution Data by Using Cubic Timmer Triangular Patches



**Fatin Amani Mohd Ali, Samsul Ariffin Abdul Karim,  
Sarat Chandra Dass, Vaclav Skala, Mohammad Khatim Hasan  
and Ishak Hashim**

This chapter discusses the application of the new cubic Timmer triangular patches constructed by Ali et al. [1] to interpolate the irregularly scattered data with  $C^1$  continuity. In order to apply the cubic Timmer triangular patches for scattered data interpolation, the data is first triangulated by using the Delaunay algorithm, and then the sufficient condition for  $C^1$  continuity is derived along the adjacent triangles. Two methods are used to calculate the cubic Timmer ordinates on each triangle. The convex combination between three local schemes  $T_i$ ,  $i = 1, 2, 3$  is used to produce the  $C^1$  surface everywhere. The proposed scheme will be tested to visualize three types of energy data sets with irregular shape properties. Numerical and graphical results are presented using MATLAB. Comparisons of the proposed scheme with some existing procedures such as cubic Ball and cubic Bézier triangular patches are also carried out. The resulting surface produced by cubic Timmer triangular patch is better than that produced using cubic Ball and cubic Bezier triangular patches with an overall coefficient of determination  $R^2$  value obtained to be larger than 0.8359.

---

F. A. M. Ali · S. A. A. Karim (✉) · S. C. Dass  
Fundamental and Applied Sciences Department, Universiti Teknologi PETRONAS,  
32610 Seri Iskandar, Perak, Malaysia  
e-mail: [samsul\\_ariffin@utp.edu.my](mailto:samsul_ariffin@utp.edu.my)

V. Skala  
Faculty of Applied Sciences, Department of Computer Science and Engineering,  
University of West Bohemia, Univerzitni 8, CZ 306 14, Pilsen, Czech Republic

M. K. Hasan  
Faculty of Information Science and Technology, Centre for Artificial Intelligence  
Technology, Universiti Kebangsaan Malaysia, 43600 UKM, Bangi, Selangor, Malaysia

I. Hashim  
Faculty of Science and Technology, Centre for Modelling and Data Science,  
Universiti Kebangsaan Malaysia, 43600 UKM, Bangi, Selangor, Malaysia



## 8.1 Introduction

Computer-Aided Geometric Design (CAGD) is a field initially developed to introduce computer-based applications to industries such as automotive, aerospace and shipbuilding. The term CAGD was proposed by Barnhill and Riesenfeld in 1974. This term was coined during a conference on the CAGD organized by them at the University of Utah, U.S.A. [2]. CAGD deals mainly with the mathematical aspects of computer-aided design such as the construction of the curves and surfaces [3].

In CAGD, the most famous and earliest method of constructing curves and surfaces is the Bèzier method. Another method of generating curves and surfaces that has similar behavior to the Bèzier method is the Ball method [4]. Both the Bèzier and Ball methods have the same properties for curves and surface construction, i.e., both fulfill positivity to ensure the convex hull condition is satisfied. The convex hull condition means that the formation of curve lies inside of the control polygon that is formed from the control points [2].

In the early 1980s, Harry Timmer proposed the Timmer method. This method is a variation of the Bèzier method [2]. Although Timmer method does not obey the convex hull property, it is more useful and easier to use in the designing of objects compared to the Bèzier method. The curve produced is nearer to its control polygon. Timmer's method may have the weakness of not obeying the convex hull property, but it is the best method for manipulating the curve [5]. Timmer's curve has a special property where the curve meets the midpoint of the line segment.

Some surfaces are more suitably represented using triangles rather than quadrilaterals since triangular regions yield a more convenient partition of the domain. Therefore, Timmer triangular patches can be used to construct surfaces over arbitrary triangular meshes. A brief overview of curve and surface construction using quadrilaterals and triangular surfaces are given in the following section. Most researchers use cubic Bèzier and cubic Ball triangular patches in scattered data interpolation. No research has been carried out using cubic Timmer triangular patches for the interpolation of scattered data. Thus, this study will focus on cubic Timmer triangular patches in scattered data.

Scattered data can be defined as the non-uniform distribution of data points such as rainfall or geological data. Scattered data are encountered in many areas of scientific applications such as in meteorology (for example, the amount of rainfall) and geology (such as the depths of underground formations). Research on scattered parametric data interpolation as well as shape preserving interpolation and range-restricted interpolation can be found in [1–53]. Meshless approach is another method that can be used for scattered data interpolation [54, 55]. However, in this chapter, the focus is given on the parametric approach.

Many researchers also have investigated surface interpolation based on triangulations for scattered data. The construction of scattered data interpolation using Bèzier triangular patches can be described as follows:

- (a) Triangulate the domain by using Delaunay triangulation,
- (b) Specify the derivatives at the data points, and then assign Bézier ordinate values for each triangular patch,
- (c) Generate the triangular patches of the surfaces, and finally,
- (d) Apply spatial data interpolation to estimate the missing value.

For instance, Chan and Ong [15] described the local scheme for range-restricted scattered data interpolation by using cubic triangular Bézier patches. The interpolating surface was obtained piecewise through convex combination of three cubic Bézier triangular patches. The sufficient conditions for the non-negativity of a cubic Bézier triangle on the Bézier ordinates were derived above certain lower bound. The gradients (first-order partial derivatives) at the data sites were modified, if necessary, to ensure that the non-negativity conditions are fulfilled.

Scattered data technique is important to visualize the geochemical images of the surface data. In the work of Karim and Saaban [32], they visualized terrain data by using cubic Ball triangular patches. The terrain data was collected at the central region of Malaysia. They claimed that cubic Ball triangular could reconstruct terrain surface with good approximation properties. Wu et al. [53] proposed a new approach to construct shape-preserving interpolating curves. This new approach was based on the use of a class of multiquadric quasi-interpolation operator and supported radial basis functions. It also has the advantages of preserving shapes and having good approximation behavior.

Several types of surfaces are concerned with non-negativity preserving interpolation on rectangular surfaces, such as in the study by Peng et al. [42]. In their study, rational splines were used to construct the non-negativity preserving interpolant of the data. Simple and explicit sufficient non-negativity conditions were derived. Experimental results illustrated the validity and feasibility of their method. Ramli and Ali [5] extended the Timmer function to higher order Timmer blending functions which were quartic and quantic functions. They were used for the designing of objects using Timmer quantic blending functions such as glass, sink, and vase. The quintic Timmer function was used because the higher order basis function would enable them to control the curve easier.

Shape-preserving scattered data interpolation is useful in geometric modeling and visualization. Ordinary interpolation methods do not preserve the data shape. In the work by Hussain et al. [31], they developed a method to preserve the shapes of scattered data when it was convex. Convexity is useful in shape property and its example applications are in telecommunication system design and approximation theory. Feng and Zhang [22] discussed a piecewise bivariate Hermite interpolation function in order to approximate three-dimensional scattered data sets. This study used local radial basis interpolation function to estimate the first derivative of each scattered point. Their methods had strong estimation ability for scattered data, and the approximation of derivatives by local radial basis interpolation had high accuracy.

Surface reconstruction is the process of generating three-dimensional surfaces from a point cloud of data of the real object. This method was significant in the area

of computer animation and industrial manufacturing. In Awang et al. [8], six different test functions were used in reconstructing the surface of scattered data points. Their research aims were to test the accuracy of Delaunay triangulation in generating different surface when the points were removed. Awang and Rahmat [7] focused on developing a smooth surface using the cubic Bézier triangular patch. The Delaunay triangulation process was chosen as the method did not require the deletion of the sample data points. Thus, it could preserve the original surface topology. The least squares minimization method was used to approximate the second-order partial derivatives. The Graphical User Interface (GUI) function was applied to represent the results and the comparison of the interpolation surface generated by six test functions were discussed.

Luo and Peng [40] described the rational spline as a piecewise rational convex combination of three cubic Bézier triangular patches that share the same boundary Bézier ordinates. The sufficient conditions for non-negativity were derived on the boundary Bézier ordinates of adjacent triangle and the normal derivatives at the data sites. If the non-negativity property is lost in any triangular patches, then the gradients at the data sites and normal derivatives at the edge knots will be modified to ensure positivity is preserved. Thus, their main scheme also requires the modification of the first order partial and normal derivatives.

Ong and Wong [3] described a globally scattered data interpolation scheme subject to constant lower and upper bounds. They used the side-vertex method for interpolation in triangles and the rational cubic spline was used for univariate interpolation along the line segments that join a vertex to the opposite edge of a triangle. The convex combination of three triangular patches then was used to construct the surface interpolation.

Piah et al. [43] improved the lower bound of Chan and Ong [15]. Their schemes still used the convex combination of three cubic Bézier triangular patches. They proposed an alternative scheme to Chan and Ong [15] which is simpler and have more relaxed conditions of positivity where the new lower bound for Bézier ordinates can become infinitely smaller compared to the lower bound of Bézier ordinates in Chan and Ong [15]. Some numerical results were presented to show the capability of the alternative scheme. The main drawback of their scheme is that the actual first-order partial derivative may be adjusted subject to the positivity sufficient conditions imposed on Bézier ordinates of each Bézier triangular patches.

Peng et al. [42] discussed the positivity preserving interpolation of data on rectangular grids. They extended the rational cubic spline of Sarfraz [49] with two parameters to construct the bivariate rational interpolating function with continuity. The concept behind their main strategy was that by converting the bivariate interpolating function to the bi-cubic Bézier representation, the sufficient conditions for the non-negativity were derived on the Bézier ordinates and they used the lower bound of Chan et al. [16]. If the positivity of the bi-cubic Bézier patches were lost, then the first-order partial derivatives would be modified by introducing the scaling factor. However, the first-order partial derivatives might still need some modifications in order to construct the positive surfaces.

Saaban et al. [47] described the positivity preserving property by using quintic triangular Bézier patches. The surface was constructed by using convex combination of quintic triangular Bézier patches. They used real rainfall data collected from various stations in West Peninsular Malaysia. Goodman et al. [19] described the local derivative estimation for scattered data interpolation. Amidor [6] and Lodha and Franke [39] provided a good survey on scattered data interpolation techniques with applications in surface reconstruction and electronic imaging systems. Hussain et al. [31] described the convexity-preserving property to preserve the shape of the scattered data arranged over a triangular grid. Bernstein–Bézier quartic function was used for interpolation.

Renka [45] described the Fortran implementation for preserving the convexity property of scattered data interpolation. Beliakov [10] developed a method to preserve the monotonicity multivariable scattered data. The proposed scheme was only applicable to preserve the shape of monotone Lipschitz continuous functions. Thus, the method could not be used to interpolate the monotone data from a function that not fall under Lipschitz continuous functions definition. Another drawback of the scheme was that the scheme involved the quadratic programming problem that needed proper choices of some initial values. The graphical results were also not visually pleasing and would not be suitable for computer display and scientific visualization purposes.

Beatson and Ziegler [9] discussed the monotonicity preserving property by using quadratic spline for monotone data arranged over triangular elements obtained by subdividing each mesh rectangle into a grid of sixteen triangles. The necessary and sufficient conditions on functional and derivatives were derived to produce the monotonic interpolant. Han and Schumaker [29] discussed the monotone interpolation problem for both gridded and scattered data by using cubic spline defined on triangulations. The Sibson split was used to split each rectangle into four triangles and calculate the gradient values at each grid point and then adjust the values to assure the monotonicity. Their scheme required adjustment of the function values to meet monotonicity preservation from scattered data to the gridded data. The main drawback of their scheme was that it might produce very small rectangles.

Dodd et al. [21] constructed a quadratic spline along boundary of each rectangular grid and constructed the rectangular patches using Gregory's blending functions. Their schemes preserved the convexity of surface along the grid lines but might fail to preserve the convexity of the data inside the rectangles. Moreover, flat spots could exist in the convex surface due to vanishing second-order mixed partial derivatives. Brodlie et al. [13] extended Butt and Brodlie's [14] idea of constructing the positivity preservation of surface data arranged over a rectangular grid. The sufficient conditions on first partial derivatives and twist values were derived and subsequently projected onto a valid interval through an efficient knots insertion algorithm.

Brodlie et al. [13] constructed the modified quadratic Shepard (MQS) method to interpolate scattered data of any dimensionality. Their scheme preserved the positivity of the data for curves and surfaces interpolation by forcing the quadratic basis functions to be positive. They also extended the method for handling other types of

constraints such as lower bound of 0, upper bound of 1 and generalized the constraint to any arbitrary functions as lower and upper bounds. However, from the numerical results, they indicated that their schemes have a 10% error bound associated with the data values. Wu et al. [53] discussed the positivity preserving property for curve and surface approximation and interpolation by using compactly supported radial basis functions (CSRBFs). To achieve the positivity, the optimization problems need to be solved. Multiquadric (MQ) functions were used as quasi-interpolation operators and the CSRBFs were used to construct the interpolation function that preserved the monotonic and convexity of planar data sets.

The objectives of the study presented in this chapter are to:

- (a) construct local scheme involving cubic Timmer triangular patches,
- (b) apply the proposed local scheme for scattered irregular data sets, and
- (c) predict the amount of energy produced.

This chapter is organized as follows: Sect. 8.1 presents a basic introduction to the subject matter including an up-to-date literature review. In Sect. 8.2, the definition of cubic Timmer triangular bases and patches are presented with some examples. In Sect. 8.3, three local schemes are discussed in detail. This includes the methods of calculating the boundary ordinates as well as three inner ordinates for each local scheme. The numerical results and discussions are given in Sect. 8.4. Comparison of the performance with scattered data interpolation schemes involving cubic Ball and cubic Bezier triangular patches, i.e., form established schemes is also given. Section 8.5 concludes the chapter with some recommended studies for future work.

## 8.2 Cubic Triangular Timmer Patches

### 8.2.1 Timmer Curve and Bi-Cubic Timmer Surface

The concept of Timmer method was proposed by Timmer [52] to produce curves and surfaces. The basic functions of the cubic Timmer are shown as follows:

$$\begin{aligned}
 T_0^3(u) &= (1 - 2u)(1 - u)^2 \\
 T_1^3(u) &= 4u(1 - u)^2 \\
 T_2^3(u) &= 4u^2(1 - u) \\
 T_3^3(u) &= (2u - 1)u^2
 \end{aligned} \tag{8.1}$$

The cubic Timmer curve can be defined as:

$$Q_3(u) = \sum_{i=0}^3 P_i T_i^3(u) \tag{8.2}$$

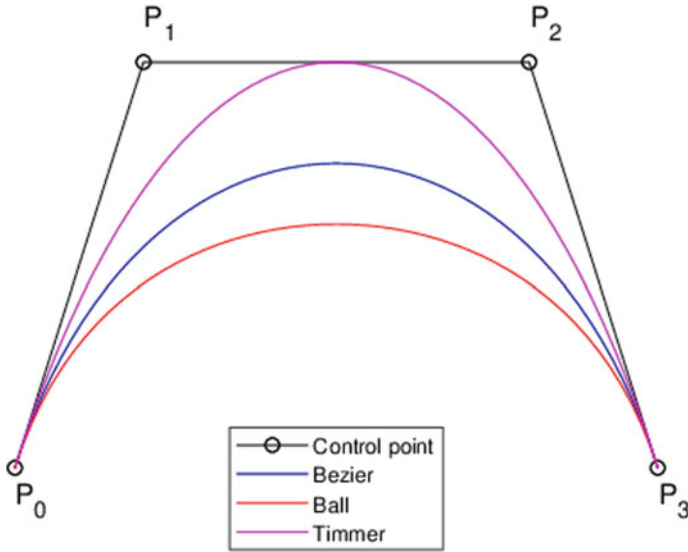


**Fig. 8.1** Cubic Bèzier, Ball and Timmer curves

$$Q_3(u) = T_0^3(u)P_0 + T_1^3(u)P_1 + T_2^3(u)P_2 + T_3^3(u)P_3 \tag{8.3}$$

where  $P_i, i = 0, 1, 2, 3$  denotes the control points while each  $T_i^3(u), i = 0, 1, 2, 3$  are cubic Timmer basis functions [2]. Figure 8.1 shows three curves of cubic Bèzier, Ball and Timmer. From this example, cubic Timmer curve approximates better the control polygon than cubic Bèzier and cubic Ball curves.

Some properties of the cubic Timmer basis functions and the resulting curve are as follows:

- (a) It will interpolate the midpoint of two inner points when  $u = 0.5, Q_3(0.5) = \frac{P_1+P_2}{2}$  which is the midpoint between control points  $P_1$  and  $P_2$  as shown in Fig. 8.2.
- (b) Positivity: Cubic Timmer curve satisfies the positivity property with few exceptions. The conditions that do not fulfill the positivity property are  $T_0^3(u) \leq 0$  when  $\frac{1}{2} \leq u \leq 1$  and  $T_3^3(u) \leq 0$  when  $0 \leq u \leq \frac{1}{2}$ .
- (c) Partition of unity:  $\sum_{i=0}^3 T_i^3(u) = 1$
- (d) Inclusion of endpoints: Cubic Timmer curve includes the endpoints as actual function values, that is,  $R(0) = P_0$  which is the first control point and  $R(1) = P_3$  which is the last control point.

Figure 8.3 shows that the bi-cubic Timmer surface where the bi-cubic Timmer surface is defined as:

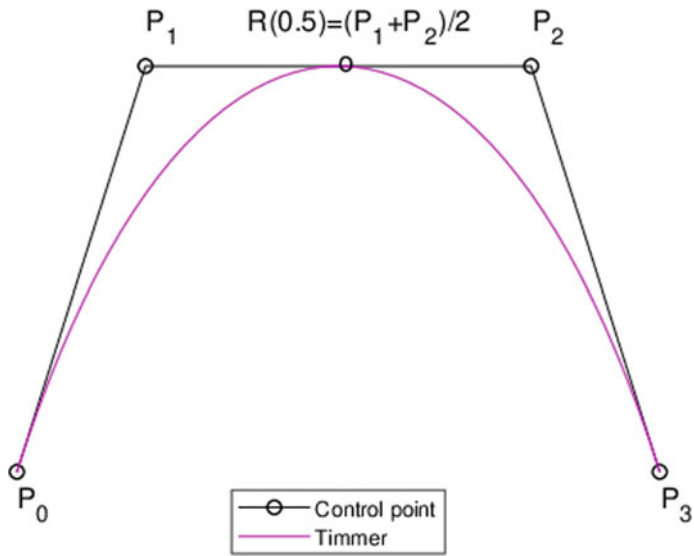


Fig. 8.2 Interpolate midpoint

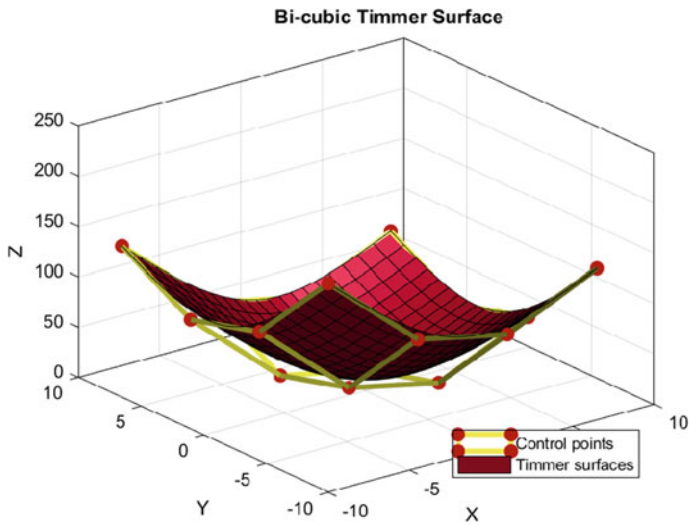


Fig. 8.3 Bi-Cubic Timmer surface

$$R(u, v) = \sum_{i=0}^3 \sum_{j=0}^3 P_{ij} T_i^3(u) T_j^3(v) \tag{8.4}$$

where  $P_{ij}$  are the 16 control points.

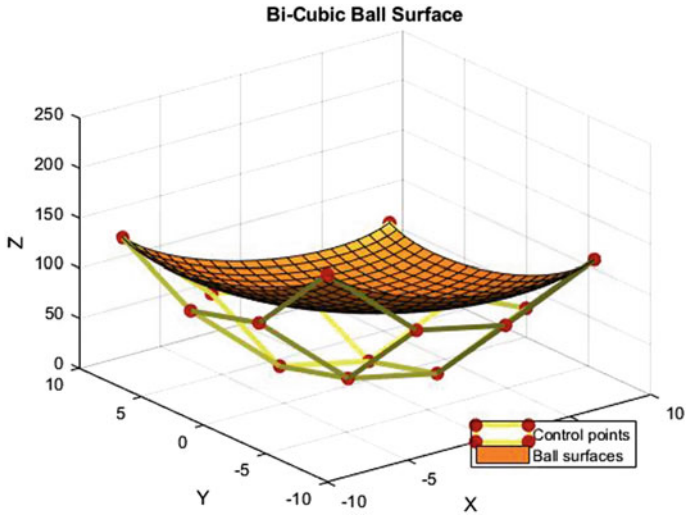


Fig. 8.4 Bi-Cubic Ball surfaces

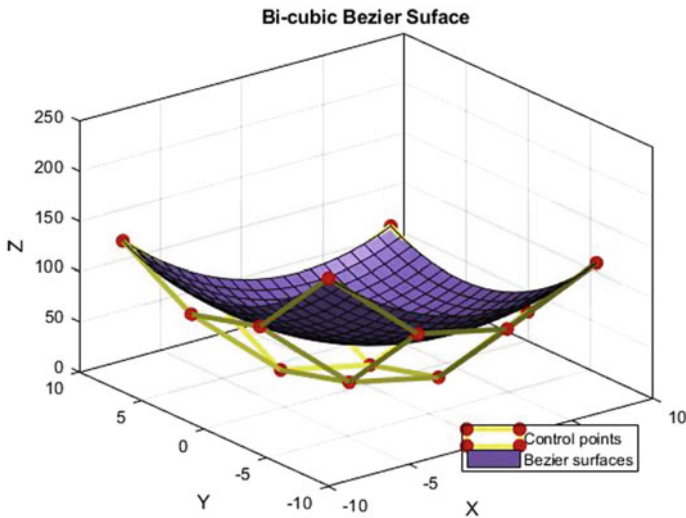


Fig. 8.5 Bi-Cubic Bèzier surfaces

The bi-cubic Ball and Bèzier surfaces are shown in Figs. 8.4 and 8.5. The surfaces used the same control points the same for the Timmer surface in Fig. 8.3.



### 8.2.2 Cubic Triangular Basis Functions

Given three vertices  $V_1, V_2, V_3$  of triangle  $T$  and the barycentric coordinates  $u, v, w$ . Any point of the triangle  $V$  can be determined as [2]:

$$V = uV_1 + vV_2 + wV_3, \quad u + v + w = 1 \tag{8.5}$$

A triangular Bèzier patch of degree  $n$  over a triangular domain is defined as [20]:

$$P(u, v, w) = \sum_{i+j+k=n} b_{ijk} B_{ijk}^n(u, v, w) \tag{8.6}$$

where  $b_{ijk}$  is the control point of the cubic Bèzier triangular patch that constructed by using de Casteljau algorithm as shown in Fig. 8.6. Meanwhile  $B_{ijk}^n(u, v, w)$  is the Bernstein polynomials defined by:

$$B_{ijk}^n(u) = \frac{n!u^i v^j w^k}{i!j!k!}, \quad i + j + k = n, \quad i, j, k \geq 0 \tag{8.7}$$

Figure 8.7 shows the cubic Bèzier triangular patch and Fig. 8.8 shows the cubic Ball triangular basis.

A cubic Bèzier triangular patch  $P(u, v, w)$  and cubic Ball triangular patch  $C(u, v, w)$  are defined as:

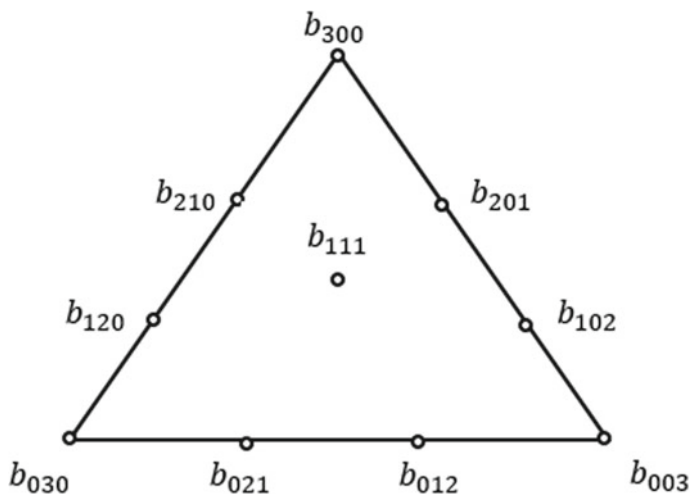
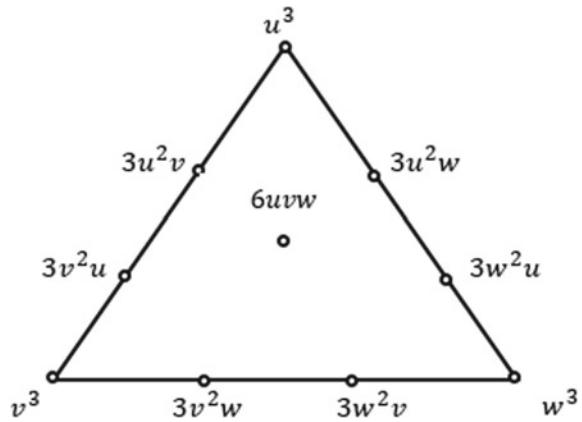
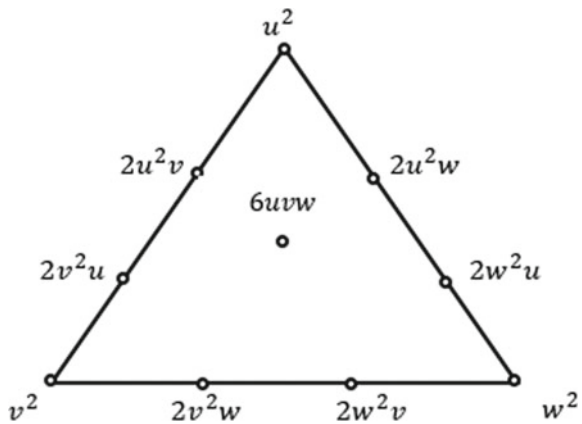


Fig. 8.6 Control points for cubic triangular patch

**Fig. 8.7** Cubic Bèzier triangular basis



**Fig. 8.8** Cubic Ball triangular basis



$$\begin{aligned}
 P(u, v, w) = & u^3b_{300} + 3u^2vb_{210} + 3u^2wb_{201} + v^3b_{030} + 3v^2ub_{120} \\
 & + 3v^2wb_{021} + w^3b_{003} + 3w^2ub_{102} + 3w^2vb_{012} + 6uvw b_{111}
 \end{aligned}
 \tag{8.8}$$

and

$$\begin{aligned}
 C(u, v, w) = & u^2c_{300} + 2u^2vc_{210} + 2u^2wc_{201} + v^2c_{030} + 2v^2uc_{120} \\
 & + 2v^2wc_{021} + w^2c_{003} + 2w^2uc_{102} + 2w^2vc_{012} + 6uvwc_{111}
 \end{aligned}
 \tag{8.9}$$

where  $b_{ijk}$  and  $c_{ijk}$  are the control point with  $u + v + w = 1$ . Figures 8.9 and 8.10 show the examples of cubic Bèzier triangular and cubic Ball triangular patches for the same control points.

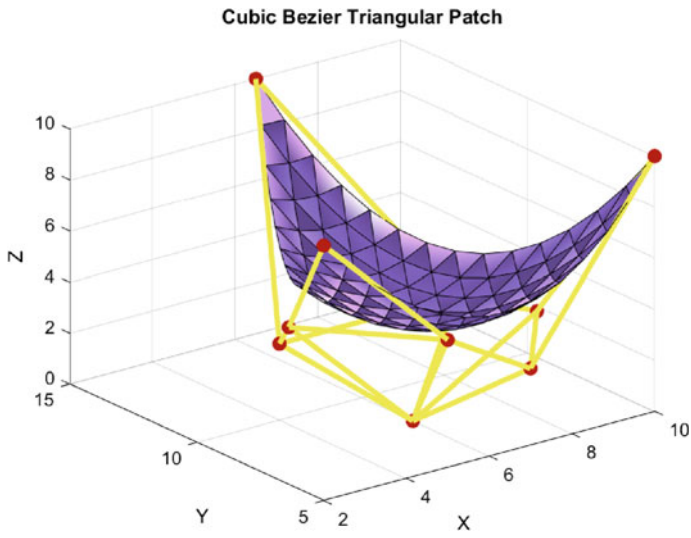


**Fig. 8.9** Cubic Bèzier triangular patch

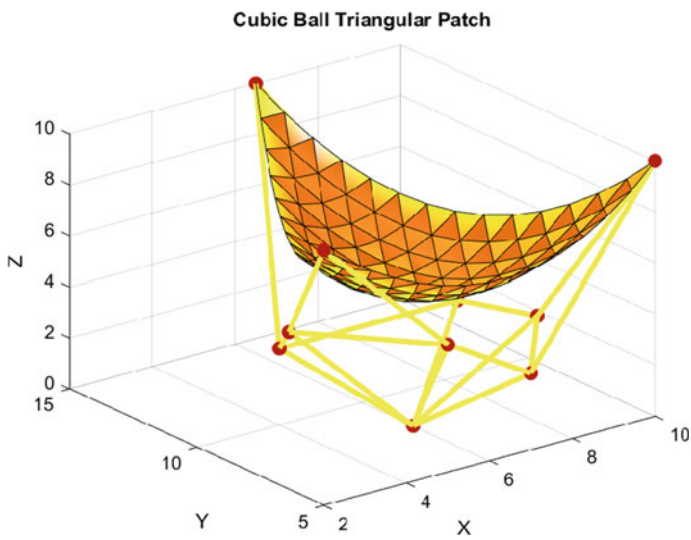


**Fig. 8.10** Cubic Ball triangular patch

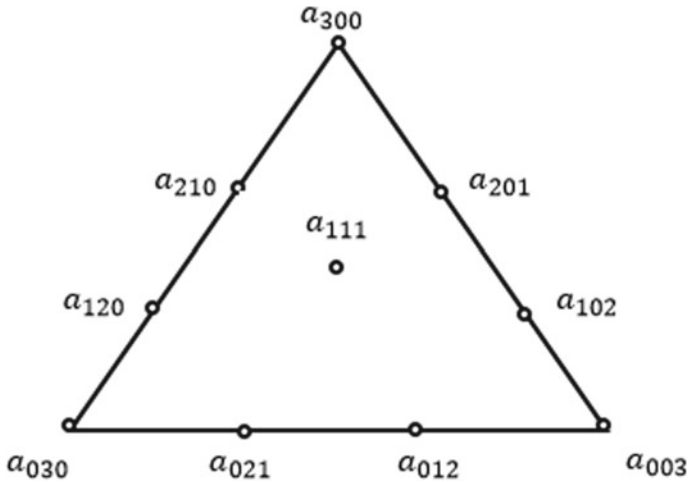


Fig. 8.11 Control points of Timmer triangular patch

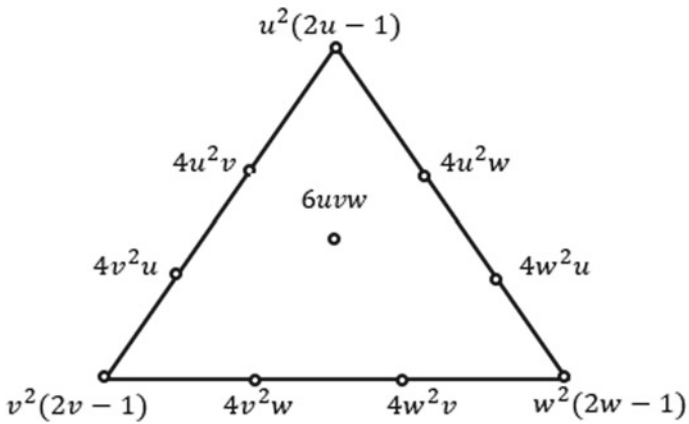


Fig. 8.12 Cubic Timmer basis functions

### 8.2.3 Cubic Timmer Triangular

The cubic Timmer triangular basis was constructed by Ali et al. [1]. Figure 8.11 shows the control points of the cubic Timmer triangular patches. Meanwhile, Fig. 8.12 shows the distribution of the cubic Timmer triangular basis functions on the triangular domain.

A cubic Timmer triangular patch is defined by:

$$T(u, v, w) = \sum_{i+j+k=n} a_{i,j,k} T_{ijk}^3(u, v, w) \tag{8.10}$$

where  $a_{i,j,k}$  denotes the Timmer ordinates of T while  $T_{ijk}^3$  are Timmer basis functions. The derivative of  $T$  with respect to the direction  $z = (z_1, z_2, z_3) = z_1 V_1 + z_2 V_2 + z_3 V_3, z_1 + z_2 + z_3 = 0$  is given by:

$$D_z T(u, v, w) = z_1 \frac{\partial T}{\partial u} + z_2 \frac{\partial T}{\partial v} + z_3 \frac{\partial T}{\partial w}$$

From (8.10), it can be shown that

$$\begin{aligned} \frac{\partial T}{\partial u} &= 4v^2 b_{120} + 4w^2 b_{102} + 6vwb_{111} \\ \frac{\partial T}{\partial v} &= (6v^2 - 2v) b_{030} + 8vwb_{021} + 4w^2 b_{012} \\ \frac{\partial T}{\partial w} &= (6w_2 - 2w) b_{003} + 4v^2 b_{021} + 8vwb_{012} \end{aligned}$$

Figure 8.13 shows the example of one patch cubic Timmer triangular and Fig. 8.14 shows some plots of cubic Timmer triangular basis functions.

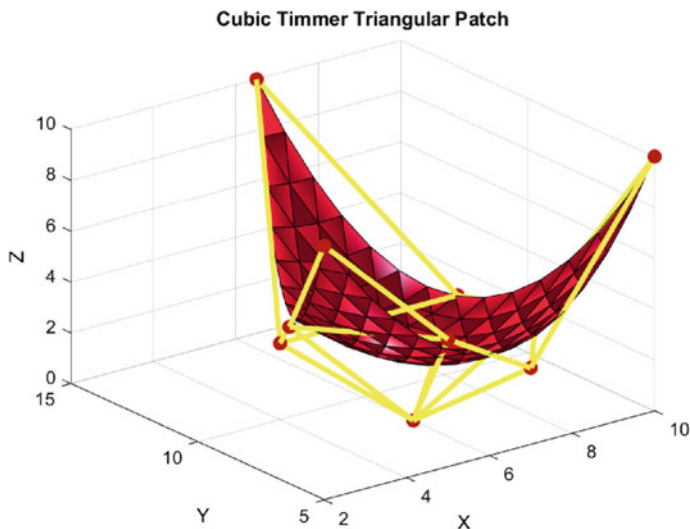


Fig. 8.13 Cubic Timmer triangular patch

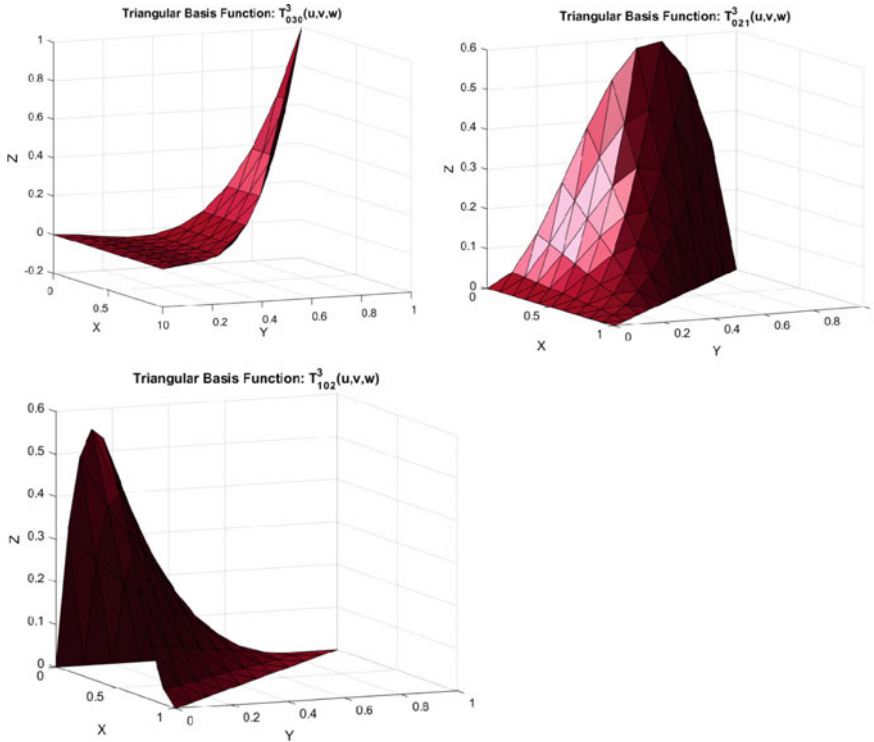


Fig. 8.14 Cubic Timmer triangular basis functions

**Some properties of cubic Timmer triangular patches are [1]:**

(a) *Partition of unity*: The property means that the sum of the Timmer triangular basis function is 1. Or, mathematically, this property can be defined as below

$$\sum_{i=0}^3 T_{ijk}^3(u, v, w) = 1$$

(b) *Symmetry*: The surfaces formed based on two different orderings of control points will be identical.

(c) *Positivity*: Each cubic Timmer triangular basis function fulfills the positivity or non-negativity behavior  $T_{ijk}^3(u, v, w) \geq 0$ , except for some cases:  $T_{300}^3(u, v, w) \leq 0$  when  $\frac{1}{2} \leq u \leq 1$  and both of  $T_{201}^3(u, v, w) \leq 0$  and  $T_{210}^3(u, v, w) \leq 0$  when  $0 \leq u \leq \frac{1}{2}$ .

(d) *Convex hull*: The Timmer triangular patches do not all lie within the convex hull of the control polygon. If the positivity property is fulfilled for the Timmer triangular patches, this will ensure the convex hull property.

### 8.3 Local Scheme for Scattered Data Interpolation

To apply cubic Timmer triangular patches for scattered data interpolation, a convex combination of three local schemes is constructed and is defined as:

$$T(u, v, w) = \frac{vwT_1 + uwT_2 + uvT_3}{vw + uw + uv} \tag{8.11}$$

where the local scheme  $T_i, i = 1, 2, 3$  is obtained by replacing the inner ordinates  $b_{111}^i, i = 1, 2, 3$  to the cubic Timmer triangular patches defined in (8.10). The main idea is to calculate the boundary ordinates by using Goodman and Said’s method [30] as well as the inner ordinates by using Foley and Opitz [31] methods. The derivations are defined as follows:

Let  $e_1 = (0, -1, 1), e_2 = (1, 0, -1)$  and  $e_3 = (0, 0, 1)$  be the direction vectors on edges  $e_1, e_2$  and  $e_3$ , respectively. Let  $n_1$  be the inward normal direction to the line segment  $U_2U_3$  which is  $e_1$  as shown in Fig. 8.15 where:

$$n_1 = -e_3 + \frac{e_3 \cdot e_1}{|e_1|^2} e_1$$

The normal derivative of local scheme  $T_1$  is given by:

$$D_{n_1}T_1 = (4b_{120} - 2b_{021} - 3b_{030})v^2 + (4b_{102} - 2b_{012} - 3b_{003})w^2 + 2(3b_{111}^1 - 2b_{021} - 2b_{012})vw + vb_{030} + wb_{003} \tag{8.12}$$

Next, consider  $n_2$  to be the inward normal direction to the line segment  $U_3U_1, e_1$  as shown in Fig. 8.16, where:

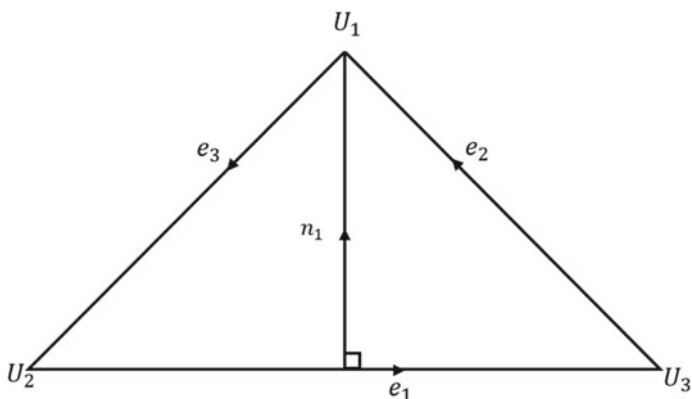


Fig. 8.15 Inward normal direction  $n_1$  to the edges

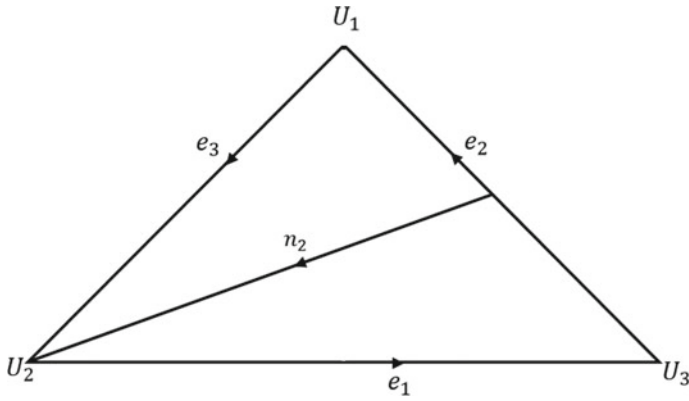


Fig. 8.16 Inward normal direction  $n_2$  to the edges

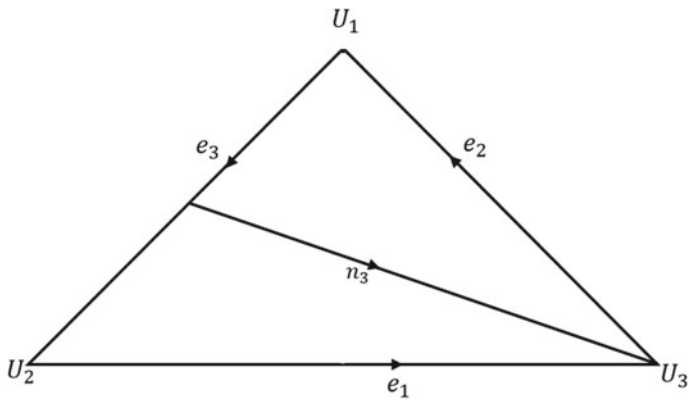


Fig. 8.17 Inward normal direction  $n_3$  to the edges

$$n_2 = -e_1 + \frac{e_1 \cdot e_2}{|e_2|^2} e_2$$

The normal derivative of the local scheme  $T_2$  is defined by

$$D_{n_2} T_2 = (4b_{120} - 2b_{021} - 3b_{030})u^2 + (4b_{102} - 2b_{012} - 3b_{003})w^2 + 2(3b_{111}^2 - 2b_{021} - 2b_{012})uw + ub_{030} + wb_{003} \tag{8.13}$$

The last inner normal direction,  $n_3$  be the inward normal directions to the edges  $U_1U_2$  which is  $e_1$  as shown in Fig. 8.17 where



$$n_3 = -e_2 + \frac{e_2 \cdot e_3}{|e_3|^2} e_3$$

Meanwhile, the normal derivative of local scheme  $T_3$  given along inward normal direction  $n_3$  is given as:

$$\begin{aligned} D_{n_3} T_3 = & (4b_{120} - 2b_{021} - 3b_{030})u^2 + (4b_{102} - 2b_{012} - 3b_{003})v^2 \\ & + 2(3b_{111}^2 - 2b_{021} - 2b_{012})uv + ub_{030} + vb_{003} \end{aligned} \quad (8.14)$$

### 8.3.1 Determination the Timmer Ordinates

Let the data  $F(U_i)$  and its first partial derivatives  $F_x(U_i)$  and  $F_y(U_i)$  for  $i = 1, 2, 3$  be given at the vertices. The Timmer ordinates that lie at the edge of the triangle  $b_{210}$  and  $b_{201}$  are determined as follows. Let the directional derivatives along  $e_3$  and  $e_2$  at  $U_1$  be:

$$\begin{aligned} \frac{\partial F}{\partial e_3} = D_{e_3} T(1, 0, 0) &= \left( \frac{\partial x}{\partial v} - \frac{\partial x}{\partial u} \right) F_x(U_1) + \left( \frac{\partial y}{\partial v} - \frac{\partial y}{\partial u} \right) F_y(U_1) \\ &= (x_2 - x_1)F_x(U_1) + (y_2 - y_1)F_y(U_1) \end{aligned} \quad (8.15)$$

and

$$\begin{aligned} \frac{\partial F}{\partial e_2} = D_{e_2} T(1, 0, 0) &= \left( \frac{\partial x}{\partial v} - \frac{\partial x}{\partial u} \right) F_x(U_1) + \left( \frac{\partial y}{\partial v} - \frac{\partial y}{\partial u} \right) F_y(U_1) \\ &= (x_1 - x_3)F_x(U_1) + (y_1 - y_3)F_y(U_1) \end{aligned} \quad (8.16)$$

Next the derivatives of Timmer triangular patches are applied as follows. For the given direction shown by the vector  $\hat{s} = (\hat{s}_1, \hat{s}_2, \hat{s}_3)$ , with  $\hat{s}_1, \hat{s}_2, \hat{s}_3 = 0$ , the directional derivative

$$D_{\hat{s}} T(r, s, t) = \hat{s}_1 \frac{\partial T}{\partial \hat{s}} + \hat{s}_2 \frac{\partial T}{\partial \hat{s}} + \hat{s}_3 \frac{\partial T}{\partial \hat{s}}$$

After applying (8.15) and (8.16) on cubic Timmer triangular patches:

$$D_{e_3} T(1, 0, 0) = 4(-b_{300} + b_{210}) \quad (8.17)$$

$$D_{e_2} T(1, 0, 0) = 4(b_{300} - b_{201}) \quad (8.18)$$

Therefore, from (8.17) and (8.18):

$$b_{210} = b_{300} + \frac{1}{4} [(x_2 - x_1)F_x(U_1) + (y_2 - y_1)F_y(U_1)]$$

and

$$b_{201} = b_{300} + \frac{1}{4} [(x_1 - x_3)F_x(U_1) + (y_1 - y_3)F_y(U_1)]$$

Similarly, the remaining boundary cubic Timmer ordinates are obtained:

$$b_{012} = b_{030} + \frac{1}{4} [(x_3 - x_2)F_x(U_2) + (y_3 - y_2)F_y(U_2)]$$

$$b_{120} = b_{030} + \frac{1}{4} [(x_2 - x_1)F_x(U_2) + (y_2 - y_1)F_y(U_2)]$$

$$b_{102} = b_{003} + \frac{1}{4} [(x_1 - x_3)F_x(U_3) + (y_1 - y_3)F_y(U_3)]$$

and

$$b_{012} = b_{003} + \frac{1}{4} [(x_3 - x_2)F_x(U_3) + (y_3 - y_2)F_y(U_3)]$$

### 8.3.2 Methods to Calculate Inner Timmer Ordinates

$$b_{111}^i, i = 1, 2, 3$$

Now it is needed to only determine the inner ordinates for each local scheme. There are two methods that can be used to calculate the inner ordinates.

#### 8.3.2.1 Goodman and Said Method

By using Goodman and Said [27] method, Condition (8.12) reduces to:

$$\begin{aligned} A &= (4b_{120} - 2b_{021} - 3b_{030}), B = 2(3b_{111}^1 - 2b_{021} - 2b_{012}), \\ C &= (4b_{102} - 2b_{012} - 3b_{003}) \end{aligned}$$

Thus,  $D_{n_1}T_1 = Av^2 + Bvw + Cw^2$ . Assume that  $B = A + C$ , then

$$D_{n_1}T_1 = Av^2 + (A + C)vw + Cw^2 = Av(v + w) + Cw(v + w) = A + Cw$$

So  $D_{n_1}T_1$ , is linear if  $B = A + C$ . Hence in order to satisfy  $C^1$  condition along edge  $e_1$  of triangle, the normal derivative  $D_{n_1}T_1$ , must be linear and the inner ordinate is following:

$$b_{111}^1 = \frac{2}{3}(b_{120} + b_{102}) + \frac{1}{3}(b_{021} + b_{012}) - \frac{1}{2}(b_{030} + b_{003}) \quad (8.19)$$

Considering the normal derivatives on edges  $V_3V_1(v = 0, u + w = 1)$  and  $V_1V_2(w = 0, u + v = 1)$  along  $n_2$  and  $n_3$  directions, respectively, so the inner ordinates are:

$$b_{111}^2 = \frac{2}{3}(b_{210} + b_{012}) + \frac{1}{3}(b_{201} + b_{102}) - \frac{1}{2}(b_{300} + b_{003}) \quad (8.20)$$

and

$$b_{111}^3 = \frac{2}{3}(b_{201} + b_{021}) + \frac{1}{3}(b_{210} + b_{120}) - \frac{1}{2}(b_{300} + b_{030}) \quad (8.21)$$

### 8.3.2.2 Foley and Opitz Method

Consider two adjacent triangles, M and N in Fig. 8.18 whose vertices are  $U_i$  and  $V_i$  with  $e_1$  is a common edge.

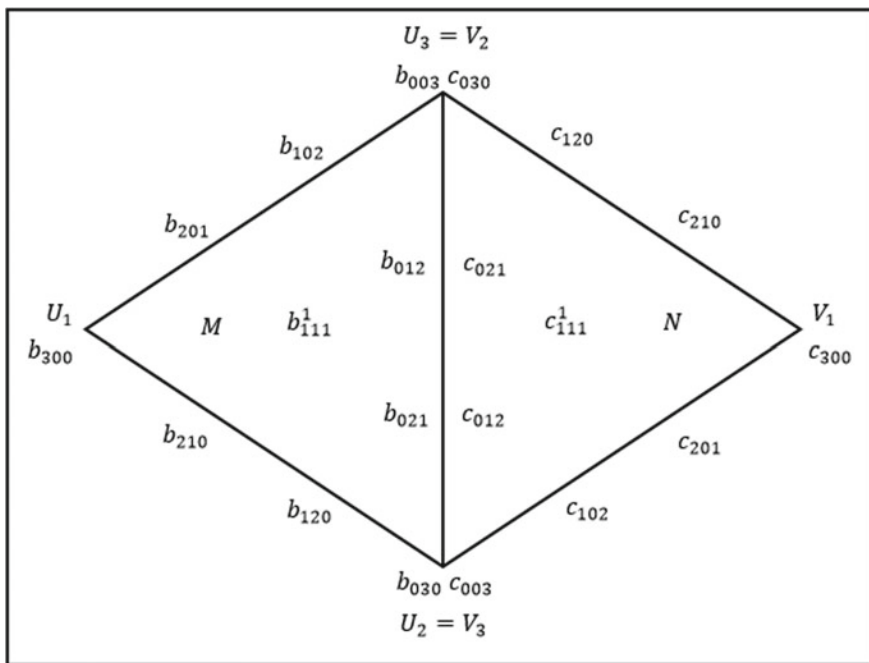


Fig. 8.18 Two adjacent cubic triangular patches

Suppose boundary control points on these two adjacent triangles are denoted as  $b_k, c_k, c \neq (1, 1, 1)$  and inner ordinates be  $b_{111}^1, c_{111}^1$  respectively. The determination of  $b_{111}^1$  and  $c_{111}^1$  are described below while the others are obtained similarly. To achieve  $C^1$  continuity along common edge and will have cubic precision, the equations must be satisfied as follows:

$$c_{201} = r^2 b_{210} + 2stb_{021} + 2rsb_{120} + s^2 b_{030} + 2rtb_{111}^1 + t^2 b_{012} \quad (8.22)$$

$$c_{210} = r^2 b_{201} + 2stb_{012} + 2rtb_{102} + s^2 b_{021} + 2rsb_{111}^1 + t^2 b_{003} \quad (8.23)$$

$$b_{201} = u^2 c_{201} + 2vwc_{012} + 2uwc_{102} + v^2 b_{021} + 2uvc_{111}^1 + w^2 c_{003} \quad (8.24)$$

$$b_{210} = u^2 c_{210} + 2vwc_{021} + 2uvc_{120} + v^2 c_{030} + 2uwc_{111}^1 + w^2 c_{012} \quad (8.25)$$

where  $V_1 = rU_1 + sU_2 + tU_3$  and  $U_1 = uV_1 + vV_2 + wV_3$ .

The overdetermined system for  $b_{111}^1$  in (8.22) and (8.23) will have a solution if the boundary control points of two patches are from a single cubic. This can be completed by adding these equations together and solving for  $b_{111}^1$ . Thus, the inner ordinates  $b_{111}^1$  can be obtained as follows:

$$b_{111}^1 = \frac{1}{2u(v+w)} (c_{201} + c_{210}) - u^2 (b_{210} + b_{201}) - v^2 (b_{030} + b_{021}) - w^2 (b_{012} + b_{003}) - 2vw(b_{021} + b_{012}) - uvb_{120} - 2uwb_{102} \quad (8.26)$$

Similarly, (8.24) and (8.25) are added together to yield

$$c_{111}^1 = \frac{1}{2r(s+t)} (b_{201} + b_{210}) - r^2 (c_{210} + c_{201}) - s^2 (c_{030} + c_{021}) - t^2 (c_{012} + c_{003}) - 2st(c_{021} + c_{012}) - rsc_{120} - 2rtc_{102} \quad (8.27)$$

### 8.3.3 Final Scheme

The final scheme of the scattered data interpolation can be written as follows:

$$T(u, v, w) = \frac{vwT_1 + uwT_2 + uvT_3}{vw + uw + uv} \quad (8.28)$$

which can be simplified to

$$T(u, v, w) = c_1 T_1(u, v, w) + c_2 T_2(u, v, w) + c_3 T_3(u, v, w)$$

where

$$c_1 = \frac{vw}{vw + uv + uw}, c_2 = \frac{uw}{vw + uv + uw}, c_3 = \frac{uv}{vw + uv + uw} \quad (8.29)$$

Or, in a much simpler form, as

$$T(u, v, w) = \sum_{\substack{i+j+k=3, \\ i \neq 1, j \neq 1, k \neq 1}} a_{i,j,k} T_{ijk}^3(u, v, w) + 6uvw(c_1 b_{111}^1 + c_2 b_{111}^2 + c_3 b_{111}^3).$$

## 8.4 Results and Discussion

To test the capability of the proposed scheme for scattered data interpolation, three different types of energy data sets are chosen. The data samples are irregular since in many applications the collected data are irregular, i.e., not in uniform sampling or regular. To measure the effectiveness on the scheme, the Root Mean Square Error (RMSE), Maximum Error and Coefficient of Determination ( $R^2$ ) are calculated. The comparison has been made between the cubic Timmer triangular patches and the cubic Ball and cubic Bezier triangular patches based on two different methods to calculate the inner ordinates, i.e., Goodman and Said [27] and Foley and Opitz [23] methods. The functions are obtained from Gilat [25].

### Example 1: Electric Potential of Two-point charge

The electric potential  $V$  around a charged particle is given by:

$$V = \frac{1}{4\pi\epsilon_0 r}$$

where  $\epsilon_0 = 8.8541878 \times 10^{-12} \frac{\text{C}}{\text{Nm}^2}$  is the permittivity constant,  $r$  is the distance from the particle in meters and  $q$  is the magnitude of the charge in Coulombs. The two particles of the electric field are calculated by using the superposition technique. The electric potential at a point of two particles is defined by:

$$V = \frac{1}{4\pi\epsilon_0} \left( \frac{q_1}{x} + \frac{q_2}{y} \right) \quad (8.30)$$

where  $q_1 = 2 \times 10^{-10} \text{ C}$  and  $q_2 = 3 \times 10^{-10} \text{ C}$  are the charges of the particles while  $x$  and  $y$  are the distance from the points to the corresponding particle. Based on the information above, cubic Timmer triangular patches will be used to interpolate the potential energy due to the two particles at points in the  $x$ - $y$  plane that are

**Table 8.1** Sample of 25 data points

x	y	V	x	y	V
-0.20	-0.20	14.2012	0.05	0.10	17.7507
-0.20	-0.05	31.3905	0.05	0.20	14.5250
-0.20	0.05	31.3905	0.10	-0.20	15.2514
-0.20	0.10	21.9368	0.10	-0.05	22.1473
-0.20	0.20	14.2012	0.10	0.05	22.1473
-0.05	-0.20	13.8398	0.10	0.10	19.9037
-0.05	-0.05	17.5928	0.10	0.20	15.2514
-0.05	0.05	17.5928	0.20	-0.20	16.7369
-0.05	0.10	16.5729	0.20	-0.05	42.1209
-0.05	0.20	13.8398	0.20	0.05	42.1209
0.05	-0.20	14.5250	0.20	0.10	28.0287
0.05	-0.05	18.9980	0.20	0.20	16.7369
0.05	0.05	18.9980			

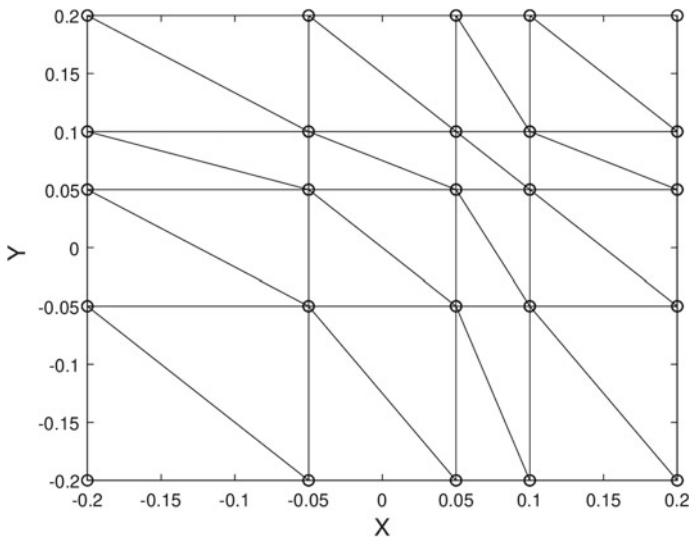


**Fig. 8.19** Delaunay triangulation for the irregular data

located in the domain  $-0.2 \leq x \leq 0.2$  and  $-0.2 \leq y \leq 0.2$ . The data are samples irregularly to 25 points as shown in Table 8.1. Figure 8.19 shows the Delaunay triangulation of the sample data.

Figure 8.20 shows the 3D linear interpolant for the irregular data, which is needed to be refined in order to produce a smooth surface. The surface interpolation for Example 1 is shown in Fig. 8.21.

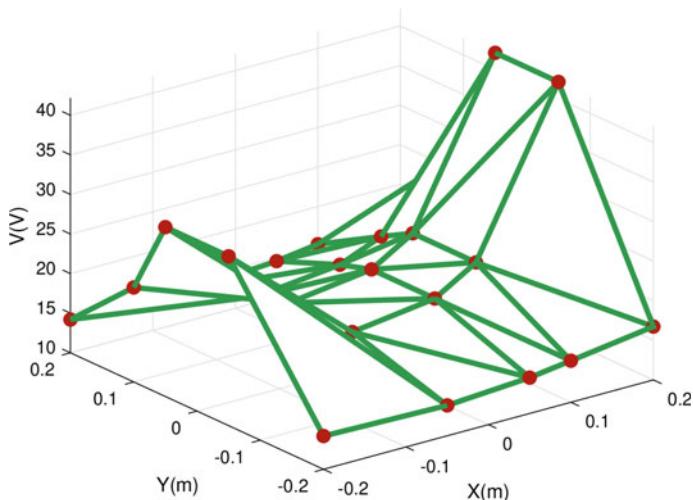


**Fig. 8.20** 3D linear interpolant

For Example 1 and from Tables 8.2 and 8.3, it is obvious that all schemes are producing the same quality of interpolating surface. Note that Goodman and Said method gives smaller RMSE compared with the Foley and Opitz method.

### Example 2: Heat Conduction in a Square Plate

Consider the scenario where one side of a rectangular plate with length  $a = 5$  m,  $b = 4$  m is kept at temperature  $80$  °C and another three sides are kept at a temperature  $0$  °C as shown in Fig. 8.22.

The temperature distribution,  $T(x, y)$  in the plate can be determined by solving the two-dimensional heat equation. For the given boundary condition,  $T(x, y)$  can be shown analytically to have Fourier series solution as given below:

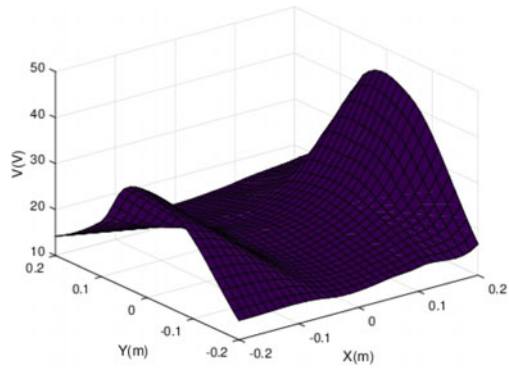
$$T(x, y) = \frac{4T_1}{\pi} \sum_{n=1}^{\infty} \frac{\sin\left[(2n-1)\frac{\pi x}{a}\right] \sinh\left[(2n-1)\frac{\pi y}{a}\right]}{(2n-1) \sinh\left[(2n-1)\frac{\pi b}{a}\right]} \quad (8.31)$$

for  $0 \leq x \leq 5$  and  $0 \leq y \leq 4$ .

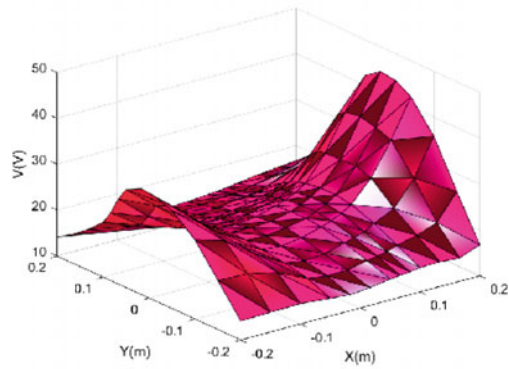
In order to apply scattered data interpolation using cubic Timmer triangular patches, the 30 irregular data points are sampled on the given domain as shown in Table 8.4.

Figure 8.23 shows the Delaunay triangulation for the data. Meanwhile, Figs. 8.24 and 8.25 show the 3D visualization of the irregular data sets and various interpolating surface for Example 2, respectively.

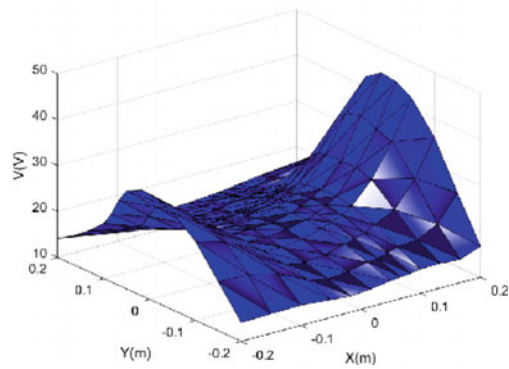
From Tables 8.5 and 8.6, the proposed scheme by using cubic Timmer triangular patches give equally results compared with cubic Ball and cubic Bezier triangular patches.



(a) True solution



(b) Cubic Timmer triangular patches using Goodman and Said



(c) Cubic Timmer triangular patches using Foley and Opitz

Fig. 8.21 Surface interpolation for Example 1



**Table 8.2** Error using Goodman and Said

Error	Bezier	Ball	Timmer
RMSE	2.0195	2.0195	2.0195
Max Error	13.3315	13.3315	13.3315
$R^2$	0.8868	0.8868	0.8868

**Table 8.3** Error using Foley and Opitz

Error	Bezier	Ball	Timmer
RMSE	2.0310	2.0133	2.0436
Max Error	13.3315	13.3315	13.3315
$R^2$	0.8855	0.8875	0.8841

**Fig. 8.22** Rectangular plate

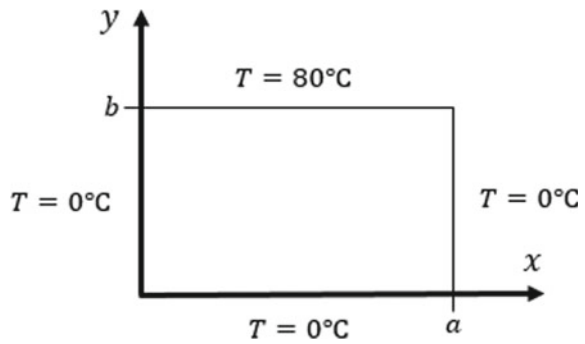


**Table 8.4** Irregular data sets for Example 2

x	y	z	x	y	z
0.0	0.0	0.0000	3.0	0.0	0.0000
0.0	0.5	0.0000	3.0	0.5	5.0220
0.0	1.0	0.0000	3.0	1.0	10.5239
0.0	3.0	0.0000	3.0	3.0	47.8679
0.0	4.0	0.0000	3.0	4.0	78.6622
0.5	0.0	0.0000	4.0	0.0	0.0000
0.5	0.5	1.6713	4.0	0.5	3.1554
0.5	1.0	3.5372	4.0	1.0	6.6567
0.5	3.0	21.7161	4.0	3.0	36.1272
0.5	4.0	75.9277	4.0	4.0	77.8402
1.5	0.0	0.0000	5.0	0.0	0.0000
1.5	0.5	4.3034	5.0	0.5	6.64E-16
1.5	1.0	9.0444	5.0	1.0	1.41E-15
1.5	3.0	44.0251	5.0	3.0	9.22E-15
1.5	4.0	78.4282	5.0	4.0	2.29E-13

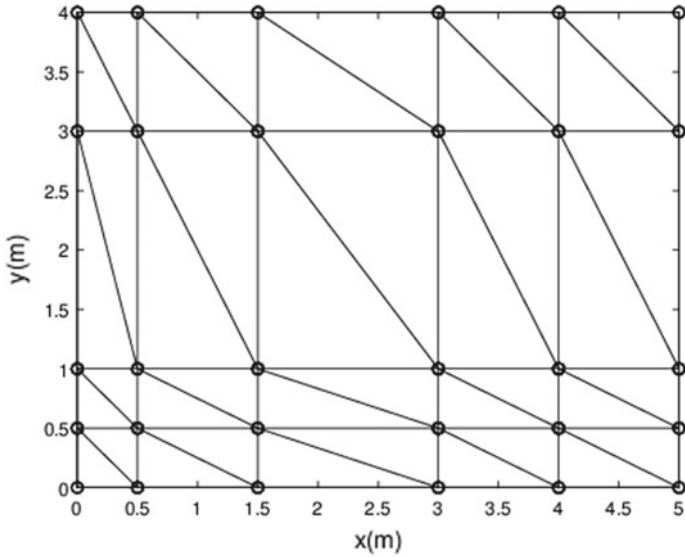


Fig. 8.23 Delaunay triangulation for data in Table 8.4

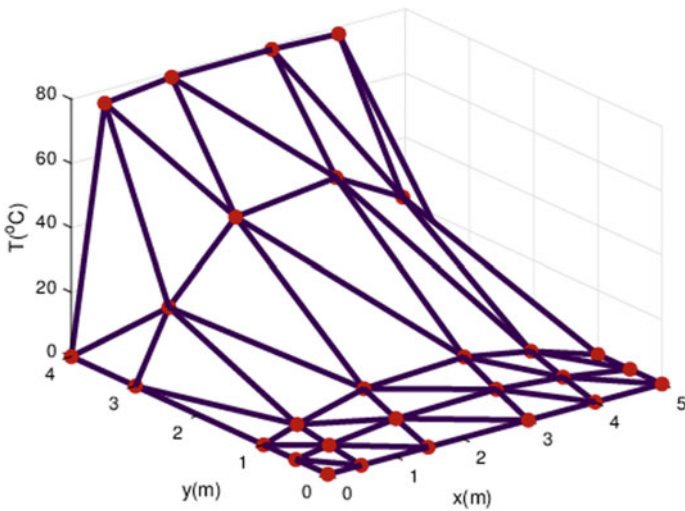
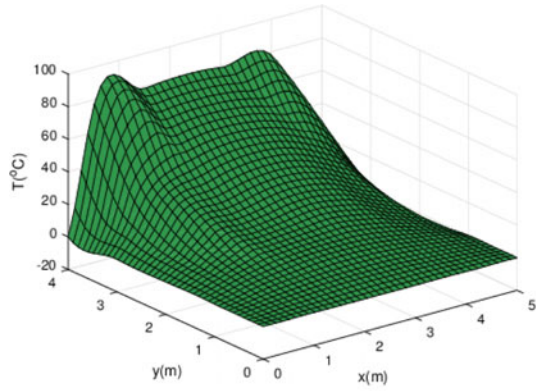


Fig. 8.24 3D linear interpolant

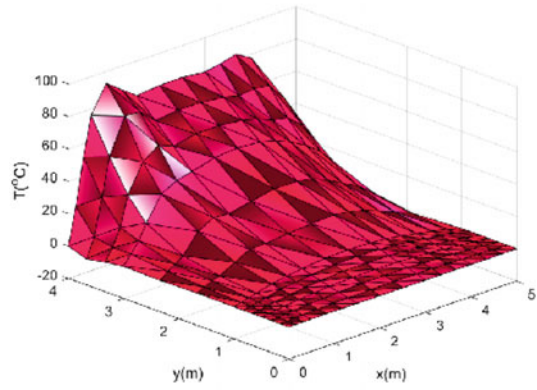
**Example 3: Kinetic Energy**

Consider the scenario where one container contains a lot of molecules of a gas moving around at different speeds. Maxwell’s speed distribution law gives the probability distribution  $P(v)$  as a function of speed and temperature as stated below:

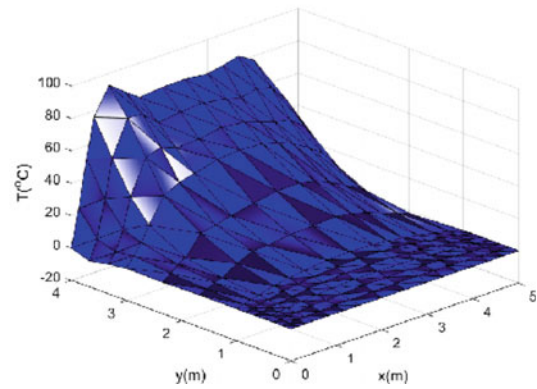
**Fig. 8.25** Various interpolating surface for Example 2



**(a)** True solution for Example 2



**(b)** Cubic Timmer triangular using Goodman and Said



**(c)** Cubic Timmer triangular using Foley and Opitz

**Table 8.5** Error using Goldman and Said

Error	Bezier	Ball	Timmer
RMSE	4.2779	4.2779	4.2779
Max Error	52.9540	52.9540	52.9540
$R^2$	0.9652	0.9652	0.9652

**Table 8.6** Error using Foley and Opitz

Error	Bezier	Ball	Timmer
RMSE	4.3100	4.3	4.3404
Max Error	52.9540	52.954	52.9540
$R^2$	0.9647	0.9648	0.9642

**Table 8.7** 36 irregular data sets for Example 3

x	y	z	x	y	z
0	70	0.000000	700	70	2.24E-07
0	100	0.000000	700	100	7.47E-06
0	180	0.000000	700	180	2.05E-04
0	250	0.000000	700	250	0.000543
0	280	0.000000	700	280	0.000686
0	320	0.000000	700	320	0.000856
250	70	0.003647	850	70	5.51E-10
250	100	0.003577	850	100	1.25E-07
250	180	0.002529	850	180	2.51E-05
250	250	0.001863	850	250	1.34E-04
250	280	0.001655	850	280	2.05E-04
250	320	0.001429	850	320	0.000311
500	70	0.000084	1000	70	3.69E-13
500	100	0.000387	1000	100	8.29E-10
500	180	0.001361	1000	180	1.79E-06
500	250	0.001758	1000	250	2.18E-05
500	280	0.001823	1000	280	4.20E-05
500	320	0.001850	1000	320	8.12E-05

$$P(v) = 4\pi \left( \frac{M}{2\pi RT} \right)^{3/2} v^2 e^{(-Mv^2)/(2RT)} \tag{8.32}$$

where  $M = 0.032 \text{ kg/mol}$  is denoted as the molar mass of the gas,  $R = 8.3145 \text{ J/(K mol)}$  is the gas constant,  $70 \leq T \leq 320 \text{ K}$  is the temperature and  $0 \leq v \leq 1000 \text{ m/s}$  is the speed of the molecules. To apply cubic Timmer triangular patches, they are sampled into 36 irregular data sets as given in the following Table 8.7.

Figure 8.26 shows the Delaunay triangulation for the irregular data. Figure 8.27 shows the 3D visualization of the irregular data sets and the surface interpolation for Example 3 is shown in Fig. 8.28 (Tables 8.8 and 8.9).

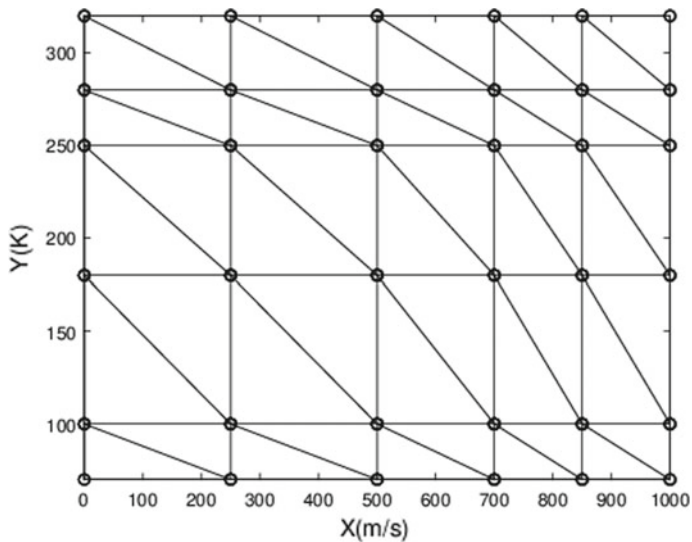


Fig. 8.26 Delaunay triangulation for data in Table 8.7

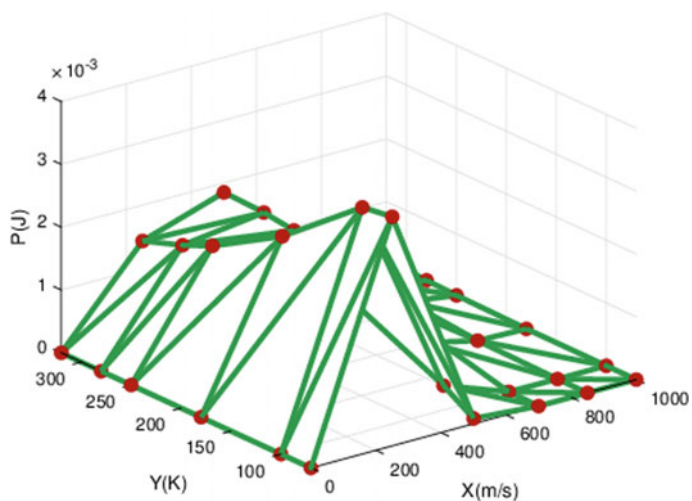
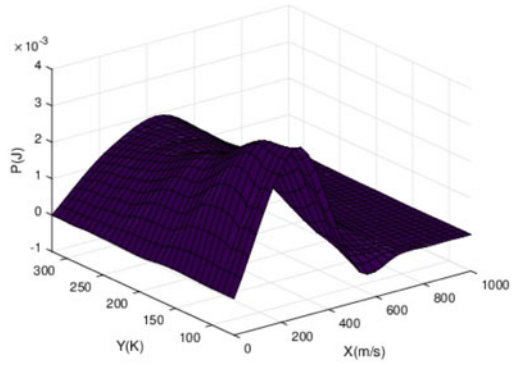


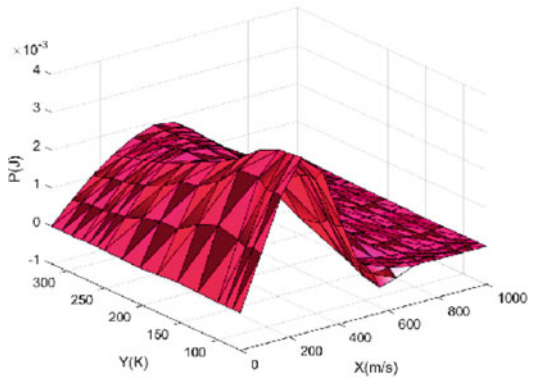
Fig. 8.27 3D linear interpolant for Example 3

For Example 3, it is found that the cubic Timmer triangular patches are the best method to interpolate irregular data sets compared to the cubic Ball and cubic Bezier triangular patches. When Goodman and Said's [33] method is used to calculate the inner ordinates for each local schemes, smaller RMSE and maximum error are obtained as compared to Foley and Opitz's [34] method. Besides that, it

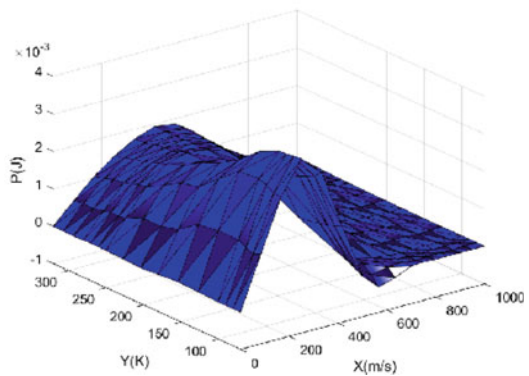
**Fig. 8.28** Scattered data interpolation



**(a)** True solution



**(b)** Cubic Timmer triangular using Goodman and Said



**(c)** Cubic Timmer triangular using Foley and Opitz

**Table 8.8** Error using Goldman and Said

Error	Bezier	Ball	Timmer
RMSE	0.0003	0.0003	0.0003
Max Error	0.0015	0.0015	0.0015
$R^2$	0.9234	0.9234	0.9234

**Table 8.9** Error using Foley and Opitz

Error	Bezier	Ball	Timmer
RMSE	0.0004	0.0004	0.0004
Max Error	0.0018	0.0018	0.0018
$R^2$	0.8356	0.8347	0.8359

**Table 8.10** Selected points

x	y	V
0.1	0.05	22.1473
0.1667	0.0667	29.5390
-0.2	0.0833	24.4048
0.05	0.05	18.9980
0.0167	0.1	16.9412
-0.15	-0.05	22.7768
0.1333	-0.15	18.5630
0.1	-0.05	22.1473
0.05	-0.2	14.5250
-0.05	-0.1	16.5729

can be seen that, the cubic Timmer gives higher  $R^2$  value compared to cubic Ball and cubic Bezier. Overall, the cubic Timmer triangular patches give the results on par with the established schemes.

Finally, the proposed scheme in this study can be used to predict the amount of energy. For this, the Goodman and Said scheme of Example 1 are considered. Supply any value of  $x$ - $y$  plane that is located in the given domain. The values of selected data points  $x$  and  $y$  as shown in Table 8.10 are taken. Then calculate the value of the electric potential at a point of two particles as follows:

$$V = \frac{1}{4\pi\epsilon_0} \left( \frac{q_1}{r_1} + \frac{q_2}{r_2} \right) = \frac{1}{4\pi\epsilon_0 r} \left( \frac{2e^{-10}}{\sqrt{(x+0.25)^2 + y^2}} + \frac{3e^{-10}}{\sqrt{(x-0.25)^2 + y^2}} \right) \tag{8.33}$$

Figure 8.29 shows the location of the selected data points in the Delaunay triangulation.

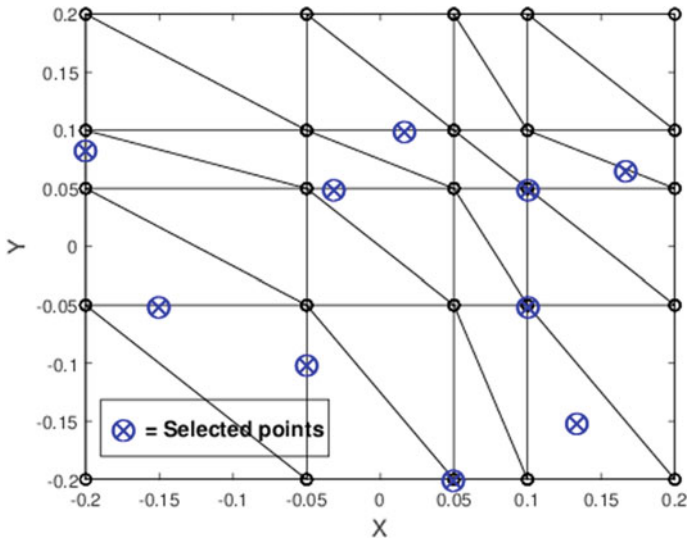


**Fig. 8.29** Location of the selected data points

**Table 8.11** Energy prediction with absolute error

$x$	$y$	Actual $V$	Prediction $V_p$	Absolute Error $ V - V_p $
0.1	0.05	22.1473	22.1473	0
0.1667	0.0667	29.5390	29.7527	$2.14 \times 10^{-1}$
-0.2	0.0833	24.4048	24.7729	$3.18 \times 10^{-1}$
0.05	0.05	18.9980	19.3508	$3.53 \times 10^{-1}$
0.0167	0.1	16.9412	16.8513	$8.86 \times 10^{-3}$
-0.15	-0.05	22.7768	22.7044	$7.24 \times 10^{-2}$
0.1333	-0.15	18.5630	18.8297	$2.67 \times 10^{-1}$
0.1	-0.05	22.1473	22.1473	0
0.05	-0.2	14.5250	14.5250	0
-0.05	-0.1	16.5729	16.9701	$3.97 \times 10^{-1}$

Then, the energy ( $V$ ) located at a selected point can be predicted by using the cubic Timmer triangular patches. The energy prediction data points are given in Table 8.11.

Table 8.11 shows the absolute error for the prediction at selected locations. It can be seen that some of the energy prediction is similar to the energy values from the true function and hence, the absolute error is equal to zero. This is due to the properties of cubic Timmer triangular patch that interpolates end points. Overall, the cubic Timmer triangular patches can be used to predict the electric potential for the data that lies inside the Delaunay triangulation.



## 8.5 Summary

In this study, the cubic Timmer triangular patches constructed in Ali et al. [1] is applied to reconstruct the surface coming from irregular scattered data. Two methods are discussed to calculate the inner ordinates for each local scheme, i.e., Goodman and Said [27] and Foley and Opitz [23]. Both methods will produce  $C^1$  surface everywhere in the given domain. The main advantage in using cubic Timmer in scattered data interpolation is that one may obtain some prediction for the geophysical event that may happen outside of the given domain. Furthermore, one can interpolate the midpoint of the data based on the cubic triangular Timmer method. Future works are underway to study the application of the cubic Timmer triangular for shape-preserving scattered data interpolation and compared with established meshless methods.

**Acknowledgements** This research is fully supported by Universiti Teknologi PETRONAS (UTP) through a research grant YUTP: 0153AA-H24 (Spline Triangulation for Spatial Interpolation of Geophysical Data).

## References

1. F.A.M. Ali, S.A.A. Karim, S.C. Dass, V. Skala, A. Saaban, M.K. Hasan, H. Ishak, New cubic Timmer triangular patches with  $C^1$  and  $G^1$  continuity. Submitted to Jurnal Teknologi (2019)
2. G. Farin, A history of curves and surfaces, in *Handbook of Computer Aided Geometric Design*, vol. 1 (2002)
3. B.H. Ong, H.C. Wong.  $C^1$  positivity preserving scattered data interpolation scheme, in *Proceedings of Advanced Topics in Multivariate Approximation*, ed. by F. Fontanella, K. Jetter, P.J. Laurent (World Scientific Publishing Company, Singapore, 1996), pp. 259–274
4. A.A. Ball, CONSURF. Part one: introduction of the conic lofting tile. *Comput. Aided Des.* **6** (4), 243–249 (1974)
5. N. Ramli, J.M. Ali. Object design using blending of rational Timmer. In *AIP Conference Proceedings*, vol. 1605, No. 1 (AIP, 2014), pp. 262–267
6. I. Amidor, Scattered data interpolation methods for electronic imaging systems: a survey. *J. Electron. Imaging* **11**(2), 157–176 (2002)
7. N. Awang, R.W. Rahmat. Reconstruction of smooth surface by using cubic Bezier triangular patch in GUI. *Malaysian J. Ind. Technol.* **2**(1) 2017
8. N. Awang, R.W. Rahmat, P.S. Sulaiman, A. Jaafar, Delaunay Triangulation of a missing points. *J. Adv. Sci. Eng.* **7**(1), 58–69 (2017)
9. R.K. Beatson, Z. Ziegler, Monotonicity preserving surface interpolation. *SIAM J. Numer. Anal.* **22**(2), 401–411 (1985)
10. G. Beliakov, Monotonicity preserving approximation of multivariate scattered data. *BIT* **45** (4), 653–677 (2005)
11. S.L. Borne, M. Wende. Domain decomposition methods in scattered data interpolation with conditionally positive definite radial basis functions. *Comput. Math. Appl.* (in press, 2018)
12. C. Bracco, C. Gianelli, A. Sestini, Adaptive scattered data fitting by extension of local approximations to hierarchical splines. *Comput. Aided Geometr. Des.* **52–53**, 90–105 (2017)
13. K. Brodlie, P. Mashwama, S. Butt, Visualization of surface data to preserve positivity and other simple constraints. *Comput. Gr.* **19**(4), 585–594 (1995)

14. S. Butt, K.W. Brodlie, Preserving positivity using piecewise cubic interpolation. *Comput. Gr.* **17**(1), 55–64 (1993)
15. E.S. Chan, B.H. Ong, Range restricted scattered data interpolation using convex combination of cubic Bézier triangles. *J. Comput. Appl. Math.* **136**(1–2), 135–147 (2001)
16. E.S. Chan, V.P. Kong, B.H. Ong. Constrained  $C^1$  interpolation on rectangular grids, in *Proceedings of the International Conference on Computer Graphics, Imaging and Visualization (CGIV'04)*, July 26–29, Penang, Malaysia (2004), pp. 239–244
17. L.H.T. Chang, H.B. Said, A triangular patch for the interpolation of functional scattered data. *Comput. Aided Des.* **29**(6), 407–412 (1997)
18. Z. Chen, F. Cao, Scattered data approximation by neural networks operators. *Neurocomputing* **190**, 237–242 (2016)
19. V. Cheutet, M. Daniel, S. Hahmann, R.L. Greca, J.C. Léon, R. Maculet, B. Sauvage, Constraint modeling for curves and surfaces in CAGD: a survey. *Int. J. Shape Model.* **13**(02), 159–199 (2007)
20. H.S. Chua, V.P. Kong. Constrained  $C^1$  scattered data interpolation using rational blend, in *AIP Conference Proceedings*, vol. 1605, No. 1 (2014), pp. 280–285
21. M.S.L. Dodd, J.A. Roulrier, Shape Preserving Spline Interpolation for specifying Bivariate Functions of Grids. *IEEE Comput. Gr. Appl.* **3**(6), 70–79 (1983)
22. R. Feng, Y. Zhang. Piecewise Bivariate Hermite Interpolations for large sets of scattered data. *J. Appl. Math.* **10**, Article ID 239703 (2013)
23. T.A. Foley, K. Opitz. Hybrid cubic Bézier triangle patches, in *Mathematical Methods in Computer Aided Geometric Design II*, ed. by T. Lyche, L.L. Schumaker (Academic Press, 1992), pp. 275–286
24. R. Franke, G.M. Nielson, Scattered data interpolation of large Sets of scattered data. *Intl. J. Numer. Methods Eng.* **15**, 1691–1704 (1980)
25. A. Gilat. *MATLAB: An Introduction with Applications* (Wiley, Hoboken, 2009)
26. R. Gobithasan, J.M. Ali, Towards  $C^2$  curve design with Timmer parametric cubic, in *Proceedings. International Conference on Computer Graphics, Imaging and Visualization, 2004. CGIV 2004* (IEEE, 2004), pp. 109–114
27. T.N. Goodman, H.B. Said, Shape preserving properties of the generalised Ball basis. *Comput. Aided Geometr. Des.* **8**(2), 115–121 (1991)
28. T.N.T. Goodman, H.B. Said, L.H.T. Chang, Local derivative estimation for scattered data interpolation. *Appl. Math. Comput.* **68**(1), 41–50 (1995)
29. L. Han, L.L. Schumaker, Fitting monotone surfaces to scattered data using  $C^1$  piecewise cubics. *SIAM J. Numer. Anal.* **34**(1), 569–585 (1997)
30. M. Herrmann, B. Mulansky, J.W. Schmidt, Scattered data interpolation subject to piecewise quadratic range restrictions. *J. Comput. Appl. Math.* **73**(1–2), 209–223 (1996)
31. M. Hussain, A.A. Majid, M.Z. Hussain, Convexity-preserving Bernstein-Bézier quartic scheme. *Egyptian Inf. J.* **15**, 89–95 (2014)
32. S.A.A. Karim, A. Saaban, Visualization terrain data using cubic Ball triangular patches. *MATEC Web Conf.* **225**, 06023 (2018)
33. S.A.A. Karim, A. Saaban, M.K. Hasan, J. Sulaiman, I. Hashim, Interpolation using cubic Bezier triangular patches. *Intl. J. Adv. Sci. Eng. Inf. Technol.* **8**(4–2), 1746–1752 (2018)
34. S.A.A. Karim, A. Saaban. *Construction of New Cubic Triangular Patches with Application in Scattered Data Interpolation Using New Cubic Triangular Patches*. (Preprint, 2018)
35. S.A.A. Karim, A. Saaban. *Scattered Data Interpolation Using New Cubic Triangular Patches*. Technical Report (Universiti Teknologi PETRONAS, Malaysia, 2018)
36. V.P. Kong, B.H. Ong, K.H. Saw. Range restricted interpolation using cubic Bézier triangles (2004)
37. M.J. Lai, C. Meile, Scattered data interpolation with nonnegative preservation using bivariate splines and its application. *Comput. Aided Geometr. Des.* **34**, 37–49 (2015)
38. C. Liu, *Theory and application of convex curves and surfaces in CAGD* (Faculty of Mathematical Sciences, University of Twente, Enschede, 2001)

39. S.K. Lodha, R. Franke. Scattered data techniques for surfaces, in *Proceedings of Scientific Visualization Conferences*, June 9–13 (Dagstuhl, Germany, 1997), pp. 1–42
40. Z. Luo, X. Peng. A  $C^1$ -rational spline in range restricted interpolation of scattered data. *J. Comput. Appl. Math.* **194**(2), 255–266 (2006)
41. B. Mulansky, J.W. Schmidt, Powell-Sabin splines in range restricted interpolation of scattered data. *Computing* **53**(2), 137–154 (1994)
42. X. Peng, Z. Li, Q. Sun. Non-negativity preserving interpolation by  $C^1$  bivariate rational spline surface. *J. Appl. Math.* Article ID 624978, 11 (2012)
43. A.R.M. Piahi, T.N.T. Goodman and K. Unsworth. Positivity-preserving scattered data interpolation. In *Mathematics of surfaces XI* (Springer, Berlin, Heidelberg, 2005), pp. 336–349
44. S. Ping, K.V. Pang. Local normal estimation for scattered data interpolation. In *AIP conference proceedings*, vol. 1522, No. 1. (AIP, 2013), pp. 448–452
45. R.J. Renka. Interpolation of scattered data with a  $C^1$  convexity-preserving surface. *ACM Trans. Math. Softw.* **30**(2), 200–211 (2004)
46. A. Saaban. Parametric interpolation to scattered data, Doctoral dissertation, Universiti Sains Malaysia, 2008
47. A. Saaban, A.A. Majid, A.R.Mt. Piahi. Visualization of rainfall data distribution using quintic triangular bézier patches. *Bullet. Malays. Math. Sci. Soc.* **32**(2), 137–150 (2009)
48. A. Saaban, A.R.M. Piahi, A.A. Majid, Performance of the triangulation-based methods of positivity-preserving scattered data interpolation. *Far East J. Math. Sci* **57**(1), 1–11 (2011)
49. M. Sarfraz, A rational cubic spline for visualization of monotonic data. *Comput. Gr.* **24**(4), 509–516 (2000)
50. L.L. Schumaker, H. Speleers, Non-negativity preserving macro-element interpolation of scattered data. *Comput. Aided Geometr. Des.* **27**, 245–261 (2010)
51. Q. Sun, F. Bao, Y. Zhang, Q. Duan, A bivariate rational interpolation based on scattered data on parallel lines. *J. Vis. Commun. Image R.* **24**, 75–80 (2013)
52. H.G. Timmer, Alternative representation for parametric cubic curves and surfaces. *Comput. Aided Des.* **12**, 25–28 (1980)
53. J. Wu, Y. Lai, X. Zhang, Radial basis functions for shape preserving planar interpolating curves. *J. Inf. Comput. Sci.* **7**(7), 1453–1458 (2010)
54. A. Crivellaro, S. Perotto, S. Zonca, Reconstruction of 3D scattered data via radial basis functions by efficient and robust techniques. *Appl. Numer. Math.* **113**, 93–108 (2017)
55. G.R. Joldes, H.A. Chowdhury, A. Wittek, B. Doyle, K. Miller, Modified moving least squares with polynomial bases for scattered data approximation. *Appl. Math. Comput.* **266**, 893–902 (2015)

# Chapter 9

## Biodiesel-Fuelled Direct Injection Compression Ignition Engine



Saheed Wasii

This chapter presents a research that was carried out mainly to partly solve the problem that comes up from the depletion of fossil fuel, through the use of biodiesel. Biodiesel is easily attained because of its renewable nature. This chapter discusses the feasibility of biodiesel as an alternative fuel in a compression ignition (diesel) engine; under certain engine's operating condition. The engine behaviour under the influence of different fractions of biodiesel (B0, B7, B10 and B20) is demonstrated.

### 9.1 Introduction

At present, an ignition compression engine or diesel engine is preferable than a gasoline engine as it is more efficient and cost-effective than the latter. Commonly, ignition compression engines are used as power generators and mechanical engines for automobiles [1, 2]. Diesel engines are used in locomotives, construction equipment, automobiles and countless industrial applications. A diesel engine runs on conventional sources which come primarily from fossil fuels such as coal and gas [2]. As of 2012, the U.S. Energy Administration reported that fossil fuels account for 84% of U.S. energy consumption. Comparing the fuels for both engines, diesel fuel has a higher density than gasoline [3]. This allows more energy to be extracted from diesel fuel than gasoline even with the same volume of fuel, resulting in higher mileages making it a better choice for any heavy-duty

---

S. Wasii (✉)

Malaysia France Institute, University of Kuala Lumpur, Jalan Damai,  
Section 14, 43650 Bandar Baru Bangi, Selangor, Malaysia  
e-mail: [engineerlk2003@yahoo.com](mailto:engineerlk2003@yahoo.com)

© Springer Nature Singapore Pte Ltd. 2020  
S. A. Sulaiman (ed.), *Energy Efficiency in Mobility Systems*,  
[https://doi.org/10.1007/978-981-15-0102-9\\_9](https://doi.org/10.1007/978-981-15-0102-9_9)

transportation and equipment. A diesel engine is built ruggedly to withstand the rigours of higher compression. Consequently, the engine usually went much longer than gasoline engine before requiring major repairs [4, 5]. However, the consumption of fossil fuels also gives out bad side effects. One of the side effects that the world is facing right now is the depletion of fossil fuel supply. As fossil fuels can be considered as one of the main natural sources, the depletion of it is slowly affecting the world, mainly economically. With fossil fuel getting scarce, the price of the fuel is also getting higher by the day, making the fuel price unstable. Fossil fuel also affects the world environmentally. This happens because of the combustion of fossil fuel produces harmful products such as nitrogen oxides, sulphur dioxide, volatile organic compound and heavy metals, all which affects the world biosphere [5].

To overcome the problems that arise from this, countless researchers have come up with a solution to replace and reduce the usage of fossil fuels [6, 7]. Some of the alternative fuels proposed by the researchers are compressed natural gas (CNG), hydrogen fuel, water in diesel emulsion (WIDE) and biodiesel. Out of all the alternative fuels that were proposed, biodiesel is the more promising alternative fuel to apply with the current scenario that the world facing as of this moment. The reason being that biodiesel is safe, produce less emission and biodegradable. Biodiesel refers to animal fats, waste cooking oil and usually vegetable oils [8–10]. This work focuses on the suitability of various fractions of biodiesel (B0, B7, B10 and B20) and its effects on performance characteristics of direct injection compression ignition engine.

## 9.2 Biodiesel as a Source of Renewable Energy

The dwindling of natural resources especially fossil fuels and the harmful effects to the nature that it has done, has led to the intensification of research and development efforts in search of renewable and nature-friendly alternative energy sources. This phenomenon had promoted biodiesel as a top choice in alternative energy source. Marginal replacement of diesel by biofuel can actually prolong the depletion of petroleum resources and subside the negative impact on environmental caused by automotive pollutants.

Malaysia through Malaysian Palm Oil Berhad (MPOB) has carried out vigorous R&D on the production of biodiesel from palm oil and its products since the 1980s. MPOB has now become one of the successful technology providers for the production of biodiesel with the building of its first commercial plant in 2006. The homegrown palm biodiesel production technology is comparable if not better than overseas technologies. This is due to the in-depth understanding of the indigenous properties and characteristics of palm oil [11].

### 9.3 Biodiesel as Alternative Fuel in Compression Ignition Engine

In general, biodiesels offer a very promising alternative to diesel oil since they are renewable and have similar properties. This can also be said in terms of its feasibility as an alternative fuel in Internal Combustion Engine. Biodiesel is defined as a trans-esterified renewable fuel derived from vegetable oils or animal fats with properties similar to or better than diesel fuel. Extensive research and demonstration projects by various institutions have shown it can be used pure or in blends with conventional diesel fuel in unmodified diesel engines. Some biodiesel such as palm biodiesel can be used directly in existing diesel engines as neat palm biodiesel (straight non-mixed biodiesel) can be used as fuel in diesel engines without any engine modifications. It can also be blended in any proportion with petroleum diesel.

Aside from its well-known advantage over conventional diesel in terms of out emission, biodiesel possesses a number of other advantages as well. As mentioned several times before, biodiesel can be locally produced from renewable resources such as palm oil and animal fats. In fact, as time progresses, many research and studies had emerged that discovered other source of biodiesel. Besides out emission, biodiesel is also biodegradable and safe to handle. In addition, most of biodiesel produced till date is compatible with quite a number of existing engines. In terms of performance, biodiesel possesses almost similar characteristics with the existing diesel. Apart from the potential prospect it contains (better overall performance characteristics when compared to diesel), biodiesel has a higher cetane level and better lubricity than conventional diesel. Several studies have found that certain blends of biodiesel (B20 and below) have a small, sometimes negligible effects on fuel economy and performance. B20 biodiesel has an 8–9% lower energy content by volume than conventional diesel, while B5 only has a 1–2% lower energy content. The higher the biodiesel blend, the lower the energy content.

Although occasionally true, biodiesel's price can be significantly lower than conventional diesel. Being renewable and could be produced from a wide variety of organic matter, added with the ever-increasing and intensive research in this field, it is only a matter of time for the best blend of biodiesel in terms of performance and emission characteristics to replace the existing diesel. Furthermore, indirectly biodiesel can open up many industries to from small to large-scaled. It could provide many job opportunities. Consequently, it could directly improve a nation's economy, especially third world nations. This is due to the fact that most of these countries own a rich amount of biodiesel source. On top of that, arguably it can also help in reducing the increasing price of daily consumer product particularly, and stabilize the current global economy generally. Although the effects of biodiesel mentioned before could not be observed clearly at the moment, with the rapid increment of technology and research, biodiesel is an alternative to the existing fossil fuels that cannot be overlooked as its impact to the humankind can be as big as fossil fuels somewhere in the future [12].

By using biodiesel, many environmental benefits can be achieved as compared to petroleum-based diesel. Biodiesel has a higher cetane number that improves engine performance and results in cleaner emissions compared to petroleum diesel.

As one of the world's top producer of palm oil, the affordability of this fuel is not a problem. Palm biodiesel is an alternative fuel derived from palm oil and can be used in compression ignition engines, diesel engines without any modifications. It refers to methyl esters derived from palm oil through a process known as 'transesterification'. MPOB is spearheading the R&D of palm oil as biodiesel and they have come a long way since they started.

### **9.3.1 Chemical Process**

Biodiesel production process starts with the mixing of catalyst and methanol. The catalyst used in this process is sodium hydroxide or potassium hydroxide. So, the catalyst and alcohol are mixed, and before the fat is added, the mixture will be charged in a closed vessel. To speed up the reaction, the temperature of reaction mixture always needs to control under alcohol's boiling point. Right after the reaction took place, glycerine and alcohol will be produced, and reactant mixture will neutralise itself at this phase before separation of glycerine and alcohol using centrifuge to separate them faster. After that, the excess alcohol is removed by using evaporation or distillation processes. Meanwhile, glycerine is brought to distil until 99% or higher purity and biodiesel purified by washing using warm water to remove the catalyst. This process will produce a clear yellow-amber liquid with the absence of free fatty acid [13].

### **9.3.2 Chemical and Physical Properties of Biodiesel**

Flash point is a point of fuel temperature when there is a spark of flame, it will ignite. For this biodiesel, the temperature is 150 °C [14]. Meanwhile, density is calculated from its mass per unit volume. Biodiesel has a quite higher density which is 950 kg/m<sup>3</sup> as compared to fossil fuels that mean greater mass of biodiesel compared to fossil fuels is injected by volumetric operating fuel pumps. Moreover, kinematic viscosity is the most important thing in biodiesel fuel which measures the internal fluid friction of oil to flow. Viscosity also an important property to lubricating oil and function of this is to calculate the wear rate of engine component. All those components are some of the physical properties of biodiesel and now, iodine value is one of chemical properties that play a significant role in biodiesel fuel. The higher the iodine value, the more drying quality of the oils. Iodine value means amount of iodine per 100 g to the oils, so the quantity of iodine value defined the quality of drying of oils. However, biodiesel can be combined with pure diesel to be implemented in standard diesel engine because diesel engine runs better when pure

diesel combined with biodiesel and the combination of conventional diesel and biodiesel will be discussed in the next section.

### ***9.3.3 Biodiesel Blend with Conventional Diesel***

In biodiesel, there are many types of biodiesel blend that can serve as promising alternative fuel in compression ignition engine. Biodiesel blend is a mixture of conventional diesel with biodiesel in different concentrations. A study was completed on biodiesel blend and emission characteristics of biodiesel and the study stated system “B” factor is used in most of the countries that refers to the amount of biodiesel fuel in the mixture [15, 16]. The common biodiesel in used are 100% biodiesel (B100), 2% biodiesel (B2), 5% biodiesel (B5) and 20% biodiesel (B20) [17]. For B100, it has already been discussed in the previous section. B20 is the mixture of 80% of conventional diesel and 20% biodiesel which is the most popular used compared to others. This is due to its cost, emission characteristics and ability to act as a solvent. Meanwhile, B5 which contain 5% biodiesel and 95% conventional diesel is having approximately the same function as conventional diesel in compression ignition engine. While B2 has only 2% biodiesel and the remaining are conventional diesel and it is usually used for off-road heavy equipment, fleets, etc. [16, 17].

## **9.4 Combustion Strategies Used in Compression Ignition Engine**

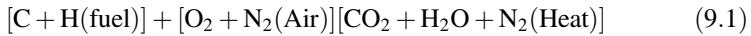
Combustion strategy is a strategy utilised in controlling the air-fuel missing in the engine cylinder so as to obtain the best engine performance and least possible engine out emission. These types are air-fuel ratio mixtures. Air-fuel ratio (AFR) is the mass ratio of air to fuel present in a combustion process in an internal combustion engine. The determination of AFR is an important measure for anti-pollution and performance-tuning reasons. There are three types of AFR, as elaborated in the following sub-sections.

### ***9.4.1 Stoichiometric***

Enough air is provided to completely burn all of the fuel. It is the ideal combustion process as the fuel is burned completely where all the Carbon (C) are burned to Carbon Dioxide (CO<sub>2</sub>), all the hydrogen (H) are burned to Water (H<sub>2</sub>O) and all the



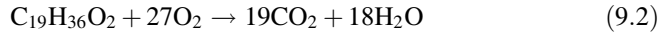
Sulphur (S) to Sulphur Dioxide (SO<sub>2</sub>). The general combustion process can be expressed by:



Any mixture greater than 15:1 is considered a lean mixture; any less than 15:1 is a rich mixture. Gasoline engines can run at stoichiometric air-to-fuel ratio because gasoline is quite volatile and is mixed (sprayed or carburetted) with the air prior to ignition.

Diesel engines, in contrast, run lean, with more air available than simple stoichiometry would require. Diesel fuel is less volatile and is effectively burned as it is injected, leaving less time for evaporation and mixing. Thus, it would form soot (black smoke) at stoichiometric ratio. For diesel fuel, the stoichiometric AFR is about 14.5:1.

For biodiesel, the stoichiometric mixture equation is quite the same as the ideal combustion:



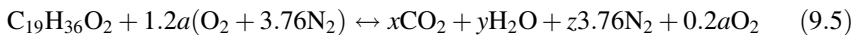
Thus, the balanced equation is:



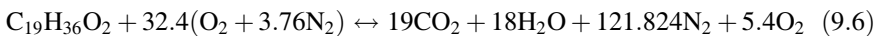
### 9.4.2 Rich

A mixture of air and fuel that has lower AFR than stoichiometric. It is less efficient, but may produce more power and burn cooler. Rich mixture can also be explained with the Equivalent Ratio. Equivalent Ratio is the ratio of actual AFR over theoretical AFR. When equivalence ratio is less than 1, it is called as lean mixture. When the equivalence ratio is greater than 1, it is called as rich mixture. And when there is exact amount of fuel and air as theoretical, it is called as stoichiometric mixture.

The rich combustion mixture which has an excess of about 20% air is given by:



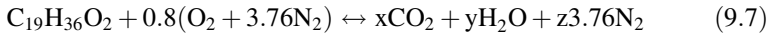
Thus, the balanced equation is:



### 9.4.3 *Lean*

Burning of fuel with an excess of air in an internal combustion engine, any mixture that has higher AFR than stoichiometric mixture. The excess of air in a lean-burn engine combusts more of the fuel and emits fewer hydrocarbons. High air–fuel ratios can also be used to reduce losses caused by other engine power management systems such as throttling losses.

For lean combustion mixture equation, the deficient air would be 20% less than the stoichiometric equation:



Thus, the balanced equation is:



For this research, the interest is in stoichiometric type mixture. There are two types of biodiesel that are generally used when calculating combustion, the C19 and the C20 chain lengths. For simplicity, only C19 (nineteen carbons in the chain) will be given focus in this chapter.

## 9.5 Implementation of Biodiesel in a Compression Ignition Engine

Up till now, there have been numerous studies and researches about biofuels. From its feasibility to its side effects, a wide area of biofuels had been covered by numerous researchers. This includes a variety of biofuel types from the vegetables to animal fats. Narrowing the scope down, the study and research on biodiesel had also covered a wide area. Biodiesel can be used in existing compression ignition engine without any retrofit (modification) on the engine. Numerous researchers from around the world have studied the implementation of biodiesel in compression ignition engine. According to Saheed et al. [1], when comparing a Euro 2M (B7) biodiesel of lower fraction with conventional fuel, at different throttle positions. The result showed that the brake thermal efficiency and brake specific fuel consumption shows a significant increment with 32% and 13%, respectively, during idle throttle and 18% during wide open throttle. Another experiment by Alireza [2], was conducted to investigate the brake torque power of a diesel engine fuelled with biodiesel (waste cooking oil) and diesel. It is concluded that with high lubricity and higher oxygen content found in biodiesel able to reduce the friction loss and improved the brake effective torque. It also compensates the heating value loss of biodiesel. Shahabuddin et al. [3], had researched towards the effects of biodiesel on

the ignition delay. It was concluded that a shorter ignition delays able to obtain through the usage of biodiesel.

Biodiesel have high viscosity, high cetane number and lower compressibility compared to the diesel fuel. Thus theoretically, with a higher percentage of biodiesel in a blend, it can prolong the shorter ignition delay. Yilmaz and Vigil [4], had investigated the potential of alcohol-vegetable oil mixtures as additives to biodiesel blends in terms of performance characteristics. It is certain that vegetable oil can improve the biodiesel lubricity properties, which contribute to better combustion. Maawa et al. [5] had conducted a research with another type of biodiesel which is the emulsified biodiesel water. The research was carried out by comparing the different percentage of emulsified water biodiesel (4, 6 and 8% of water ratio) with a B5 fuel. The result obtained shows that there are no significant differences between engine brake power and brake thermal efficiency. For the brake specific fuel consumption, it decreased as much as 12.75% when tested with 4% of water ratio but experienced an increase of 17.19% when tested with 8% of water ratio.

Onuh and Freddie [6], investigated on waste cooking oil which is another type of biodiesel. Waste cooking oil able to give a good engine performance because of its high level of saturation and single bond making it more stable and predictable. Lopez et al. [7], had a work of their own on the effects of olive-pomace oil biodiesel in compression ignition engine by analysing the exergy aspect. Even though a higher content of biodiesel in a blend reduced the exergy flow, the reduction is very minimal. Hence, the olive-pomace oil biodiesel can be considered to substitute diesel fuel. As studied by Tesfa et al. [8], the biodiesel types, mixture fraction values and physical properties of biodiesel do affect the compression ignition engine in-cylinder pressure, heat release and the brake specific fuel consumption. Due to biodiesel low heating value, high density and viscosity, the brake specific fuel consumption was increased up to 15%. Moreover, Prbakaran and Viswanathan [9] had investigated the effects of ethanol added in blends of biodiesel (cottonseed oil) in compression ignition engine. It is found that the biodiesel blends gave a higher brake thermal efficiencies and brake specific fuel consumption (at lower load) than the diesel fuel. In furtherance, Wahab et al. [10] had in their own executed experimental investigation on biodiesel. It was concluded that biodiesel showed a positive result regarding the performance and overcoming emission-related issues.

Even though a lot of works has been done related to the implementation of biodiesel in an internal combustion engine (compression-ignition engine), further literature survey confirmed that most of the biodiesel implementation was at lower fractions such as B0, B5 up to B7. Thus, it is apparent that up till now, there is still a technical communication gap on the implementation of higher fractions of biodiesel such as B10 up to B20 in direct injection compression ignition engine. Therefore, this study will be focusing on analysing the performance characteristics of the direct injection compression ignition engine under the influence of different fractions of biodiesel (B0, B7, B10 and B20) and clarifying the engine behaviours under these operating conditions.

### 9.6 Experimental Methodology

The research was conducted by experiment in the Centre of Automotive Research, University Kebangsaan Malaysia (UKM), using single-cylinder four (4) strokes direct injection compression ignition engine. Table 9.1 provides the technical operating parameters of the engine while Fig. 9.1 shows the schematic diagram of the experimental set-up.

This section focuses on the reason for selecting the technical operating parameters that were utilised in this experiment for optimum performance characteristics of the engine. The research used wide open throttle (WOT) load. It is to guarantee a maximum induction of air for the optimum performance characteristics of the internal combustion engine (compression-ignition engine). The engine speed (N) with a range from 1000 to 1750 rpm was utilised. It is to determine the best engine speed that can be guaranteed the best performance characteristics in a

**Table 9.1** Technical operating parameters

Operating parameters	Specification
Load	Idle load (10 kW), part load (20 kW), full load (40 kW)
Engine speed	1000–1750 RPM
Fuel	Biodiesel (B0, B7, B10 and B20)
Fuel injection timing	Maximum brake torque injection timing
Combustion strategy	Stoichiometry mixture

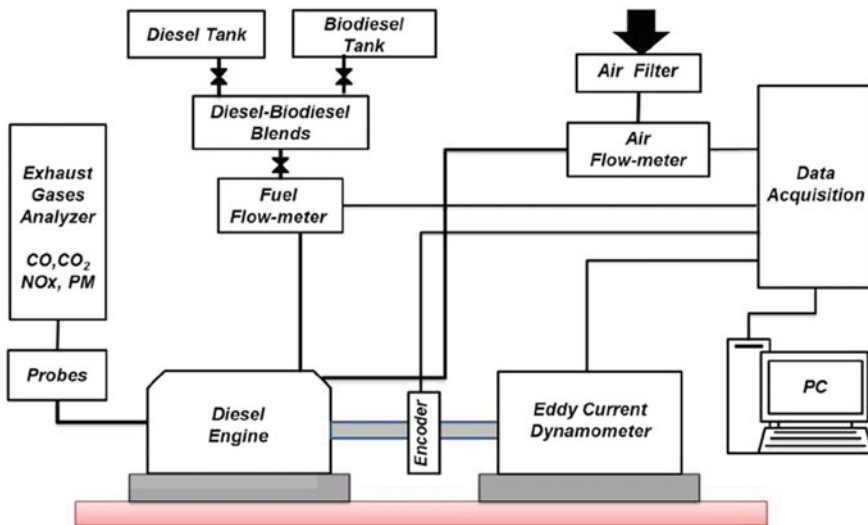


**Fig. 9.1** Schematic of the experiment set up

compression ignition engine while different fractions of biodiesel which are B0, B7, B10 and B20 were implemented. The reason for selecting the fractions of biodiesel up to B20 is to determine which biodiesel fraction guarantees the best performance in a compression ignition engine. In addition, Maximum Brake Torque Injection Timing (MBT Injection Timing) was utilised to determine the best injection timing that able to ensure maximum performance and lowest fuel consumption. For this research, the combustion strategy that was applied is the stoichiometry combustion strategy. It is to gain a uniform air-fuel mixing and a complete combustion of the engine. This can guarantee optimum performance and low engine emission. However, Table 9.1 shows the summary of the technical operating parameters that were used in this study.

## 9.7 Description of the Experimental Procedure

Table 9.2 shows the specification of the engine while Fig. 9.1 shows the schematic diagram of the experimental set up. For the experiment set up, the supply system of the engine comprises of biodiesel tank, pressure regulator, flow meter, etc. The experiment begins after the engine had been run for a period of time in order for the oil and coolant temperature to be stable in between 70 and 100 °C. The engine cylinder was injected with biodiesel fuel. This research was conducted at various throttle loads (idle, part and full load), maximum brake torque timing (MBT-Timing) and a range of engine speed from 1000 to 1750 rpm. Electronic Control Unit (ECU) was used to control the technical operating parameters during the experiment. The technical operating parameters such as engine speed (N), stoichiometry air-fuel ratio, throttle loads (idle, part and full load), etc. Eddy Current Dynamometer was used to collect the performance characteristics data such as Brake Power (BP), Brake Specific Fuel Consumption (BSFC) and Brake Thermal Efficiency (BTE).

**Table 9.2** Engine specification

Engine	YANMAR TF90
General details	4 stroke single cylinder compression ignition engine
Bore and stroke	85 mm × 86 mm
Compression ratio	18:1
Displacement volume	493 cm <sup>3</sup>
Connecting rod length	130 mm
Cooling system	Water-cooled (radiator)
Maximum power output	40 kW at 2500 rpm

## 9.8 Results and Discussion

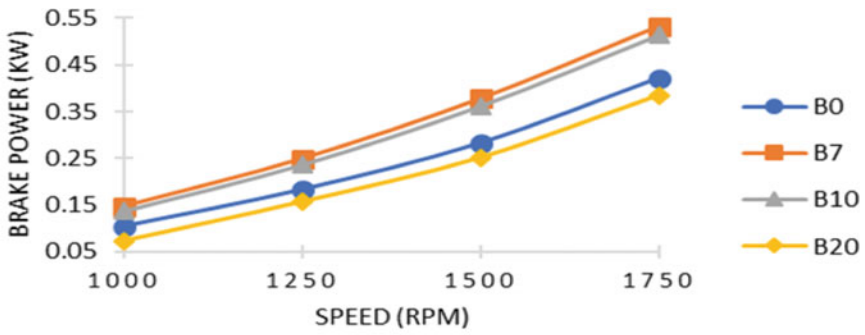
This section focused on the results obtained from the experiment of single-cylinder four-stroke direct injection compression ignition engine (Yanmar TF90). The experiment was conducted under the technical operating conditions such as engine speed (N) which ranges from 1000 to 1750 rpm, different throttle loads which are idle load (10 kW), part load (20 kW) and full load (40 kW), stoichiometry mixture and different fractions of biodiesel that ranges from B0, B7, B10 and B20. The results obtained are shown in Figs. 9.2, 9.3 and 9.4 and are fully discussed in the next section.

### 9.8.1 Brake Power

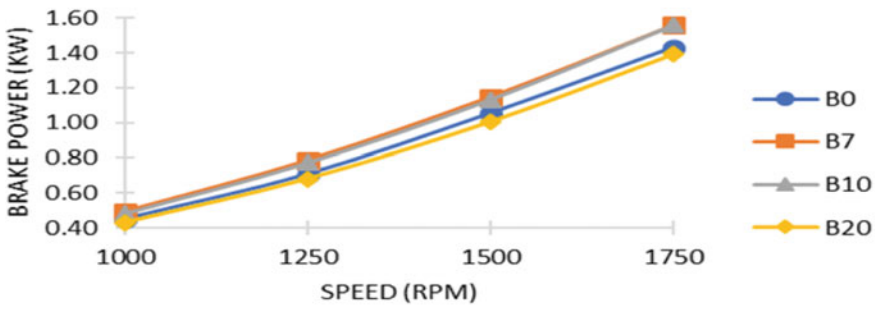
Figures 9.2a–c show the relationship between the brake power with different engine speed at three different throttle load conditions. It is apparent from the graphs that the increase of engine speed brings about an increment in brake power for all loading conditions under consideration. This might be due to the increase in burning velocity that reciprocated with the increased engine speeds. Comparing the brake power at different biodiesel fraction, it shows that B7 gives the highest brake power at operating conditions under consideration. This might be due to the low viscosity of B7 that gives a good atomisation which leads to efficient mixing of air and fuel, contributing to a good combustion in the engine.

Furthermore, by analysing the brake power at different loading conditions, it is shown that the maximum brake power occurred at full load, which is 3.68 kW. The idle load and part load are 0.53 kW and 1.56 kW, respectively. The reason being that at full load, there is maximum induction of air which increased the volumetric efficiency as this intensified the turbulence within the cylinder. The relationship between the two parameters is that the higher the volumetric efficiency, the higher the brake power is obtained. Moreover, consider the data point of brake power at full load for B0 and B7 at engine speed of 1000 and 1750 rpm, respectively. For B0 at 1000 and 1750 rpm, the brake powers are 1.16 kW and 3.56 kW, respectively. This shows an approximately 67% increment of brake power at this operating condition.

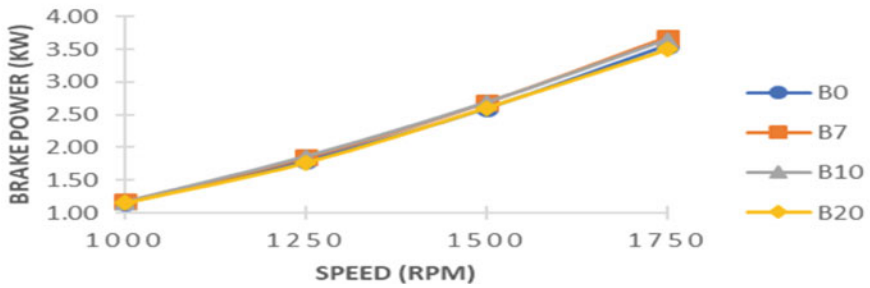
For B7, under the same operating conditions, the brake powers are 1.17 kW and 3.68 kW respectively. This shows a nearly 68% increment of brake power at this operating condition. Thus, it can be concluded that an approximately similar percentage of increment of brake power is obtained for the two biodiesel fuels under the same engine operating conditions. This is probably due to increase in friction occasioned by increase in pumping work. Good agreement was achieved between these experimental results and the reported work elsewhere [1, 18].



(a) Idling (10 kW)

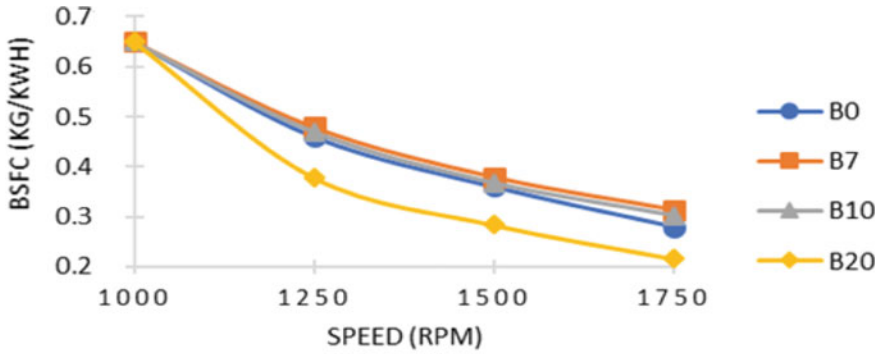


(b) Part load (20 kW)

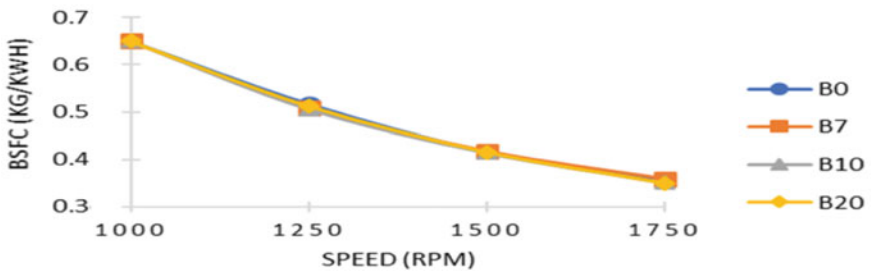


(c) Full load (40 kW)

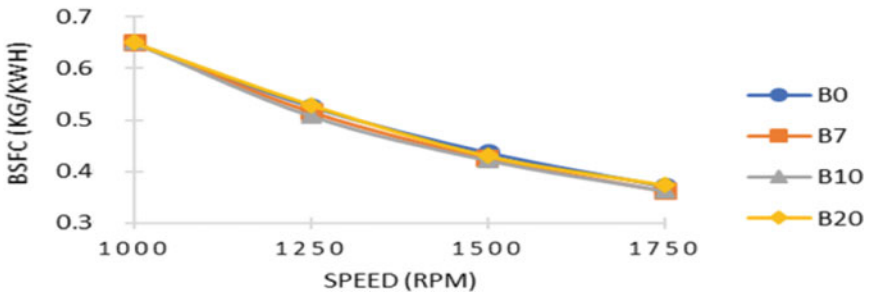
Fig. 9.2 Variations of brake power with multiple engine speed at different throttle loads



(a) Idling (10 kW)



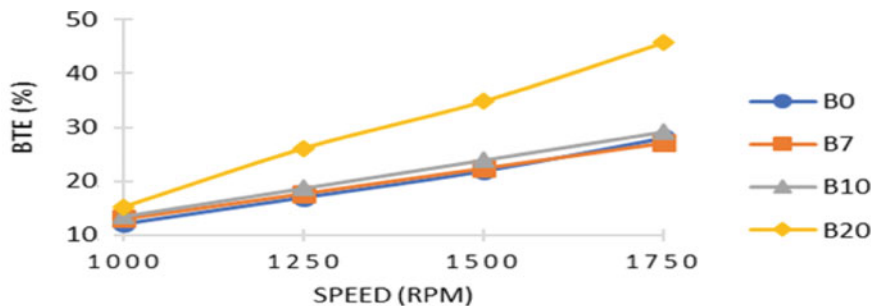
(b) Part load (20 kW)



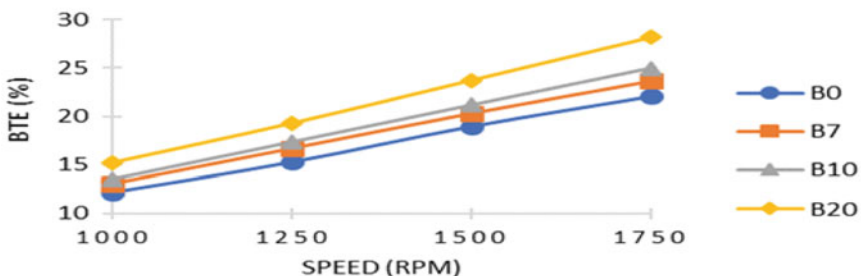
(c) Full load (40 kW)

Fig. 9.3 Variations of brake specific fuel consumption with multiple engine speeds at different throttle loads

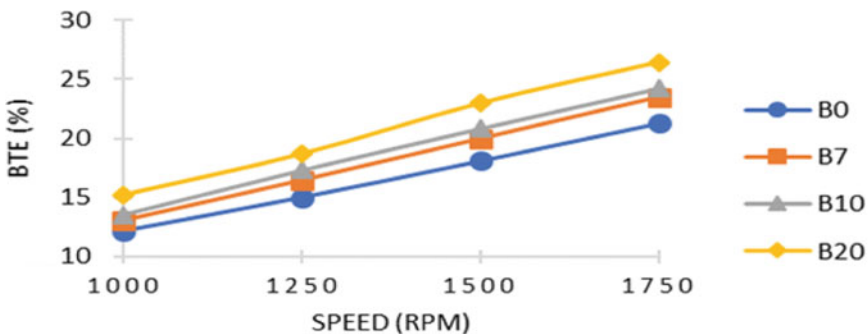




(a) Idling (10 kW)



(b) Part load (20 kW)



(c) Full load (40 kW)

Fig. 9.4 Variations of brake thermal efficiency with multiple engine speed at different throttle loads

### 9.8.2 Brake Specific Fuel Consumption

Figures 9.3a–c show the relationship between brake specific fuel consumption (BSFC) against different engine speed at three different throttle loads conditions. It is obvious from the graphs that with the increased engine speed, brake specific fuel consumption decreased for all loading conditions under consideration. This represents an improvement in fuel consumption. This reason being is that as the engine speed increases, it produced a high percentage of oxygen atom which leads to a late burning of heavier components of biodiesel in the expansion stroke.

From Figs. 9.3a, b comparing the BSFC between the different biodiesel fractions, it is apparent that B20 produced the best BSFC (the least BSFC) at the operating conditions under consideration. The reason is because of the lower heating value of B20 where more fuel is needed to generate the engine output power. From further observation, an exemption is found for Fig. 9.3c where the least BSFC is obtained from B10. This might due to the cycle-by-cycle combustion occasioned by the variation of mixture composition in the engine cylinder. Furthermore, consider the BSFC at the different loading conditions, the minimum BSFC is found occurring at idle load where the BSFC is 0.22 kg/kWh. While at part load is 0.35 kg/kWh and at full load is 0.37 kg/kWh. The reason being that idle load gives out a lower induction of air (lower volumetric efficiency), which caused lesser fuel to be needed for combustion, and so, produced the least BSFC. Furthermore, consideration should be given to the data point of the BSFC at idle load for B0 and B20 at engine speed of 1250 rpm and 1750 rpm, respectively. For B0 at 1250 and 1750 rpm, the BSFC is 0.46 kg/kWh and 0.28 kg/kWh respectively. This shows an approximately 64% decrement of BSFC under this operating condition. For B20, under the same engine operating conditions, the BSFC is 0.38 kg/kWh and 0.22 kg/kWh, respectively. This shows an approximately 73% decrement of BSFC under this operating condition. From the foregoing analysis, a significant decrement is obtained at B20 compared to B0 which might be due to the higher viscosity and density of B20. The results obtained here are coherent with the ones reported in the literature [10].

### 9.8.3 Brake Thermal Efficiency

Figures 9.4a–c show the relationship between brake thermal efficiency (BTE) against different engine speed at three different throttle loads. From the observation on the BTE graphs, it is seen that the BTE is increasing with the engine speed for all loading conditions under consideration. This observation can be explained by the increment of combustion quality as the engine speed increases. Based on the data resulting from different biodiesel fractions, it obvious that B20 produced a high BTE compared with the other biodiesel fractions at the operating conditions under consideration. This is probably because of a high percentage of biodiesel tends to

cause a reduction in heat loss and the developed power is increased. In addition, considering the different loading conditions, it observed that the maximum BTE occurred at idle load which is approximately 46%. Whereas, at part load and full load, the BTE values are nearly 28% and 26% respectively. It is because at idle load, lesser fuel is needed for combustion and thus, the lower combustion the higher the BTE will be obtained. Moreover, consider the data points of BTE at idle load for B0 and B20 at an engine speed of 1000 rpm and 1750 rpm respectively. For B0 at 1000 and 1750 rpm, the BTE are around 12% and 28%, respectively. This shows a nearly 57% increment of BTE under this operating condition. For B20 at 1000 and 1750 rpm, the BTE is roughly 15% and 46%, respectively. This shows an approximately 67% increment of BTE under this operating condition. Based on the above analysis, it is shown that an obvious increment in BTE is obtained with B20. This might be probably due to the high lubricity and oxygen present in the biodiesel that helps to improve the BTE during the combustion process in the cylinder. Good agreement is achieved between these experimental results and those reported elsewhere [19, 20].

## 9.9 Summary

This research has proven the feasibility of the direct injection compression ignition engine under the various fractions of biodiesel. A superior performance characteristic was obtained with biodiesel compression ignition engine as compared to pure diesel compression-ignition engine due to better ignition quality of the biodiesel fuel. Unlike the scarcity of fossil fuel, biodiesel is easily attained because of its renewable nature and its price can be significantly lowered than the conventional diesel fuel. Being renewable and could be produced from a wide variety of organic matter, added with the ever-increasing and intensive research in this field, it is only a matter of time for the best blend of biodiesel in terms of performance and emission characteristics to replace the existing diesel. Although the effects of biodiesel could not be observed clearly at the moment, with the rapid increment of technology and research, biodiesel is an alternative to the existing fossil fuels that cannot be overlooked as its impact to the humankind can be as big as fossil fuels somewhere in the future.

## References

1. S. Wasiu, R. Aziz, S. Ramlan, N. Mohamed, Performance characteristics of the direct injection compression ignition engine fuelled by biodiesel. *Intl. J. Appl. Eng. Res.* (2018)
2. A. Shirneshan, Brake torque of a diesel engine fuelled with biodiesel and diesel. *Intl. J. Renew. Sustain. Energy* **2**, 242 (2013)

3. W. Maawa, R. Mamat, G. Najafi, O. Majeed Ali, R. Aziz, Engine performance and emission of compression ignition engine fuelled with emulsified biodiesel-water. *IOP Conf. Ser. Mater. Sci. Eng.* **100**(1) (2015)
4. M. Shahabuddin, A. Liaquat, M. Masjuki, H. Kalam, M. Mofijur, Ignition delay, combustion and emission characteristics of diesel engine fueled with biodiesel. *Renew. Sustain. Energy Rev.* **21**, 623–632 (2013)
5. N. Yilmaz, F. Vigil, Potential use of a blend of diesel, biodiesel, alcohols and vegetable oil in compression ignition engines. *Fuel* **124**, 168–172 (2014)
6. E. Onuh, F. Inambao, A comparative evaluation of biodiesel derived from waste restaurant oil and Moringa (2017)
7. I. López, C. Quintana, J. Ruiz, F. Cruz-Peragón, M. Dorado, Effect of the use of olive-pomace oil biodiesel/diesel fuel blends in a compression ignition engine: preliminary exergy analysis. *Energy Convers. Manag.* **85**, 227–233 (2014)
8. B. Tesfa, R. Mishra, C. Zhang, F. Gu, A. Ball, Combustion and performance characteristics of CI (compression ignition) engine running with biodiesel. *Energy* **51**, 101–115 (2013)
9. B. Prbakaran, D. Viswanathan, Experimental investigation of effects of addition of ethanol to bio-diesel on performance, combustion and emission characteristics in CI engine. *Alex. Eng. J.* **57**(1), 121–130 (2018)
10. M. Wahab, M. Ma'arof, I. Ahmad, H. Husain, Potential utilization of biodiesel as alternative fuel for compression ignition engine in Malaysia. *IOP Conf. Ser. Mater. Sci. Eng.* **257**(1) (2017)
11. Official Palm Oil Information Source, Retrieved 01 June 2017, from [http://www.palmoilworld.org/about\\_mpob.html](http://www.palmoilworld.org/about_mpob.html)
12. Y. Li, G. Tian, H. Xu, Application of biodiesel in automotive diesel engines (2012)
13. A. Gianfrancesco, Worldwide overview and trend for clean and efficient use of coal materials for ultra-supercritical and advanced ultra-supercritical power plants, 543–687 (2017)
14. K. Breda, K. Marko, P. Stanislav, *Green Diesel Engine* (Springer Nature America, Inc., 2013)
15. E. Shahid, Y. Jamal, Production of biodiesel: a technical review. *Renew. Sustain. Energy Rev.* **15**, 4732–4745 (2011)
16. J. Nair, J. Deepthi, K. Kalyani, Study of biodiesel blends and emission characteristics of biodiesel. *Intl. J. Innov. Res. Sci. Eng. Technol.* **2** (2013)
17. S. Arindam, C. Akoijam, P. Kannan, *An overview of production, properties and use of biodiesel from vegetable oil* (Springer Nature, Berlin, 2016), p. 2016
18. S. Siraj, R. Kale, S. Deshmukh, Effects of thermal, physical and chemical properties of biodiesel and diesel blends, **2**, 24–31 (2017)
19. I. Adam, R. Aziz, S. Yusup, Performance and emission characteristics of an IDI diesel engine fuelled biodiesel (rubber seed oil and palm oil mix) diesel blends (2014)
20. N. Abu-Hamdeh, K. Al Nefaie, A comparative study of almond and palm oils as two bio-diesel fuels for diesel engine in term of emissions and performance. *Fuel* **150**, 318–324 (2015)

# Chapter 10

## A Study on Handling of Stranded Motorcycles in Malaysia



**Shaharin Anwar Sulaiman, Choo Sin Keat, Bong Hong Seng,  
M. Syahir Sazali and M. Ashraf Azhar**

In Malaysia, motorcycles are well known as vehicles with significantly low fuel consumption due to its low weight. Nevertheless, motorcycles also contribute to many issues such as emission, noise, traffic, and a few others. On top of that, motorcycle riders are exposed to various situations such as exposure to harsh weather, tendency of being hit by larger vehicles, and unexpected breakdown. This chapter discusses a study on the handling of motorcycles in the event when they are stranded. The primary concern here is on the safety of the riders and other road users. Although this chapter is not directly related to energy efficiency, it looks into an important aspect of a transport system that has a significant feature of low fuel consumption. The study was conducted through a survey and also via an interview with the local authority.

### 10.1 Introduction

Motorcycles are one of the main transportation in Malaysia. According to the Ministry of Transport Malaysia, in 10 out of 14 states, motorcyclists are recorded as the majority. Malaysia has the highest road facility risk per 100,000 populations among the ASEAN countries, and 50% of the road accidents involve motorcyclists. From the police records, 61% of the road accidents involving motorcyclists usually occur in rural areas. However, there are insufficient data on whether these road accidents involved improper towing of the damaged motorcycle or whether the motorcyclists have limited options and knowledge on how to transport their

---

S. A. Sulaiman (✉) · C. S. Keat · B. H. Seng · M. Syahir Sazali · M. Ashraf Azhar  
Department of Mechanical Engineering, Universiti Teknologi PETRONAS, 32610 Seri  
Iskandar, Perak, Malaysia  
e-mail: [shaharin@utp.edu.my](mailto:shaharin@utp.edu.my)

© Springer Nature Singapore Pte Ltd. 2020  
S. A. Sulaiman (ed.), *Energy Efficiency in Mobility Systems*,  
[https://doi.org/10.1007/978-981-15-0102-9\\_10](https://doi.org/10.1007/978-981-15-0102-9_10)



**Fig. 10.1** Towing a broken motorcycle using leg

damaged motorcycle which may lead to dangerous acts such as towing with their own leg with the help of another moving motorcycle, as shown in Fig. 10.1.

Motorcyclists may occasionally find themselves stranded on the roadside. The onus is on the riders that towing services are not common for motorcycles. One of the popular options is to call a friend who will ride to the place and then help the unlucky rider to tow him the workshop or to home. Such an act requires skill. At the same time, it may cause traffic congestion and fatal accidents if the motorcyclist's presence is not noticed. In an attempt to understand the problem, survey is conducted among motorcyclists, who are asked questions pertaining to how to act when stranded and the preferred approach in managing the situation.

There are strict laws to abide when it comes to towing a vehicle and limited guidance to them which then poses a difficulty on designing a proper towing device which can aid motorcyclists on towing their damaged motorcycle. For instance, according to The National Road Traffic Act, 1996 (Act No. 93 of 1996) and the National Road Traffic Regulations published in Government Notice No. R.225 of 17 March 2000, Regulation 330, no person shall operate a vehicle on a public road towing another vehicle if the towed vehicle is connected to the towing vehicle in

such a manner that both vehicles are not under control. In view of this, an interview with the Road Transport Department Malaysia was conducted to understand the regulations.

## 10.2 Accident Cases Involving Motorcycles

Towing a motorbike using leg is indeed a dangerous act, although it is a common sight in Malaysia. A student was reported killed by a four-wheel-drive car on 29 May 2012 when he was towing his motorcycle [1]. According to a witness, the victim was about to go home after having meal at a restaurant with his friends but unfortunately the motorcycle had a problem and he had to tow it with the help of a friend. However, suddenly there was a car coming from behind and hit them. A police spokeswoman said the incident occurred when the victim who rode a motorcycle with his brother-in-law towed the motorcycle assisted by another friend following as their motorcycle running out of oil. The case was investigated under Section 41 (1) of the Road Transport Act 1987. This case is only one of the many other similar accidents.

Figure 10.2 shows the statistic of Malaysia’s road accidents involving motorcycles, from 2008 to 2017, adopted from the Public Works Department of Malaysia [2]. The total number of accidents involving motorcycles is always high. The highest number of accident in motorcycle was in year 2016 with 135,181 cases.

Moreover, the data obtained from the official website of Road Safety of Malaysia [3] shows that there have been high numbers of reported accidents and deaths and 70% of the data resulted from the motorcyclist. Based on the data, the total number

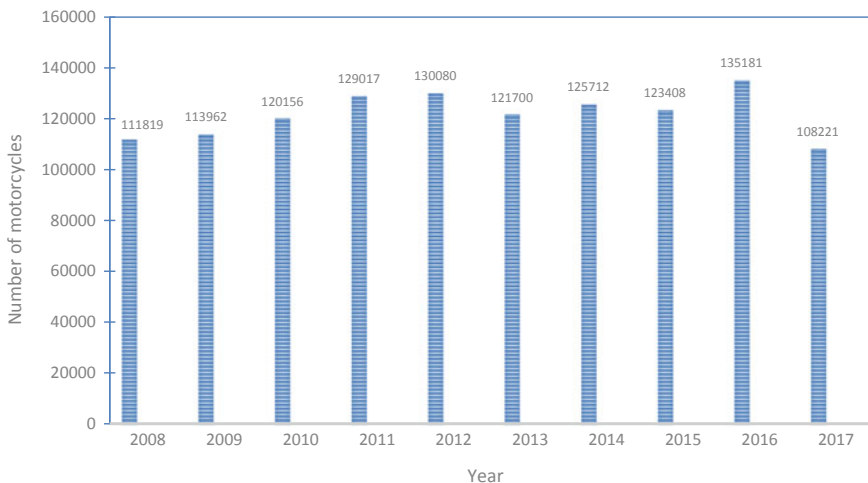


Fig. 10.2 Statistics of road accidents in Malaysia involving motorcycles

of accident was increasing from 2016 to 2017 but the total number of fatal accident was decreasing [4]. In addition, the total number of fatality also decreasing from 2016 to 2017.

### **10.3 Common Practice in Public**

Motorcycle breakdown is so common in Malaysia that it can be seen almost every day if one spends most of the time-traveling on the road. When a motorcycle breaks down, most probably the motorcyclist will be stranded by the roadside and will be unable to continue with the journey. Being stranded by the roadside while waiting for assistance, and with heavy traffic passing by, such situation exposes motorcyclists and other road users to danger. The broken motorcycle needs to be brought to a nearby workshop for repair or to be brought to the nearest rest area for towing services. One of the most common solutions is to push the broken motorcycle by hand to the nearest workshop in town or the nearest rest area on highway. Although this practice can get the broken motorcycle to a safer place instead of being stranded by the roadside, such practice exposes motorcyclists to potential road hazards while pushing the motorcycle. With traffics on the road, motorcyclists have the potential of being hit by other vehicles due to various reasons.

Other than that, the improper yet highly popular way of getting out of being stranded is by pushing the broken motorcycle using the leg of the motorcyclist on the running motorcycle. Such practice is the easiest way to solve this problem and most passing motorcyclists are willing to lend a hand by pushing the broken motorcycle to a nearby workshop or rest area. The danger lies within such practice is that both motorcyclists might lose balance while going through uneven terrain or corners thus exposes potential road hazards to both motorcyclist and other road users. Besides, for the case of being stranded due to punctured tyres, broken absorbers or tyre rims, the broken parts will be incurred further damages if it is towed improperly.

### **10.4 Safety Issue and Regulations of On-the-Road Motorcycle**

Safety issue on the road is important when towing a vehicle. Without the attention to safety procedures and regulations, towing any vehicle could be dangerous to the driver and other road users. When designing a towing device, a designer needs to know the capabilities of the device and must adhere to the rules and regulations on the road. A driver who tows another vehicle also must be aware of challenges such as decreased acceleration, braking performance, reduced vehicle control, and maneuverability when towing a vehicle.



Any drivers and vehicles on the road must obey the road law of a certain, which in this case the Law of Malaysia Act 333 Road Transport Act (1987). For instance, in Malaysia, any matters regarding road traffic can be referred in the Road Transport Act 1987. This law is important to facilitate the regulation of motor vehicles and traffic in streets. Besides, it also provides protection against other parties and risks arising from the use of motor vehicles in addition to assigning a method/way for construction and the use of motor vehicles.

In the Road Transport Act, there are several clauses that are relevant to the classification, registration and licensing. In this section, the act explains the classification of motorized vehicle and the prohibition of motorized vehicle which do not comply with rules. For towing a device, the classification can be put under trolley vehicles. This classification is used to determine the fees, the compound.

In the various section, it touches on the methods of prescribing the construction, maintenance, use, age, equipment used and the conditions without affecting the previous provision. As stated in the Law of Malaysia Act 333 Road Transport Act (1987), the minister may make regulation of the towing or drawing of motor vehicles by tow-trucks or motor vehicles and the manner of attachment. However, after several research is done, there is no specific law and regulation on modification tools and additional tools to the motorbike neither from Law of Malaysia nor from the minister of transportation.

## 10.5 Interview with the Road Transport Department

In order to implement new modification on a motorized vehicle, a designer needs to follow certain procedure to get verification for the license. Besides, the designer also needs to meet the road regulations and get approvals from several authorities such as Ministry of Road Transport, PUSPAKOM (Pusat Pemeriksaan Kenderaan Berkomputer) and consulting agencies.

On a general view, one needs to refer to the book of "*Kaedah-kaedah Pengangkutan Jalan.*" This book specifies the main Act (APJ 1987) which is updated regularly depending on the policy stated by the law. Inside the book, there are methods about anything related to road transport be it licensing, motorized vehicles, road traffics and so on. Referring to "*Kaedah-Kaedah Pengangkutan Jalan,*" one of the methods that governs the construction and usage of the motorized vehicles on the road are as follows:

Kaedah-Kaedah Kenderaan Bermotor (Pembuatan dan Penggunaan) 1959.

Based on the methods found in the textbook, there are several clauses that describe the concept of towing of motorized vehicle. The clauses are described as follow:

Tiada kenderaan bermotor yang melebihi Panjang 24 kaki boleh menarik sesuatu treler dengan syarat bahawa kaedah ini tidak terpakai pada mana-mana kenderaan rosak yang

ditarik oleh suatu kenderaan bermotor akibat kerosokan itu; dan tiada motosikal boleh menarik treler. Tiada pengangkut yang tidak sah boleh menarkik treler; da tiada treler boleh digunakan bagi mengangkut penumpang-penumpang yang menyewa atau yang membayar.

But in some cases, there are possible clauses that allow a motorcycle to be modified. Referring to Clause 138, "*Kenderaan yang melanggarkaedah-kaedah*", the clauses that allow a motorcycle to be modified are outline as follow:

keadaan atau dalam cara yang melanggar atau gagal mematuhi apa-apa Kaedah-Kaedah ini sebagaimana ia terpakai bagi pembuatan, peralatan, jenis kegunaan, cara penggunaan, bagi kenderaan itu atau jenis kenderaan itu, melainkan kenderaan itu telah secara nyata dikesualikan oleh Ketua Pengarah daripada mematuhi apa-apa Kaedah-Kaedah ini yang sepatutnya terpakai kepada kenderaan sedemikian. Berhubung dengan penggunaan jejak tayar peruntukan mana-mana undang-undang bertulis yang melarang penggunaan jejak tayar di atas jalan raya hendaklah juga terpakai.

Furthermore, a design can be put into Clause "*94. Keadaan Kenderaan (Aksesori)*" where the design can be assumed the same as the ice cream motorcycle with the side compartment. But the motorcycle with the side compartment needs to follow certain requirements as stated in Clause "*94. Keadaan Kenderaan (Aksesori)*"

Keadaan mana-mana kenderaan bermotor yang digunakan di atas jalan dan semua bahagian dan aksesoriya hendaklah pada setiap masa tidak menyebabkan bahaya atau mungkin menyebabkan bahaya kepada mana-mana orang di atas kenderaan atau di atas jalan.

The Road Transport Department (RTD) is a Malaysia's government agency that is responsible of undertaking registration and licensing of drivers and all motor vehicles and trailers in Malaysia. According to the Road Transport Act, the enforcement and regulatory duties are under the roles and responsibilities of RTD. Based on a consultation with an RTD officer, any heavy things can be put into the side compartment of the motorcycle, as long it meets the requirement of Clause 94. A design also needs to meet the specification stated by the act. For example, there is one clause that mentioned the specifications of tire "*46. Tayar*". It stated that the tire needs to be in tube tire (tire with air) if want to be implemented on the road. Besides, if new tire is suggested to be implemented, the tire need to be tested and approved by consultant, RTD director and PUSPAKOM. The clauses are as follow:

- (1) Semua tayar kenderaan hendaklah dipasang dengan tayar pneumatik dari saiz dan rekabentuk yang sesuai.
- (2) Tayar pneumatik di bawah subkeadah (1) hendaklah menurut spesifikasi berikut, seperti yang dikehendaki:
  - (a) Spesifikasi MS 1394 untuk Tayar Pneumatik Baru bagi Kenderaan Lebuhraya lain daripada Kenderaan Penumpang atau Peraturan UN ECE 54 Peruntukan Seragam Mengenai Kelulusan Tayar Pneumatik bagi Kenderaan Perdagangan dan Trelernya atau Standard No. 119 Tayar Pneumatik Baru bagi Kenderaan Lebuhraya lain daripada Kenderaan Penumpang;
  - (b) Spesifikasi MS 149 untuk Tayar Pneumatik Baru Kenderaan Penumpang atau Peraturan UN ECE 30 Peruntukan Seragam Mengenai Kelulusan Tayar Pneumatik

- bagi Kenderaan Motor dan Trelernya Standard FMVSS N0. 119 Tayar Pneumatik Baru bagi Kenderaan Penumpang; atau
- (c) Spesifikasi MS 224 untuk Tayar Celup Pneumatik Getah bagi Kenderaan Penumpang dan Kenderaan Perdagangan atau Peraturan UN ECE 108 Peruntukan Seragam Mengenai Kelulusan bagi Pengeluaran Tayar Celup Pneumatik bagi Kenderaan Motor dan Trelernya dan Peraturan UN ECE 109 Peruntukan Seragam Mengenai Kelulusan bagi Pengeluaran Tayar Celup Pneumatik bagi Kenderaan Perdagangan dan Trelernya.

Upon understanding the laws and regulation of the modification of private vehicles, a designer can apply for exceptions. Firstly, the designer needs to know category of the modified motorcycle. This is important to know the fees and for further classifications. A design also needs to meet the specification stated by the clause. For example, the tire needs to be in tube tire (tire with air) if want to be implemented on the road. Besides, if new tire is suggested to be implemented, the tire needs to be tested.

### 10.6 Questionnaire Survey

A questionnaire survey is designed to gather information about the public awareness pertaining to stranded motorcycle situations. The survey was conducted on 76 university students regardless of their faculties and seniority. This survey is done by using Google form with a total of 8 questions.

As shown in Fig. 10.3, 60.5% of the students are aware about the condition of their motorcycle. Another 39.5% of the respondents imply that they are not aware of their motorcycle condition due to not owning a motorcycle themselves. By knowing the motorcycle condition, one can prevent unwanted breakdown to happen at an important moment by performing preventive maintenance in advance.

Figure 10.4 shows the result pertaining to the experience of getting stranded. It is shown in the figure that 52.6% of the students have, in the past, experienced stranded by the roadside due to malfunction of motorcycle. With more than 50% of

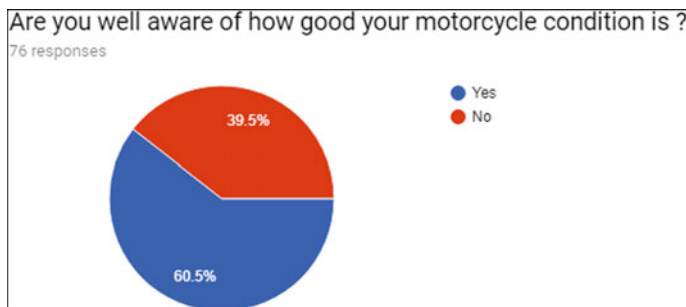


Fig. 10.3 Awareness on motorcycle condition

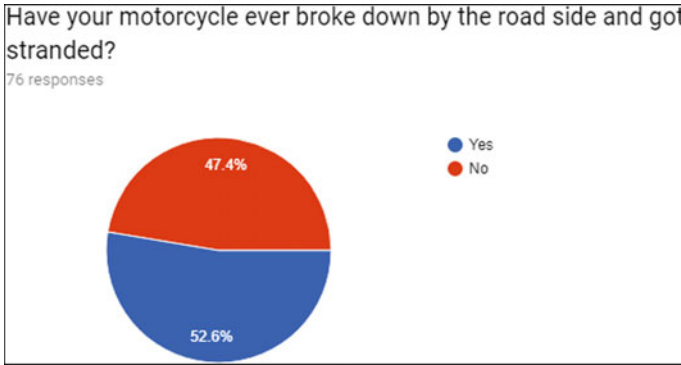


Fig. 10.4 Experience of getting stranded

students have ever faced such incident, this unfavorable figure shows that there might be a lack of exposure on motorcycle maintenance among the riders. The frequency of such incident to happen can be reduced with consistent practice of preventive maintenance by motorcycle owner.

With 85.5% of the students having awareness about the danger lies within stranded by the roadside, Fig. 10.5 shows that the exposures and teachings of road safety among university students are effective. Only 14.5% of students are unaware of the dangers that can happen when one got stranded by the roadside. By knowing the potential hazards on the road, one can prevent unwanted incident from happening by not doing any unsafe act that leads to it.

Figure 10.6 shows the choice of actions by respondents in the event of breakdown. As shown in the figure, 21.1% of them prefer to call for a proper motorcycle tow truck or any insurance company that they have subscribed to on a monthly basis. These services might not be cost-efficient because payment needs to be made on a monthly basis but their presence is in need once in a blue moon. Besides, 25%

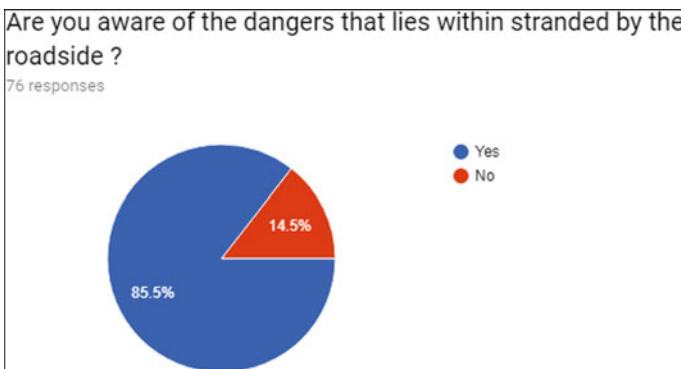


Fig. 10.5 Awareness on danger when getting stranded by the roadside

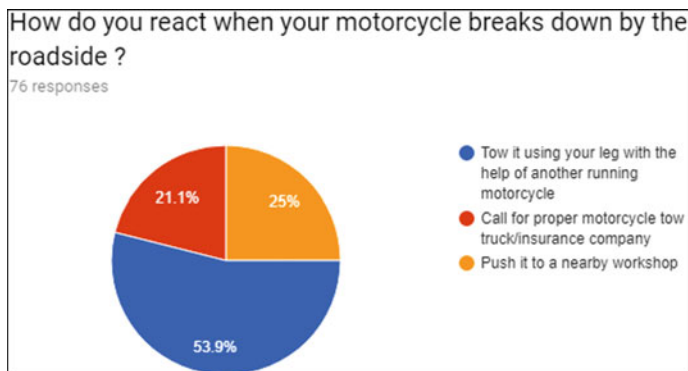


Fig. 10.6 Ways of handling a broken motorcycle by the roadside

of the students are willing to push the stranded motorcycle to the nearby workshop. This action leads students to potential exposure to dangers due to traffic on the road especially during peak hours. The remaining 53.9% of the students opt for towing the stranded motorcycle by using leg with the help of another running motorcycle. This kind of practice is the most commonly found on the road and it does not only expose both motorcyclists to great danger, it also has the potential to incur further damage to the broken motorcycle in the case of a punctured tyre.

In relation to the previous question, it is shown in Fig. 10.7 that almost 60% of students have actually experienced the dangerous practice of towing a broken motorcycle with their own leg. This unfavorable percentage shows that such dangerous practice is opted to be the solution due to the lack of safety awareness and a selfish way of solving the problem regardless of the safety of other road users.

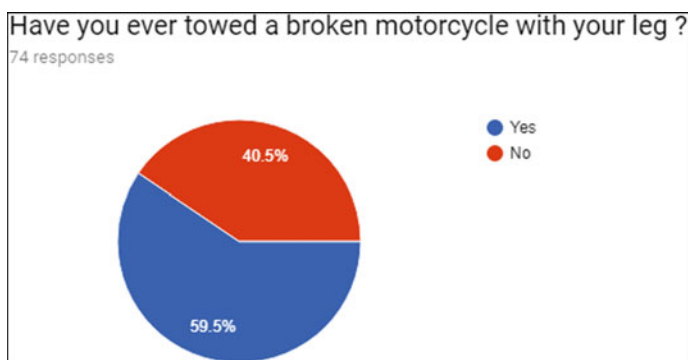


Fig. 10.7 Experience in towing a broken motorcycle

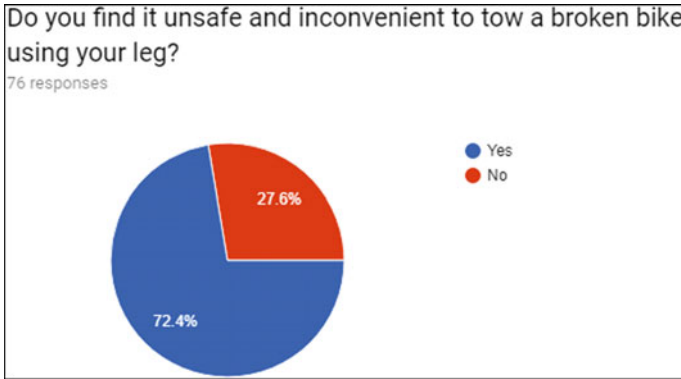


Fig. 10.8 Opinion on towing a broken motorcycle by using leg

With almost 60% of students having ever towed a broken motorcycle with a leg as shown in Fig. 10.7, this question shown in Fig. 10.8 is designed to find out the safety awareness of these students. A result of 72.4% of the students understood that towing the broken motorcycle using leg instead of proper device is unsafe and inconvenient. Despite knowing the potential hazard lies within this unsafe act, based on Fig. 10.7 there are still almost 60% of the students performing this towing technique due to one’s selfish way of handling the situation.

The maximum speed that a vehicle can travel when towing another vehicle with a rigid towing system is limited to 90 km/h. It is shown in Fig. 10.9 that about 79% of the respondents do not know about the maximum speed for towing a stranded motorcycle and 21% of them already knew about this matter. Towing a broken motorcycle at a high speed can cause further damage to the broken motorcycle in the case of punctured tyre or broken rim and absorber. Besides, it can also affect the

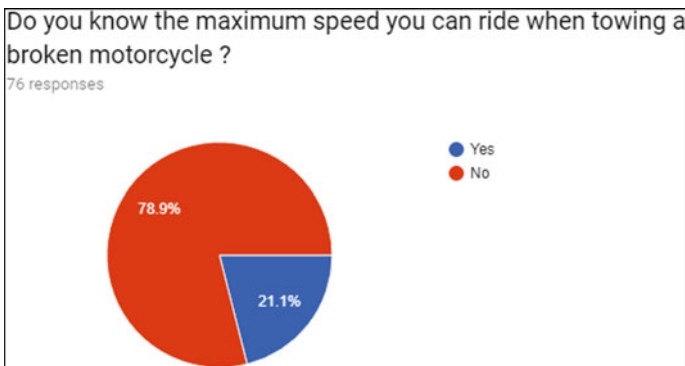
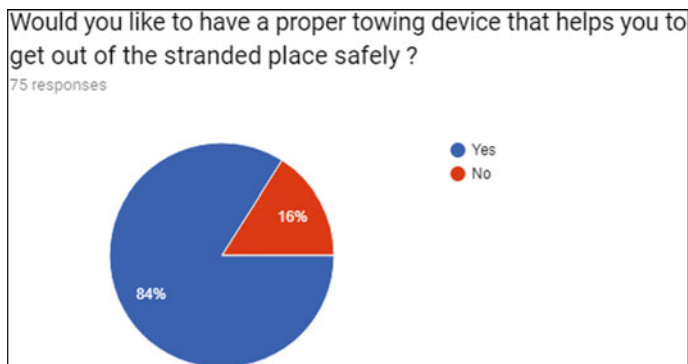


Fig. 10.9 Knowledge on maximum cruising speed during towing process



**Fig. 10.10** Market demand for proper towing device

safety of both motorcyclist and other road users when it is towed at high speed as it is harder to control the broken motorcycle thus more prone to an accident.

The common way of towing a broken motorcycle is by using leg to push the broken motorcycle while riding on the functional one. Based on Fig. 10.8, such towing practice is dangerous and risking the motorcyclists and other road user's life. In order to ensure the safety of all road users, a proper towing device is needed to put an end to this improper yet dangerous towing practice. According to Fig. 10.10, as much as 84% of the students would like to have a proper towing device to be used in an emergency situation. With the aid of a proper towing device, road users can get out of being stranded safely without risking the life of road users and also incur further damage to the broken motorcycle.

## 10.7 Summary

This study focuses on identifying the general conduct and practices when motorcyclists are stranded with their damaged motorcycle and the problems that arise with it. Once they are identified, the laws that govern towing procedure are studied as well to allow the proper design of a towing device without obstructing any road regulations.

## References

1. Dirempuh ketika tunda motor, Sinar Harian, 30 May 2010, p. 4
2. Jabatan Keselamatan Jalan Raya, Analisis Statistik Perbandingan Kemalangan, Kemalangan Maut Dan Kematian Op Selamat 9/2016 Dan Op Selamat 11/2017 (2017), <http://www.jkjr.gov.my/ms/berita-terkini/467-berita-terkini/2963-analisis-statistik-perbandingan-kemalangan,-kemalangan-maut-dan-kematian-op-selamat-9-2016-dan-op-selamat-11-2017.html>

3. Malaysian Institute of Road Safety Research (2019), [www.miros.gov.my](http://www.miros.gov.my). Accessed 1 Apr 2019
4. Ministry of Transport Malaysia, Transport Statistics Malaysia (2017), <http://www.mot.gov.my/my/Statistik%20Tahunan%20Pengangkutan/Statistik%20Pengangkutan%20Malaysia%202017.pdf>